# IMPERIALCOLLEGEOFSCIENCE, TECHNOLOGY ANDMEDICINE

University of London

# SENSITIVITY ANALYSIS OF MECHANICAL STRUCTURES USING EXPERIMENTAL DATA

*by*

**Wai Ming TO**

Dynamics Section
Department of Mechanical Engineering
Imperial College of Science, Technology and Medicine
London SW7, U.K.

October 1990

# ABSTRACT

This thesis presents the development and application of linear and non-linear sensitivity analysis techniques for determining the revised modal properties in a structural modification analysis using analytical or experimentally-derived modal data. Since the quality of experimentally-derived modal models is dependent on the accuracy and the reliability of measurement and structural identification techniques, the associated methods for frequency response function (FRF) measurement and structural identification are also presented.

The traditional model for a FRF measurement using either single-shaker or multi-shaker modal testing is an open-loop form. However, inevitable physical constraints in practical implementation cause such FRF measurements to be inherently of a closed-loop form. By modelling the structure-shaker(s) interaction in proper detail, a closed-loop model for single- or multi-shaker modal testing has been developed from which it is shown that the previously hidden feedback paths introduce noise and leakage problems on current FRF estimators. The complexity of multi-shaker modal testing is illustrated by using a multi-input multi-output model from which a new frequency domain technique has been developed to give noise-free estimates of the FRFs.

Despite the highly sophisticated development of finite element (FE) methods, a comparison of the experimental and the analytical models for a structure's dynamic behaviour often reveals quite considerable discrepancies between the test structure and its FE model. The orthogonal constraint and the eigendynamic constraint methods for localizing the structural modification sites using modal data have been developed and shown to be successfully applicable the validation or updating of the FE model when a sufficient number of measured modes is available and when the measured coordinates

or degrees of freedom (DoFs) are complete. The effects of coordinate incompleteness and of simulated measurement errors on these methods are presented.

In recent years, first- and/or higher-order sensitivity analyses have been used to predict the dynamic characteristics of modified mechanical structures. However, the applicability of these techniques is in general limited to small modifications and by the complexity in computing the higher-order **eigenvalue** and eigenvectors derivatives. In this thesis, some inherent limitations to such sensitivity analysis methods are discussed and an alternative structural modification method based on **Rayleigh** quotient iteration is proposed. By retaining the nonlinear terms not accounted for in a first- or **higher**-order sensitivity analysis, a new computation procedure for determining the modified structure's modal properties has been developed. A comprehensive case study of an aluminium casing is presented which demonstrates the applicability of error localization and non-linear sensitivity analysis techniques. By combining the **first**-order eigenvalue sensitivity and one of these structural reanalysis techniques, it is possible to enhance the efficiency and the accuracy of structural optimization techniques for determining the optimum condition of a mechanical structure specified by an analyst.

# ACKNOWLEDGEMENTS

# NOMENCLATURE

The following list gives the principal use of the symbols in this thesis. However, a given symbol might be used to denote different quantities under special situations. The interpretation to be given to a symbol will be clear from the context in which it is employed.

| A | Coefficient defined in equation 2.39 |
| $a_{ij}$ | *ijth* element of matrix [A] |
| $_rA_{ij}$ | Modal constant of *rth* mode for receptance $H_{ij}(\omega)$ |
| [A] | Coefficient matrix defined in equation 4.14 *(Chapter 4)* <br> System matrix of a generalised eigenvalue problem <br> $[A]\{x\}=\lambda[B]\{x\}$ *(Chapter 5)* |
| $[A_1]$, $[A_2]$ - | Coefficient matrices defined in equation 7.7 |
| $[\Delta A]$ | Finite change in matrix [A] |
| B | Coefficient defined in equation 2.39 |
| $\{b\}$ | Coefficient vector defined in equation 4.14 |
| [B] | System matrix of a generalised eigenvalue problem <br> $[A]\{x\}=\lambda[B]\{x\}$ |
| C | Coefficient defined in equation 2.39 <br> A constant dependent upon the time-window shape <br> *(Chapter 2 : eqns. 2.47 and 2.48)* |
| $c_{rs}$ | Mode participation factors |
| $C_{jj}$ | Static flexibility at point j |
| $\mathbb{C}^{NxN}$ | Complex space with dimensions *NxN* |
| [C] | Viscous damping matrix of the original structure |
| $[\Delta C]$ | Viscous damping modification matrix |
| e | Number of mass/stiffness error coordinates |
| $\{EV\}$ | Error vector defined in equation 7.14 |
| [EM] | Error matrix defined in equation 7.11 |
| f(t) | Applied force in the time-domain |
| f'(t) | Measured force signal in the time domain |

| | | |
|---|---|---|
| $F(\omega)$ | | Applied force in the frequency-domain |
| $\{f\}$ | | Applied force vector |
| $\{F(\omega)\}$ | - | Applied force vector in the frequency domain |
| $\{F'(\omega)\}$ | | Measured force signals in the frequency domain |
| $G(\omega)$ | | Frequency domain function defined in equation 2.29 |
| $h_{ij}(t)$ | - | Impulse response function between points i and j |
| $H(\omega)$ | | **Frequency** response function |
| $_1H(\omega), _2H(\omega)$ | | Conventional FRF estimators |
| $_3H(\omega)$ | - | Instrumental FRF estimator |
| $_vH(\omega)$ | | Geometric mean FRF estimator |
| $H_{em}(\omega)$ | - | FRF representing the electro-mechanical properties of the shakers |
| $H_{ij}(\omega)$ or $H_{ij}$ | - | Receptance between points i and j |
| $H_s(\omega)$ | | FRF representing the mechanical properties of the shakers |
| $\{H_A(\omega)\}$ | - | A complete column of the receptance matrix of the analytical model |
| $\{H_X(\omega)\}$ | - | A complete column of the measured receptance matrix |
| $[h(\omega)]$ | - | Impulse response function matrix of the structure |
| $[h_{em}(t)]$ | - | Diagonal matrix describing the electro-mechanical properties of shakers in the time-domain |
| $[h_s(t)]$ | - | Diagonal matrix describing the mechanical properties of shakers in the time-domain |
| $[H(\omega)]$ | - | Receptance matrix of the original structure |
| $[H'(\omega)]$ | - | Receptance matrix of the modified structure |
| $[H_o(\omega)]$ | - | **Open** loop FRF matrix |
| $[H_s(\omega)]$ | - | Diagonal matrix describing the mechanical properties of shakers |
| $[H_{XF}(\omega)]$ | | FRF matrix for test structure |
| $[I]$ | - | Unit matrix |
| $\{J\}$ | | Coefficient matrix defined in equation 4.19 |
| $k$ | - | Stiffness of a **SDoF** system |
| $k_e$ | - | Effective stiffness of the test structure at resonance |
| $k_i$ | | Stiffness value of *ith* spring elements |
| $k_s$ | - | Suspension stiffness of shaker |
| $K_{fg}$ | | Stiffness of force gauge |
| $\Delta k_{ij}$ | | Change in stiffness between points i and j |

| | | |
|---|---|---|
| $[K]$ | - | System stiffness matrix of the original structure |
| $[_AK_{11}]$ | - | Stiffness matrix of the analytical model corresponding to measured (master) DoFs |
| $[_AK_{12}]$ | - | Stiffness matrix of the analytical model corresponding to measured (master) and unmeasured(slave) DoFs |
| $[_AK_{22}]$ | - | Stiffness matrix of the analytical model corresponding to unmeasured (slave) DoFs |
| $[\Delta K]$ | - | Stiffness error matrix (Chapter 4) |
| | - | Stiffness modification matrix *(Chapters 5 &* 6) |
| $[\Delta K_{BARUCH}]$ | - | Baruch's stiffness error matrix |
| $[\Delta K_{PSEUDO}]$ | - | Pseudo-stiffness error matrix |
| $[K_A]$ | - | System stiffness matrix of the analytical model |
| $[K_{fg}]$ | - | Diagonal matrix describing the properties of force gauges |
| $\{L(\bar{x}_r')\}$ | - | Displacement vector defined in equation 6.18 |
| $[L]$ | - | Coefficient matrix defined in equation 4.19 |
| m | - | Number of averages *(Chapter 2 : eqns 2.19-2.21)* |
| | - | Mass of a SDoF system *(Chapter 2: eqns 2.24-2.48)* |
| | - | Number of measured modes *(Chapters 4-7)* |
| $m_i$ | - | *ith* mass elements where $i = 1, \ldots N$ |
| m(t) | - | Measurement noise in applied force signal |
| $m_e$ | - | Effective mass of the test structure at resonance |
| $m_s$ | - | Moving mass of excitation mechanism |
| $M(\omega)$ | - | Magnitude of FRF |
| $\{M(\omega)\}$ | - | Measurement noise vector of the applied-force signals in the frequency-domain |
| MCOH(i)($\omega$) | - | Multiple coherence functions of *ith* output |
| $[M]$ | - | Rotation matrix defined in equation 4.6 *(only for eqn.4.6)* |
| | - | System mass matrix of the original structure |
| $[_AM_{11}]$ | - | Mass matrix of the analytical model corresponding to measured (master) DoFs |
| $[_AM_{12}]$ | - | Mass matrix of the analytical model corresponding to measured (master) and unmeasured(slave) DoFs |
| $[_AM_{22}]$ | - | Mass matrix of the analytical model corresponding to unmeasured (slave) DoFs |
| $[\Delta M]$ | - | Mass error matrix *(Chapter 4 )* |
| | - | Mass modification matrix *(Chapters 5 & 6)* |
| $[\Delta M_{BERMAN}]$ | - | Berman's mass error matrix |
| $[m_A]$ | - | Matrix defined in equation 4.10 |

| | | |
|---|---|---|
| $[M_A]$ | | System mass matrix of the analytical model |
| $n$ | | Number of measured(master) coordinate |
| $n(t)$ | | Measurement noise of response signal |
| $N$ | | Number of degrees-of-freedom |
| $\{N(\omega)\}$ | - | Measurement noise vector of the response signals in the frequency-domain |
| $P$ | | Number of mass elements |
| $\{P\}$ | | Coefficient vector defmed in equation 4.19 |
| $q$ | | Electric charge *(Chapter 2 only for Fig.2.3)* <br> Number of spring elements *(Chapters 4-7)* |
| $r$ | | ***Structural*** parameter of the test structure |
| $r_A$ | | Structural parameter of the analytical model |
| $r(t)$ | | External input signal in the time domain |
| $R_o$ | | Constant external input signal in the frequency domain |
| $R(\omega)$ | | External input signal in the frequency domain |
| $S_{fx'}(\omega)$ | | Cross-spectrum between measured input $f$ and measured output $x'$ |
| $S_{ff}(\omega),\ S_{x'x'}(\omega)$ | - | Auto-spectra of measured input f and measured output $x'$ |
| $S_{mm}(\omega),\ S_{nn}(\omega)$ | - | Auto-spectra of measurement noise |
| $[S_{F'F'}(\omega)]$ | - | Cross-spectrum matrix of $\{F'(o)\}$ |
| $[S_{F'X'}(\omega)]$ | - | Cross-spectrum matrix of $\{F'(\omega)\}$ and $\{X'(o)\}$ |
| $[S_{X'F'}(i)(\omega)]$ | - | Augmented cross-spectrum matrix of the ***ith*** input |
| $T$ | | Sample duration |
| $T_1(\omega),\ T_2(\omega)$ | - | Frequency response functions defined in Figure 2.6 |
| $[U]$ | | Matrix formed of left singular vectors |
| $\{v\}$ | | A set of data points defined in equation 4.6 |
| $[V]$ | | Matrix formed of right singular vectors |
| $W(\omega)$ | | Windowing function |
| $[W]$ | | A matrix defined in equation 6.21 |
| $x(t)$ | | Displacement function in the time-domain |
| $x'(t)$ | | Measured displacement signal in the time-domain |
| $X(\omega)$ | | Measured displacement signal in the frequency-domain |
| $\{x\}$ | | Coefficient vector defined in equation 4.14 *(only for 4.14)* <br> Displacement vector of the original structure *(Chapters 5 & 6)* |
| $\{\ddot{x}\}$ | | Acceleration vector of the original structure |

| | | |
|---|---|---|
| $\{x'\}$ | - | Displacement vector of the modified structure |
| $\{\bar{x}_r'\}$ | - | Displacement vector contains only the **DoF's** affected by the modification |
| $\{X'(\omega)\}$ | - | Measured displacement vector in the frequency domain |
| $\{Z(\omega)\}$ | - | Measurement noise vector defined in equation 3.35 |
| $[\Delta Z(\omega)]$ | - | Dynamic stiffness matrix of structural changes |
| $\alpha$ | - | Design parameter |
| $\alpha_i$ | - | Fractional change to element $i$ (where i = 1, . . . . **N**) |
| $\Delta\alpha$ | - | Incremental change of design parameter |
| $^{ii}\beta_k$ | - | *kth* zero for $H_{ij}$ |
| $\gamma$ | | Norm of a matrix defined in equation 5.37 |
| $\gamma(\omega)^2$ | - | Ordinary coherence function |
| $\Gamma(\omega)$ | - | A function defined in equation 2.48 |
| $\delta$ | - | Norm of a matrix defined in equation 5.37 |
| $\delta_{ij}$ | | Kronecker delta |
| $\epsilon$ | | Coefficient defined in equation 5.46 |
| $\eta$ | - | Damping loss factor of a **SDoF** system |
| $\eta_e$ | - | Damping loss factor of the test structure at resonance |
| $_A\lambda_r$ | - | *rth* eigenvalue of the analytical model |
| $\lambda_r$ | - | Measured eigenvalue of *rth* mode *(Chapter 4)* |
| | - | *rth* eigenvalue of the original structure *(Chapters 5 & 6)* |
| $\lambda_R$ | - | **Rayleigh** quotient |
| $\lambda'_r$ | - | *rth* eigenvalue of the modified structure |
| $\Delta\lambda_r$ | - | Finite change of *rth* eigenvalue |
| $\mu$ | - | Norm of a matrix defined in equation 5.37 |
| $\theta_r$ | - | the angle between *rth* left- and right-hand eigenvectors |
| $\{\theta\}_r$ | - | *rth* normalised right-hand eigenvector for viscously-damped system |
| $\{_l\theta\}_r$ | - | *rth* normalised left-hand eigenvector for viscously-damped system |
| $\rho_{LS}$ | - | least-squares norm of a matrix |
| $\rho_{rs}$ | - | Coefficient defined in equation 5.27 |
| $\sigma_{rs}$ | - | **Coefficient** defined in equation 5.28 |
| $[\Sigma]$ | - | Rectangular matrix of singular values |
| $\tau_r$ | - | Arbitrary constant |

| | | |
|---|---|---|
| $\nu$ | - | Norm of a matrix defined in equation 5.37 |
| $\phi_{ij}$ | - | *jth* element of *ith* **mode** |
| $\phi(\omega)$ | - | Argument of FRF |
| $\{\phi\}_r$ | - | Measured eigenvector of *rth* mode *(Chapter 4)* |
| | - | *rth* mass-normalised right-hand eigenvector of the original structure *(Chapters 5 &* 6) |
| $\{\phi'\}_r$ | - | *rth* mass-normalised right-hand eigenvector of the modified structure |
| $\{_A\phi\}_r$ | - | *rth* eigenvector of the analytical model |
| $\{_A\phi_1\}_r$ | - | *rth* eigenvector corresponding to measured(master) DoFs |
| $\{_A\phi_2\}_r$ | - | *rth* eigenvector corresponding to unmeasured(slave) DoFs |
| $\{_l\phi\}_r$ | - | *rth* normalised left-hand eigenvector of the original structure |
| $\{_l\phi'\}_r$ | - | *rth* normalised left-hand eigenvector of the modified structure |
| $\{_X\phi\}_r$ | - | *rth* expanded mode shape vector of the modified structure |
| $\{_X\phi_1\}_r$ | - | *rth* measured mode shape vector of the modified structure |
| $\{_X\phi_2{}^*\}_r$ | - | *rth* expanded mode shape vector of the modified structure corresponding to unmeasured DoFs |
| $[\Phi]$ | - | Measured mode shape matrix *(Chapter 4)* |
| | - | Mass-normalised eigenvector matrix of the original structure *(Chapters 5 &* 6) |
| $[\Phi_A]$ | - | Mode shape matrix of the analytical model |
| $\{\varphi\}_r$ | - | Estimate of *rth* eigenvector |
| $\{\psi\}_r$ | - | Arbitrarily scaled *rth* right-hand eigenvector of the original structure |
| $\{\psi'\}_r$ | - | Arbitrarily scaled *rth* right-hand eigenvector of the modified structure |
| $\{_l\psi\}_r$ | - | Arbitrarily scaled *rth* left-hand eigenvector of the original structure |
| $\{_l\psi'\}_r$ | - | Arbitrarily scaled *rth* left-hand eigenvector of the modified structure |
| $\omega_r$ | - | *rth* natural frequency of the original structure |
| $_A\omega_r$ | - | *rth* natural frequency of the analytical model |
| $_X\omega_r$ | | Measured natural frequency of *rth* mode |
| $\Delta\omega$ | - | Finite change of natural frequency |
| $\lceil\omega^2\rfloor$ | - | Measured natural frequency squared matrix *(Chapter 4)* Natural frequency squared matrix of the original structure *(Chapters 5 &* 6) |

## Operators

| | |
|---|---|
| adj{[ ]} | **Adjoint** of a matrix |
| arg | **Argument(phase)** |
| det [ ] | Determinant of a matrix |
| E[ ] | Expected value of [ ] |
| rank [ ] | Rank of a matrix |
| trace [ ] | Trace of a matrix |
| var [ ] | Variance of [ ] |
| $\Delta_{ij}$ | *(i,j)th* cofactor of a matrix |
| * | Complex conjugate |
| \| \| | **Modulus(magnitude)** |
| [ ]$^{-1}$ | Inverse of a matrix |
| [ ]$'$ | Generalised inverse of a matrix |
| [ ]$^T$ | Transpose of a matrix |
| [ ]$^H$ | Complex-conjugate transpose of a matrix |
| \|\|[ ]\|\|$_2$ | 2-norm of a matrix |
| \|\|[ ]\|\|$_F$ | Frobenius norm of a matrix |

## Diacritical

| | |
|---|---|
| $'$ | Derivative with respect to frequency |
| $\cdot$ | Derivative with respect to time |
| $\wedge$ | Averaged sample |

## Abbreviations

| | |
|---|---|
| ARMA | Auto-regression moving average |
| COMAC | - Coordinate modal assurance criterion |
| DoF(s) | Degree(s) of freedom |
| ERA | Eigensystem realisation |
| FE | Finite element |

| | |
|---|---|
| FFT | Fast Fourier transform |
| FRF | Frequency response function |
| IRF | Impulse response function |
| MAC | Modal assurance criterion |
| MDoF | Multi-degree-of-freedom |
| MIMO | Multi-input multi-output |
| SDoF | Single degree-of-freedom |
| SIMO | Single-input multi-output |
| SISO | Single-input single-output |
| SVD | Singular value decomposition |

# LIST OF FIGURES

| **Table** | **Title** | **Page** |
|---|---|---|

# TABLE OF CONTENTS

# 1 INTRODUCTION

*Gauss's dictum, " When a building is completed no one should be able to see any trace of the scaffolding," is often used by pure mathematicians as an excuse for neglecting the motivation behind their work and the history of their field. It is also used by practical engineers as an excuse for ignoring the original aim of their work and the historical development of their methods.*

## 1.1 THE STRUCTURAL VIBRATION PROBLEM

Because of resource scarcity and the escalating costs of materials and fabrication, structural optimization becomes an important stage in product design for many high-capital industries, such as the ship-building and aerospace industries. In those industries, the revenue is dependent on the payload of the vehicle so that the desire to reduce structural weight without unduly compromising structural integrity has been a strong driving force behind the development and application of structural optimization methods for many years.

In past decades, structural analysts have sought to evolve the "optimum" structural designs which normally possess pre-defined strengths with the minimum weights. In static analysis, the optimum structural designs can be accomplished analytically by employing some elegant mathematical techniques, such as total least-squares method or steepest descent method. Unfortunately, sometimes what is "optimum" or "best" design for one aspect may be a "bad" or "worst" design for another aspect.

The use of light-weight materials, truss frameworks and components milled from solid material makes a modem structure usually very stiff in all directions and provides an ideal solution for the structural optimization problem under a statically-loaded condition. However, this type of light-weight structures will have many **flexural** modes in the low-frequency range and is more likely to be excited into resonance under normal working conditions which may then cause human discomfort, fatigue cracking and, at worst, result in catastrophic failure. To this end, the incorporation of vibration analysis in product design has grown considerably in recent years.

## 1.2 **THE IMPORTANCE OF MODAL TESTING IN STRUCTURAL ANALYSIS**

Many fundamental vibration problems can be investigated and minimized by the use of theoretical vibration analysis and reanalysis techniques during the design stage of a manufacturing process.

Due to the advances in numerical methods and the availability of powerful computing facilities, finite element analysis (**FEA**) has become the most commonly-used analytical technique in structural dynamic analysis. In FEA a complicated continuous structure is usually represented by an assembly of well-defined discrete elements such as shell, plate and beam elements. To overcome the intractability of the structural modelling, various procedures and methods of discretisation have been proposed by structural analysts from time to time. All involve an *approximation* which, it is to be hoped, is of such a kind that it approaches, as closely as desired, the true characteristics of the continuous structure as the number of *discrete state variables* or *degrees-of-freedom* (**DoFs**) increases. However, many features of mechanical components and/or real structures are difficult to model or to discretise accurately in a finite element (FE)

model and, the approximations introduced during the structural modelling can lead to wide variations in the predicted dynamic response of the structure. A survey 'DYNAS'[1] has been conducted to show the existence of potential hazards when carrying out dynamic FE analyses for structures.

The use of such idealistic **FE** models alone should be considered to be inadequate. Once the prototype of a component (or the whole structure) has been produced, modal testing and analysis have to be performed in order to validate the FE model of the component (or the whole structure) and, if possible, to update the FE model so that it can be further used in structural analysis. It should be noted that after years of continued improvement in measurement equipment and development of structural identification techniques, there is a general agreement that the measured response data or experimentally-derived modal data are reckoned as more "correct" than their counterparts obtained from **FE** analysis, provided sufficient care is given to the experimental and identification procedures. Also, it should be noted that the experimentally-determined response and modal models can be used directly in coupling, structural modification and optimization analyses.

## 1.3 HISTORICAL DEVELOPMENT OF MODAL TESTING

The theoretical and practical considerations of performing a modal test have been investigated at length, and numerous erudite papers have been published in the technical literature over a period of several decades. A brief historical development of modal testing is presented here, a more thorough description of testing techniques is provided in some later chapters when specific techniques are classified or referred to in more detail.

Before the 1940s, the 'Peak-Amplitude' method was widely-used in determining the natural frequencies and mode shapes of mechanical structures. In 1947, Kennedy and Pancu [2] recognized the inadequacy of the 'Peak-Amplitude' method and suggested that certain characteristics of vector response plots - the real and imaginary vector components of vibration response with respect to the applied forces - could be more useful, and discussed their utility in the conduct and interpretation of modal testing. Following the 'characteristic phase lag theory' of damped structures given by Fraeijs de Veubeke (1956) [3], Bishop and Gladwell [4] in 1963 provided the theoretical background to the problem of resonance testing. In addition to Kennedy & Pancu's method, Bishop and Gladwell also assessed the accuracy of several modal testing techniques developed by Lewis and Wrisley [5] in 1950, Trasill-Nash [6] in 1958 and Asher [7] in 1958, respectively. In the 1960s and 1970s, there were major advances in vibration measurement equipment and different modal testing techniques which are currently used were established.

More recently, with the availability of computer-controlled measurement equipment and special-purpose analysis software, both the measurement time and human effort have been reduced and the reliability and accuracy of measured response and experimentally-derived data have also been improved significantly. The details of practical implementation of modal testing have been fully discussed by Ewins [8].

## 1.4 SCOPE OF PRESENT WORK

The research work presented in this thesis is concerned with structural reanalysis techniques using experimental data. Since the experimental data play an important role in structural reanalysis of real mechanical structures, the research work encompasses

many aspects of experimental modal analysis and, thus, the thesis is mainly formed of four constituent parts as described next.

**(i)    - Sensitivity Analysis of Measurement Techniques** is the subject of chapter 2. In this chapter, the classification of measurement techniques is presented and their characteristics are given.  Also, the specific advantages and limitations of each technique are discussed. The central part of chapter 2 is devoted to investigate the sensitivity of different FRF estimators with respect to the effects of noise and leakage for single-shaker modal testing using random excitation. Because of the advent of computer-aided testing systems and cheap Fast Fourier Transform processors, broadband testing techniques using random excitation are currently amongst the most popular vibration measurement techniques. Following the presentation of chapter 2, the classical multi-input multi-output identification techniques are presented and examined in chapter 3. There is a general belief that multi-shaker modal testing must provide a more consistent estimation of resonance frequencies, mode shapes and damping loss factors than a series of single-point tests, especially when the size of test structure is large and is assembled from a number of flexible components. However, practical experience shows that the shaker-structure interactions introduce unwanted internal feedbacks that cause difficulties in maintaining the orthogonality property of measured applied forces in a sine-dwell test and in ensuring the incoherence of measured force auto-spectra in a random excitation test. By carefully considering the effect of shaker-structure interactions in multi-shaker modal testing, a new closed-loop model is presented to reflect the 'true' or at least 'more realistic' physical situation in vibration measurement. The closed-loop model reveals the hidden feedback paths which has caused uncertainty in FRFs estimation for many years. As the classical MIMO identification techniques cannot handle highly correlated measured force signals in the vicinity of structural resonances, a new frequency domain technique is presented whereby the inability to estimate the FRFs due to the rank deficiency of measured

force cross-spectrum matrix, is overcome by using two cross-spectrum matrices that relate the measured response signals to the external input signals and the measured applied-force signals to the external input signals.

**(ii)  -  Structural Identification and Model Updating Techniques are** presented in chapter 4. Direct structural identification techniques include all traditional parameter extraction (modal analysis) methods in the frequency-domain and the time-domain. A concise description of commonly-used parameter extraction methods is provided from which the advantages and limitations of each method are addressed. In practice, only the **_response model_** is directly measurable and the _modal_ **model** can be derived from the measured FRF using curve-fitting techniques. The **_spatial model,_** which consists of mass, stiffness and damping properties of the structure, is neither measurable nor obtainable without the use of an analytical model. In order to determine the spatial properties of the structure (a good spatial model) which can reproduce the **_measured_** and **_unmeasured_** characteristics of the test structure, reconciliation processes including model correlation and model updating/validation must be performed. Several commonly-used correlation techniques are presented. By using these correlation techniques, the comparison between experimental modal data and FE results can be quantified in terms of real- or complex-valued numbers. Direct matrix-update methods are investigated and discussed in detail because although they have been long used by numerous researchers and practicing engineers for updating analytical/FE models, the reasons why these methods could not produce accurate mass and stiffness error matrices, even though a large number of modes have been measured, have not been well understood. Alternative model updating techniques using the orthogonal constraints and eigendynamic constraints are proposed. The sensitivity of these techniques with respect to the modal and coordinates incompleteness, and to simulated random noise is also investigated.

**(iii) - Linear and Non-linear Sensitivity Analysis of Mechanical Structures** constitute the subjects of chapter 5 and 6, respectively. It has already been stated that a good spatial model must be able to replicate the measured and unmeasured dynamic characteristics of the test structure. However, there are many situations where the dynamic response of the updated analytical/FE model does not satisfy the requirements set by the structural analyst (designer). In such situations, a practical solution is to alter the response properties by changing/redesigning the spatial properties of the structure. In chapter 5, first-order and higher-order sensitivity analyses are presented and their limitations in structural modification analysis are carefully discussed. By identifying the inherent limitations of sensitivity analysis, an alternative structural reanalysis technique using **Rayleigh** quotient iteration is proposed. Also, another structural reanalysis technique using inverse iteration is presented. It should be noted that these reanalysis techniques can be applied to some specific cases in which the mass and stiffness matrices, some eigenvalues and the corresponding eigenvectors of the original structure, the mass modification and stiffness modification matrices are provided or given. Chapter 6 presents a new computation procedure for determining the revised properties in a structural modification analysis where only the eigenvalues and the corresponding eigenvectors of the original structure, and the mass modification and stiffness modification matrices are given. This method has a distinct advantage because coordinate incompleteness will not introduce prediction errors provided the responses are available at the modification sites. The sensitivity of this reanalysis technique with respect to modal incompleteness and to simulated random noise is also investigated.

**(iv) - An Experimental Case Study** is presented in chapter 7. The physical expansion techniques are presented to resolve the incompatibility problem between the experimentally-derived and analytically-derived modal data sets. Central to this chapter are the results obtained on actual modified structures. They represent the

ultimate test of the capability of non-linear sensitivity analysis in predicting the effects of a simple practical modification on a real structure.

Finally, chapter 8 presents the general conclusions and contributions of the current work and suggestions for further research are also recommended.

# 2 SENSITIVITY ANALYSIS OF MEASUREMENT TECHNIQUE FOR SINGLE-SHAKER MODAL TESTING

## 2.1 INTRODUCTION

The experimental determination of the modal properties of mechanical structures is typically a costly and technically-demanding task that requires both measurement and analytical expertise. The reliability and accuracy of measured data are very important as they are required to create a modal model or a spatial model of the mechanical structure. Success in structural identification, modal updating, sensitivity analysis, structural assembly analysis and structural optimization lies in the ability to obtain 'good' measured results.

The importance of the reliability of measured data was realized by the Naval Research Laboratory (USA) which conducted the "Round Robin" survey in the early 1960s [9]. This survey invited some twenty laboratories in the USA, all of whom were actively engaged in performing structural dynamic testing, to take part in obtaining the mobility data of some pre-defined test structures. Their respective mobility data sets were collated and compared, resulting in the realisation that a high degree of unreliability existed in mobility measurement techniques at that time. Some years later, in the late 1970s, a similar survey was conducted in Europe under the codename "SAMM' (State-of-the-art Assessment of Mobility Measurements)[10]. Although this survey indicated that there existed considerable scope of improvement in some of the testing techniques used, it highlighted that the reliability and accuracy of measured mobility

data still depended on the competence of modal test practitioners and that considerable care was required during the measurement stage.

More recently, the availability of sophisticated computer-controlled measurement facilities makes the acquisition of frequency response functions (FRFs) much easier, much faster and possibly more reliable than in the past. However, the reliability and accuracy of measured data is very difficult to justify unless a thorough understanding of the sensitivity of measured FRFs with respect to different excitation methods and different FRF estimators is established.

## 2.2 OVERVIEW OF MEASUREMENT TECHNIQUES

Over the years, measurement techniques have been developed continuously to improve the accuracy of measured FRFs and to reduce the testing time, and therefore the cost, of experimental modal testing. Historically, these measurement techniques have been categorised into two main groups; Phase-Resonance methods and Phase-Separation methods.

### 2.2.1 PHASE-RESONANCE METHODS

Phase-Resonance methods consist of those procedures that attempt to establish natural modes of vibration by direct measurement of the test structure's forced vibration by multi-point excitation.

In order to establish natural modes of vibration, multi-shaker excitation is used to exert sinusoidally varying forces on the test structure. The frequency of excitation and the relative force levels of the electrodynamic shakers are adjusted to isolate the target

mode response from all other modes. The modal properties are then taken from direct measurement of the forced vibration response. A significant advantage of these methods is that it can be used to determine the modal properties' of a structure with high modal density i.e. close modes. However, in tuning the shakers to excite the mode of interest, one should have a reasonably good knowledge about the nature of that particular mode and the tuning procedure is very cumbersome. As a result, **Phase-**Resonance methods are rarely used because they are time-consuming, and therefore costly. In addition, their success sometimes seemed to be dependent upon the competence of the modal test practitioners.

### 2.2.2 PHASE-SEPARATION METHODS

Phase-Separation methods consist of those procedures that attempt to identify modal properties of the test structure by post-processing the measured frequency response functions or time domain free response data.

There are a number of test and analysis procedures that have been proposed and developed by modal test practitioners to extract the modal properties by post-test analysis of **FRFs** which are obtained using sine-sweep or other excitations. In the past 20 years, the introduction of the Fast Fourier Transform (**FFT**) algorithm, the availability of digital data processing equipment and powerful mini- and micro-computers has led to the development of test procedures that make no attempt to excite the test structure at discrete frequencies. Instead, all modes within the frequency range of interest are simultaneously excited with either a single broadband randomly varying force using an **electrodynamic** shaker, or multiple uncorrelated broadband randomly varying forces using multiple-shakers, or an impulsive force using an instrumented hammer. The measured response data are then digitally processed to yield estimates of

the **FRFs,** from which modal properties are extracted using any one of several modal analysis curve-fitting techniques **[8].**

In addition to the frequency-domain identification procedures, other workers, including Ibrahim *et* al. [**11**]**,** have proposed analysis procedures that attempt to obtain modal properties (natural frequencies and damping loss factors) by post-test analysis of measured time-domain free response data. However, as noted by Ewins **[8],** many of these time domain identification procedures currently lack the ability to identify the **mass-normalised** mode shapes of complex structures which play a significant role for model updating and structural modification analysis because only free-response data are recorded.

Although each approach has specific advantages and disadvantages, the selection of a testing technique is usually based on the type of equipment available rather than its suitability for a particular job. In what follows, the sensitivity of different FRF estimators with respect to the effects of noise and leakage for single-shaker modal testing will be investigated.

## 2.3  IDENTIFICATION OF A REALISTIC MEASUREMENT-SYSTEM MODEL

Most **FRF** measurement methods require the attachment of an **electrodynamic** shaker and transducers to the structure under test. The transducers convert the force transmitted to the structure and the response of the structure to electric signals which, once filtered through signal conditioning equipment, are digitised and used to develop estimates of **FRF** in a spectrum or frequency analyser. However, because of its very nature, the excitation mechanism interferes with the test structure. Ewins [S] inter alia,

has noticed that if this interference is not controlled to negligible proportions, it may result in the acquisition of poor data, with the consequence of loss of quality in the final model of the structure.

Shaker-structure interaction is always a concern in FRF measurement because it introduces the problem of "force drop-out" at structural resonances. In recent years, there have been a number of publications [12-14] which document the force drop-out phenomenon at structural resonances and give excellent models of both the mechanical and electrical systems for an excitation mechanism. Also, there is a focus of interest in the estimation of **FRFs** of mechanical structures and various alternative FRF estimators have been introduced and investigated [15-17] for single-shaker modal testing using random excitation. Unfortunately, none has attempted to investigate the effect of shaker-structure interaction on those FRF estimates although it is obvious that the inevitable physical constraints cause such FRF measurements to be inherently of a closed-loop form rather than of the open-loop form usually supposed to apply. As will subsequently be made clear, the practical importance of the analysis of a FRF measurement system with feedback is quite significant.

Figure 2.1 shows a traditional measurement-system model used to describe the FRF measurement when noise is present on both measured force and response signals. This model has widely been accepted and used to determine the characteristics of conventional FRF estimators, $_1H(\omega)$ and $_2H(\omega)$, which are available in most commercially-available frequency analysers.

Figure 2.1 Measurement-system model
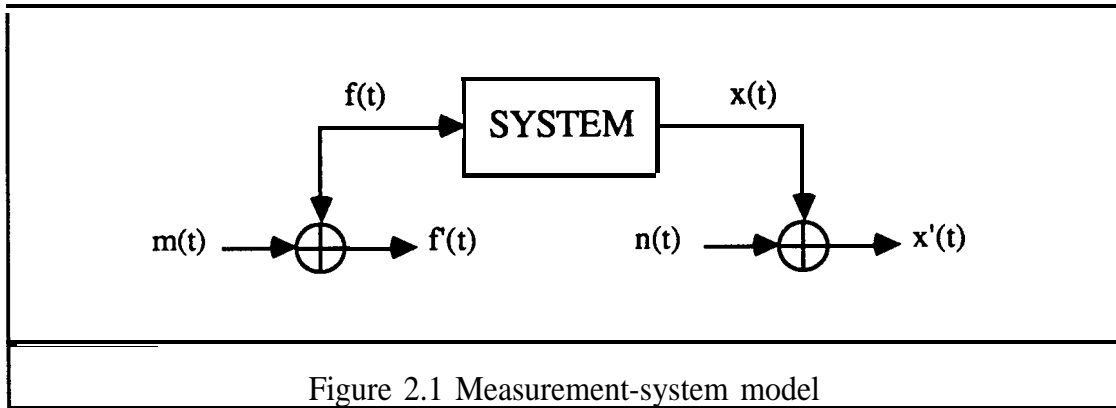
Goyder [18] and Mitchell et al. [17] have pointed out that an estimator can extract the FRF (H(o)) with minimum errors incurred through noise by using the ratio of two complex cross-spectral estimates.   The computation scheme of Figure 2.1 can be extended to include the external input signal r(t), broad-band white noise, generated by a signal source generator as shown in Figure 2.2. This measurement technique was used by Wellstead [ 19,201 for determining transfer functions in control systems with a feedback path, and the estimator was called the "instrumental frequency response function estimator" ($_3H(\omega)$).



$$_3H(\omega) = \frac{S_{rx'}(\omega)}{S_{rf'}(\omega)}$$

Figure 2.2 An open-loop measurement-system model with external reference signal
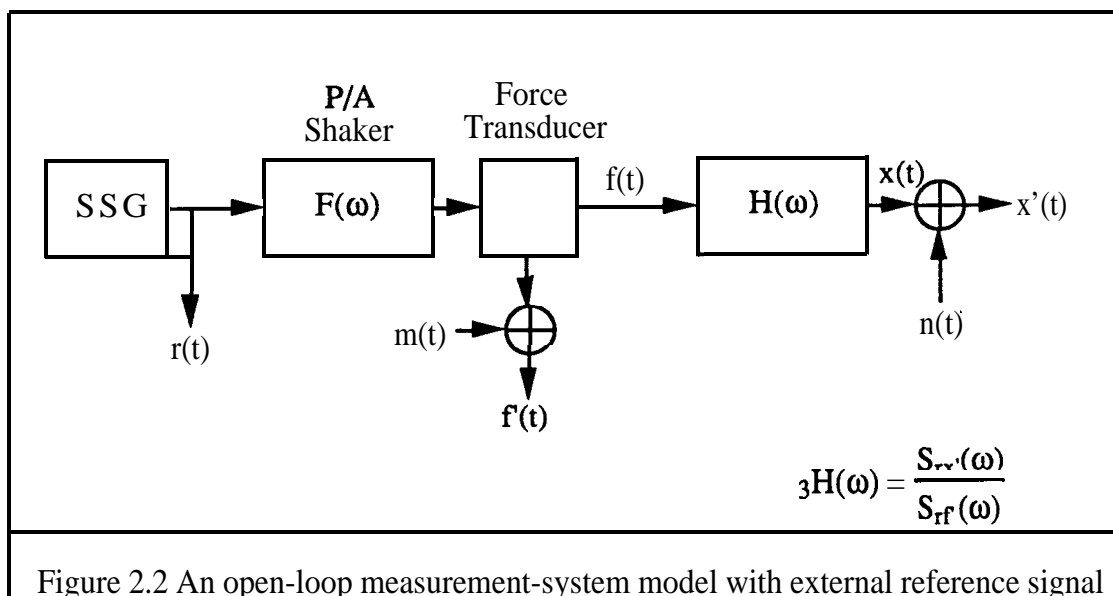
However, the models shown in Figures 2.1 and 2.2 cannot be used to explain what causes the drop-out 'notches' in the input force spectrum at structural resonance frequencies. Since a realistic model is vital in mathematical analysis, an alternative model for the measurement-system is proposed which seeks to reflect the true physical situation of a FRF measurement.

In order to establish a realistic measurement-system model it is necessary to **characterise** in detail the components of the excitation mechanism consisting of a force transducer and an electrodynamic shaker.

A force transducer is the simplest type of piezoelectric transducer and its configuration is illustrated in Figure 2.3. The relative displacement of the upper and lower plates of the cell generates a charge, q, which is proportional to the transmitted force.



Figure 2.3   Piezoelectric force transducer
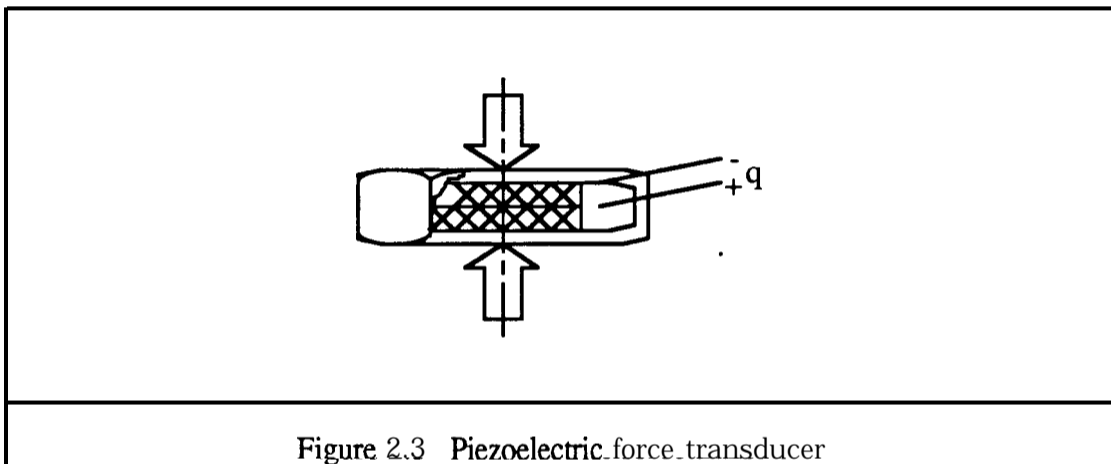
The force transducer is placed between the test structure and an electrodynamic shaker so it can be **modelled** as a spring with stiffness $K_{fg}$.  By considering the electrodynamic shaker to have a suspension stiffness k,, and an armature mass m,, a greatly-simplified diagram of an excitation mechanism with the test structure as used for a point FRF measurement is shown in Figure 2.4.
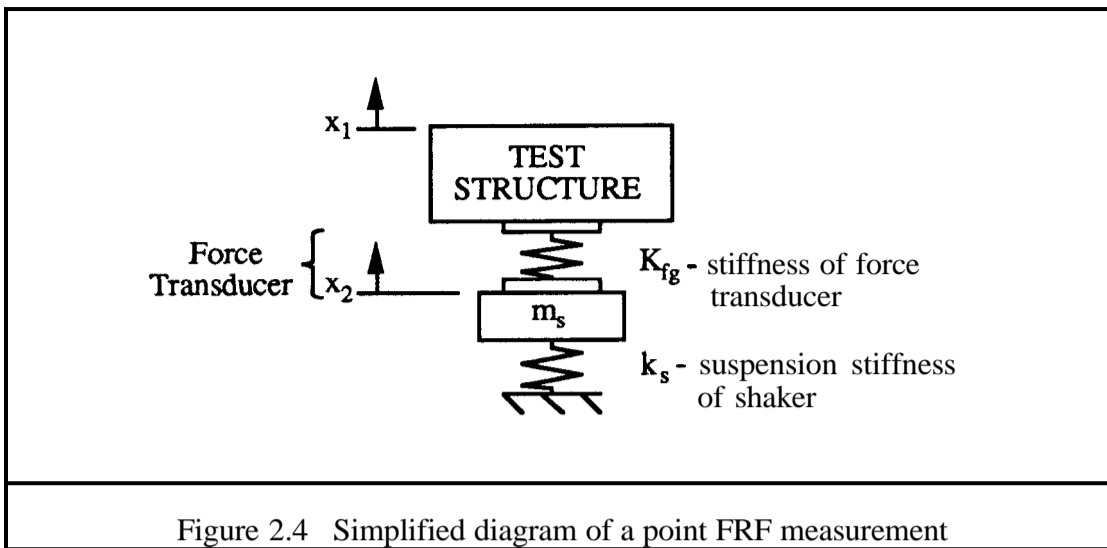
Figure 2.4   Simplified diagram of a point FRF measurement

It can be seen that by transforming the above figure into a block diagram, a closed-loop model is established for a point FRF measurement as shown in Figure 2.5. The signal-source generator (SSG) provides a driving signal r(t), assumed constant, to a power amplifier.  The dynamic response of the power amplifier is assumed to be linear and thus to produce constant driving force p(t) on the armature of the shaker . The measured force f(t) is an internal force across the force transducer with uncorrelated measurement noise, m(t), and the measured acceleration is $x_1'(t)$ which is contaminated by uncorrelated measurement noise, n(t).



where        $H_s(\omega) = \dfrac{1}{k_s - m_s\omega^2}$
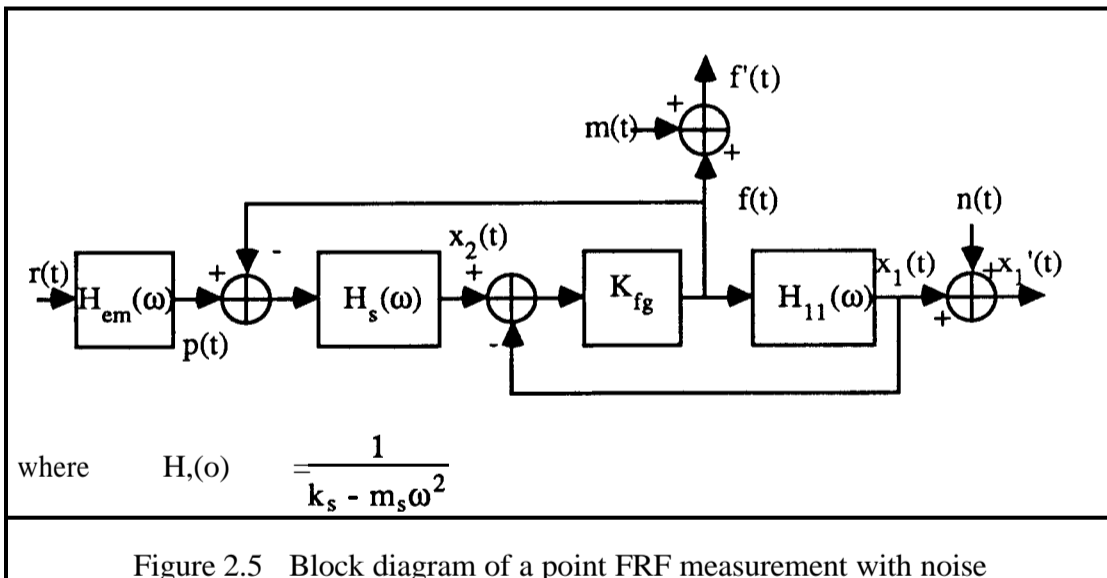
Figure 2.5   Block diagram of a point FRF measurement with noise

The use of a reference test signal r(t) for an estimate of FRF $_3H(\omega)$ has been established for many years in control engineering and the associated basic statistical properties have been described by Wellstead [19,20] for a single feedback control system. However, there are two interrelated feedback paths existing in a point FRF measurement, as shown in Figure 2.5, and the following sections reveal the effect of noise and the bias error due to leakage on FRF estimators.

### 2.3.1 THE EFFECT OF NOISE ON FRF ESTIMATORS

With reference to Figure 2.5, one can simplify the block diagram to produce an equivalent single-input/two-output system as illustrated in Figure 2.6. It is noted that the measured force signal is one of the output signals for a point FRF measurement. Figure 2.6 shows that only the driving signal r(t) generated from the signal-source generator is not influenced by the excitation mechanism and hence is the only input signal for a point FRF measurement. Here one can readily observe that f(t) contains the characteristics of the test structure as well as of the excitation mechanism itself.



where

$$T_1(\omega) = \frac{H_{em}(\omega)H_s(\omega)K_{fg}}{1 + K_{fg}(H_s(\omega)+H_{11}(\omega))}$$

$$T_2(\omega) = \frac{H_{em}(\omega)H_s(\omega)K_{fg}H_{11}(\omega)}{1 + K_{fg}(H_s(\omega)+H_{11}(\omega))}$$

Figure 2.6   An alternative model of a point FRF measurement
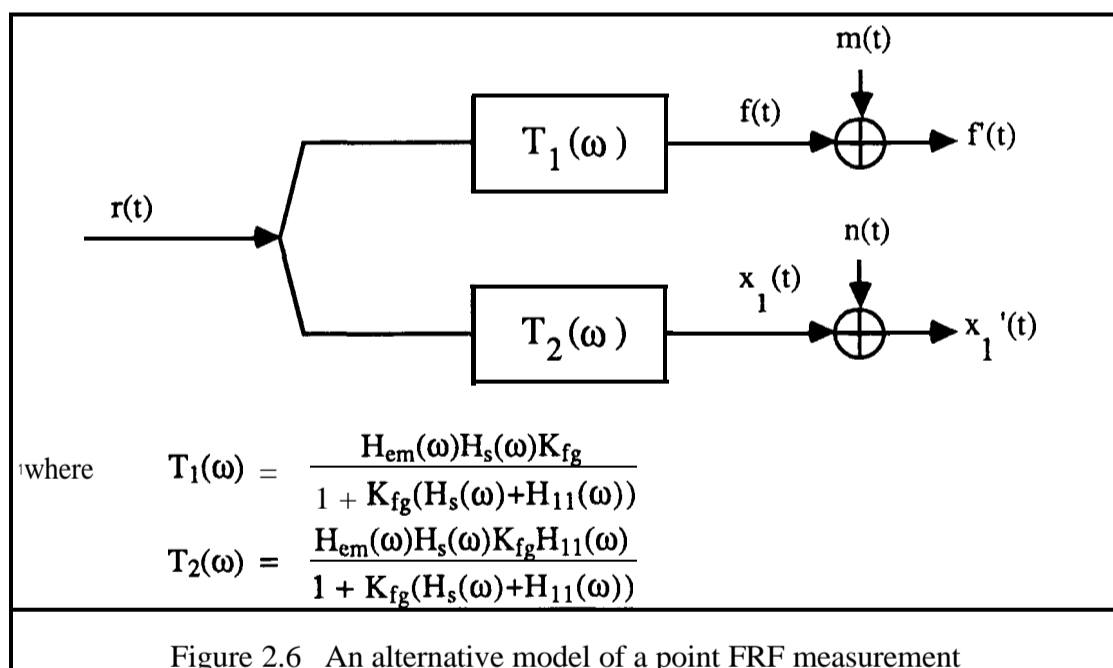
It is reasonable to assume that the noise terms m(t) and n(t) are uncorrelated with each other and with the input r(t), and therefore, the following frequency domain equations apply to this model.

$$S_{rm}(\omega) \quad = \quad S_{fm}(\omega) = S_{rn}(\omega) = S_{x_1n}(\omega) = S_{mn}(\omega) = 0 \qquad (2.1)$$

$$S_{ff}(\omega) \quad = \quad S_{ff}(\omega) + S_{mm}(\omega) \quad = \quad |T_1(\omega)|^2 S_{rr}(co) + S_{mm}(\omega) \qquad (2.2)$$

$$S_{x_1'x_1'}(\omega) \quad = \quad S_{x_1x_1}(\omega) + S_{nn}(\omega) \quad = \quad |T_2(\omega)|^2 S_{rr}(co) + S,(o) \qquad (2.3)$$

$$S_{rf'}(\omega) \quad = \quad S_{rf}(\omega) \quad = \quad T_1(\omega) S_{rr}(\omega) \qquad (2.4)$$

$$S_{rx_1'}(\omega) \quad = \quad S_{rx_1}(\omega) = T_2(\omega) S_{rr}(\omega) \qquad (2.5)$$

$$S_{fx_1'}(\omega) \quad = \quad S_{fx_1}(\omega) = T_1(\omega)^* T_2(\omega) S_{rr}(\omega) \qquad (2.6)$$

The conventional frequency response function estimator of $H_{11}(\omega)$ is described by

$$_1H_{11}(\omega) = \frac{S_{fx_1'}(\omega)}{S_{ff}(\omega)} = \frac{T_1(\omega)^* T_2(\omega) S_{rr}(\omega)}{|T_1(\omega)|^2 S_{rr}(\omega) + S_{mm}(\omega)} = \frac{H_{11}(\omega)}{1 + \dfrac{S_{mm}(\omega)}{S_{ff}(\omega)}} \qquad (2.7)$$

Mitchell [ 15] has shown the same result by using the model given in Figure 2.1 and has pointed out that the input force spectrum drops drastically near resonance, but without mathematical explanation because the model gave no information on the structure-shaker interaction. In contrast, the closed-loop model reveals that the measured force signal contains the characteristics of the test structure as well as of the excitation measurement. The auto-spectrum of the measured force is expressed by :

$$S_{ff}(\omega) = |T_1(\omega)|^2 S_{rr}(\omega) = \left| \frac{H_{em}(\omega) H_s(\omega) K_{fg}}{1 + K_{fg}(H_s(\omega) + H_{11}(\omega))} \right|^2 S_{rr}(\omega) \qquad (2.8)$$

By representing the receptance of the test structure in terms of an effective stiffness ($k$,) and an effective mass ($m$,) at a structural resonance, equation (2.8) can be rewritten as:

$$S_{ff}(\omega)=\left|\frac{H_{em}(k_e-m_e\omega^2+i\eta k_e)}{\frac{1}{K_{fg}}(k_e-m_e\omega^2+i\eta k_e)(k_s-m_s\omega^2)+(k_e-m_e\omega^2+i\eta k_e)+(k_s-m_s\omega^2)}\right|^2 S_{rr}(\omega)$$

$$(2.9)$$

When the excitation frequency ($\omega$) approaches the structural resonance frequency ($\omega_r$), $S_{fx_1}(\omega)$ is noise-free but the noise-to-signal ratio decreases due to the peak response of force spectrum $S_{ff}(\omega)$, if the structural resonance frequency is greater than the combined structure-shaker resonance frequency in equation (2.9). There is a drastic change in the small frequency range around the structure's resonance. The force drops to a minimum so that the noise-to-signal ratio increases from a minimum to a maximum, and when the excitation frequency is increased beyond the structural resonance frequency, the noise-to-signal ratio decreases again.

An alternative frequency response function estimator of $H_{11}(\omega)$ is described by

$$_2H_{11}(\omega) = \frac{S_{x_1'x_1'}(\omega)}{S_{x_1'f}(\omega)} = \frac{|T_2(\omega)|^2 S_{rr}(\omega)+S_{nn}(\omega)}{T_2(\omega)^* T_1(\omega)S_{rr}(\omega)} = H_{11}(1+\frac{S_{nn}(\omega)}{S_{x_1x_1}(\omega)}) \qquad (2.10)$$

One can readily observe that this estimator is contaminated only by the noise-to-signal ratio of the measured response. In the closed-loop model, it can be shown that the auto-spectrum of the measured response is given by

$$S_{x_1x_1}(\omega) = |T_2(\omega)|^2 S_{rr}(\omega) = \left|\frac{H_{em}(\omega)H_s(\omega)K_{fg}H_{11}(\omega)}{1+K_{fg}(H_s(\omega)+H_{11}(\omega))}\right|^2 S_{rr}(\omega) \qquad (2.11)$$

When the excitation frequency approaches a structural anti-resonance frequency, the noise-to-signal ratio increases to a maximum as the response auto-spectrum $S_{x_1 x_1}(\omega)$ becomes a minimum. Equation (2.11) shows a drop in the response auto-spectrum resulting from the nature of $H_{11}(\omega)$ at a structural anti-resonance. When the excitation frequency is increased beyond the structural anti-resonance frequency, the noise-to-signal ratio decreases. At resonance one recalls that $S_{mm}$, the input noise, can become significant. However, $_2H(\omega)$ is insensitive to such effect, and, moreover, the response at resonance is still large compared to $S_{nn}$ thus allowing equation (2.10) to provide a better estimate of $H_{11}(\omega)$ than equation (2.7).

Since $_1H(\omega)$ is a lower bound estimator and $_2H(\omega)$ is an upper bound estimator, one can calculate the average or the geometric mean of $_1H(\omega)$ and $_2H(\omega)$ to obtain another FRF estimate. The expression for the FRF estimator, $_vH(\omega)$, which is the geometric mean of $_1H(\omega)$ and $_2H(\omega)$ and lies between the upper and lower bound of the FRF estimate, is given as :

$$_vH_{11}(\omega) \; = \; \sqrt{_1H_{11}(\omega) \; _2H_{11}(\omega)} \; = \; H_{11}(\omega) \sqrt{(1+\frac{S_{nn}(\omega)}{S_{x_1 x_1}(\omega)})(1+\frac{S_{mm}(\omega)}{S_{ff}(\omega)})^{-1}}$$

$$(2.12)$$

This estimator has taken the contamination in measured force and response auto-spectra into consideration. In the case when the noise-to-signal ratios for measured force and response signals are 'small' and approximately the same, $_vH_{11}(\omega)$ should provide the better picture of the true FRF. However, practical experience and the afore-mentioned analytical analysis show that those noise-to-signal ratios vary with the excitation frequency and their magnitude depends on the structure's properties as well as the excitation mechanism, hence, this FRF estimator is unlikely to provide a meaningful result from a mathematical point of view.

The normal frequency response function estimators of $H_{11}(\omega)$ based upon equations (2.7) and (2.10) are systematically in error when the measured signals f(t) and x'(t) are contaminated by noise, m(t) and n(t).   This difficulty can be avoided by introducing the independent external input signal r(t), as shown in Figure 2.5, where r(t) is a zero-mean random signal. Because r(t) is independent of m(t) and n(t), and is statistically orthogonal to the disturbances m(t) and n(t), the cross-spectra S,(o) and S,(o) are identically zero. Hence, the instrumental frequency response estimator is given by:

$$_3H_{11}(\omega) = \frac{S_{rx_1'}(\omega)}{S_{rf}(\omega)} = \frac{S_{rx_1}(\omega)}{S_{rf}(\omega)} = \frac{T_2(\omega)S_{rr}(\omega)}{T_1(\omega)S_{rr}(\omega)} = H_{11}(\omega)$$

(2.13)

Equations (2.7) and (2.10) show that $_1H(\omega)$ and $_2H(\omega)$ give biassed results in the presence of measurement noise.   On the other hand, the instrumental frequency response function estimator $_3H(\omega)$ does not suffer from this limitation and yields gain and phase estimates which are well-behaved, provided that due attention is paid to the statistical error caused by windowing for a finite amount of data. This is discussed in more detail in Section 2.3.3 below.

### 2.3.1.1    ORDINARY COHERENCE FUNCTION

Figures (2.5) and (2.6) show that the measured force and response signals, f(t) and x'(t), are jointly related, but they do not quantify the degree of correlation.   Such information is provided by the ordinary coherence function $\gamma_{fx_1'}(\omega)^2$ defined by

$$\gamma_{fx_1'}(\omega)^2 = \frac{|S_{fx_1'}(\omega)|^2}{S_{ff}(\omega)\,S_{x_1'x_1'}(\omega)} = \frac{|S_{fx_1'}(\omega)|^2}{S_{ff}(\omega)\,S_{x_1'x_1'}(\omega)} = \gamma_{rf}(\omega)^2\,\gamma_{rx_1'}(\omega)^2$$

(2.14)

which is the result following from the fact that

$$|S_{fx_1'}(\omega)|^2 = |T_1(\omega)^*T_2(\omega)S_{rr}(\omega)|^2 = (|T_1(\omega)|^2 S_{rr}(\omega))(|T_1(\omega)|^2 S_{rr}(\omega))$$

$$= S_{ff}(\omega)S_{x_1x_1}(\omega) \tag{2.15}$$

$$\gamma_{rf}(\omega)^2 = \frac{|S_{rf}(\omega)|^2}{S_{rr}(\omega)S_{ff}(\omega)} = \frac{|T_1(\omega)S_{rr}(\omega)|^2}{S_{rr}(\omega)S_{ff}(\omega)} = \frac{S_{ff}(\omega)}{S_{ff}(\omega)} \tag{2.16}$$

$$\gamma_{rx_1'}(\omega)^2 = \frac{|S_{rx_1'}(\omega)|^2}{S_{rr}(\omega)S_{x_1'x_1'}(\omega)} = \frac{|T_2(\omega)S_{rr}(\omega)|^2}{S_{rr}(\omega)S_{x_1'x_1'}(\omega)} = \frac{S_{x_1x_1}(\omega)}{S_{x_1'x_1'}(\omega)} \tag{2.17}$$

One can visualise the ordinary coherence function as being a normalised coefficient of correlation between the measured force and response signals evaluated at each frequency. In practice, the ordinary coherence function is always greater than zero but less than unity. When the ordinary coherence function is less than unity, one or more of the following four main conditions exist.

1.  Extraneous noise is present in the FRF measurements.

2.  Resolution bias errors are present in the spectral estimates.

3.  The system relating f(t) and x'(t) is not linear.

4.  The measured response x'(t) is due to other external inputs besides r(t).

The ordinary coherence function shown in equation (2.14) can be rewritten as:

$$\gamma_{fx_1'}(\omega)^2 = \frac{|S_{fx_1'}(\omega)|^2}{S_{ff}(\omega)S_{x_1'x_1'}(\omega)} = \frac{_1H(\omega)}{_2H(\omega)} \tag{2.18}$$

This formulation can be used to determine the $_2H(\omega)$ estimate from the $_1H(\omega)$ estimate in the spectrum analyzer. Hence if the coherence is unity, the three estimates, $_1H(\omega)$, $_2H(\omega)$ and $_vH(\omega)$, for calculating the frequency response function are identical.

2.3.2        VARIANCE ERROR ON FRF ESTIMATORS

When analysing the measured force and response signals for random excitation, it is not sufficient to compute Fourier Transforms because the signals are not deterministic in nature. Additional consideration must be drawn to the statistical reliability and accuracy of FRF estimates. Generally, it is necessary to perform an averaging of several individual time records, or samples, to reduce the random fluctuation in the estimation of **FRFs.**

These time records are normally independent, so that if *m* time records are averaged, the variability of the estimates will decrease inversely with *m* and will depend on the degree to which f(t) and x(t) are correlated. The variability of the magnitude and phase of the $_1H(\omega)$ estimate is given approximately by

$$\frac{var[|_1\hat{H}_{11}(\omega)|]}{|H_{11}(\omega)|^2} = var[arg_1\hat{H}_{11}(\omega)] = \frac{1}{2m}(\frac{1}{\gamma_{fx_1}{'}(\omega)^2} -1) \qquad (2.19)$$

where the circumflex indicates an estimated quantity.

The variability of the instrumental FRF estimator can, to a first approximation, be assessed by taking a Taylor series expansion about the expected values of $\hat{H}_{11}(\omega)$. In this manner it can be shown that :

around resonance;

$$\frac{var[|_3\hat{H}_{11}(\omega)|]}{|H_{11}(\omega)|^2} = var[arg_3\hat{H}_{11}(\omega)] \approx \frac{1}{2m}(\frac{S_{mm}(\omega)}{S_{rr}(\omega)|T_1(\omega)|}) \qquad (2.20)$$

and around anti-resonance :

$$\frac{var[|_3\hat{H}_{11}(\omega)|]}{|H_{11}(\omega)|^2} = var[arg_3\hat{H}_{11}(\omega)] \approx \frac{1}{2m}(\frac{S_{nn}(\omega)}{S_{rr}(\omega)|T_2(\omega)|}) \qquad (2.21)$$

Here, the functions $T_1(\omega)$ and $T_2(\omega)$ are the equivalent closed-loop transfer functions used in Figure (2.6). The desirable feature of the $_3H(\omega)$ estimate is that the variance of its magnitude and phase is inversely proportional to the number of averages($m$) and the spectral power associated with r(t).

### 2.3.3     BIAS ERROR DUE TO THE EFFECT OF LEAKAGE ON FRF ESTIMATORS

As mentioned in the preceding section, noise is not the only source of error in FRF measurement. The frequency resolution obtained from an **FFT-based** spectrum analyzer is 1/T Hz, where T is the record length employed. The process is not equivalent to a frequency sweep using sinusoidal excitation where readings are taken at discrete frequencies.   The spectral components obtained from an FFT-based analyzer are average values across the band of the **FFT** "filter". Therefore, maxima (resonances) in the FRF tend to be underestimated while minima (anti-resonances) tend to be overestimated. This inaccuracy is a bias error and is known as 'leakage'.

A model for the measurement of a noise-free point FRF measurement is presented in Figure 2.7 in which a single-degree-of-freedom (**SDoF**) system comprising a mass (m), spring (k), with hysteretic loss factor ($\eta$), and its natural frequency ($\omega_r$) is excited with a force generated by a reference random signal of constant spectral power, R(o).

where $H_{11}(\omega) = \dfrac{1}{k(1+i\eta) - m\omega^2}$

Figure 2.7. A noise-free point FRF measurement
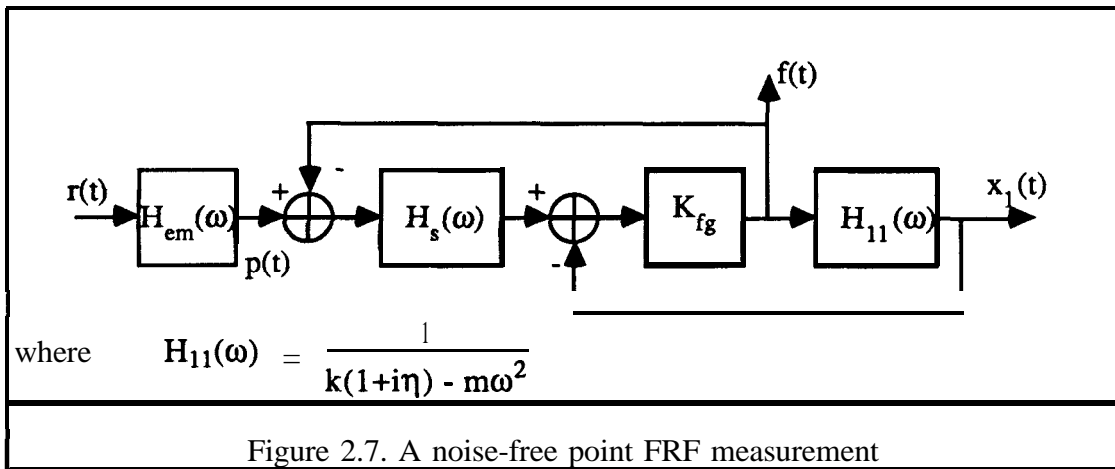
The relationship between the displacement signal and the input signal produced by the random signal generator is shown as follows :

$$\frac{X_1(\omega)}{R(\omega)} = \frac{H_{em}(\omega)H_s(\omega)H_{11}(\omega)K_{fg}}{1+K_{fg}(H_s(\omega)+H_{11}(\omega))} \tag{2.22}$$

The relationship between the force signal and the input signal is :

$$\frac{F(\omega)}{R(\omega)} = \frac{H_{em}(\omega)H_s(\omega)H_{11}(\omega)}{1+K_{fg}(H_s(\omega)+H_{11}(\omega))} \tag{2.23}$$

For a SDoF system employing the symbols used in Figure 2.4, equations (2.22) and (2.23) can be rewritten as:

$$\frac{X_1(\omega)}{R(\omega)} = \frac{H_{em}(\omega)}{\frac{1}{K_{fg}}(k-m\omega^2+i\eta k)(k_s-m_s\omega^2)+(k-m\omega^2+i\eta k)+(k_s-m_s\omega^2)} \tag{2.24}$$

$$\frac{F(\omega)}{R(\omega)} = \frac{H_{em}(\omega)\, m(\omega_r^2-\omega^2+i\eta\omega_r^2)}{\frac{1}{K_{fg}}(k-m\omega^2+i\eta k)(k_s-m_s\omega^2)+(k-m\omega^2+i\eta k)+(k_s-m_s\omega^2)} \tag{2.25}$$

As the stiffness of the force transducer approaches infinity, the following approximate expression is derived :

$$\frac{F(\omega)}{R(\omega)} \approx \frac{H_{em}(\omega)\, m(\omega_r^2 - \omega^2 + i\eta\omega_r^2)}{m\left[(\omega_r^2 - \omega^2 + i\eta\omega_r^2) + (\frac{k_s}{m} - \frac{m_s}{m}\omega^2)\right]} \qquad (2.26)$$

This last expression is similar to the equation derived by Cawley [21].

The estimates of the spectra produced by an **FFT-based** analysis are derived as follows:

$$S_{x_1 x_1}(\omega) = \int_{-\infty}^{\infty} \frac{|H_{em}(\Omega)|^2}{|G(\Omega)|^2} R_o W(\Omega - \omega) d\Omega \qquad (2.27)$$

$$S_{x_1 f}(\omega) = \int_{-\infty}^{\infty} \frac{|H_{em}(\Omega)|^2}{|G(\Omega)|^2} (k - m\Omega^2 + i\eta k) R_o W(\Omega - \omega) d\Omega \qquad (2.28)$$

where W is a function of the window,eg. Boxcar or Hanning and

$$G(\Omega) = \frac{1}{K_{fg}}(k - m\Omega^2 + i\eta k)(k_s - m_s\Omega^2) + (k - m\Omega^2 + i\eta k) + (k_s - m_s\Omega^2) \qquad (2.29)$$

Substituting the estimates of the auto- and cross-spectra shown in equations (2.27) and (2.28) into equation (2.10), the expression of $_2H(\omega)$ for a point FRF measurement is derived,

$$_2H_{11}(\omega) = \frac{S_{x_1 x_1}(\omega)}{S_{x_1 f}(\omega)} = \frac{\displaystyle\int_{-\infty}^{\infty} \frac{|H_{em}(\Omega)|^2}{|G(\Omega)|^2} R_o W(\Omega - \omega)\, d\Omega}{\displaystyle\int_{-\infty}^{\infty} \frac{|H_{em}(\Omega)|^2}{|G(\Omega)|^2} (k - m\Omega^2 + i\eta k) R_o W(\Omega - \omega)\, d\Omega} \qquad (2.30)$$

Setting $\quad A \quad = \int\limits_{-\infty}^{\infty} \frac{|H_{em}(\Omega)|^2}{|G(\Omega)|^2} R_o W(\Omega-\omega) d\Omega$ (2.3 1)

$\quad\quad B \ = \int\limits_{-\infty}^{\infty} \frac{|H_{em}(\Omega)|^2 (\Omega)^2}{|G(\Omega)|^2} R_o W(\Omega\ \omega) d\Omega$ (2.32)

**gives**

$$_2H_{11}(\omega) \ = \ \frac{A}{m(A\omega_r^2 - B + iA\eta\omega_r^2)} \ = \ \frac{1}{m(\omega_r^2 - \frac{B}{A} + i\eta\omega_r^2)}$$ (2.33)

While the true frequency response function is given by

$$H_{11}(\omega) \ = \ \frac{1}{m(\omega_r^2 - \omega^2 + i\eta\,\omega_r^2)}$$ (2.34)

Comparison of equations (2.33) and (2.34) reveals that the expressions for the FRF estimate, $_2H_{11}(\omega)$, and the true value, $H_{11}(\omega)$, are of the same form and are identical if $B/A = \omega_r^2$. This condition is only satisfied at a very high frequency resolution. In general, the estimate $_2H_{11}(\omega)$ lies on the true modal circle but at different positions around the circle.

By using a similar analysis, one can derive the FRF estimate $_1H_{11}(\omega)$ based on the cross-spectrum and the measured force auto-spectrum which are defined as follows:

$$S_{fx_1}(\omega) \ = \ \int\limits_{-\infty}^{\infty} \frac{|H_{em}(\Omega)|^2}{|G(\Omega)|^2} (k - m\Omega^2 - i\eta k) R_o W(\Omega-\omega) d\Omega$$ (2.35)

$$S_{ff}(\omega) \quad = \ \int\limits_{-\infty}^{\infty} \frac{|H_{em}(\Omega)|^2}{|G(\Omega)|^2} [(k - m\Omega^2)^2 + (\eta k)^2] R_o W(\Omega-\omega) d\Omega$$ (2.36)

Using the estimates of the cross- and auto-spectra derived in equations (2.35) and (2.36), the estimate of $_1H_{11}(\omega)$ is expressed by :

$$_1H_{11}(\omega) = \frac{S_{fx_1}(\omega)}{S_{ff}(\omega)} = \frac{\displaystyle\int_{-\infty}^{\infty} \frac{|H_{em}(\Omega)|^2}{|G(\Omega)|^2}(k-m\Omega^2-i\eta k)R_oW(\Omega-\omega)d\Omega}{\displaystyle\int_{-\infty}^{\infty} \frac{|H_{em}(\Omega)|^2}{|G(\Omega)|^2}[(k-m\Omega^2)^2+(\eta k)^2]R_oW(\Omega-\omega)d\Omega} \qquad (2.37)$$

now setting

$$C = \int_{-\infty}^{\infty} \frac{|H_{em}(\Omega)|^2}{|G(\Omega)|^2}\Omega^4 R_oW(\Omega-\omega)d\Omega \qquad (2.38)$$

gives

$$_1H_{11}(\omega) = \frac{A\omega_r^2-B-iA\eta\omega_r^2}{m(A\omega_r^4-2B\omega_r^2+C+A\eta^2\omega_r^4)}$$

$$= \frac{\omega_r^4-2\frac{B}{A}\omega_r^2+(\frac{B}{A})^2+\eta^2\omega_r^4}{\omega_r^4-2\frac{B}{A}\omega_r^2+\frac{C}{A}+\eta^2\omega_r^4}\,_2H_{11}(\omega) \qquad (2.39)$$

Hence, the estimates of $_1H_{11}(\omega)$ have the same phase as those of $_2H_{11}(\omega)$ but in general the magnitudes are smaller and, as a result, the estimate $_1H_{11}(\omega)$ always lies inside the true model circle.  If the frequency resolution is increased, so reducing the leakage error, $_1H_{11}(\omega)$ tends towards $_2H_{11}(\omega)$ which tends to the true FRF and all three FRF estimates $(_1H_{11}(\omega), _2H_{11}(\omega)$ and $_vH_{11}(\omega))$ give the correct magnitude and phase of the frequency response data.

The formulation of the instrumental FRF estimator, $_3H_{11}(\omega)$, is different and requires the derivation of the estimates of two cross-spectra shown as follows :

$$S_{rx_1}(\omega) = \int^{\infty} \frac{H_{em}(\Omega)}{G(\Omega)} R_o W(\Omega-\omega)d\Omega \qquad (2.40)$$

$$S_{rf}(\omega) = \int_{-\infty}^{\infty} \frac{H_{em}(\Omega)}{G(\Omega)} (k-m\Omega^2+i\eta k)R_o W(\Omega-\omega)d\Omega \qquad (2.41)$$

Using these estimates of the cross-spectra, the estimate of $_3H_{11}(\omega)$ is expressed by :

$$_3H_{11}(\omega) = \frac{S_{rx_1}(\omega)}{S_{rf}(\omega)} = \frac{\int_{-\infty}^{\infty} \frac{H_{em}(\Omega)}{|G(\Omega)|^2} G^*(\Omega)R_o W(\Omega-\omega)d\Omega}{\int_{-\infty}^{\infty} \frac{H_{em}(\Omega)}{|G(\Omega)|^2} G^*(\Omega)(k-m\Omega^2+i\eta k)R_o W(\Omega-\omega)d\Omega} \qquad (2.42)$$

where $G^*(Q)$ is the complex conjugate of $G(R)$

It is very difficult to express this complicated equation in terms of functions of $\Omega$. No simple or enlightening relation between $_3H_{11}(\omega)$ and the true $H_{11}(\omega)$ exists, and so computer simulation is employed to explore the bias error of the $_3H_{11}(\omega)$ FRF estimator.

Two special cases are considered to illustrate the relationships between $_3H_{11}(\omega)$ and $_2H_{11}(\omega)$ and between $_3H_{11}(\omega)$ and $_1H_{11}(\omega)$. First, it is important to assume that the relationship between the generator signal r(t) and the force applied to the armature of the shaker p(t) is simple and linear so that the transfer function $H_{em}(\omega)$ is constant.

(i) When the stiffness of the force transducer $(K_{fg})$ and the suspension stiffness of the electrodynamic shaker (k,) are much greater than that of the SDoF system, (k), the following approximations can be made :

$$S_{rx_1}(\omega) \approx \int_{-\infty}^{\infty} \frac{H_{em}}{|G(\Omega)|^2} R_o W(\Omega-\omega) d\Omega \tag{2.43}$$

$$S_{rf}(\omega) \approx \int_{-\infty}^{\infty} \frac{H_{em}}{|G(\Omega)|^2} (k-m\Omega^2+i\eta k) R_o W(\Omega-\omega) d\Omega \tag{2.44}$$

Hence in this case, $_3H_{11}(\omega)$ is approximately equal to $_2H_{11}(\omega)$.

(ii)    When the stiffness of the force gauge ($K_{fg}$) is finite, and the mass (m,) and suspension stiffness ($k_s$) of the armature for the electrodynamic shaker are very small,

$$S_{rx_1}(\omega) \approx \int_{-\infty}^{\infty} \frac{H_{em}}{|G(\Omega)|^2} (k-m\Omega^2+i\eta k) R_o W(\Omega-\omega) d\Omega \tag{2.45}$$

$$S_{rf}(\omega) \approx \int_{-\infty}^{\infty} \frac{H}{|G(\Omega)|^2} [(k-m\Omega^2)^2+(\eta k)^2] R_o W(\Omega-\omega) d\Omega \tag{2.46}$$

Here $_3H_{11}(\omega)$ is approximately equal to $_1H_{11}(\omega)$.

Jenkins and Watts [22] have shown that the effect of windowing upon a frequency response function estimator is to introduce a phase-dependent bias error. One can follow the procedure provided in [22] and use the Taylor series expansion about the expected value of $|_3\hat{H}_{11}(\omega)|$ to obtain the approximate expressions shown below :

$$\text{Bias } [|_3\hat{H}_{11}(\omega)|] = E[|_3\hat{H}_{11}(\omega)|-|H_{11}(\omega)| ]$$
$$\approx \frac{C}{T^2} \{\ddot{M}(\omega) + 2\frac{\dot{M}(\omega)\dot{L}(\omega)}{L(\omega)} - M(\omega)[\dot{\phi}(\omega)]^2 - \dot{\phi}(\omega)\dot{\Gamma}(\omega) \} \tag{2.47}$$

$$\text{Bias } [\text{arg}_3\hat{H}_{11}(\omega)] = E[\text{arg}_3\hat{H}_{11}(\omega) - \text{arg}H_{11}(\omega)]$$
$$\approx \frac{C}{T^2} \{\ddot{\phi}(\omega) + 2\frac{\dot{M}(\omega)}{M(\omega)}[2\dot{\phi}(\omega) - \dot{\Gamma}(\omega)] + \frac{\dot{L}(\omega)}{L(\omega)}\dot{\phi}(\omega)\} \tag{2.48}$$

where the dash notation denotes derivatives with respect to angular frequency and

$T$ = the sample duration

$M(\omega) = |H_{11}(\omega)|$

$\phi(\omega) = \arg H_{11}(\omega)$

$\Gamma(\omega) = \arg S_{rx_1}(\omega) + \arg S_{rf}(\omega)$

$C$ = a constant dependent upon the time-window shape

It is noted that the gain estimate has a bias term which is proportional to the square of the rate of change of $\arg H_{11}(\omega)$ with frequency. This implies that the bias error will become significant in a small range around a structural resonance.

### 2.3.3.1 COMPUTER SIMULATION RESULTS

Generally speaking, the external reference signal generated by the signal source generator, r(t), is uniform over a wide frequency range. When the electro-mechanical response of the shaker armature is simple and linear a constant force, p(t), is generated and applied to the armature of the shaker. Therefore the maximum response occurs at the resonance frequency of the combined shaker-structure system while at the resonance frequency of the structure itself the force input to the structure is reduced considerably since most of the available force is used to accelerate the armature of the shaker.

Consider a single-degree-of-freedom system with mass m, and stiffness k, and hysteretic loss factor $\eta$, excited through a force gauge with stiffness $K_{fg}$ and a shaker with effective mass m,, and effective suspension stiffness k,. The predicted variations of the FRF estimators for different armature suspension stiffness of the shaker are shown in Figure 2.8. It should be noted that the value of $H_{em}(\omega)$ is unity so that the external input signal has a uniform frequency spectrum R,. The integration of

equations (2.30), (2.37) and (2.42) was carried out numerically in which the bandwidth of true spectra was limited. A Hanning window was chosen in all cases.

The three curves in Figure 2.8 show how the estimates $_1H(\omega)$, $_2H(\omega)$ and $_3H(\omega)$ vary as the ratio of the armature suspension stiffness for the shaker to the stiffness of SDoF system varies. When this stiffness ratio was small, $_3H(\omega)$ was close to $_1H(\omega)$. When the ratio was large, $_3H(\omega)$ was close to $_2H(\omega)$. These results confirmed the predictions given in the preceding section. The FRF data were then analysed by using a SDoF curve-fitting algorithm [8] and the bias errors for the resulting modal properties of the SDoF system are shown in Figures 2.9(a)-(d).

Figure 2.9(a) shows a graph of the bias error on natural frequency estimate against the stiffness ratio. The natural frequency of the SDoF system is overestimated when the stiffness ratio is below 0.1% for $_1H(\omega)$, 0.1% for $_2H(\omega)$ and 1% for $_3H(\omega)$ FRF estimates, respectively. The natural frequency is underestimated when the stiffness ratio increases. All estimates of natural frequency approach the correct analytical solution when the stiffness ratio is equal to or greater than 10. Figure 2.9(b) shows a graph of the radius of the modal circle against the stiffness ratio from which it can be seen that only $_2H(\omega)$ always lies on the true modal circle. Both the curves $_1H(\omega)$ and $_3H(\omega)$ lie inside the true modal circle in most cases. Figure 2.9(c) shows a graph of the bias error on the damping loss factor against the stiffness ratio. The damping loss factor is overestimated for all $_1H(\omega)$ FRF estimates. When the stiffness ratio is equal to or greater than 10, the $_2H(\omega)$ and $_3H(\omega)$ FRF estimates give accurate results for the identified damping loss factor. The bias error on the modal constant against the stiffness ratio is shown in Figure 2.9(d) from which it can be seen that those estimates produce accurate results when the stiffness ratio is equal to or larger than 10.

Figure 2.8   Predicted variations of the FRF estimators for different armature suspension stiffnesses of the shaker $(M_s = 1\%)$



Figure 2.9(a)-(d)   The effect of the armature suspension stiffness of the shaker on the estimations of the modal properties (M, = 1 %)

**RCEPTANCE (Ms = 10%)**

SDOF system
k = 100000 N/m
m = 9.895 kg
$\alpha_n$ = 100.59 rad/s = 16 Hz
$\eta$ IO.05
Hanning window
A f = 3 rad/s

Figure 2.10   Predicted variations of the FRF estimators for different armature
suspension stiffnesses of the shaker (M, = 10 %)



Figure 2.11 (a)-(d)   The effect of the armature suspension stiffness of the shaker on
the estimations of the modal properties (M, = 10 %)

Figures 2.10 and 2.11 (a)-(d) show the computational and analytical results of different
**FRF** estimators when the mass of the armature for the shaker increased from 1 percent
to 10 percent of the effective mass of the **SDoF** system. The trends of identified
modal properties shown in Figures 2.1 l(a)-(d) are similar to the ones mentioned
earlier.

## Analogue Computer Tests

**The** predictions of the previous section have been checked using an analogue computer
and a Solartron 1202 analyzer. The analogue computer was set up as a **SDoF** system
with a natural frequency of about 16 Hz and a Q factor of 20 $(\eta \approx .05)$. The properties
of the excitation mechanism were varied and a uniform power spectrum was applied to
the armature of the shaker (m,). The frequency resolution was adjusted to 1.25 Hz
and a Hanning window was used in all the measurements.

The results of this simulation are shown in Figures 2.12 and 2.13. Good agreement is
indicated between these results and the analytical results being calculated numerically.



Figure 2.12   Analogue computer simulation results (M, = 1 %)

**RECEPTANCE (Ms=10%) EAL380**
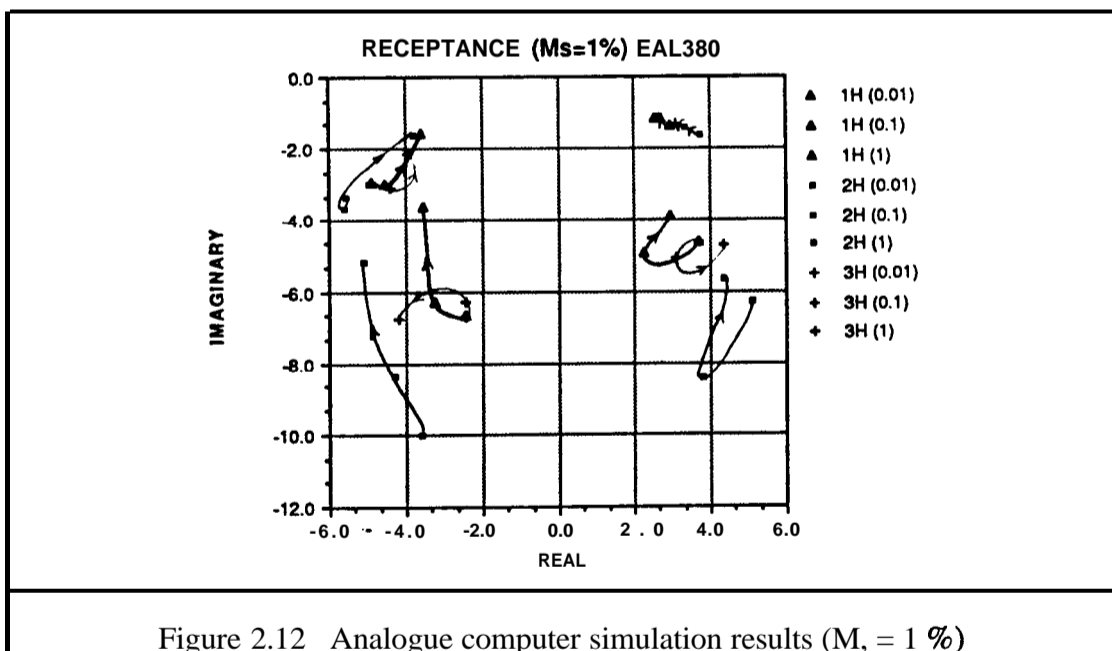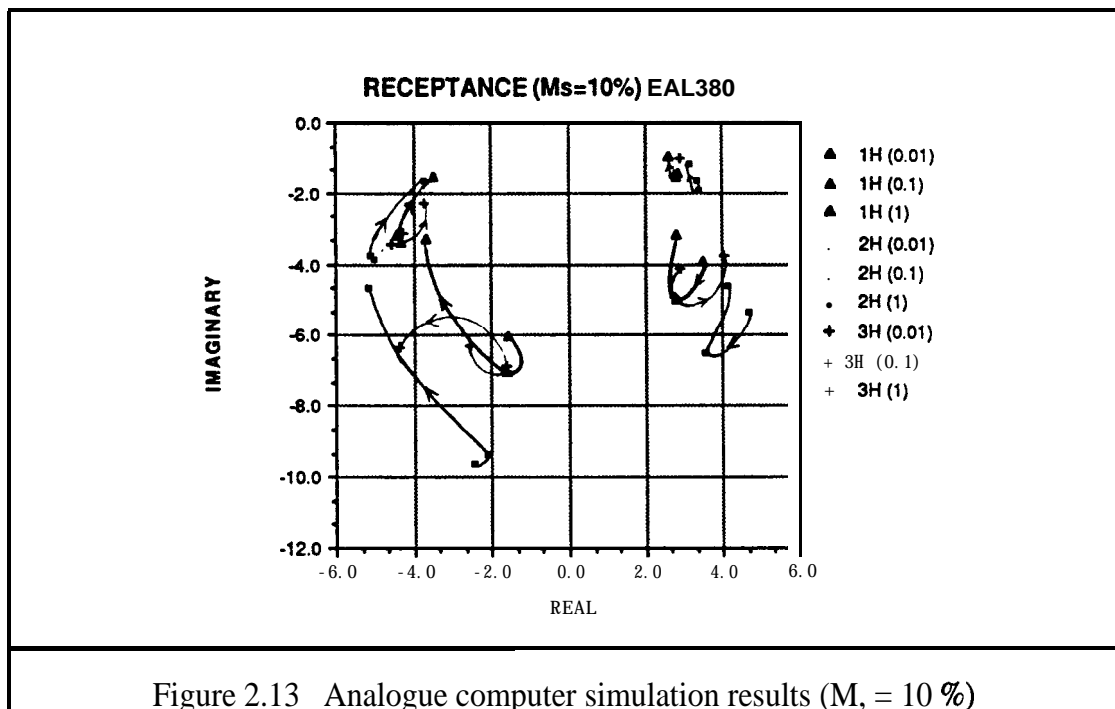


Figure 2.13   Analogue computer simulation results (M, = 10 %)

## 2.4 CONCLUDING REMARKS

In this chapter, a closed-loop model for a single-shaker FRF measurement scheme with the potential of uncorrelated measurement noise is developed. This model explains the variation in the input force spectrum near structural resonances . It also reveals the relationships between the measured force and acceleration signals to the properties of a test structure and the excitation mechanism.

In Section 2.3 it is proved that even if a specified amount of uncorrelated noise exists in the measured force and acceleration, the overall percentage of the noise-to-signal ratio for $_1H(\omega)$ and $_2H(\omega)$ FRF estimators is no longer a constant because of the frequency-dependent characteristics of the auto-spectra. Therefore, the reliability of both conventional FRF estimators is greatly influenced by measurement noise, especially in the vicinity of structural resonances and anti-resonances. In contrast, the

instrumental FRF estimator $_3H(\omega)$ is a noise-free estimator whose variance is directly reduced by increasing the number of averages. Nevertheless, the instrumental FRF estimator $_3H(\omega)$ has a phase-dependent bias error due to leakage (windowing effect). Bias errors for the different FRF estimators have been studied analytically and numerically. The computer-simulation results show that the only estimate which will lie on the true modal circle is $_2H(\omega)$. When the ratio of the armature suspension stiffness for the shaker to the effective stiffness of the structure is large, both $_2H(\omega)$ and $_3H(\omega)$ FRF estimators give very accurate results for the modal properties using a SDoF circle-fitting technique.

Unlike $_1H(\omega)$ and $_2H(\omega)$, $_3H(\omega)$ requires another channel of data acquisition, and thus requires more expensive equipment. It should also be noted that the damping of the structure will affect the time delays between the reference source signal and measured force signal, and any large time delays in F(o) will cause rapidly changing phase characteristics in $S_{rf}(\omega)$ and $S_{rx_1}{}'(\omega)$ and thus increases bias in the gain estimates.

# 3 A CLOSED-LOOP MODEL FOR MULTI-SHAKER MODAL TESTING

## 3.1 INTRODUCTION

The preceding chapter was devoted to a proper understanding and description of the effect of feedback paths on currently-used FRF estimators for single-shaker modal testing. In some cases, a single shaker is unable to accomplish the requirements of a particular test, such as a need for application of large forces and linearization of non-linear structures. In such situations, one solution to these problems is to use two or more shakers acting together. There are various forms of excitation signal for multi-shaker modal testing amongst which the sine-dwell and random excitations are the most common forms employed by modal test practitioners.

For a multi-shaker sine dwell test, the phase difference of the input signals applied to electrodynamic shakers is controlled in order to maintain the orthogonality property of shaker-applied forces. However, test experience indicates that interaction between the test structure and the shakers introduces phase distortions between the shaker-applied forces even though the input signals to the shakers are well controlled. This problem was reported to be overcome by introducing a time delay for one shaker force signal relative to the others, thereby adjusting for any phase distortions [23]. However, this task is time-consuming and requires considerable operator input. For multi-shaker random excitation tests, uncorrelated signals are introduced to the shakers but the correlation of the shaker-applied forces (by the structure itself) not only varies from

shaker to shaker, but also as a function of frequency at each shaker. This makes it considerably more difficult (than for sinusoidal excitation) to maintain the required incoherence of the shaker-applied forces.

## 3.2 MOTIVATIONS FOR MULTI-SHAKER MODEL TESTING

In the aerospace industry, a large complicated flexible structure is normally assembled from a number of components through numerous joints and inherently has a significant amount of damping. During single-point excitation testing of this structure, there may exist large differences in the response amplitudes at various locations because of the dissipation of the excitation energy within the structure. When such a situation occurs, the use of multi-shaker modal testing may be preferable to a series of single-point tests as two or more shakers acting together are able to provide a better energy distribution in a test structure, resulting in a more consistent estimation of resonance frequencies, mode shapes and damping loss factors.

Another advantage of multi-shaker modal testing is the ability to excite all modes in a frequency range of interest. This is in contrast to single-shaker modal testing where (i) some modes cannot be observed if the force is applied to a location close to the node point for some particular modes, and (ii) inconsistencies may occur in the measured **FRFs** as the set of force and response transducers are moved to all the required locations on the structure.

Another deficiency of single-point excitation is that, in an effort to excite remote regions in a large structure, the single point forcing level is sometimes increased to excessive levels, thereby inducing non-linear behaviour, especially in the region of the excitation point. With multiple-input excitation, the response amplitudes across the

structure will be more uniform, with a consequent decrease in the effect of non-linearities.

## 3.3 CLASSICAL MULTI-INPUT MULTI-OUTPUT SYSTEM IDENTIFICATION THEORY

For multi-shaker modal testing, the theoretical basis of existing FRF analysis is well documented in a number of publications [24-26]. The existing theories have been developed based on the general case of *n* inputs and *m* outputs measured during a modal test as shown in Figure 2.1 from which an open-loop multi-input multi-output (MIMO) system is identified.



Figure 3.1   Traditional multi-input multi-output (FRF Measurement) Model
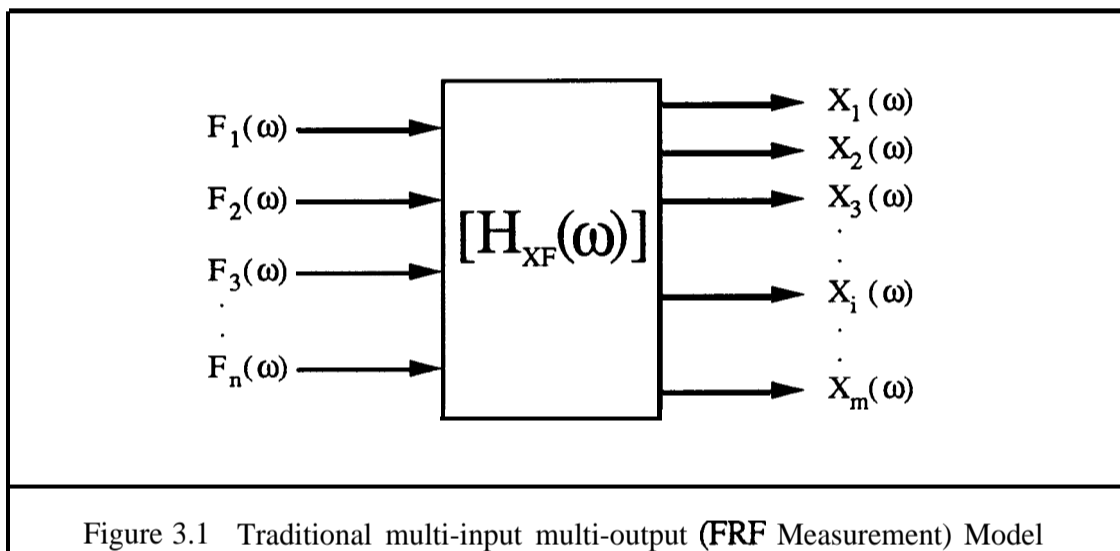
By considering the test structure to be a linear and time-invariant system, a measured output (response) signal X'(o) which is contaminated by an output noise is expressed as :

$$X_i'(\omega) \;=\; \sum_{j=1}^{n} H_{ij}(\omega)\, F_j(\omega) + N_i(\omega) \tag{3.1}$$

Using matrix notation, the measured output vector of a MIMO system is written as :

$$\{X'(\omega)\} = [H_{XF}(\omega)] \{F(\omega)\} + \{N(\omega)\} \tag{3.2}$$

The complex conjugate of (X'(0)) is :

$$\{X'(\omega)\}^* = [H_{XF}(\omega)]^* \{F(\omega)\}^* + \{N(\omega)\}^* \tag{3.3}$$

Post-multiplying both sides of equation (3.3) by $\{F(\omega)\}^T$ and taking expected values give the following matrix equation in terms of output/input and input cross-spectrum matrices as the measured output noise vector and input vector are not correlated.

$$[S_{X'F}(\omega)] = [H_{XF}(\omega)]^* [S_{FF}(\omega)] \tag{3.4}$$

As a result, the least-squares estimate of the FRF matrix can be computed by :

$$[H_{XF}(\omega)] = [S_{FX'}(\omega)] [S_{FF}(\omega)]^{-1} \tag{3.5}$$

Although most of the literature considers the effect of noise in measured output signals only, in practice, both the measured input and measured output signals are contaminated by uncorrelated random noise. The measured input (force) vector can be considered as a summation of the input vector (F(o)) and a measurement noise vector {M(o)) as :

$$\{F'(\omega)\} = \{F(\omega)\} + \{M(\omega)\} \tag{3.6}$$

Substituting equation (3.6) into equation (3.3) gives

$$\{X'(\omega)\}^* = [H_{XF}(\omega)]^* (\{F'(\omega)\} - \{M(\omega)\})^* + \{N(\omega)\}^* \tag{3.7}$$

Post-multiply both sides of equation (3.6) by (F'(o)) and take expected values to obtain

$$[S_{X'F}(\omega)] = [H_{XF}(\omega)]^* [ [S_{FF}(\omega)] - [S_{MM}(\omega)] ] \tag{3.8}$$

where $[S_{MM}(\omega)]$ is a diagonal matrix whose elements represent noise auto-spectra at each transducer. Since it is not feasible to separate the input noise auto-spectrum matrix from the measured input (force) cross-spectrum, the estimate of FRF matrix is written as:

$$[_1H_{XF}(\omega)] = [S_{FX'}(\omega)] [S_{FF}(\omega)]^{-1} \tag{3.9}$$

It is noted that the measured input cross-spectrum matrix must be inverted at every frequency in the frequency range of interest. Equation (3.9) is valid when all the measured input signals are not fully correlated. However, practical experience shows that there are a number of situations where the input cross-spectrum matrix $[S_{FF}(\omega)]$ is singular at specific frequencies or over specific frequency intervals. When this happens, the inverse of $[S_{FF}(\omega)]$ will not exist and thus equation (3.9) cannot be used to determine the estimate of FRFs.

As there is no indication for the interrelationships between various measured input signals in a open-loop model, the concept of the coherence function needs to be expanded to include the variety of relationships among the various measured input signals.

3.3.1      ORDINARY COHERENCE FUNCTION

An ordinary coherence function is defined as the correlation coefficient describing the possible causal relationship between an output and an input for a single-input single-output (SISO) system.   Mathematically, the ordinary coherence function $\gamma_{xf}^2$ between an output (f) and an input (x) can be computed from equation (2.14) in Section 2.3.1.1.

For the multi-input single-output case, there may be relationships between the various inputs as well as those between inputs and output. When all inputs are uncorrelated with each other, the ordinary coherence function between each pair of inputs is zero, hence $S_{f_i f_j}(\omega) = 0$ for $i \neq j$. The input cross-spectrum matrix, $[S_{F'F'}(\omega)]$, is diagonal so that the system reduces to a set of single-input single-output systems.   In this case, the ordinary coherence function analysis can be used to determine the contribution of each input to the output. However, in the general case the ordinary coherence function between each pair of inputs will not be equal to zero. In other words, the inputs will be partially coherent.   The summation shown in equation (3.1) will not be one of independent quantities but one with interference among the summed inputs, so that the ordinary coherence function becomes difficult to interpret. The situation is further complicated when there are multiple outputs since the various interfering power sources at each output may themselves be related.

3.3.2      PARTIAL COHERENCE FUNCTION

In order to deal with the complicated multi-input multi-output situation, a partial coherence function - defined as the ordinary coherence function between two conditioned signals - was developed [27,28]. Practically, the output and input signals are conditioned by removing the potential contributions to the output and input from

other inputs consecutively. The removal of the effects of the other inputs is formulated on a linear least-squares basis and there will be a partial coherence function for every input/output combination for all permutations of coherence. However, the order of removal has a definite effect upon the partial coherence if some of the inputs are mutually correlated and, hence, there may exist many solutions of the **FRFs** estimation. As a result, the main function of partial coherence with respect to the estimation of **FRFs** is to explore the correlation(s) between the various input signals. In this case, a low value of partial coherence is desirable.

### 3.3.3      MULTIPLE COHERENCE FUNCTION

Multiple coherence is defined as the correlation coefficient describing the possible causal relationship between an output and all known inputs. There will be a multiple coherence function for every output. The formulation of multiple coherence functions can be expressed in a concise form by using the input cross-spectrum matrix $[S_{XX'}(\omega)]$ and the output cross-spectrum matrix $[S_{FF}(\omega)]$ to construct an augmented input cross-spectrum matrix. For the *ith* output, the augmented input cross-spectrum matrix is written as :

$$
[S_{X'FF}(i)(\omega)] = \begin{bmatrix} [S_{x_ix_i}(\omega)] & [S_{x_if_1}(\omega)] & [S_{x_if_2}(\omega)] & [S_{x_if_3}(\omega)] & \cdots\cdots & \cdots\cdots \\ [S_{x_1f_i}(\omega)] & [S_{f_1f_1}(\omega)] & [S_{f_1f_2}(\omega)] & \cdots\cdots & \cdots\cdots\cdots \\ [S_{x_2f_i}(\omega)] & [S_{f_2f_1}(\omega)] & \cdots\cdots & \cdots\cdots & \cdots\cdots\cdots \\ \cdots\cdots & \cdots\cdots & \cdots\cdots & \cdots\cdots & \cdots\cdots\cdots \\ \cdots\cdots & \cdots\cdots & \cdots\cdots & \cdots\cdots & \cdots\cdots\cdots\,I \end{bmatrix}
$$

$$(3.10)$$

Therefore, as a check on the determination of the FRF matrix, the multiple coherence functions can be computed from the following equation:

$$MCOH(i)(\omega) = 1 - \frac{DET[S_{X'FF}(i)(\omega)]}{DET[S_{x_i x_i}(\omega)]\, DET[S_{FF'}(\omega)]} \qquad (3.11)$$

When the multiple coherence of the *ith* output is near unity then, in most cases, the *ith* output can be well predicted from the set of inputs using the least-squares estimate of the **FRFs.** A multiple coherence function less than unity can indicate that there is/are (i) extraneous noise on the output, (ii) non-linear effects in the system, (iii) additional system inputs that have not been included in the calculation or (iv) a severe problem - interrelationship between various inputs. In general, the multiple coherent output spectrum indicates the part of the output that is linearly related to all of the measured inputs.

## 3.4 A NEW CLOSED-LOOP MODEL FOR MULTI-SHAKER MODAL TESTING

There are a variety of situations that can cause difficulties in the computation of the **FRFs** using equation (3.9). One of the most troublesome arises in the case of coherent inputs because if two of the measured inputs are highly coherent, there is no unique estimate of the **FRFs** associated with those inputs. This can be confirmed by computing the ordinary coherence function between each pair of inputs.

In practice, the external signals used as inputs to the **electrodynamic** shakers are independent, band-limited white noise with constant amplitude and random phases. However, due to the inability to isolate the excitation mechanism from the test structure completely, an ordinary coherence function between each pair of measured forces with values other than zero is observed, particularly at the structural resonances.

Following the methodology presented in Chapter 2, a new closed-loop model for multi-shaker modal testing can be devised to explain the correlation between measured force signals in a multi-shaker modal test that has caused uncertainty in structural identification for many years.

### 3.4.1 TWO-SHAKER SINE-DWELL TESTS

For the purpose of investigating the potential of a closed-loop approach to multi-shaker excitation, the natural place to begin is with two-shaker excitation. A two-shaker sine-dwell test is shown in Figure 3.2.



Figure 3.2. Two-shaker FRF measurement
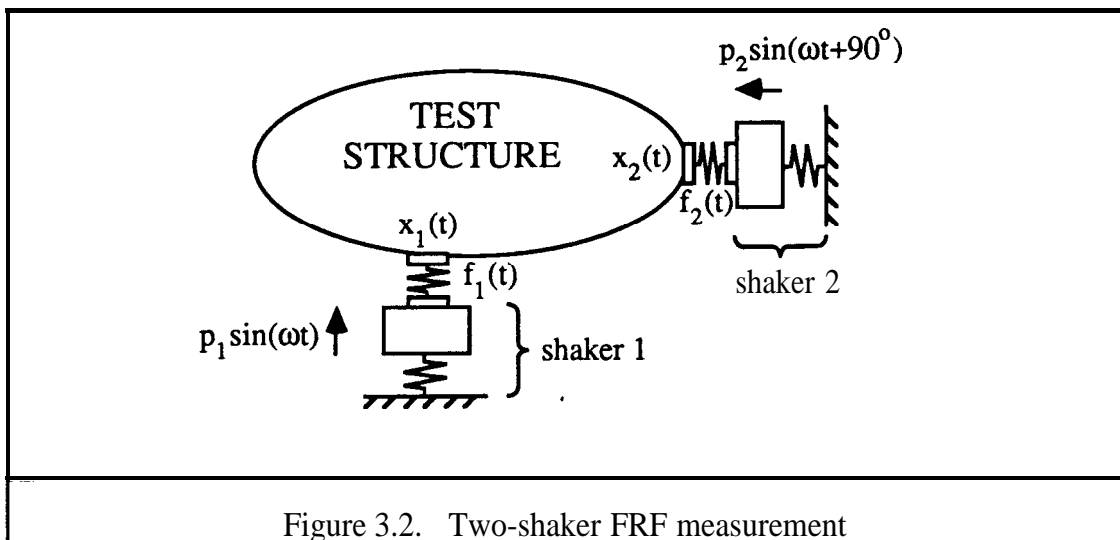
Following the methodology shown in Section 2.3, an equivalent block diagram for the two-shaker sine-dwell test is constructed and shown schematically in Figure 3.3.
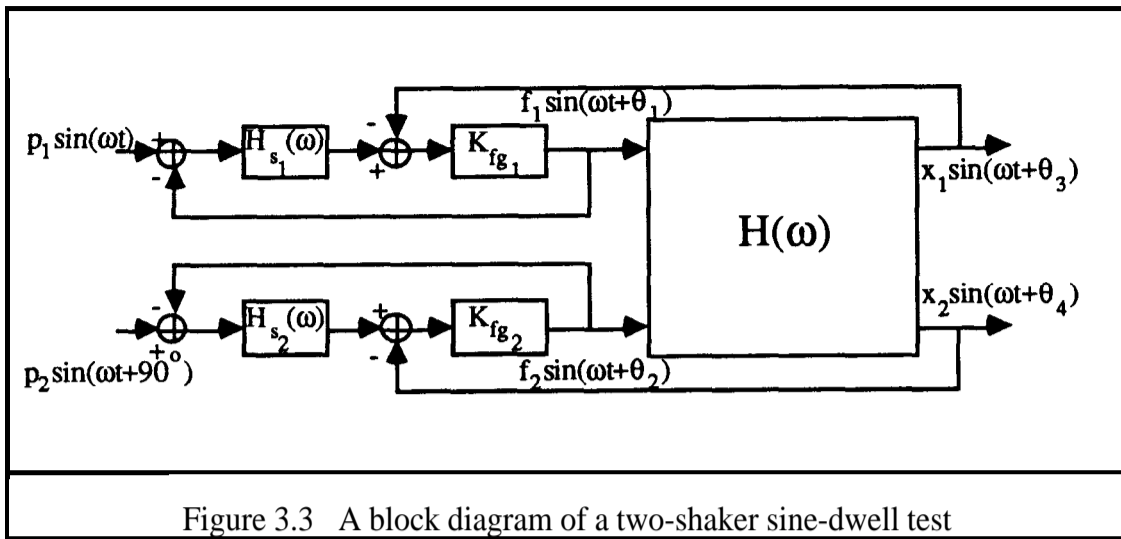
Figure 3.3 A block diagram of a two-shaker sine-dwell test

where $r_1(t)$ and $r_2(t)$ are the external input signals provided by the signal source generators; $p_1(t)$ and $p_2(t)$ are the forces generated at the armature of electrodynamic shakers 1 and 2 respectively; $K_{fg_1}$ and $K_{fg_2}$ are the stiffnesses of force transducers 1 and 2 respectively; $f_1(t)$ and $f_2(t)$ are the measured applied forces; and $x_1(t)$ and $x_2(t)$ are the associated responses where the shaker-applied forces act on the structure.

As a sinusoidal excitation test always produces high signal-to-noise ratios in measured applied forces as well as the associated responses, a noise-free condition for the closed-loop model is assumed in this case. The relationships between the shaker-applied forces, $f_1(t)$ and $f_2(t)$, and the responses $x_1(t)$ and $x_2(t)$, are described by

$$x_1(t) = \int_0^t h_{11}(\tau)f_1(t-\tau)d\tau + \int_0^t h_{12}(\tau)f_2(t-\tau)d\tau \qquad (3.12)$$

$$x_2(t) = \int_0^t h_{21}(\tau)f_1(t-\tau)d\tau + \int_0^t h_{22}(\tau)f_2(t-\tau)d\tau \qquad (3.13)$$

Applying the Fourier transform, equations (3.12) and (3.13) can be rewritten :

$$X_1(\omega) = H_{11}(\omega) F_1(\omega) + H_{12}(\omega) F_2(\omega) \qquad (3.14)$$

$$X_2(\omega) = H_{21}(\omega) F_1(\omega) + H_{22}(\omega) F_2(\omega) \tag{3.15}$$

With reference to Figure 3.3, one can express the input force signal $F_1(\omega)$ in terms of the signal generated by the signal source generator, $R_1(\omega)$, and the response signal $X_1(\omega)$ as follows:

$$[(H_{em_1}(\omega)R_1(\omega) - F_1(\omega))H_{s_1}(\omega) - X_1(\omega)] K_{fg_1} = F_1(\omega) \tag{3.16}$$

Therefore:

$$K_{fg_1}H_{s_1}(\omega)H_{em_1}(\omega)R_1(\omega) = F_1(\omega) (1 + K_{fg_1}H_{s_1}(\omega)) + K_{fg_1}X_1(\omega) \tag{3.17}$$

where $H_{em_1}(\omega)$ represents a FRF that converts the input excitation signal, $R_1(\omega)$, to the mechanical force applied to the armature mass and $H_{s_1}(\omega)$ is a FRF describing the mechanical properties of the shaker.

Substituting the expression for $X_1(\omega)$ (equation (3.14)) into equation (3.17) and rearranging :

$$F_1(\omega) = \frac{K_{fg_1}(H_{s_1}(\omega)H_{em_1}(\omega)R_1(\omega)-H_{12}(\omega)F_2(\omega))}{1 + K_{fg_1}(H_{s_1}(\omega)+H_{11}(\omega))} \tag{3.18}$$

and, following a similar analysis, one can also derive :

$$F_2(\omega) = \frac{K_{fg_2}(H_{s_2}(\omega)H_{em_2}(\omega)R_2(\omega)-H_{21}(\omega)F_1(\omega))}{1 + K_{fg_2}(H_{s_2}(\omega)+H_{22}(\omega))} \tag{3.19}$$

By considering equation (3.18) alone, it can be seen that the measured force signal, $F_1(\omega)$, is not only affected by the shaker-structure interaction but also by the measured

force signal, $F_2(\omega)$. When the excitation frequency is not close to a structural resonance frequency, or to a combined shaker-structure resonance frequency, $R_1(\omega)$ and $F_1(\omega)$ are in phase with each other because the cross-coupling term, $H_{12}(\omega)F_2(\omega)$, is relatively insignificant when compared with $H_{s_1}(\omega)H_{em_1}(\omega)R_1(\omega)$. It should be noted that $H_{12}(\omega)$ represents a cross receptance, $X_1(\omega)$ is in phase with $F_2(\omega)$ for a lightly damped structure except at the resonance frequencies where the phase of $H_{12}(\omega)$ changes significantly. A similar phenomenon is observed in $F_2(\omega)$, as shown in equation (3.19). This implies that the measured force signals $F_1(\omega)$ and $F_2(\omega)$ affect each other in a small range around each resonance. Another factor that affects the phase distortion at the structural resonances is the relative magnitude of two driving forces.

It is noted that if the position of one of the shakers, for example shaker 2, is located at a node point of a particular mode, $H_{12}(\omega)F_2(\omega)$ will give a zero magnitude even at resonance so that $F_1(\omega)$ and $F_2(\omega)$ are uncorrelated for this particular mode.

As mentioned earlier, phase distortion of the input force signals in a small range around each structural resonance for a two-shaker sine-dwell test can be overcome by adjusting the phase difference between two generator signals until $F_1(\omega)$ and $F_2(\omega)$ are $90^o$ out of phase, using the information given in equations (3.18) and (3.19).

### 3.4.2    TWO-SHARER RANDOM EXCITATION TESTS

The same closed-loop model as used above in two-shaker sine-dwell testing is applicable to a modal test with broad-band random excitation. First assume that there is no measurement noise contaminating the measured force and response signals at location 1 and 2, then the input force signals are given by:

$$F_1(\omega) = \frac{K_{fg_1}}{1 + K_{fg_1} H_{s_1}(\omega)} (H_{s_1}(\omega)H_{em_1}(\omega)R_1(\omega) - X_1(\omega))$$

(3.20)

$$F_2(\omega) = \frac{K_{fg_2}}{1 + K_{fg_2} H_{s_2}(\omega)} (H_{s_2}(\omega)H_{em_2}(\omega)R_2(\omega) - X_2(\omega))$$

(3.21)

For stationary and ergodic random data, the input force power spectra can be written as:

$$S_{f_1 f_1}(\omega) = \frac{K_{fg_1}{}^2}{1 + |K_{fg_1}H_{s_1}(\omega)|^2} (|H_{s_1}(\omega)H_{em_1}(\omega)|^2 S_{r_1 r_1}(\omega) - H_{s_1}{}^*(\omega)H_{em_1}{}^*(\omega)S_{r_1 x_1}(\omega)$$

$$-H_{s_1}(\omega)H_{em_1}(\omega)S_{x_1 r_1}(\omega) + S_{x_1 x_1}(\omega))$$

(3.22)

$$S_{f_2 f_2}(\omega) = \frac{K_{fg_2}(\omega)^2}{1 + |K_{fg_2}H_{s_2}(\omega)|^2} (|H_{s_2}(\omega)H_{em_2}(\omega)|^2 S_{r_2 r_2}(\omega) - H_{s_2}{}^*(\omega)H_{em_2}{}^*(\omega)S_{r_2 x_2}(\omega)$$

$$-H_{s_2}(\omega)H_{em_2}(\omega)S_{x_2 r_2}(\omega) + S_{x_2 x_2}(\omega))$$

(3.23)

where

$$S_{x_1 x_1}(\omega) = |H_{11}(\omega)|^2 S_{f_1 f_1}(\omega) + H_{11}{}^*(\omega)H_{12}(\omega)S_{f_1 f_2}(\omega) + H_{12}{}^*(\omega)H_{11}(\omega)S_{f_2 f_1}(\omega)$$

$$+ |H_{12}(\omega)|^2 S_{f_2 f_2}(\omega)$$

(3.24)

$$S_{x_2 x_2}(\omega) = |H_{21}(\omega)|^2 S_{f_1 f_1}(\omega) + H_{21}{}^*(\omega)H_{22}(\omega)S_{f_1 f_2}(\omega) + H_{22}{}^*(\omega)H_{21}(\omega)S_{f_2 f_1}(\omega)$$

$$+ |H_{22}(\omega)|^2 S_{f_2 f_2}(\omega)$$

(3.25)

Substituting $S_{x_1 x_1}(\omega)$ and $S_{x_2 x_2}(\omega)$ into equations (3.22) and (3.23), one can derive :

$$S_{f_1 f_1}(\omega) = \frac{K_{fg_1}{}^2}{1 + K_{fg_1}{}^2(|H_{s_1}(\omega)|^2 - |H_{11}(\omega)|^2)} \left[ |H_{s_1}(\omega)H_{em_1}(\omega)|^2 S_{r_1 r_1}(\omega) - H_{s_1}{}^*(\omega)H_{em_1}{}^*(\omega)S_{r_1 x_1}(\omega) \right.$$

$$- H_{s_1}(\omega)H_{em_1}(\omega)S_{x_1 r_1}(\omega) + H_{11}{}^*(\omega)H_{12}(\omega)S_{f_1 f_2}(\omega)$$

$$\left. + H_{12}{}^*(\omega)H_{11}(\omega)S_{f_2 f_1}(\omega) + |H_{12}(\omega)|^2 S_{f_2 f_2}(\omega) \right]$$

(3.26)

$$S_{f_2f_2}(\omega) = \frac{K_{f_{g_2}}^2}{1+K_{f_{g_2}}^2(|H_{s_2}(\omega)|^2-|H_{22}(\omega)|^2)} \left[|H_{s_2}(\omega)H_{cm_1}(\omega)|^2 S_{r_2r_2}(\omega) - H_{s_2}^*(\omega)H_{cm_2}^*(\omega)S_{r_2x_2}(\omega)\right.$$

$$-H_{s_2}(\omega)H_{cm_2}(\omega)S_{x_2r_2}(\omega) + H_{21}^*(\omega)H_{22}(\omega)S_{f_1f_2}(\omega)$$

$$\left. + H_{22}^*(\omega)H_{21}(\omega)S_{f_2f_1}(\omega) + |H_{21}(\omega)|^2 S_{f_1f_1}(\omega)\right]$$

(3.27)

The coherence function between two measured force signals $f_1$ and $f_2$ is defined [29] as :

$$\gamma_{f_1f_2}(\omega)^2 = \frac{|S_{f_1f_2}(\omega)|^2}{S_{f_1f_1}(\omega)S_{f_2f_2}(\omega)}$$

(3.28)

In most cases, the auto-power spectra $S_{f_1f_1}(\omega)$ and $S_{f_2f_2}(\omega)$ are partially correlated and the cross-spectrum $S_{f_1f_2}(\omega)$ is not zero, so that the coherence function $\gamma_{f_1f_2}(\omega)$ is not zero. When the cross receptance $H_{12}(\omega)$ is zero, the coherence function approaches zero because $R_1(\omega)$ and $R_2(\omega)$ are uncorrelated.

Unlike the two-shaker sine-dwell test, there is no way of obtaining two uncorrelated shaker-applied force signals for a two-shaker random excitation test unless adaptive control methodology is employed.

### 3.4.3    MULTI-SHAKER MODAL TESTS

Based on the traditional open-loop FRF measurement model, Leuridan [26] has noted that a unique solution for the MIMO problem can be worked out for the case where the measured inputs are not correlated and has pointed out also that most solution techniques applied to the MIMO situation can handle the case of some correlation between the measured inputs but fail if the measured inputs become highly correlated. This condition implies that the spectrum matrices are rank deficient and is unavoidable

due to shaker-structure interactions. However, as will subsequently be shown, it is possible to determine the dynamic characteristics of a test structure by using the cross-spectrum matrices even though, the measured force signals are highly correlated. A new FRF technique is developed below which can give noise-free estimates of FRFs and requires minimum post-processing calculation.

The closed-loop model used above for simple two-exciter systems can be generalized to produce a model for multi-shaker modal testing as illustrated in the simplified block diagram in Figure 3.4. For simplicity, a special case with $n$ measured shaker-applied forces and $n$ corresponding output signals is considered.
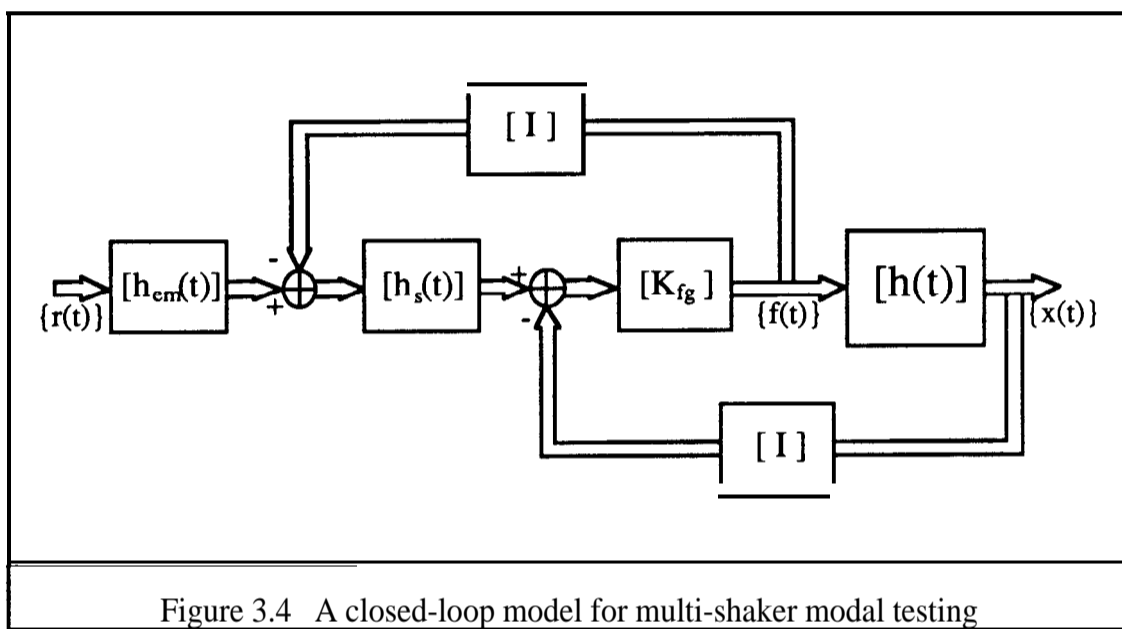


Figure 3.4   A closed-loop model for multi-shaker modal testing

The dynamic response for all components is assumed to be linear and time-invariant so that the measured output signals can be expressed by the linear vector difference equation as :

$$\{x(t)\}_{nx1} \;=\; [h(t)]_{nxn}\{f(t)\}_{nxl} \tag{3.29}$$

$$\{f(t)\}_{nx1} = [K_{fg}]_{nxn}[h_s(t)]_{nxn}[h_{em}(t)]_{nxn}\{r(t)\}_{nx1} - [K_{fg}]_{nxn}[h_s(t)]_{nxn}\{f(t)\}_{nx1}$$

$$- [K_{fg}]_{nxn}\{x(t)\}_{nx1} \qquad\qquad (3.30)$$

where $\{f(t)\}$ and $\{x(t)\}$ are the $nx1$ input and output vectors respectively, $\{r(t)\}$ is the $nx1$ external input vector. $[h_{em}(t)]$, $[H_s(t)]$, $[K_{fg}]$ and $[H]$ are described by

$$[h_{em}(t)] = \begin{bmatrix} h_{em_1}(t) & & 0 \\ & \ddots & \\ 0 & & h_{em_n}(t) \end{bmatrix} = \text{diag} \ (h_{em_i}(t)) \qquad (3.31)$$

$$[h_s(t)] = \begin{bmatrix} h_{s_1}(t) & & 0 \\ & \ddots & \\ 0 & & h_{s_n}(t) \end{bmatrix} = \text{diag} \ (h_{s_i}(t)) \qquad (3.32)$$

$$[K_{fg}] = \begin{bmatrix} K_{fg_1} & & 0 \\ & \ddots & \\ 0 & & K_{fg_n} \end{bmatrix} = \text{diag} \ (K_{fg_i}) \qquad (3.33)$$

$$[h(t)] = \begin{bmatrix} h_{11}(t) & .. & h_{1n}(t) \\ \vdots & \ddots & \vdots \\ h_{n1}(t) & .. & h_{nn}(t) \end{bmatrix} \qquad (3.34)$$

$$i = 1, 2, ......, n \qquad\qquad j = 1, 2, ......, n$$
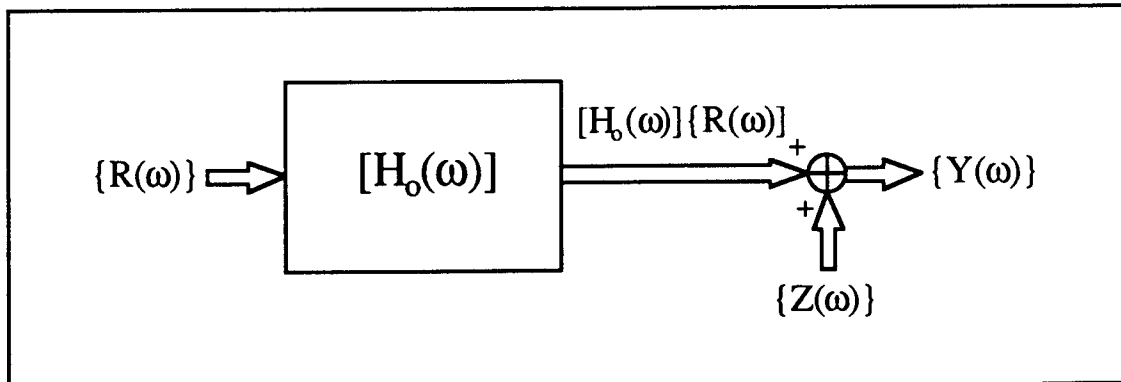


Figure 3.5   An alternative model for a multi-shaker modal test with measurement noise

Figure 3.5 illustrates an equivalent open-loop system model for the multi-shaker modal test system with measurement noise in the frequency domain. $\{R(\omega)\}_{nx1}$ is an $nx1$ external input vector. The output vector $\{Y(\omega)\}_{2nx1}$, is subdivided into two parts, $\{F'(\omega)\}_{nx1}$ and $\{X'(\omega)\}_{nx1}$, where $\{F'(\omega)\}_{nx1}$ and $\{X'(\omega)\}_{nx1}$ are the measured force and measured response vectors respectively. The equivalent open-loop FRF matrix $[H_o(\omega)]_{2nxn}$, is partitioned into two square matrices $[H_F(\omega)]_{nxn}$ and $[H_X(\omega)]_{nxn}$, where $[H_F(\omega)]_{nxn}$ and $[H_X(\omega)]_{nxn}$ are the equivalent open-loop FRFs for the measured forces and measured responses respectively. The contaminating noise vector $\{Z(\omega)\}_{2nx1}$, is also subdivided into two parts, $\{M(\omega)\}_{nx1}$ and $\{N(\omega)\}_{nx1}$, and is defined to be incoherent with $\{R(\omega)\}_{nx1}$, as expressed by :

$$E\left[\{Z(\omega)\}^*\{R(\omega)\}^T\right]_{2nxn} = 0 \tag{3.35}$$

The output $\{Y(\omega)\}_{2nx1}$ can be written as follows :

$$\{Y(\omega)\}_{2nx1} = [H_o(\omega)]_{2nxn}\{R(\omega)\}_{nx1} + \{Z(\omega)\}_{2nx1} \tag{3.36}$$

Equation (3.36) can be rewritten as :

$$\left\{\begin{array}{c}[F'(\omega)]_{nx1}\\ \text{---------}\\ [X'(\omega)]_{nx1}\end{array}\right\}_{2nx1} = \left[\begin{array}{c}[H_F(\omega)]_{nxn}\\ \text{---------}\\ [H_X(\omega)]_{nxn}\end{array}\right]_{2nxn}\{R(\omega)\}_{nx1} + \left\{\begin{array}{c}\{M(\omega)\}_{nx1}\\ \text{---------}\\ \{N(\omega)\}_{nx1}\end{array}\right\}_{2nx1}$$

$$\tag{3.37}$$

Post-multiplying both sides of the complex conjugate of equation (3.36) by $\{R(\omega)\}_{nx1}^T$ and taking expected values, we get

$$E[\{Y(\omega)\}^*\{R(\omega)\}^T]_{2nxn} = [H_o(\omega)]^*_{2nxn}E[\{R(\omega)\}^*\{R(\omega)\}^T]_{nxn} + E[\{Z(\omega)\}^*\{R(\omega)\}^T]_{2nxn}$$

$$\tag{3.38}$$

Equation (3.38) can be expressed in terms of the auto- and cross-spectra, therefore,

$$[S_{YR}(\omega)]_{2nxn} = [H_o(\omega)]^*_{2nxn} [S_{RR}(\omega)]_{nxn} \tag{3.39}$$

from which, the FRF matrix $[H_o(\omega)]_{2nxn}$ is obtained.

$$[H_o(\omega)]_{2nxn} = [S_{RY}(\omega)]_{2nxn} [S_{RR}(\omega)]^{-1}_{nxn} \tag{3.40}$$

or

$$\begin{bmatrix} [H_F(\omega)]_{nxn} \\ \text{---------} \\ [H_X(\omega)]_{nxn} \end{bmatrix}_{2nxn} = \begin{bmatrix} [S_{RF'}(\omega)]_{nxn} \\ \text{---------} \\ [S_{RX'}(\omega)]_{nxn} \end{bmatrix}_{2nxn} [S_{RR}(\omega)]^{-1}_{nxn} \tag{3.41}$$

A necessary and sufficient condition for the inverse of $[S_{RR}(\omega)]$ to exist is that none of the external input signals are completely coherent with any other so that $[S_{RR}(\omega)]$ is nonsingular.

After the equivalent open-loop FRF matrix $[H_o(\omega)]_{2nxn}$ has been obtained, the FRFs of the system are derived:

$$\begin{aligned} [H_{XF}(\omega)]_{nxn} &= [H_X(\omega)]_{nxn} [H_F(\omega)]^{-1}_{nxn} \\ &= [S_{RX'}(\omega)]_{nxn} [S_{RR}(\omega)]^{-1}_{nxn} ([S_{RF'}(\omega)]_{nxn} [S_{RR}(\omega)]^{-1}_{nxn})^{-1} \\ &= [S_{RX'}(\omega)]_{nxn} [S_{RF'}(\omega)]^{-1}_{nxn} \end{aligned} \tag{3.42}$$

From equations (3.41) and (3.42), the uniqueness of the estimate of $[H_{XF}(\omega)]_{nxn}$ is seen to be determined by the rank of the matrix $[S_{RR}(\omega)]_{nxn}$. If this matrix has full rank then equation (3.42) provides a unique least-squares solution. Otherwise, any solution will be an arbitrary point in the kernel of $[H_{XF}(\omega)]_{nxn}$. It can be concluded that the effect of measurement noise in the estimation of the FRFs for a multi-shaker random excitation test can be minimized by using equation (3.42). A requirement of

this method is that the point FRF measurements associated with the coordinates at which the shaker-applied forces act on the structure should be obtained.

As mentioned in the preceding section, classical techniques for MIMO analysis are based on either ordinary and partial coherence functions or principal inputs calculation [24-27] because there are a number of situations where the cross-spectrum matrix of measured force signals is singular at specific frequencies or frequency intervals. Bendat [28] presented a frequency-domain technique based on the calculation of coherence and partial coherence functions to evaluate the correlation between signals. The operations involved with the calculation of the coherence and partial-coherence functions are identical to the operations that are used to an LU decomposition of the following matrix, using Gauss eliminations:

$$
\begin{bmatrix}
[S_{F'F'}(\omega)]_{n \times n} & [S_{F'X'}(\omega)]_{n \times n} \\
[S_{X'F'}(\omega)]_{n \times n} & [S_{X'X'}(\omega)]_{n \times n}
\end{bmatrix}_{2n \times 2n}
$$

More recently, Leuridan [26] suggested an alternative technique based on the calculation of a set of principal inputs. The operation involved with the calculation of the minimum set of uncorrelated signals, or a set of principal inputs, is basically equivalent to the spectral decomposition of the afore-mentioned matrix. Estimates of the FRFs can be obtained once the ordinary and partial coherence functions, or principal inputs are determined. Both techniques involve a lot of post-processing calculations and, moreover, the estimate of $[H_{XF}(\omega)]_{n \times n}$ is contaminated by the measurement noise existing either in the measured force signals or in the measured response signals because the auto-spectra are used. The $[_1H(\omega)]_{n \times n}$ estimator will converge to a biassed, lower-bound estimate of the true $[H_{XF}(\omega)]_{n \times n}$ since the cross-spectrum matrix $[S_{FF'}(\omega)]_{n \times n}$ is used. On the other hand, the $[_2H(\omega)]_{n \times n}$ estimator

will give a biassed, upper-bound estimate of the true $[H_{XF}(\omega)]_{nxn}$ since the cross-spectrum matrix $[S_{XX'}(\omega)]_{nxn}$ is used.

However, it should be noted that when the technique proposed in this section is applied to the estimation of **FRFs** in multi-shaker modal testing with *n* measured force signals and *n* measured response signals, 3n processing channels are needed because an additional $2n^2$ cross-spectrum terms are needed for the $[S_{RF'}(\omega)]$ and $[S_{RX'}(\omega)]$ matrices respectively.

### 3.4.4    EXPERIMENTAL VERIFICATION

In the preceding sections, only the pure theoretically aspects of the closed-loop model have been discussed. However, as a realistic mathematical model, the applicability of the closed-loop model for a multi-shaker modal testing must be checked on an actual mechanical structure.

A circular disk was chosen to validate the application of the closed-loop model in a two-shaker sine-dwell test. The disk was excited at two locations simultaneously, with two point response signals measured.   Sinusoidal excitation signals were generated by a Solartron 1254 frequency response analyser and were arranged to be $90^o$ out of phase. The measured force signals were orthogonal when the frequency of the excitation signals is well below or above the structural resonance frequencies. However, it was observed that the phase difference between two measured force signals, $F_1(\omega)$ and $F_2(\omega)$, approached zero at most structural resonance frequencies.

An experiment was then carried out by disconnecting the power from one of the electrodynamic shakers, while all four signals (two force signals and two response signals) were still measured.   Figure 3.6 shows the resulting **FRFs**. A zoom

will give a biassed, upper-bound estimate of the true $[H_{XF}(\omega)]_{nxn}$ since the cross-spectrum matrix $[S_{XX'}(\omega)]_{nxn}$ is used.

However, it should be noted that when the technique proposed in this section is applied to the estimation of **FRFs** in multi-shaker modal testing with *n* measured force signals and *n* measured response signals, 3n processing channels are needed because an additional ***2n²*** cross-spectrum terms are needed for the $[S_{RF'}(\omega)]$ and $[S_{RX'}(\omega)]$ matrices respectively.

### 3.4.4    EXPERIMENTAL VERIFICATION

In the preceding sections, only the pure theoretically aspects of the closed-loop model have been discussed. However, as a realistic mathematical model, the applicability of the closed-loop model for a multi-shaker modal testing must be checked on an actual mechanical structure.

A circular disk was chosen to validate the application of the closed-loop model in a two-shaker sine-dwell test. The disk was excited at two locations simultaneously, with two point response signals measured.   Sinusoidal excitation signals were generated by a Solartron 1254 frequency response analyser and were arranged to be $90^o$ out of phase. The measured force signals were orthogonal when the frequency of the excitation signals is well below or above the structural resonance frequencies. However, it was observed that the phase difference between two measured force signals, $F_1(\omega)$ and $F_2(\omega)$, approached zero at most structural resonance frequencies.

An experiment was then carried out by disconnecting the power from one of the **electrodynamic** shakers, while all four signals (two force signals and two response signals) were still measured.   Figure 3.6 shows the resulting **FRFs**. A zoom

measurement for the response (acceleration) at location 1 divided by the applied force at location 1 in the frequency range from 5 to 139 Hertz is shown in Figure 3.7 in which a dominant mode was identified at 72.1 Hz.

With reference to Figure 3.3, one can observe that even though one of the external input signals, for example $R_1(\omega)$, is set to zero, there will still be a response $\ddot{X}_1(\omega)$ and a force signal $F_1(\omega)$ because of the existence of the interrelated feedback paths. It can easily be shown that, under these conditions, $\ddot{X}_1(\omega)/F_1(\omega)$ contains the dynamic characteristics of electrodynamic shaker 1.

The predicted results were checked by exciting electrodynamic shaker 1 by another shaker via an impedance head. The measured FRF data are shown in Figures 3.8 and 3.9. Good agreement is indicated between these two set of experimental FRF results.

Figure 3.6 The FRFs of a a two-shaker sine dwell test
(the power for shaker 1 was disconnected)



Figure 3.7   A zoom measurement of $\ddot{X}_1(\omega)/F_1(\omega)$ (the power for shaker 1 was
disconnected and the frequency range was set to 5- 139 Hz)
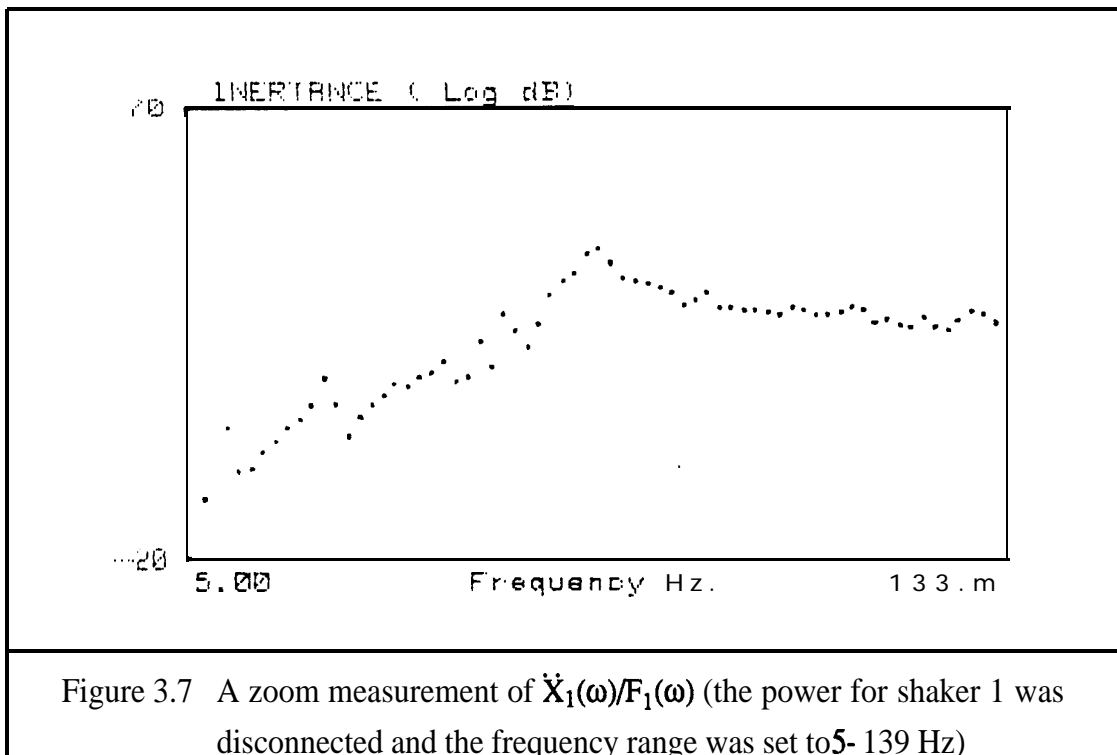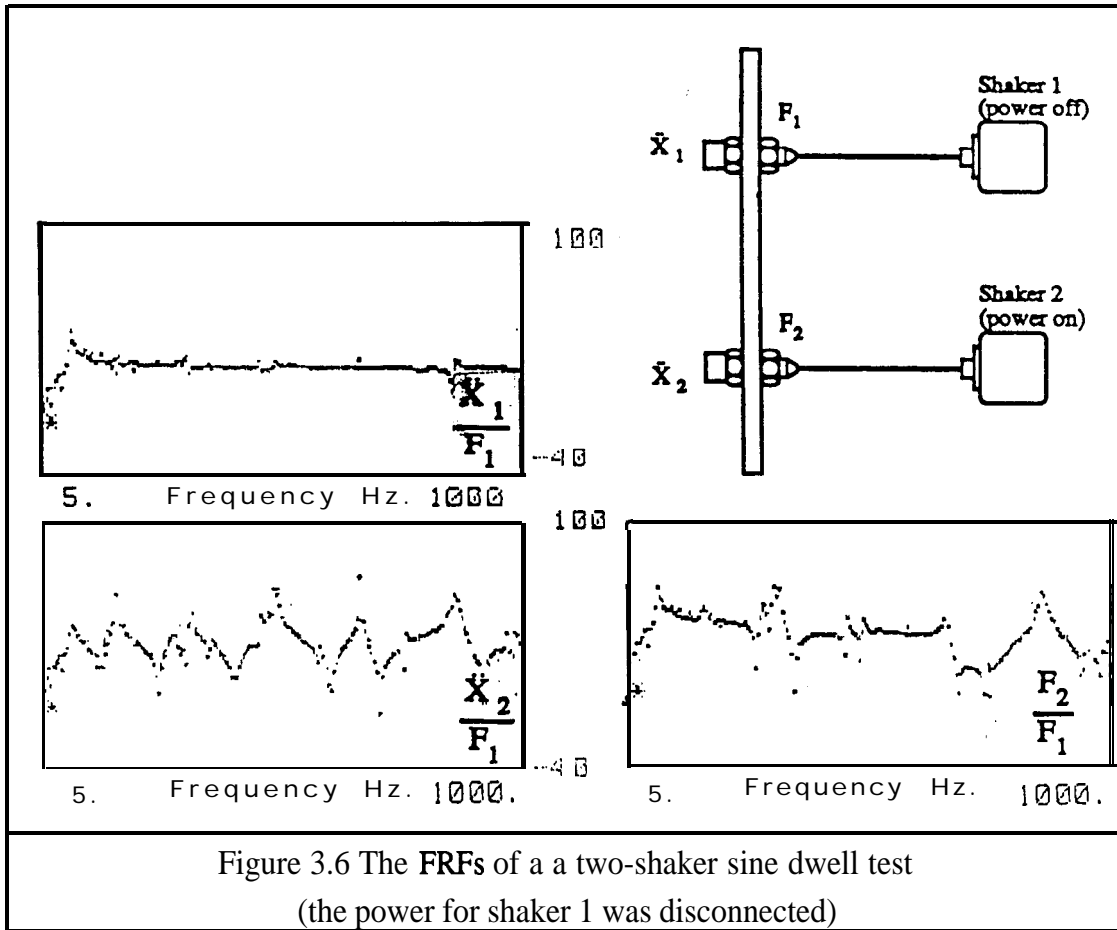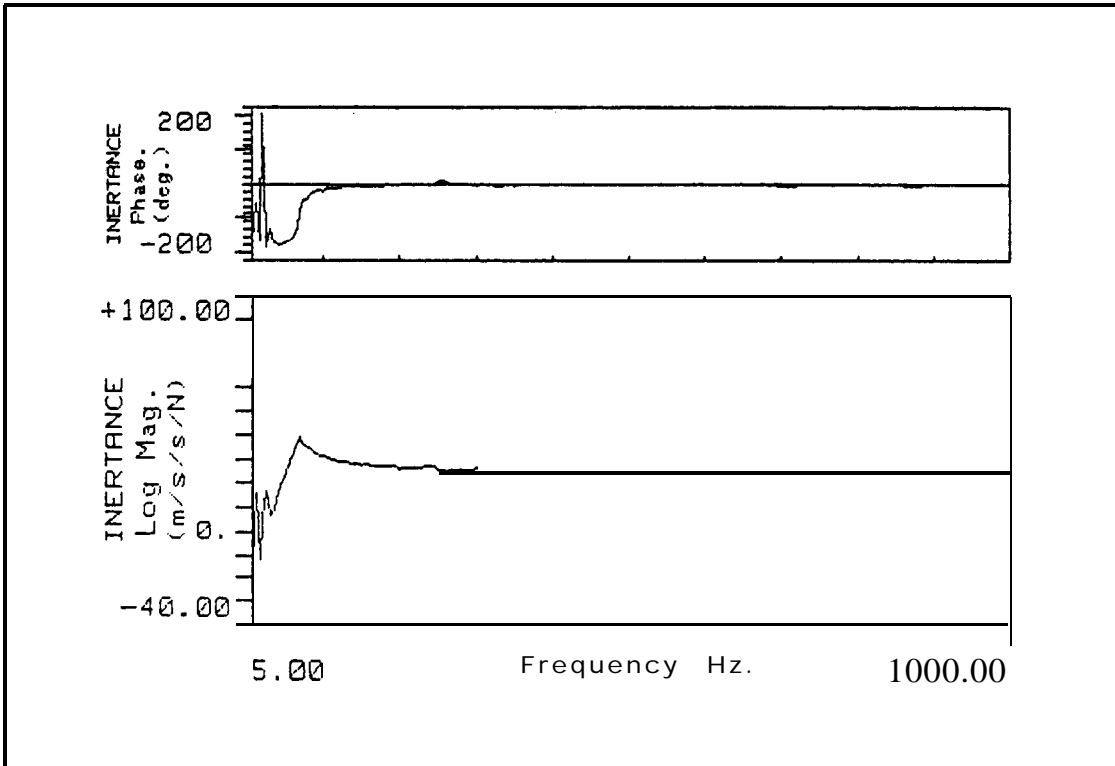
Figure 3.8   The FRF of the **electrodynamic** shaker with a push **rod**
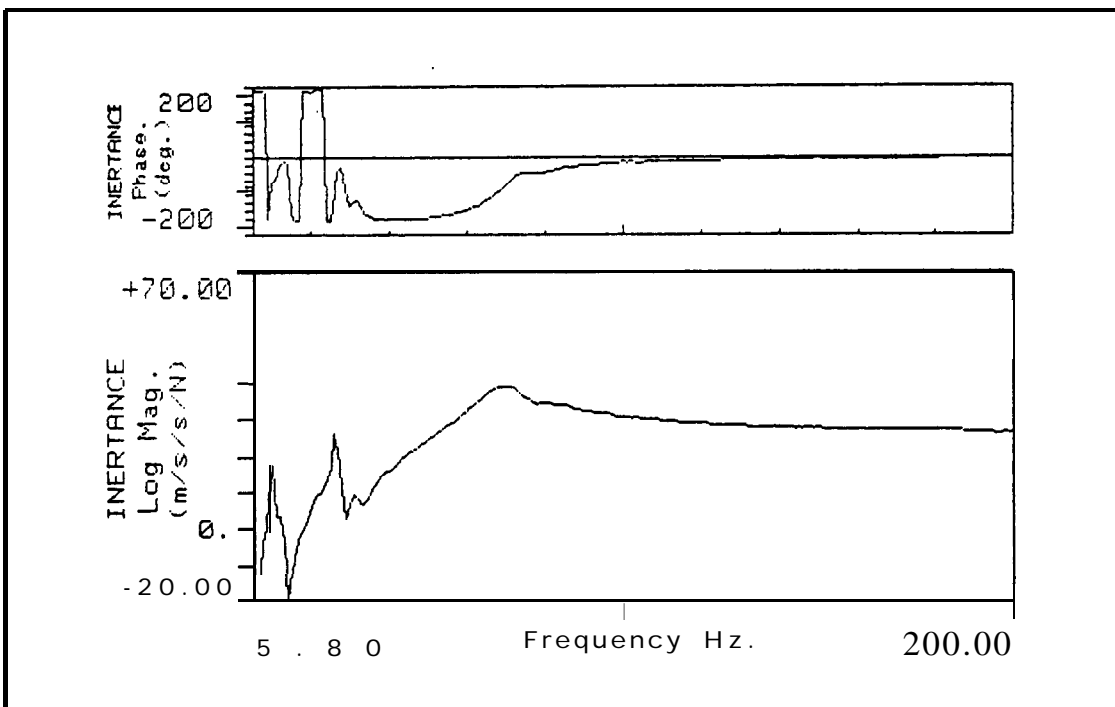
Figure **3.9**   A zoom measurement of the **FRF** (the frequency range
was set to **5-200** Hz)

## 3.5 CONCLUDING REMARKS

Classical FRF estimation techniques based on the ordinary, partial and multiple coherence function calculations have been reviewed. These techniques are able to handle cases where there is some correlation between the measured inputs, but they fail when the measured inputs become highly correlated. Unfortunately, the measured inputs (force signals) in most practical cases are highly correlated in the vicinity of each of the structural resonances even though (i) the orthogonality property of the external input signals to the shakers is well maintained in a multi-shaker sine-dwell test ; or (ii) the external input signals are uncorrelated in a multi-shaker random excitation test. The difficulty arising in controlling the measured force signals is mainly due to the fact that it is physically impossible for the shakers to excite the test structure without interfering with it.

Since the traditional open-loop FRF measurement model cannot be used to explain the correlation between the various input signals in a multi-shaker modal test, the closed-loop model developed in Chapter 2 has been generalised to explore the complexity of shaker-structure interactions for multi-shaker modal testing. The generalised model can be used to explain what causes the difficulties arising in maintaining the orthogonality condition in a sine dwell test and in ensuring the incoherence of the shaker-applied forces in a random excitation test. After identifying the inter-relationships between the excitation mechanism and the test structure, a frequency domain technique is developed to give a unique estimate of the FRFs in a multi-shaker random excitation test. The proposed technique is superior to classical FRF estimation techniques since it can be applied to all frequencies of interest, even if the shaker-applied forces are highly correlated at specific frequencies or over specific frequency intervals. In addition, the effect of measurement noise on the FRF estimation is

minimised because the proposed technique only requires the computation of the cross-spectra between the measured response signals and the external input signals, and between the measured force signals and the external input signals. Experimental results have verified the applicability of the closed-loop model in a two-shaker sine dwell test.

# 4 IDENTIFICATION AND MATHEMATICAL MODELLING OF LINEAR STRUCTURES

## 4.1 INTRODUCTION

Structural identification problems can be divided into two categories. One is the "black box" problem where the physical description of a structure is totally unknown : the widely-used modal testing or experimental modal analysis approach for determining response models and modal models of mechanical structures are such black box identification methods. Various modal testing techniques have been discussed in the preceding sections and different experimental modal analysis techniques in the frequency and time domain methods will be given in Section 4.2.

The second category of problem is that where some knowledge of the structure, such as its total mass/inertia or its physical connectivity, is known or given a priori. Thus this problem can be that of determining some unknown parameters or parameter changes within a finite element (FE) or analytical model of this structure in accordance with a stated correlation function. The most recent methods of structural identification and model updating are based on the philosophy depicted in Figure 4.1. An appropriate correlation function must be judiciously chosen which can be optimized in order to accomplish the goal of structural identification or model updating - deriving a good representation model. In general, this function determines how good will be the fit of the model response to that of the test structure. In recent years many techniques

for adjustment of the unknown parameter changes and different correlation functions have been developed.
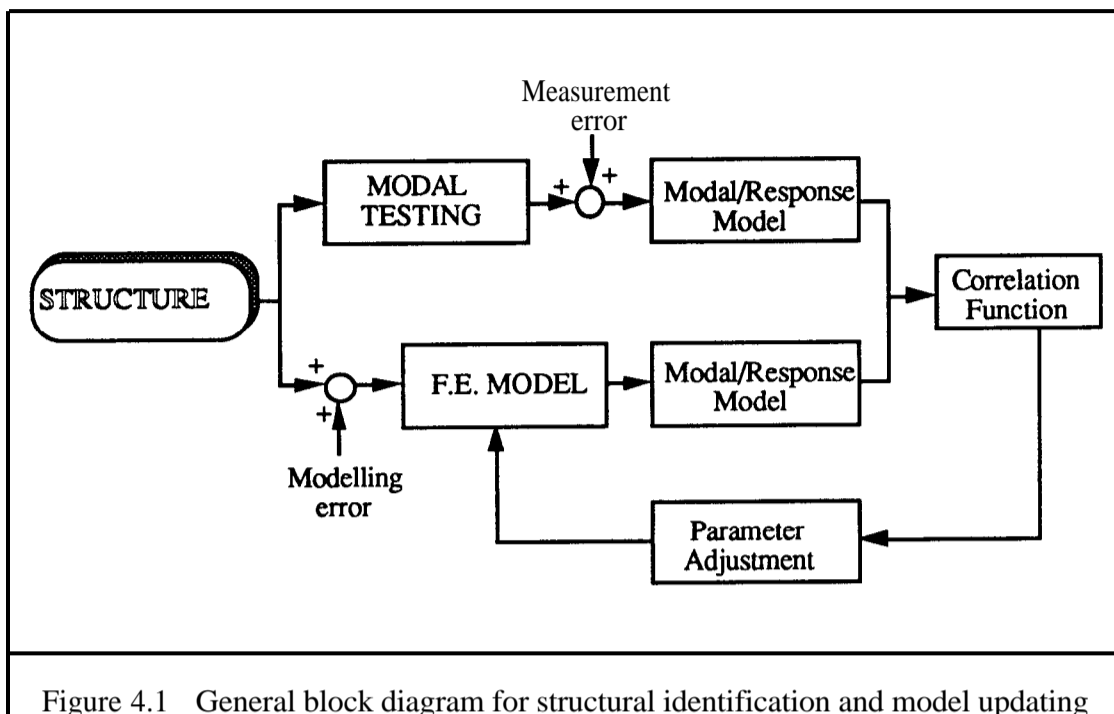


Figure 4.1   General block diagram for structural identification and model updating

However, the accuracy of structural identification and model updating results is impaired - sometimes severely - by a combination of measurement error, numerical error in the computations, modelling error and the modal and coordinate incompleteness of the measured data.   In the preceding chapters, the subject of measurement errors has been studied in some detail. Here, the numerical error in the computations is discussed below.   The error existing in FE/analytical structural modelling will be fully discussed in Section 4.3. The problems caused by the modal and coordinate incompleteness in measured data will be investigated in the subsequent sections where the problem of reconciliation between the theoretical and experimentally-derived models is addressed.

The continued technical improvements in the design of mainframe, mini- and micro-computers are coupled with an ever-increasing variety of numerical techniques to solve

mathematical problems. Some numerical methods work effectively for numerically-stable problems but may be inadequate for certain types of ill-conditioned problem, especially for some experimental engineering and physical problems. It should be emphasized that it is meaningless to assert that a matrix is ill-conditioned without stating which type of calculation to be performed. For example, a matrix may be ill-conditioned with respect to the calculation of its inverse or the calculation of its eigenvalues or eigenvectors but ill-condition with respect to one of these will not in general imply ill-condition with respect to any other. For structural identification problems, it can be shown that the ratio of the extreme eigenvalues is a dominant factor in determining condition.  The stiffness matrix of a mechanical structure depends largely on the high-frequency modes and the mass matrix of the structure depends largely on the low-frequency modes. For a structural parameter extraction problem, "physical noise" caused by the inevitable errors of the measurement equipment cannot be reduced beyond a specific level which depends on the refinement of the physical measurement devices. However, "arithmetical noise", introduced by the finite accuracy of numerical computations, can be reduced to an arbitrarily low level by increased computer capacity and by more circumspect coding using more reliable and numerical stable techniques.  A good example is the recent wide use of singular value decomposition (SVD) in modal-parameter estimation [30] and coupling of sub-structures [31].

## 4.2 DIRECT STRUCTURAL IDENTIFICATION TECHNIQUES

The purpose of direct structural identification techniques is to extract or to determine the structural parameters from experimental FRFs or time response data. Since the early 1970s, a wide variety of methods have been developed. The bases of many of the parameter extraction methods commonly used nowadays have been developed and

presented in works by Brown, Allemang, Zimmerman and Mergeay [32], Ewins [8], Stroud [33] and Füllekrug [34].

### 4.2.1 THEORETICAL AND EXPERIMENTAL ROUTES TO VIBRATION ANALYSIS

Three main categories of system model are identified in Figure 4.2, these being the Spatial Model (consisting of mass, stiffness and damping properties), the Modal Model (comprising the natural frequencies and mode shapes) and the Response Model (consisting of a set of frequency response functions or a set of time response data). For a theoretical analysis, such as an FE analysis, it is a normal practice for a structural analyst to create the spatial model of a structure and then subsequently to derive the modal model and response model of the structure. In contrast, practical experience shows that only the response model of the structure is directly measurable, so the relative sequence of mathematical models is Response-Modal-(Spatial ) for an experimental study. However, neither the experimentally-derived modal model nor the response model of the structure is complete in terms of the number of modes and/or the number of degrees-of-freedom **(DoFs)**. As a result, the direct derivation of a representative spatial model from experimental data is very difficult to achieve successfully.

Figure 4.2  Theoretical and experimental routes to vibration analysis
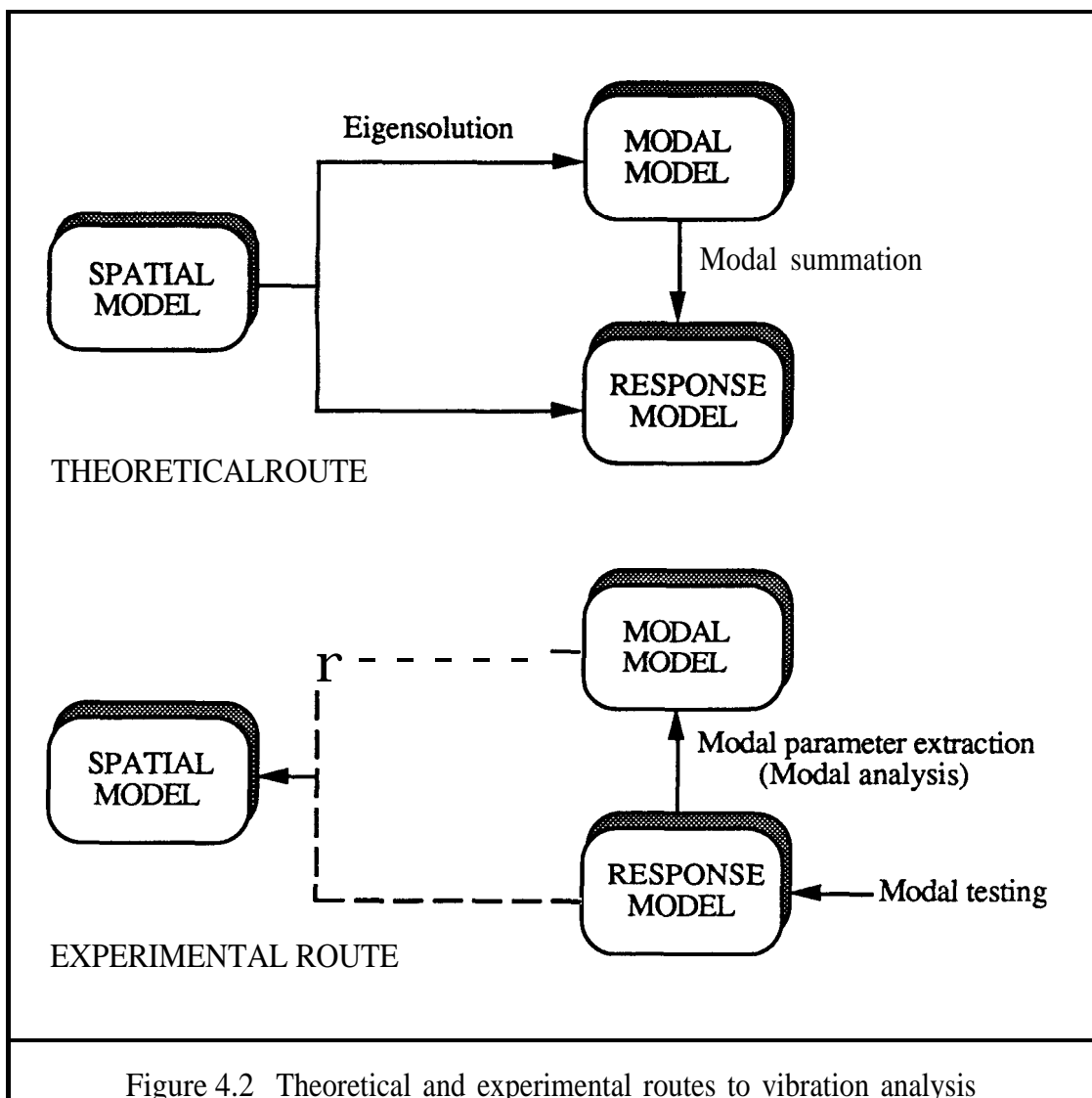
## 4.2.2     PARAMETER EXTRACTION METHODS IN THE FREQUENCY

DOMAIN

In the frequency domain, some modal parameter extraction (or modal analysis)

methods are applied to a single FRF at a time. These are called "single-reference" or

"local" single degree-of-freedom (SDoF) and multi-degree-of-freedom (MDoF) SISO

methods. The basic assumption of the SDoF methods is that the response of a

structure in the vicinity of a structural resonance is dominated by one single mode.  It

is well known that for the general SDoF system a Nyquist plot of FRF produces

circle-like curves and, it has been proved by Ewins [8] that if the appropriate type of damping model is chosen, this Nyquist plot will produce an exact circle. Based on this assumption, the modal parameters of the structure can be determined by **circle**-fitting the Nyquist plot of the FRF data around each of the structural resonances. There are alternative procedures available which work within the same assumption of the **SDoF** circle-fit method, such as the **SDoF** inverse method. Here, by plotting the reciprocal of the FRF around a structural resonance, the modal parameters can be determined by least-squares straight line-fits through the measured data points. The **MDoF** methods can be seen as an extension of **SDoF** method. They relax the restrictive assumption that the effect of all the other modes shall be represented by a constant (for every mode in a **SDoF** analysis), and so are likely to produce more precise modal parameters from a set of FRF data

Some methods allow for several **FRFs** to be analysed simultaneously, with responses taken at various points on the structure, but using one excitation point only. These are called "global" or single-input multi-output (SIMO) methods. The philosophy behind these methods is that the natural frequencies and damping loss factors do not vary (theoretically) from point to point on the structure, and thus it should be possible to obtain a consistent and unique set of modal properties by processing several **FRFs** at the same time. One of the main advantages of these methods is that any variation of the identified modal properties (such as is often found with repeated SISO analysis) will be removed by the parameter extraction procedure.

Finally, there are other methods that can process all the available **FRFs** simultaneously, from various excitation and response locations. These methods are usually called "polyreference" or multi-input multi-output (**MIMO**) methods.

### 4.2.3    PARAMETEREXTRACI'ION METHODS IN THE TIME DOMAIN

In the frequency domain there are **SDoF** and **MDoF** analysis methods, while in the time domain only **MDoF** analysis is applicable. The normal starting point of the time domain methods is based on the following equation:

$$h_{ij}(t) = \sum_{r=1}^{2N} {}_rA_{ij}e^{\lambda_r t} \tag{4.1}$$

where $h_{ij}(t)$ is the impulse response function (IRF) at particular time and ${}_rA_{ij}$ is the modal constant which contains the initial conditions implicitly. The response data do not require the free decay vibrations to be measured in reality: they can be obtained by taking the inverse Fourier Transform of the measured receptances in the frequency domain.

The complex exponential method is a local approach for SISO analysis, because the natural frequencies and the damping loss factors are determined from the time history of one single measurement point. This method is based on describing equation (4.1) at a number of equally-spaced time intervals and taking a number of samples which is equal to or larger than the number of time intervals in order to obtain an exactly- or over-determined system of equations from which the complex eigenvalues natural frequencies and damping loss factors - are determined using the Prony method. Afterwards, the eigenvectors can be determined by employing the time histories of other measurement points.

The polyreference complex exponential method is an extension of the basis complex exponential method which uses the time history of several measurement points and excitation points simultaneously. In contrast to the complex-exponential method, the polyreference method is a global approach.  It is capable of producing consistent

modal data, of separating closely-spaced (or even identical-frequency) modes and of handling the heavily damped responses obtained from a complex structure.

The Ibrahim time domain method **(ITD)** is likewise a global approach. With this method, a unique set of modal parameters - natural frequencies, damping loss factors and mode shapes - are obtained from a set of free vibration measurements in a single analysis. This method is based on constructing an equation relating a matrix which contains sets of free response measurements with matrices which contain mode shape vectors, complex eigenvalues and the response measurement times. By using a second set of measured response data with a time shift At and then constructing another matrix equation, the desired modal parameters are calculated from a transformation matrix that relates the first set of data to the second set.

Other time domain methods are the eigensystem realization (ERA) and the **ARMA** methods, the former one being similar to the Ibrahim time domain method and the latter being based on finite difference equations.

## 4.3 STRUCTURAL MODELLING

Modelling errors inevitable arise when a continuous structure is represented by a discrete FE mesh. In general the accuracy and reliability of the FE solution is dependent on the shape function of the chosen elements and thus on the elements used in the dynamic analysis. There exist many types of elements in FE packages, e.g. bar, beam, shell, plate, block etc., and each is described by different shape functions. The choice of elements depends to a great extent on the geometry of the structure and to some extent on individual preference, as there is more than one element that can be

used to create the FE model. For most complex structures a combination of several types of elements is necessary for an (efficient and) accurate analysis.

A complex structure is usually assembled from different components through a number of joints. Unfortunately, the modelling of structural joints is still an under-developed area in structural dynamics and their idealisation normally assumes the elements/nodes between joints to be perfectly connected through fixed-fixed interfaces. Some FE analysts suggest that the nodes between joints may not be directly connected and some forms of joint stiffnesses must be defined. However, this immediately increases the number of degrees of freedom in the model and usually the spring values of a joint are not well-defined in all rotational directions.

Nothing has yet been said regarding the modelling of damping. For most engineering structures the damping values are both small and ill-defined so that the damping matrix cannot be **modelled** in the same detail as the mass and stiffness matrices of the structure. Finally, the boundary conditions of a test structure and an FE model cannot be matched exactly as it is very difficult either (i) to achieve a free-free or perfect clamped conditions in practice or (ii) to model the elastic boundaries of the measurement stage in detail.

## 4.4 THE USEFULNESS AND LIMITATION OF CORRELATION TECHNIQUES

There are several techniques available for correlating the modal data obtained from FE analysis and from experimental modal analysis which can be used to quantify the comparison between two sets of modal data and to represent the correlation of modal data in terms of real- or complex-valued numbers. In order to explore the

characteristics of these correlation techniques in a broader sense, the formulae given below assume that the mode shape vectors are complex.

1.  Cross Orthogonality Method (COM)

$$[COM(A,X)] = [\Phi_A]^H [M_A] [\Phi_X] \tag{4.2}$$

2.  Mixed Orthogonality Check (MOC)

$$[MOC(A,X)] = [\Phi_X]^H [M_A] [\Phi_X] \tag{4.3}$$

3.  Modal Assurance Criterion (MAC)

$$MAC(A_j,X_k) = \frac{|\{\phi_A\}_j^H\{\phi_X\}_k|^2}{|\{\phi_A\}_j^H\{\phi_A\}_j| \, |\{\phi_X\}_k^H\{\phi_X\}_k|} \tag{4.4}$$

Both the cross orthogonality method and the mixed orthogonality check [35] include the analytical mass matrix in their formulation and will produce meaningful results only when the number of coordinates for the experimentally-derived mode shape vectors is equivalent to the number of DoFs in the analytical model.

In contrast, the modal assurance criterion (MAC) [36] requires only the eigenvectors and is therefore ideally suited to quantifying the correlation of two incomplete sets of mode shape vectors. However, the MAC values do not present the whole picture of correlation because these values cannot identify whether random scatter or systematic error is responsible for the deviations. It can be seen that the MAC values vary between zero and unity, the former limit indicating no correlation and the latter complete correlation. An alternative correlation technique called COMAC (coordinate modal assurance criterion) was proposed by Lieven and Ewins [37] to identify the coordinates at which the test/model do not agree. The COMAC for coordinate i is defined as :

$$COMAC(i) = \frac{(\sum\limits_{r=1}^{L}|(_i\psi_{Ar})(_i\psi_{Xr}{}^*)|)^2}{\sum\limits_{r=1}^{L}(_i\psi_{Ar})^2\sum\limits_{r=1}^{L}(_i\psi_{Xr}{}^*)^2} \qquad (4.5)$$

where L is the total number of well-correlated modes as indicated by the MAC. Again a value close to 1 suggests good correlation.

For the case of proportional damping and no repeated modes, each mode shape vector of a structure is orthogonal to all other mode shape vectors of the structure when weighted by the mass, stiffness, or damping matrices. In addition, the mode shape vectors obtained either from the FE analysis or from experimental results are mass-normalised and this orthogonality relationship is stated as :

$$\{\phi_i\}^H [M] \{\phi_j\} = \delta_{ij} \qquad (4.6)$$

where $\delta_{ij}$ is Kronecker delta and should be equal to 1 when i=j.

When the structure has a diagonal mass matrix with identical elements, the mode shape vectors are orthogonal to each other directly, and so in comparison the MAC value of the mode shape vectors with themselves is unity. However, the mass matrix for mechanical structures does not in general possess this diagonal property and the mass elements are seldom identical. As a result, the mode shape vectors are not orthogonal to each other directly. Therefore, even though the value of all diagonal terms is unity, the MAC matrix obtained by comparing the mode shape vectors with themselves is no longer unity because some off-diagonal terms are nonzero.

In general, a MAC value close to unity indicates that the mode shape vectors concerned are consistent. This does not necessarily mean that they are correct because the mode shape vectors can be consistent for a number of reasons, including :

1.  the mode shape vectors have been incompletely measured. This situation can occur whenever incomplete response coordinates have been included in the experimental determination of the mode shape vector. This is analogous to the aliassing problem associated with digital spectral analysis for which the existence of very high frequencies in the original signal may well be misinterpreted if the sampling rate is too slow; and,

2.  the mode shape vectors represent the same mode shape vector with a different arbitrary scaling factor.

In conclusion, it is very important to notice that the modal assurance criterion can only indicate consistency, not validity.

## 4.5 MODEL UPDATING

Due to the sophisticated developments in measurement and modal parameter extraction techniques, it is usually assumed that the experimental **FRFs** or experimentally-derived modal data are correct or at least close to the true representation of a test structure. On the other hand, there inevitably exist idealisations in structural modelling, and the properties of joints and damping have not been fully explored and, thus, the dynamic responses obtained from the FE analysis are reckoned to be less correct. However, the FE model does contain the spatial properties of the structure which are required for structural sensitivity, modification and optimization analysis. Therefore, model updating is one of the most active research topics in current structural dynamics research.

## 4.5.1    DIRECT-MATRIX UPDATE METHOD

In 1965, there was an interesting problem [38] titled "A Least Squares Estimate of Satellite Attitude" given in SIAM (Society of Industrial and Applied Mathematics) Review. The mathematical problem was that if two sets of $N$ data points, [V] and [V]*, are given, can we find the rotation matrix [M] which brings the first set into the best least squares coincidence with the second set. That is, find [M] which minimizes .

$$\sum_{r=1}^{n} \| \{v\}_r^* - [M](v), \|^2 \qquad (4.7)$$

The solution was given by Farrell *et.al.* [39] in SIAM Review, one year later. In 1968, **Brock** presented a paper [40] named "Optimal Matrices Describing Linear Systems" in which the method of determination of optimal symmetric positive-definite compliance matrices for structural elements was developed based on the theory given in [39]. In 1976, Bar-Itzhack, Mayer **&** Fuhermann [41] and Bar-Itzhack **&** Meyer [42] presented a computation procedure for determining the Direction Cosine Matrix which plays a key role in strapdown attitude determination, especially in navigation, control and simulation of aerospace vehicles. Based on the work done in navigation [38-42], Baruch and Bar-Itzhack [43] presented the direct-matrix update method (DMU) to correct the analytical stiffness matrix using experimental data through a minimisation process. Since then, different formulations to correct the mass and stiffness matrix using modal data have been developed and investigated by Berman [44], **Wei** [45] and Caeser [46]. In general, the DMU method uses mass and stiffness matrices [$M_A$] and [$K_A$] from the FE analysis (assumed to be incorrect) and experimentally-derived modal data (assumed to be correct). The mathematical techniques employed are elegant. In Berman's paper, a high rank matrix was obtained

by post- and pre-multiplying a low rank matrix by the analytical mass matrix $[M_A]$. The analysis given in his paper is quoted below:

> "$[M_A]$ is an ($N x N$) analytical mass matrix and $[\Phi]$ is an ($N x m$) measured modal matrix. $m$ is the number of modes and N is the number of degrees of freedom which must correspond to the measurement points on the structure and $m < N$. The measured individual modes have been normalized so that $\{\phi_i\}^T[M_A]\{\phi_i\}=1$. [AM] represents changes in the mass matrix required to satisfy the orthogonality relationship:
>
> $$[\Phi]^T[M_A+\Delta M][\Phi] = [I]$$
>
> or
>
> $$[\Phi]^T[\Delta M][\Phi] = [I] - [m_A] \tag{1}$$
>
> where $[m_A]$ is the nondiagonal $[\Phi]^T[M_A][\Phi]$ having unit diagonal elements. Since $[\Phi]$ is rectangular (and has no inverse) there are an infinite number of [AM] matrices which will satisfy equation (1). It is possible to find that [AM] which has some minimum weighted Euclidean norm within the constraint of equation (1).
>
> It is physically reasonable and mathematically convenient to minimize the function
>
> $$\epsilon = II[N]^{-1}[\Delta M][N]^{-1} II \tag{2}$$
>
> where $[N] = [M_A]^{1/2}$ as in [43]. Note that it is not necessary to compute $[N]$ since only $[N]^2 = [M_A]$ appears in the final result.
>
> Defining a Lagrangian multiplier $\lambda_{ij}$ for each element in equation (1), the following Lagrangian function may be rewritten:
>
> $$\psi = \epsilon + \sum_{i=1}^{m} \sum_{i=1}^{m} \lambda_{ij} ([\Phi]^T[\Delta M][\Phi] - [I] + [m_A]) \tag{3}$$
>
> Differentiating equation (3) with respect to each element of [AM] and setting these results equal to zero will satisfy the minimisation of equation (2) if the constraint of equation (1) is also satisfied. This process results in the matrix equation
>
> $$2[M_A]^{-1}[\Delta M][M_A]^{-1} + [\Phi][\Lambda]^T[\Phi]^T = [0]$$
>
> or
>
> $$[AM] = -\frac{1}{2}[M_A][\Phi][\Lambda]^T[\Phi]^T[M_A] \tag{4}$$
>
> where [A] is a square ($m x m$) matrix of $\lambda_{ij}$.
>
> Substituting equation (4) into equation (1) allows the solution for [A]
>
> $$[\Lambda] = -2[m_A]^{-1}([I] - [m_A])[m_A]^{-1} \tag{5}$$

which is then substituted into equation (4) to obtain

$$[\Delta M] = [M_A][\Phi] \, ([m_A])^{-1} \, ([I] - [m_A]) \, ([m_A])^{-1} \, [\Phi]^T[M_A] \quad (6)''$$

However, it must be noted that, in general, it is not physically reasonable to minimise the function $\varepsilon$ defined in [44] because in doing so, the problem in determining the exact mass error matrix is changed to finding a mass modification matrix which can reproduce the measured properties of the structure without considering the banded nature of the system mass matrix. In most cases the connectivity of the structure will not be preserved as the only constraint imposed is to minimize the summation of all elements of $[N]^{-1}[\Delta M][N]^{-1}$.

For a modal incomplete case (i.e. not all modes included, but all coordinates included), the eigenvector matrix $[\Phi]$ is rectangular and there exists a pseudo-inverse (Moore-Penrose generalised inverse) which satisfies the following relationship:

$$[\Phi]^+ \, [\Phi] = [\, I \,] \qquad\qquad (4.8)$$

The pseudo-inverse $[\Phi]^+$ can be obtained by calculating the singular value decomposition (SVD) of $[\Phi]$ $(=[U][\Sigma][V]^T)$ and the product of $[V][\Sigma]^+[U]^T$. This pseudo-inverse is a least-squares solution that minimizes a Frobenius norm of the problem : $\min_{[\Phi] \in R^{n \times m}} \| [\Phi][\Phi]^+ - [I]_{nxn} \|_F.$

There also exists a pseudo-inverse $([\Phi]^T)^+$ which is a right-inverse of $[\Phi]^T$ and which satisfies :

$$[\Phi]^T \, ([\Phi]^T)^+ = [\, I \,] \qquad\qquad (4.9)$$

This pseudo-inverse has a similar characteristic to the pseudo-inverse of $[\Phi]$ that minimizes a Frobenius norm of the problem : $\min_{([\Phi]^T)^+ \in R^{n \times m}} \| ([\Phi]^T)^+[\Phi]^T - [I]_{nxn} \|_F.$

The orthogonality relationship of the test structure can be written in the following form
.

$$[\Phi]^T[\Delta M] [\Phi] = [I] - [m_A] \tag{4.10}$$

where

$$[m_A] = [\Phi]^T[M_A][\Phi] \tag{4.11}$$

Rx-e-multiplying both sides of equation (4.10) by $([\Phi]^T)^+$ and post-multiplying both sides of equation (4.10) by $[\Phi]^+$ gives:

$$([\Phi]^T)^+[\Phi]^T[\Delta M] [\Phi][\Phi]^+ = ([\Phi]^T)^+([I] - [M_A])[\Phi]^+ \tag{4.12}$$

At this juncture, it is advantageous to examine what has been done in **[44]**. By substituting $[m_A] = [\Phi]^T[M_A][\Phi]$ into equation (6) of **Ref.[44]** we obtain

$$[\Delta M_{BERMAN}] \overset{\Delta}{=} [M_A][\Phi] ([\Phi]^T[M_A][\Phi])^{-1} ([I] - [m_A]) ([\Phi]^T[M_A][\Phi])^{-1} [\Phi]^T[M_A] \tag{4.13}$$

Pre-multiplying equation (4.13) by $[\Phi]^T$ and post-multiplying it by $[\Phi]$ gives equation (4.10), but equation (4.13) is mathematically inaccurate. It can be shown that $[M_A][\Phi]([\Phi]^T[M_A][\Phi])^{-1}$ is a right-inverse of $[\Phi]^T$ and $([\Phi]^T[M_A][\Phi])^{-1} [\Phi]^T[M_A]$ is a left-inverse of $[\Phi]$. They are equivalent to the pseudo-inverse of $[\Phi]^T$ and the pseudo-inverse of $[\Phi]$ when $[M_A]$ is a unit mass matrix. This explains why, in most cases, numerical results obtained from the R.H.S. of equation (6) of **Ref.[44]**, do not give the correct mass error matrix [AM] and do not preserve the model connectivity.

In conclusion, it is found that equation (6) of **Ref.[44]** is mathematically incorrect unless a complete modal vector matrix is used (trivial solution) so that alternative model updating methods must be developed.

## 4.5.2      ORTHOGONALIN CONSTRAINT METHOD

It has been shown that it is impossible to determine the mass error matrix by pre-multiplying and post-multiplying the orthogonality relationship of the mass matrix by rectangular matrices. In practice, it is reasonable to assume that the mass and stiffness matrices should be updated/changed in such a fashion that the connectivity and physical characteristics of an FE/analytical model are preserved. This implies that the mass and stiffness elements of the original FE/analytical model are only scaled by arbitrary factors. In such a case, the orthogonality relationship can be transformed to a set of simultaneous equations. For a structure with diagonal mass matrix, for example, the following set of equations can be derived :

$$
\begin{aligned}
\phi_{11}\alpha_1 m_1 \phi_{11} + \phi_{12}\alpha_2 m_2 \phi_{12} + \quad \ldots \quad + \quad \phi_{1N}\alpha_N m_N \phi_{1N} \;&=\; 1 \\
\phi_{11}\alpha_1 m_1 \phi_{21} + \phi_{12}\alpha_2 m_2 \phi_{22} + \quad \ldots \quad + \quad \phi_{1N}\alpha_N m_N \phi_{2N} \;&=\; 0 \\
\cdots \qquad\qquad\qquad\qquad \cdots\qquad\qquad\qquad\qquad\quad \\
\cdots \qquad\qquad\qquad\qquad\qquad\qquad\qquad\qquad\quad \cdots \\
\cdots \qquad\qquad\qquad\qquad\qquad\qquad \cdots\qquad\qquad\qquad \\
\phi_{m1}\alpha_1 m_1 \phi_{m\text{-}1\ 1} + \phi_{m2}\alpha_2 m_2 \phi_{m\text{-}1\ 2} + \ldots + \phi_{mN}\alpha_N m_N \phi_{m\text{-}1\ N} \;&=\; 0 \\
\phi_{m1}\alpha_1 m_1 \phi_{m1} + \phi_{m2}\alpha_2 m_2 \phi_{m2} + \quad \ldots \quad + \quad \phi_{mN}\alpha_N m_N \phi_{mN} \;&=\; 1
\end{aligned}
$$

$$(4.14)$$

Here, there are $m^2$ equations but some of them are identical pairs because of the symmetrical property of the orthogonality relationship. Hence, there are *(m+1)m/2* equations in N unknowns so that this system of equations is overdetermined if

$(m+1)m/2$ is greater than N. As a result, the mathematical problem of model updating is simplified to that of determining the least-squares(LS) solution of a system of equations, ie., the minimisation of $\|$ [A] $\{ x$ $-\{b\}$ $\|_2$ where

$$[A] = \begin{vmatrix} \phi_{11}\phi_{11} & \phi_{12}\phi_{12} & \cdots & \phi_{1N}\phi_{1N} \\ \phi_{11}\phi_{21} & \phi_{12}\phi_{22} & \cdots & \phi_{1N}\phi_{2N} \\ & \cdot & & \\ & & \cdot & \\ & \cdot & & \\ \phi_{m1}\phi_{m1} & \phi_{m2}\phi_{m2} & \cdots & \phi_{mN}\phi_{mN} \end{vmatrix} \quad \{x\} = \begin{Bmatrix} \alpha_1 m_1 \\ \alpha_2 m_2 \\ \\ \alpha_N m_N \end{Bmatrix} \quad and(b) = \begin{vmatrix} 1 \\ 0 \\ \cdot \\ 1 \\ 0 \\ \cdot \\ 1 \end{vmatrix}$$

(4.15)

If [A] is rank-deficient, then the LS problem has an infinite number of solutions, but there is just one possessing a minimal 2-norm. We denote this unique solution by $\{x\}_{LS}$ and the minimum sum of squares by $\rho_{LS}^2$: $\rho_{LS}^2 = \|$ [A]$\{x\}_{LS}-\{b\}$ $\|_2^2$. The best available technique to solve this problem employs the Moore-Penrose generalised inverse with SVD.

Following a similar analysis a stiffness error matrix can be determined. The stiffness matrix of an analytical model satisfies the following orthogonality relationship :

$$[\Phi]^T[K_A+\Delta K] [\Phi] = [\ulcorner\omega^2\lrcorner]$$  (4.16)

Again, the stiffness error matrix cannot be determined by pre-multiplying andpost-multiplying this equation by square or rectangular matrices. A tridiagonal stiffness matrix is shown below to illustrate that it is possible to transform this unsolved problem into a set of simultaneous equations that may have a unique solution. For this particular case, equation (4.16) is rewritten as follows :

$$\begin{bmatrix} \phi_{11} & \cdots & \phi_{1N} \\ & \cdot & \\ \phi_{m1} & \cdots & \phi_{mN} \end{bmatrix} \begin{bmatrix} \alpha_1 k_1 + \alpha_2 k_2 & -\alpha_2 k_2 & \cdot & & 0 \\ -\alpha_2 k_2 & \alpha_2 k_2 + \alpha_3 k_3 & & & 0 \\ \cdot & & & \cdot & \\ 0 & & \alpha_{N-1}k_{N-1}+\alpha_N k_N & -\alpha_N k_N & \\ 0 & \cdot & -\alpha_N k_N & \alpha_N k_N + \alpha_{N+1}k_{N+1} \end{bmatrix} \begin{bmatrix} \phi_{11} \cdot \phi_{m1} \\ \cdot & \cdot \\ \cdot & \cdot \\ \cdot & \cdot \\ \phi_{1N} \cdot \phi_{mN} \end{bmatrix} = \begin{bmatrix} \ddots & \\ & \omega_r^2 \\ & & \ddots \end{bmatrix}$$

$$(4.17)$$

Analogous to the preceding paragraph, the above orthogonality relationship can be transformed into a set of *(m+1)m/2* simultaneous equations in *(N+1)* unknowns. This system of equations is overdetermined when *(m+1)m/2* is greater than *(N+1)*.

For most structural dynamics problems, the mass and stiffness **matrices** of an FE/analytical model are generally sparse because "many" of their elements are equal to zero. Assuming that the *NxN* **mass(or** stiffness) matrix has *p* mass (or *q* spring) elements. For a well-defined FE model, it is generally true that the connectivity is correct even though the mass and spring elements may not be assigned the right values. As a result, it can be shown that *m* specified normal modes are required to determine mass and stiffness error matrices where *(m+1)m/2* is greater than or equal to **max(***p,q***)** by using the orthogonality property of the mass and stiffness matrices.

### 4.5.3        EIGENDYNAMIC CONSTRAINT METHOD

The orthogonality constraint method can recover the values of mass and spring elements for the FE model of a mechanical structure. However, Lin **[47]** has shown that the formulation based on the orthogonality relationships is mathematically incomplete in the sense that some information of the measured modes has been lost during the formulation of the problem. In 1985, **Gladwell** and Gbadeyan **[48]** presented a stripping procedure for constructing the mass and stiffness parameters of

the discrete model from a knowledge of some of the measured modes. Their analysis concentrated on a specific fixed-free mass-spring chain system. After developing the stripping procedure, Gladwell[49] established the necessary and sufficient conditions for a given vector to be one of the eigenvectors of the system and proved that it is possible to reconstruct the simple chain system by using two modes which satisfy certain conditions, although the thus-reconstructed system is not unique in the sense that it can be scaled by an arbitrary factor. The eigendynamic constraint method generalises Gladwell's theory for structural identification and model updating of general mechanical structures. This method is based on the information of measured modal data, eigenvalues and eigenvectors, and by making use of the mass normalisation property of measured modes, the problem of non-uniqueness of the identified system is resolved.

The eigendynamic constraint method is formulated based on the following the equation for free motion for a mechanical structure and mass normalisation relationship:

$$-\omega_i^2[M_A+\Delta M]\{\phi\}_i + [K_A+\Delta K]\{\phi\}_i = \{0\} \tag{4.18}$$

$$\{\phi\}_i^T [M_A+\Delta M]\{\phi\}_i = 1 \tag{4.19}$$

As mentioned before, the physical connectivity of the FE/analytical model is usually preserved for model updating problems, and so it can be assumed that the updated model should have the same connectivity as that of the original FE/analytical model. When the connectivity information is employed, equations (4.18) and (4.19) can be combined and, after some mathematical manipulation, turned into a system of linear algebraic equations :

$$[L]_{(N+1)x(p+q)}\{P\}_{(p+q)x1} = \{J\}_{(N+1)x1} \tag{4.20}$$

the discrete model from a knowledge of some of the measured modes. Their analysis concentrated on a specific fixed-free mass-spring chain system. After developing the stripping procedure, Gladwell[49] established the necessary and sufficient conditions for a given vector to be one of the eigenvectors of the system and proved that it is possible to reconstruct the simple chain system by using two modes which satisfy certain conditions, although the thus-reconstructed system is not unique in the sense that it can be scaled by an arbitrary factor. The eigendynamic constraint method generalises Gladwell's theory for structural identification and model updating of general mechanical structures. This method is based on the information of measured modal data, eigenvalues and eigenvectors, and by making use of the mass normalisation property of measured modes, the problem of non-uniqueness of the identified system is resolved.

The eigendynamic constraint method is formulated based on the following the equation for free motion for a mechanical structure and mass normalisation relationships:

$$-\omega_i^2[M_A + \Delta M]\{\phi\}_i + [K_A + \Delta K]\{\phi\}_i = \{0\} \tag{4.18}$$

$$\{\phi\}_i^T [M_A + \Delta M]\{\phi\}_i = 1 \tag{4.19}$$

As mentioned before, the physical connectivity of the FE/analytical model is usually preserved for model updating problems, and so it can be assumed that the updated model should have the same connectivity as that of the original FE/analytical model. When the connectivity information is employed, equations (4.18) and (4.19) can be combined and, after some mathematical manipulation, turned into a system of linear algebraic equations :

$$[L]_{(N+1)x(p+q)}\{P\}_{(p+q)x1} = \{J\}_{(N+1)x1} \tag{4.20}$$

where {P} is a vector containing the unknown total design variables in the mass and stiffness matrices; [L] and {J} are the coefficient matrix and vector formed using the modal data of mode $i$.

To illustrate how [L] and {J} are constructed, a simple mass-spring chain model with fixed-fixed boundary condition is used. For this specific model, when the first mode is used, equations (4.18) and (4.19) can be written as :

$$-\omega_1^2\phi_{11}\alpha_1 m_1 + \phi_{11}\alpha_{N+1}k_1 + (\phi_{11}-\phi_{12})\alpha_{N+2}k_2 \qquad = \quad 0$$

$$\cdot \qquad \cdot \qquad \qquad \cdot \qquad \qquad \cdot$$

$$\cdot \qquad \qquad \cdot \qquad \qquad \cdot$$

$$-\omega_1^2\phi_{1N}\alpha_N m_N + (-\phi_{1N-1}+\phi_{1N})\alpha_{2N}k_N + \phi_{1N}\alpha_{2N+1}k_{N+1} = 0$$

$$\phi_{11}\phi_{11}\alpha_1 m_1 + \phi_{12}\phi_{12}\alpha_2 m_2 + \cdots\cdots + \phi_{1N}\phi_{1N}\alpha_N m_N \quad = \quad 1 \qquad\qquad (4.21)$$

Therefore, the matrix [L] and the vectors {P} and {J} are

$$[L] \; = \; \begin{bmatrix} -\omega_1^2\phi_{11}\, 0 \;\cdot\; \cdot\; 0 & \phi_{11} & \phi_{1\bar{1}}\phi_{12} & 0 & \cdot\cdot\; 0 \\ 0 -\omega_1^2\phi_{12}\, 0 \cdot 0 & 0 & -\phi_{11}^+\phi_{12}\;\phi_{1\bar{2}}\,\phi_{13} & 0 & \cdot\; 0 \\ \cdot \qquad \cdot & \cdot & \cdot & \cdot & \cdot \\ \cdot \qquad \cdot & \cdot & \cdot & \cdot & \cdot \\ 0 \cdot\; \cdot\; 0 -\omega_1^2\phi_{1N}\, 0 & \cdot\; \cdot & 0 & -\phi_{1N-1}^+\phi_{1N} & \phi_{1N} \\ \phi_{11}^{\,2} \;\; \phi_{12}^2 \;\cdot\; \phi_{1N}^2\, 0 \cdot & \cdot & \cdot & \cdot & 0 \end{bmatrix}$$

$$\{P\} \; = \; \begin{Bmatrix} \alpha_1 m_1 \\ \cdot \\ \cdot \\ \alpha_N m_N \\ \alpha_{N+1}k_1 \\ \cdot \\ \cdot \\ \alpha_{2N+1}k_{N+1} \end{Bmatrix} \quad \& \; \{V\} \; = \; \begin{Bmatrix} 0 \\ \cdot \\ \cdot \\ 0 \\ \cdot \\ \cdot \\ 1 \end{Bmatrix} \qquad\qquad (4.22)$$

When there are *m* modes available, the total number of linear algebraic equations becomes *(N+1)m* and, again, if *(N+1)m* is greater than the number of unknowns in {P}, the problem becomes overdetermined and generalised inverse techniques (least-squares) can be used to solve for {P} .

## Minimum number of measured modes in modal updating :-

For an FE model, the following two conditions can be considered:

$(m+1)m/2 \geq max(p,q)$            for orthogonality constraint method

$(N+1)m \geq (p+q)$            for eigendynamic constraint method

       where *m* is the number of measured modes, N is the number of **DoFs** and

       *p,q are the* numbers of mass and spring elements for the system respectively.

It is not unusual for the number of measured modes required to determine the mass error and stiffness error matrices to be reduced by using the eigendynamic constraint method. A unique solution for the mass and stiffness error matrices can be obtained provided that the second inequality shown above is satisfied.

4.5.4       NUMERICAL EXAMPLES

(a) Direct-matrix update method (Berman- mass updating)

A numerical example of the 10 **DoF** spring-mass model shown in Figure 4.3 is used to demonstrate the application of DMU method. This model has a diagonal unit mass matrix. Suppose that the mass-spring model was incorrectly constructed and that the mass errors lay at points 2, 5 and 8. Berman's "AM" matrix obtained from equation (6) of **Ref.[44]** using six modes of the incorrect model is plotted in Figure 4.4 from

When there are $m$ modes available, the total number of linear algebraic equations becomes $(N+1)m$ and, again, if $(N+1)m$ is greater than the number of unknowns in $\{P\}$, the problem becomes **overdetermined** and generalised inverse techniques (least-squares) can be used to solve for $\{P\}$.

## Minimum number of measured modes in modal updating :-

For an FE model, the following two conditions can be considered:

$(m+1)m/2 \geq \mathbf{max(p,q)}$                    for orthogonality constraint method

$(N+1)m \geq (p+q)$                    for eigendynamic constraint method

where $\boldsymbol{m}$ is the number of measured modes, N is the number of **DoFs** and $\boldsymbol{p,q}$ $\boldsymbol{are}$ $\boldsymbol{the}$ numbers of mass and spring elements for the system respectively.

It is not unusual for the number of measured modes required to determine the mass error and stiffness error matrices to be reduced by using the eigendynamic constraint method. A unique solution for the mass and stiffness error matrices can be obtained provided that the second inequality shown above is satisfied.

### 4.5.4    NUMERICAL EXAMPLES

(a) Direct-matrix update method (Berman- mass updating)

A numerical example of the 10 **DoF** spring-mass model shown in Figure 4.3 is used to demonstrate the application of DMU method. This model has a diagonal unit mass matrix. Suppose that the mass-spring model was incorrectly constructed and that the mass errors lay at points 2, 5 and 8. Berman's "AM" matrix obtained from equation (6) of **Ref.[44]** using six modes of the incorrect model is plotted in Figure 4.4 from

which it is shown that this solution does not preserve the physical characteristics of the mass-spring model although the peaks in these figures do contain valuable information for mismodelling sites. Figure 4.5 shows the product of left-hand side for equation (4.12). Comparing Figure 4.4 with Figure 4.5 and checking the numerical data show these matrices to be identical. Figure 4.6 shows the actual mass error matrix for this updating problem.



$$M = 1\,kg$$
$$K_1 = 1E4\ N/m$$
$$K_2 = 2E4\ N/m$$
$$K3 = 3E4\ N/m$$

Figure 4.3   A lumped mass-spring model with 10 degrees-of-freedom



Figure 4.4 Berman "AM" matrix



Figure 4.5 The product of right-hand side for eouation (4.12)

Figure 4.6   Exact mass error matrix
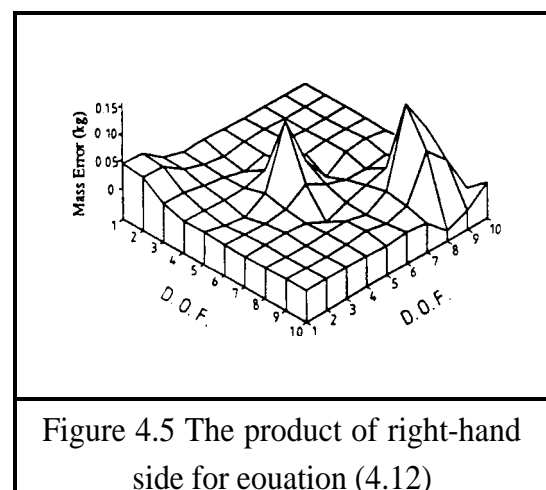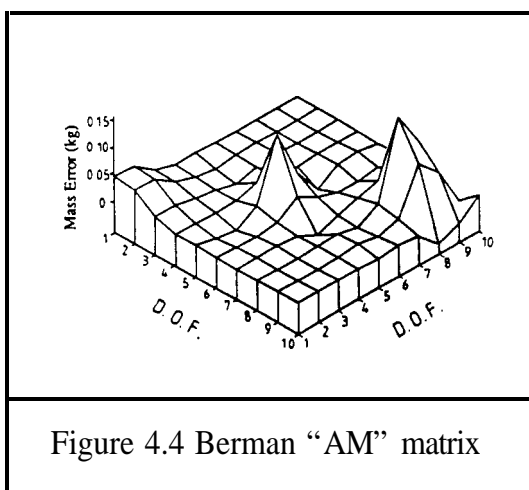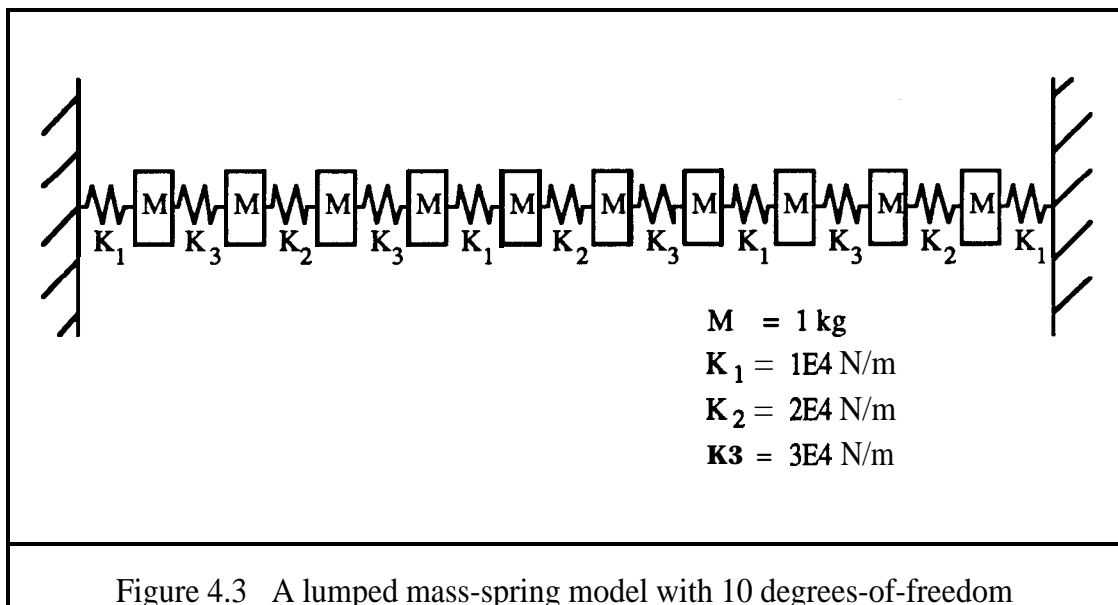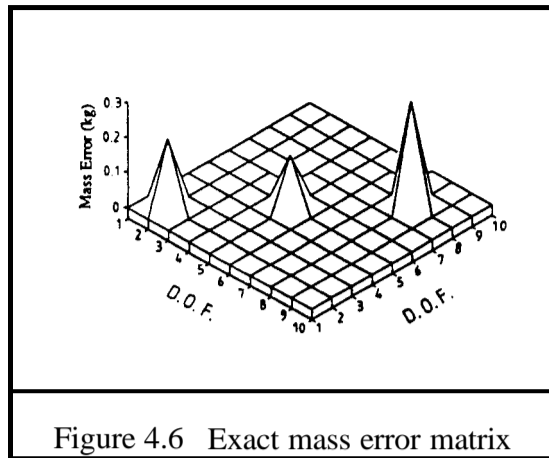
A second 10 DoF spring-mass model shown in Figure 4.7 was used to check the DMU method for a more general mass matrix. Three mass errors were introduced at points 1, 4 and 8 to simulate the mismodelling problem. Berman's "AM" matrix and the product of the left-hand side of equation (4.12) using six modes of the "measured" modes are plotted in Figures 4.8 and 4.9 respectively. The exact mass error matrix for this problem is shown in Figure 4.10. Neither Figures 4.8 nor 4.9 shows a solution with realistic physical characteristics of the mass-spring model. Berman's "AM" matrix was able to provide a better correlation with the expected solution shown in Figure 4.10 because the left-inverse of $[\Phi]^T$ and the right-inverse of $[\Phi]$ were calculated using a weighted function $[M_A]$.

$$M_1 = 1.0 \text{ kg} \quad K_1 = 1E4 \text{ N/m}$$
$$M_2 = 0.2 \text{ kg} \quad K_2 = 2E4 \text{ N/m}$$
$$M_3 = 0.1 \text{ kg} \quad K_3 = 3E4 \text{ N/m}$$
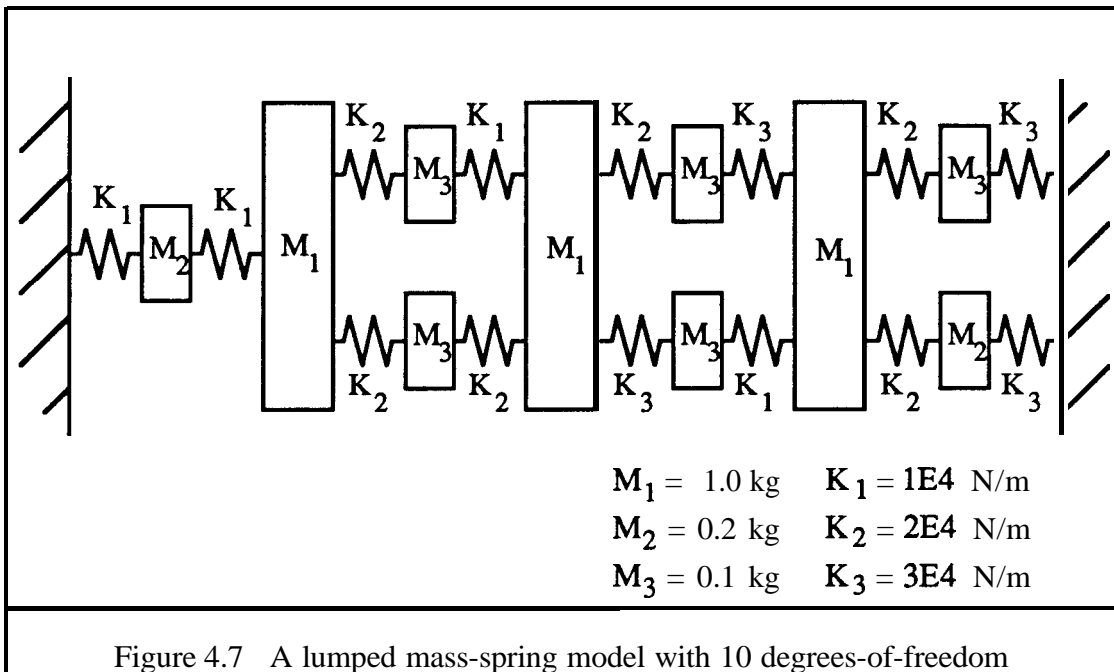
Figure 4.7 A lumped mass-spring model with 10 degrees-of-freedom
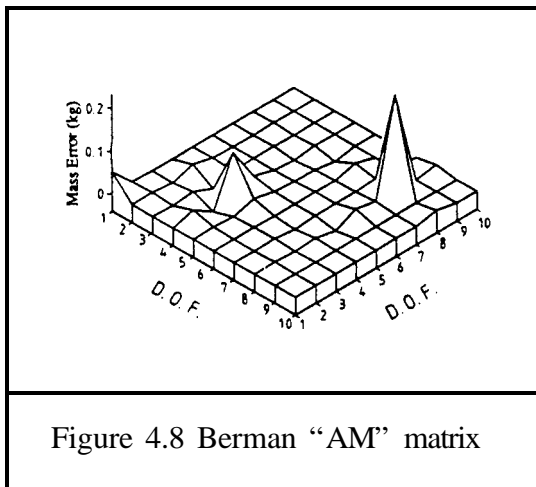


Figure 4.8 Berman "AM" matrix
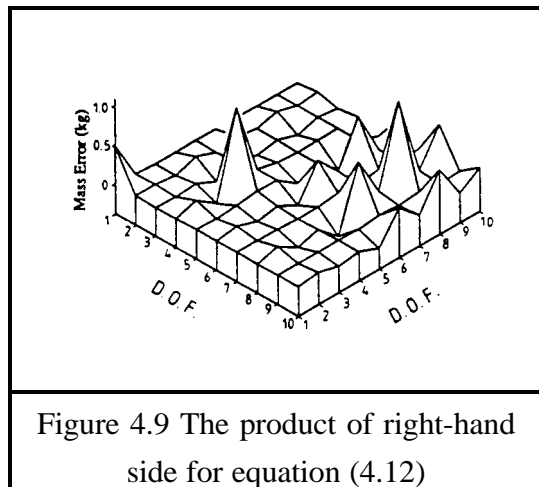


Figure 4.9 The product of right-hand side for equation (4.12)
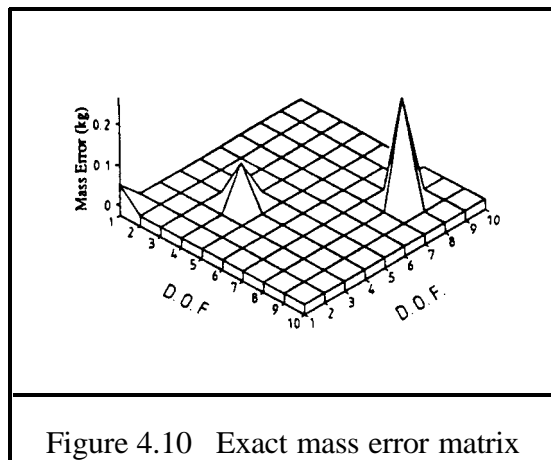


Figure 4.10 Exact mass error matrix

**(b)** Orthogonality Constraint Method

The spring-mass model shown in Figure 4.3 was next used to evaluate the orthogonality constraint method (OCM). Mass errors at points 2, 3, 5 and 8 and stiffness errors between points **2&3, 5&6** and **6&7** were introduced to the original model. It can be seen that five "measured" modes have satisfied the criterion that $(m+1)m/2$ is greater than $\max(p,q)$ where $m, p$ and $q$ have been defined in Section 4.5.3. Berman's "AM" matrix, Baruch's "AK" matrix (using analytical stiffness and correct mass matrices), and mass and stiffness error matrices using the OCM are plotted in Figures 4.11-4.14. As expected, Berman's "AM" and Baruch's "AK" matrices could not exactly locate the mismodelling sites. Comparing Figures 4.13 and 4.14 with the exact mass and stiffness error matrix shown in Figures 4.15 and 4.16, it can be seen that both error matrices were accurately determined by the OCM. Figures 4.17 and 4.18 show the mass and stiffness error matrices obtained when the "measured" five eigenvalues and the corresponding eigenvectors were contaminated by 1 percent and 5 percent Gaussian random noise respectively. It can be seen that those identified matrices are different from the true solution. However, the thus updated model is an optimized model in the sense that it preserves the connectivity of the system and can reproduce the measured **modal** properties quite accurately.
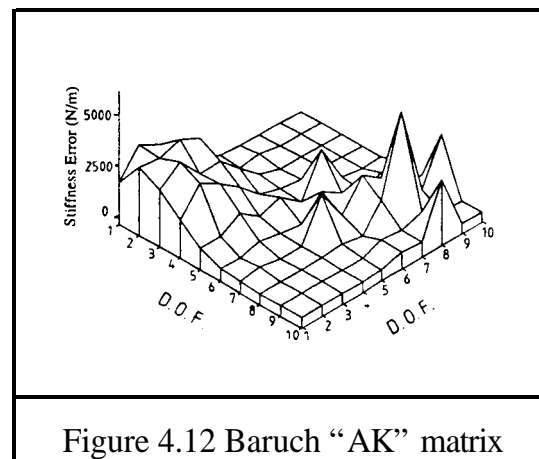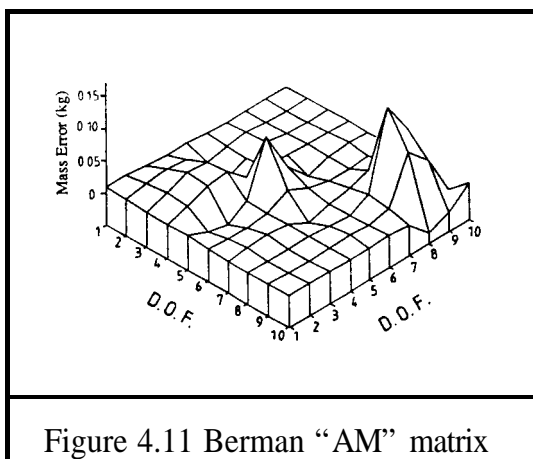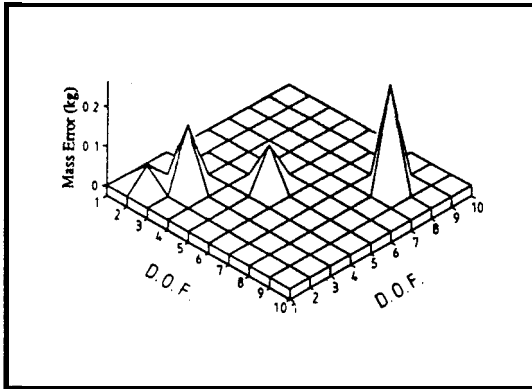


| Figure 4.11 Berman "AM" matrix | Figure 4.12 Baruch "AK" matrix |
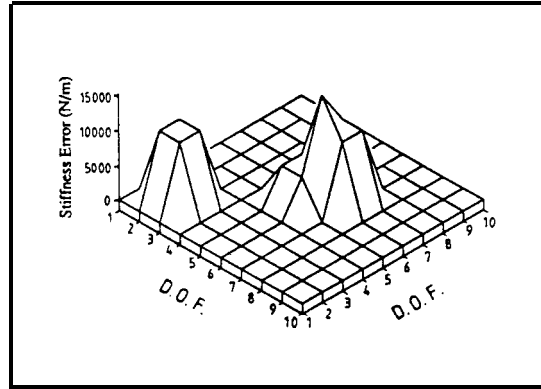
Figure 4.13 Predicted mass error
matrix using the OCM

Figure 4.14 Predicted stiffness error
matrix using the OCM

Figure 4.15  Exact mass error matrix

Figure 4.16 Exact stiffness error matrix

Figure 4.17   Predicted mass error
matrix using the OCM
(Eigenvalues:±1%  Eigenvectors:±5%   )

Figure 4.18 Predicted stiffness error
matrix using the OCM
(Eigenvalues:±1%  Eigenvectors:±5%   )

Figure 4.13 Predicted mass error
              matrix using the OCM

Figure 4.14 Predicted stiffness error
              matrix using the OCM
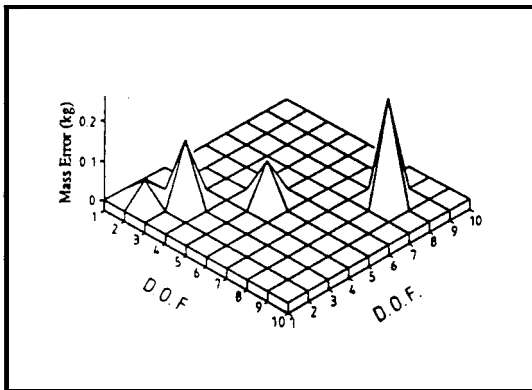
Figure 4.15  Exact mass error matrix
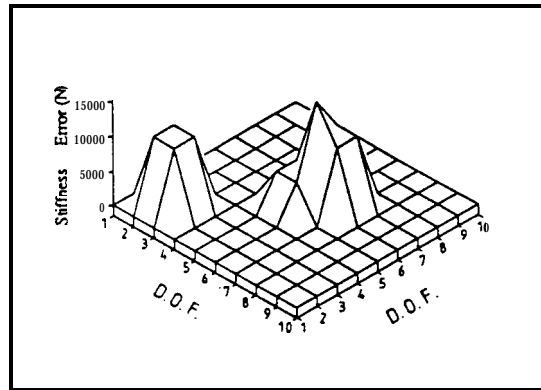
Figure 4.16 Exact stiffness error matrix
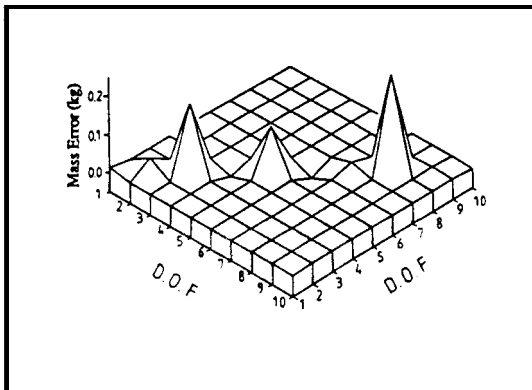
Figure 4.17  Predicted mass error
              matrix using the OCM
(Eigenvalues:±1%  Eigenvectors:±5%   )
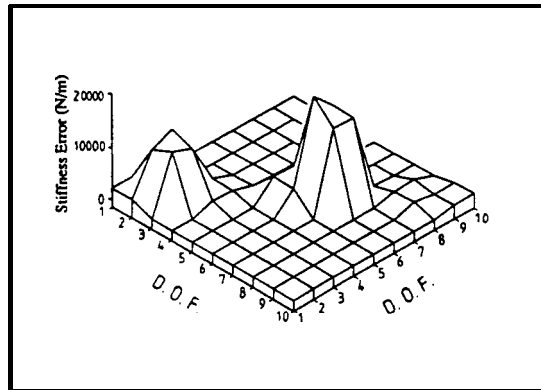
Figure 4.18 Predicted stiffness error
              matrix using the OCM
(Eigenvalues:±1%  Eigenvectors:±5%   )
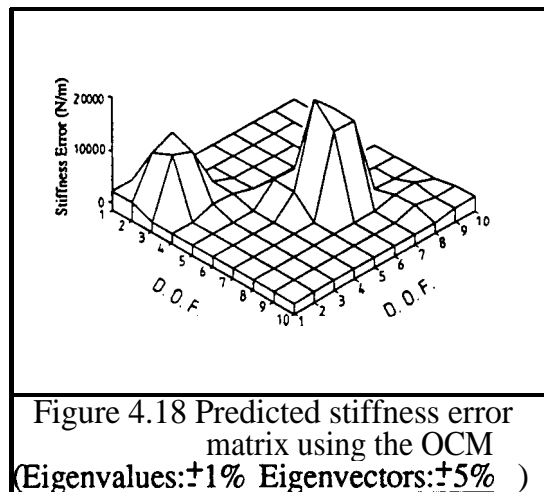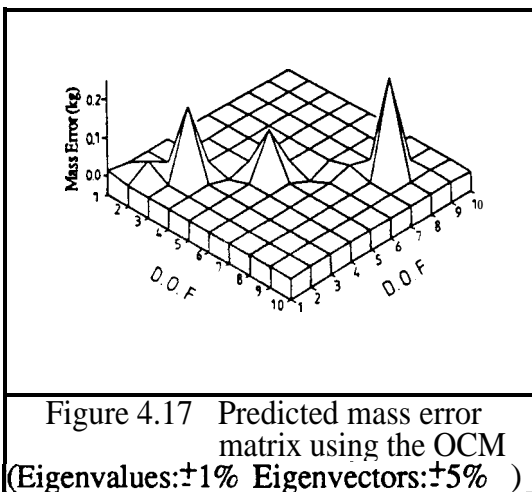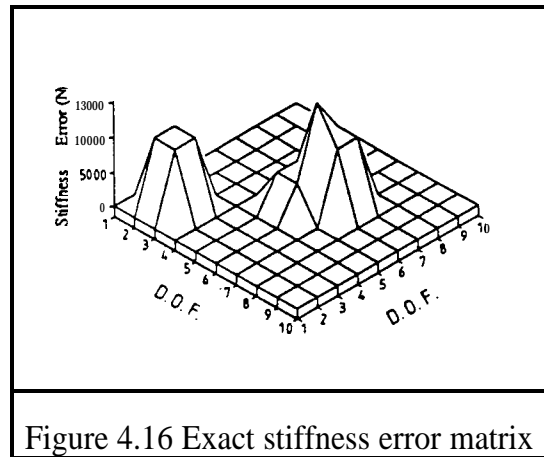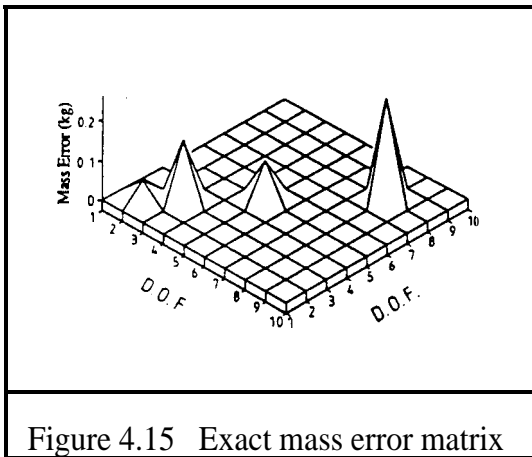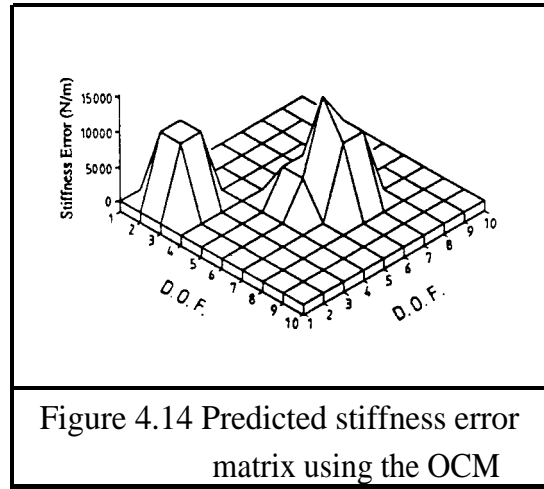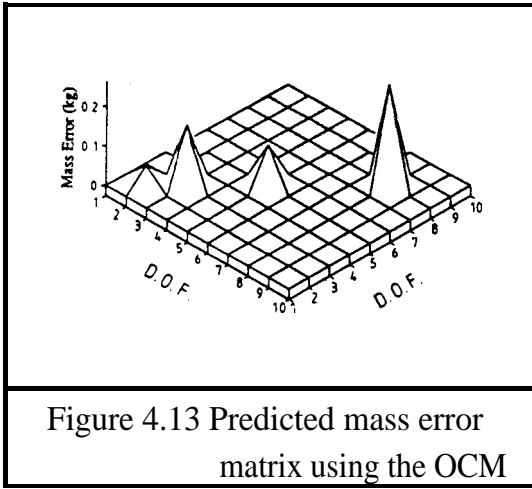
(c) Eigendynamic constraint method

The mass-spring model shown in Figure 4.7 was used to verify the eigendynamic constraint method (ECM) for a model with complicated connectivity. Mass errors at points 1, 4, 7 and 10 and stiffness errors between points **2&3, 5&7** and lo-ground were introduced to provide "measured" dynamic characteristics. In this case three modes satisfy the criterion that *(N+1)m* is greater than *(p+q)* where *m, p* and *q* have been defined in Section 4.5.3. Mass and stiffness error matrices predicted using the ECM are plotted in Figures 4.19 and 4.20. Comparing these figures with the exact mass and stiffness error matrices shown in Figures 4.21 and 4.22, it can be seen that the mass error and stiffness matrices were accurately determined. Figures 4.23 and 4.24 show the mass and stiffness error matrices obtained when the measured three eigenvalues and the corresponding eigenvectors were contaminated by 0.1 percent and 0.2 percent Gaussian random errors respectively. From these figures, it can be seen that the solutions are very sensitive with respect to the simulated random errors because the coefficient matrix [L] in equation (4.19) is very ill-conditioned with respect to the calculation of its pseudo-inverse. The conditioning for the calculation of its pseudo-inverse could be significantly improved when more modes were used.



Figure 4.19 Predicted mass error matrix using the ECM



Figure 4.20 Predicted stiffness error matrix using the ECM
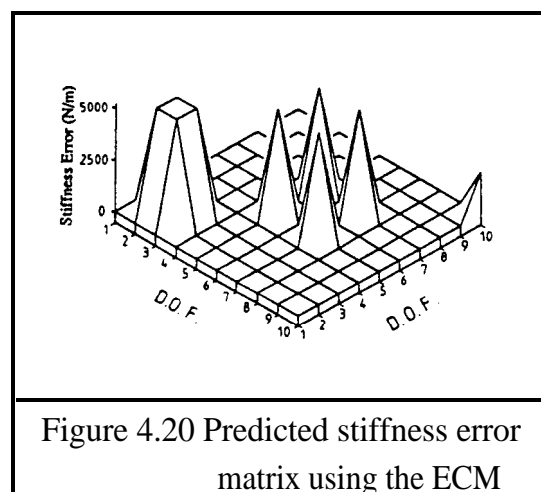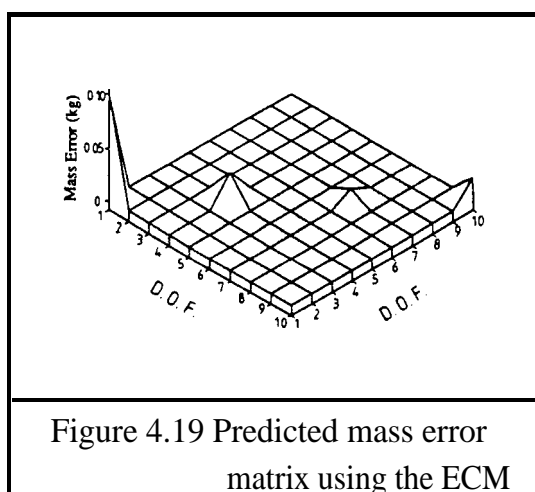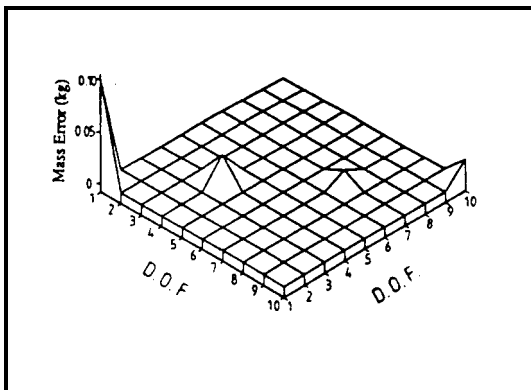
Figure 4.21   Exact mass error matrix
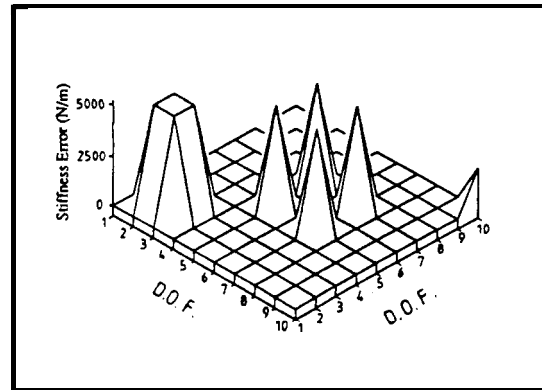


Figure 4.22 Exact stiffness error matrix
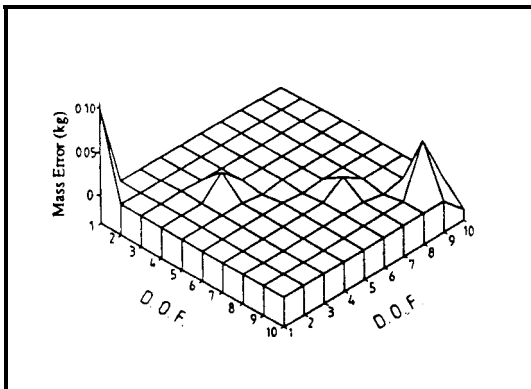


Figure 4.23 Predicted mass error
matrix using the ECM
(Eigenvalues:$\pm$0. 1%
Eigenvectors:$\pm$0.2% )
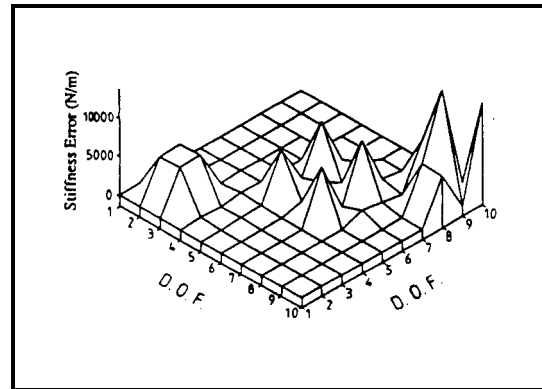


Figure 4.24 Predicted mass error
matrix using the ECM
(Eigenvalues:$\pm$0. 1%
Eigenvectors:$\pm$0.2% )

### 4.5.5     THE EFFECT OF COORDINATE INCOMPLETENESS IN MODEL UPDATING

The method for updating the mass and stiffness matrices for a mechanical structure based on the **orthogonality** relationships of the mass and stiffness matrices has been investigated in Section 4.5.2. In Section 4.5.3, it was noticed that the number of modes required to update or to improve the FE model could be *greatly* reduced by using the ECM. This section extends the ECM to investigate the effect of coordinate incompleteness in model updating. The numerical results show that if the connectivity of an FE model has been given, there are many identified systems which can reproduce the measured modal properties quite accurately when only a few natural

frequencies and responses at a few coordinates of the structure have been measured. Thus-identified systems would be optimum from a mathematical point of view.

In order to assess the effect of coordinate incompleteness in model updating, some numerical calculations have been carried out using the 10 **DoF** spring-mass systems shown in the preceding section.

The simple mass-spring system shown in Figure 4.3 consists of ten masses and eleven springs. Two special cases were investigated in which only the first two modes, specified for only half of the coordinates, were available. Since the ECM requires all the coordinates in the formulation of the updating problem, the unmeasured coordinates were therefore expanded using the analytical model itself based on Kidder's [50] method. Only two stiffness errors were introduced - between points **3&4** and **6&7** - and no mass error was added to the original model. The exact stiffness error matrix is shown in Figure 4.25. For the first case, coordinates $x3, x_4$, $x_6, x_7$ and $x_9$ have been measured, which included the stiffness errors introduced between coordinates $x_3$-$x_4$ and $x_6$-$x_7$. The identified stiffness error matrix was accurately determined as shown in Figure 4.26 and zero mass error was also identified. For the second case, only coordinates $x_1, x_3, x_5, x_7$ and $x_9$ have been measured. The predicted stiffness error and mass error matrices are shown in Figures 4.27 and 4.28. Clearly these matrices are different from the true solution. However, they can produce an optimized model in the sense that the updated model is able to reproduce the measured modal properties quite accurately.

Figure 4.25   Exact stiffness error matrix



Figure 4.26 Predicted stiffness error matrix (only measured coordinates contain errors)



Figure 4.27   Predicted mass error matrix (some unmeasured coordinates contain errors)



Figure 4.28 Predicted stiffness error matrix (some unmeasured coordinates contain errors)
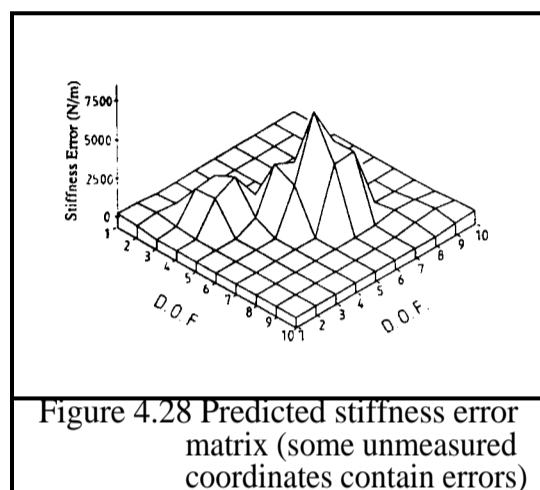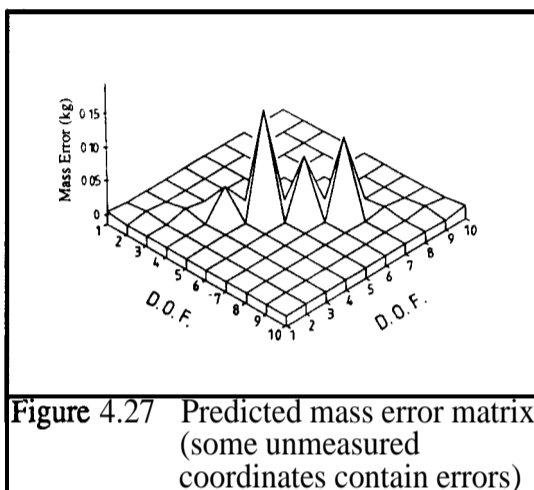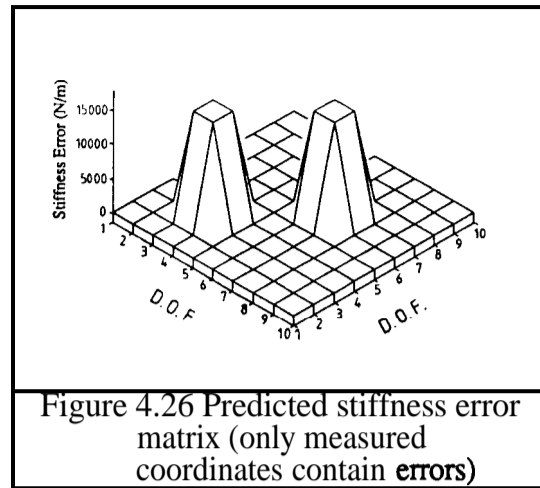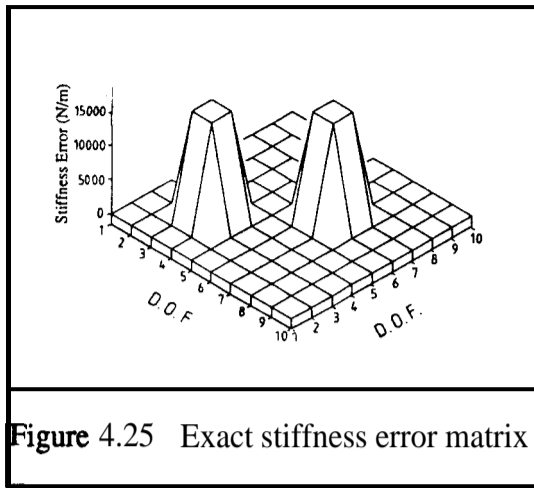
The second mass-spring system shown in Figure 4.7 consists of ten masses and fourteen springs with complicated connectivity. As before, mass errors at points 1, 4, 7 and 10 and stiffness errors between 2&3, 5&7 and lo-ground were introduced. The first three eigenvalues and the corresponding eigenvectors having the first eight out of the ten response coordinates from the modified system were "measured". By filling the last two rows of these three eigenvectors with the last two rows of the eigenvectors for the original system, the ECM could be applied. The results of the mass error matrix and stiffness error matrix prediction are plotted in Figures 4.29 and 4.30. It can be seen that the identified system was different from the actual mass error and actual stiffness error matrices shown in Figures 4.21 and 4.22. However, there was significant improvement for the error location as shown in Figures 4.3 1 and 4.32 and

a better agreement between the identified error matrices and the exact solution was obtained when a weighted least-squares method (see Appendix A) was employed. This was because, in general, the last two rows of those eigenvectors which had been filled by the last two rows of the eigenvectors for the original system were incorrect, therefore the columns of the coefficient matrix containing the information of the last two rows of those eigenvectors should be differently weighted/scaled. In this example, a scaling factor of (1/1000) was chosen in order to obtain the results in Figures 4.31 and 4.32. It should be noted that sometimes the selection of scaling factor can be based on an a priori knowledge of the uncertainties in the coefficient matrix. Again, the updated system either using the least-squares or weighted least-squares method is able to reproduce the measured modal properties quite accurately.



Figure 4.29 Predicted mass error matrix (least-squares method)



Figure 4.30 Predicted stiffness error matrix (least-squares method)
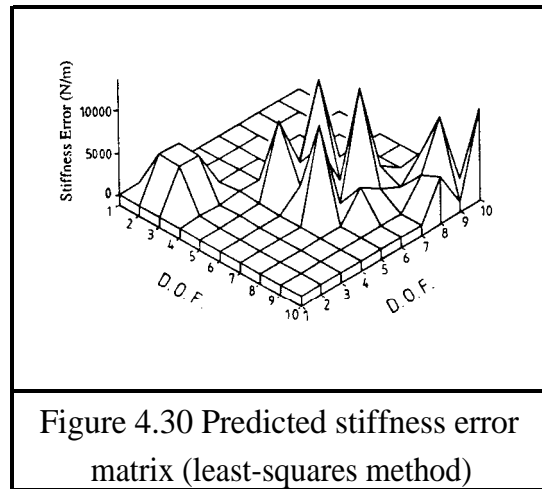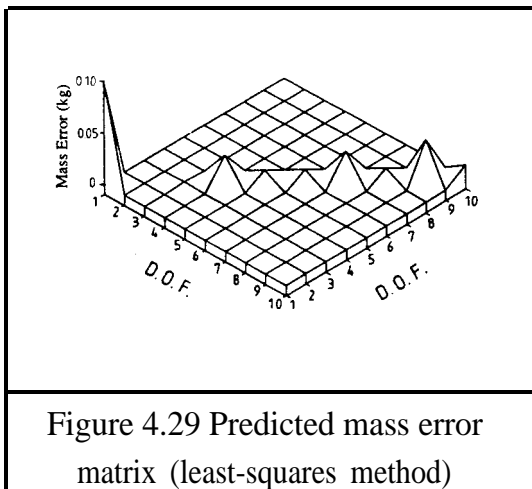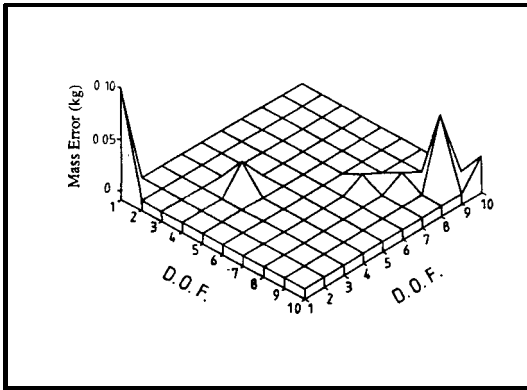
Figure 4.3 1  Predicted mass error natrix (weighted least-squares method)



Figure 4.32 Predicted stiffness error matrix (weighted least-squares method)

### 4.5.6      CHARACTERISTICS OF DIRECT MATRIX-UPDATE METHODS

Although Berman's "AM" matrix is not the actual mass error matrix, there is a close relationship between them. It is sometimes necessary in practice to understand the relationship between these two matrices or two $NxN$ subspaces. How close are they ? Do they intersect ? Can one be "rotated"/"projected" into the other ? and so on. In the following paragraphs it will be shown how questions like these can be answered using the SVD.

The updated mass matrix satisfies the orthogonality relationship :

$$[\Phi]^T[\Delta M][\Phi] \; = \; [I] - [m_A] \tag{4.23}$$

Post-multiplying equation (4.13) by $[\Phi]^T$ and pre-multiplying equation (4.13) by $[\Phi]$ gives

$$[\Phi]^T[\Delta M_{BERMAN}][\Phi] \; = \; [I] - [m_A] \tag{4.24}$$

It can be seen from equation (4.24) that Berman's "AM" matrix may be described as a projection of the actual mass error matrix in an $NxN$ subspace.

From equation **(4.24),** the rank of [AM**BERMAN**] is seen to be smaller than or equal to the minimum value of **(rank[Φ], rank[M$_A$], rank([I]-[m$_A$]))**. In all cases, this minimum value is either equal to **rank[Φ]** or equal to **rank([I]-[m$_A$])** that is smaller than or equal to the minimum value of **(rank[Φ], rank[ΔM])** from equation (4.12). Hence, when the number of measured modes $m$ is smaller than the number of mass error sites, e , *the rank* of Berman's "AM" matrix is smaller than or equal to the number of measured modes, $m$. When the number of measured modes $m$ is equal to or greater than the number of mass error sites, e, the rank of Berman's "AM" matrix is smaller than or equal to the number of mass error sites, e.  Mathematically speaking, it can be stated that :

for  $m <$ e,      rank[ΔM$_{BERMAN}$] $\leq m$                                    (4.25)

   $m \geq$ **e,**      rank[ΔM$_{BERMAN}$] $\leq e$                                    (4.26)

Alternatively, a comparison of equations (4.24) and (4.23) gives

$$[\Phi]^T[\Delta M]\,[\Phi] = [\Phi]^T[\Delta M_{BERMAN}]\,[\Phi] \qquad\qquad (4.27)$$

This implies that the ranks of $[\Phi]^T[\Delta M][\Phi]$ and $[\Phi]^T[\Delta M_{BERMAN}][\Phi]$ are the same and hence the conditions shown in (4.25) and (4.26) are justified.

In practice it is more useful to consider the case when the number of measured modes $m$ is equal to or greater than the number of mass error sites e. From equation**(4.27),** it is shown that

$$\text{rank}([\Phi]^T[\Delta M][\Phi]) = \text{rank}([\Phi]^T[\Delta M_{BERMAN}][\Phi]) \qquad (4.28)$$

and Berman's "AM" matrix can be factorised by the SVD as:

$$[\Delta M_{BERMAN}] = [U][\Sigma][V]^T \qquad (4.29)$$

where $[U]$ is an $NxN$ orthogonal matrix, $[V]$ is an $NxN$ orthogonal matrix, and $[\Sigma]$ is a diagonal matrix of rank $[\Delta M_{BERMAN}]$ whose non-negative diagonal elements are the singular values of $[\Delta M_{BERMAN}]$.

As a result, in general the rank of $[\Delta M_{BERMAN}]$ is equal to the number of mass error sites when the number of measured modes $m$ is equal or greater than the number of mass error sites e.

Furthermore, conditions given in (4.25) and (4.26) will not be affected by the number of stiffness error sites because equation (4.13) has been derived without using the information of system stiffness matrix [44].

Berman's "AM" matrix is one of the projections of the actual mass error matrix in an $NxN$ space. An $NxN$ matrix obtained using the left hand side of equation (4.12) in Section 4.5.1 is another projection of the actual mass error matrix since pre-multiplying both sides of equation (4.12) by the transpose of the mode shapes matrix and post-multiplying both sides of equation (4.12) by the mode shapes matrix the orthogonality relationship is satisfied in most cases. Hence, we can state that:

$$\text{for } m < e, \qquad \text{rank}[([\Phi]^T)^+ ([I] - [\Phi]^T[M_A][\Phi]) ([\Phi])^+] \le m \qquad (4.30)$$

$$m \ge e, \qquad \text{rank}[([\Phi]^T)^+ ([I] - [\Phi]^T[M_A][\Phi]) ([\Phi])^+] \le e \qquad (4.3\,1)$$

In contrast, Baruch's "AK" matrix is able to determine the rank of an actual stiffness error matrix only when sufficient modes are available and the correct mass matrix is used. It is because Baruch [43] derived his formula using a known symmetric positive definite mass matrix so inherently the correct mass matrix was used to obtain the Baruch"s "AK" matrix. His formula for a stiffness error matrix is given as follows :

$$[\Delta K_{BARUCH}] \overset{A}{=} -[K_A][\Phi][\Phi]^T[M_A] - [M_A][\Phi][\Phi]^T[K_A] + [M_A][\Phi][\Phi]^T[K_A][\Phi][\Phi]^T[M_A]$$
$$+ [M_A][\Phi][\omega^2][\Phi]^T[K_A] \tag{4.32}$$

In order to determine the rank of the stiffness error matrix without using the system mass matrix, the application of pseudo-inverse would be advantageous. We can define a pseudo-stiffness error matrix as :

$$[\Delta K_{PSEUDO}] = ([\Phi]^T)^+ ([\omega^2] - [\Phi]^T[K_A][\Phi]) ([\Phi])^+ \tag{4.33}$$

Pre-multiplying both sides by $[\Phi]^T$ and post-multiplying both sides by $[\Phi]$ gives

$$[\Phi]^T[\Delta K_{PSEUDO}] [\Phi] = [\omega^2] - [\Phi]^T[K_A][\Phi]$$
$$= [\Phi]^T[\Delta K] [\Phi] \tag{4.34}$$

It can be seen that in general the pseudo-stiffness error matrix is a projection of the actual stiffness error matrix in an $NxN$ space. Once again, we can state that :

for $m < e,$      rank$[\Delta K_{PSEUDO}] \leq m$ \qquad\qquad (4.35)

$m \geq e,$      rank$[\Delta K_{PSEUDO}] \leq e$ \qquad\qquad (4.36)

A 10 degree-of-freedom spring-mass model shown in Figure 4.3 was used to check the above analysis for a general mass matrix. Three mass errors have been introduced

at points 1, 4 and 8 to obtain the modified mode shape matrix. Berman's "AM" matrices were calculated using 1 to 10 modes for the modified system. The ranks of Berman's "AM" matrices were determined by the SVD and are plotted in Figure 4.33, it can be seen that the rank of Berman's "AM" matrix was 3 when three or more measured modes were available. The singular values of Berman's "AM" matrices are tabulated in Table 4. I.



Figure 4.33 The rank of Berman's "AM" man-ix against the number of measured modes
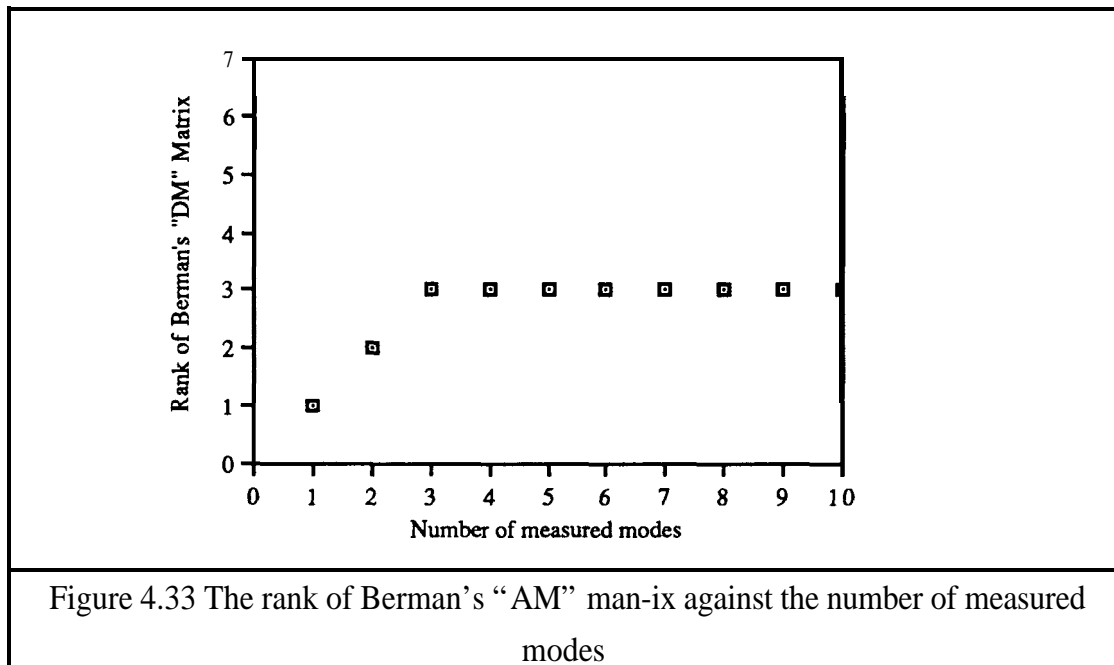
| The number of measured modes (*n* | | | | | | | | | |
|---|---|---|---|---|---|---|---|---|---|
| 1 | 2 | 3 | 4 | 5 | 6 | 7 | 8 | 9 | 10 |
| 0.061 | 0.123 | 0.208 | 0.208 | 0.208 | 0.222 | 0.223 | 0.223 | 0.224 | 0.250 |
| 0.000 | 0.046 | 0.047 | 0.050 | 0.099 | 0.099 | 0.100 | 0.100 | 0.100 | 0.100 |
| **0.000** | 0.000 | 0.018 | 0.044 | 0.050 | 0.050 | 0.050 | 0.050 | 0.050 | 0.050 |
| 0.000 | 0.000 | 0.000 | 0.000 | 0.000 | 0.000 | 0.000 | **0.000** | 0.000 | 0.000 |
| 0.000 | 0.000 | 0.000 | 0.000 | 0.000 | **0.000** | 0.000 | 0.000 | 0.000 | 0.000 |
| 0.000 | 0.000 | 0.000 | 0.000 | 0.000 | 0.000 | 0.000 | 0.000 | 0.000 | 0.000 |
| 0.000 | 0.000 | 0.000 | 0.000 | 0.000 | 0.000 | 0.000 | 0.000 | 0.000 | 0.000 |
| 0.000 | 0.000 | 0.000 | 0.000 | 0.000 | 0.000 | 0.000 | 0.000 | 0.000 | 0.000 |
| 0.000 | 0.000 | 0.000 | 0.000 | 0.000 | 0.000 | 0.000 | 0.000 | 0.000 | 0.000 |
| 0.000 | 0.000 | 0.000 | 0.000 | 0.000 | 0.000 | 0.000 | 0.000 | 0.000 | 0.000 |
| 0.000 | 0.000 | 0.000 | 0.000 | 0.000 | 0.000 | 0.000 | 0.000 | 0.000 | 0.000 |

Table 4.1  The singular values of Berman's "AM" matrices for the first case

The second case study was carried out on the same analytical model. In this case mass errors at points 2, 3, 5 and 8 and stiffness errors between points **2&3 5&6** and **6&7** have been added to the original model. Berman's "AM" matrices were calculated using 1 to 10 modes for the modified system and their ranks were determined by the SVD as shown in Figure 4.34. Again, the rank of Berman's "AM" matrix was equal to the number of mass error sites when sufficient measured modes were available, and was not affected by the number of stiffness errors made on the structure. The singular values of Berman's "AM" matrices are tabulated in Table 4.2. Table 4.3 shows the singular values of Berman's "AM" matrices when the measured mode shape vectors were contaminated by 2 percent Gaussian random noise, and it can be seen that the numerical rank was 4 when four or more measured modes were available. A careful definition of numerical rank has been given in a paper by Golub et *al.* [51]. The essential idea is briefly described as follows. In order to look at the "nonzero singular values" of Berman's "AM" matrices, a number $\delta$ must be chosen as a "zero threshold". The choice of $\delta$ was based on measurement errors (information about the uncertainty of the measured data) incurred in estimating the coefficients of those Berman's "AM" matrices. In this case, two percent random noise was applied to the

measured mode shape vectors so that by considering the round off and the measurement errors in the matrix computation the value of $\delta$ was set to 0.02 time the spectral norm of Berman's "AM" matrix.
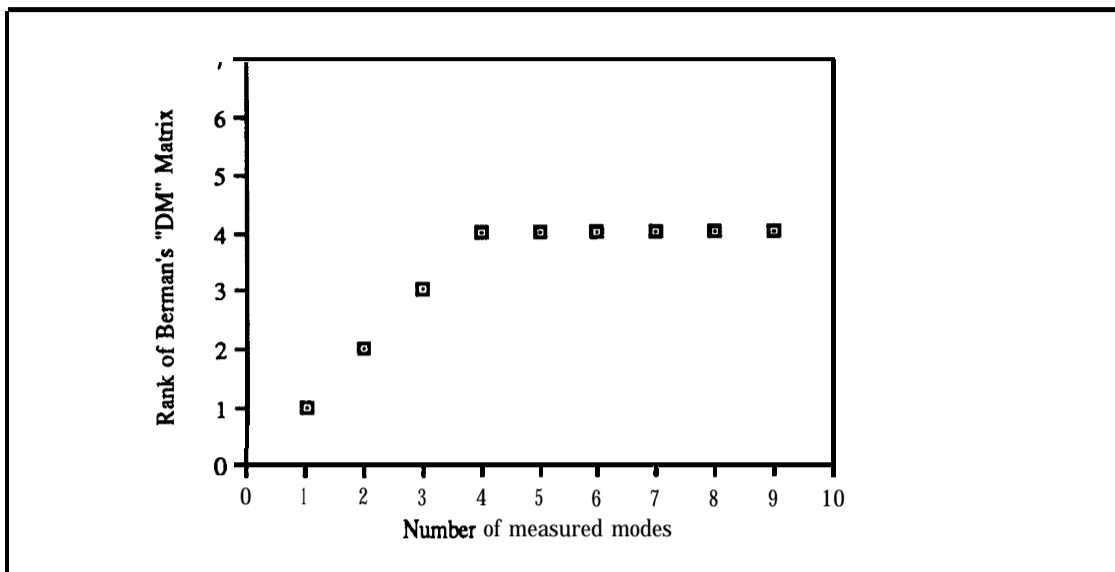


Figure 4.34 The rank of Berman's "AM" matrix against the number of measured modes

| The number of measured modes (n | | | | | | | | | |
|---|---|---|---|---|---|---|---|---|---|
| 1 | 2 | 3 | 4 | 5 | 6 | 7 | 8 | **9** | 10 |
| 0.022 | 0.039 | 0.074 | 0.100 | 0.100 | 0.100 | 0.100 | 0.100 | 0.100 | 0.100 |
| 0.000 | 0.009 | 0.014 | 0.014 | 0.014 | 0.025 | 0.025 | 0.025 | 0.025 | 0.025 |
| 0.000 | 0.000 | 0.004 | 0.004 | 0.004 | 0.006 | 0.008 | 0.010 | 0.020 | 0.020 |
| 0.000 | 0.000 | 0.000 | 0.002 | 0.002 | 0.003 | 0.004 | 0.004 | 0.010 | 0.010 |
| 0.000 | 0.000 | 0.000 | 0.000 | 0.000 | 0.000 | 0.000 | 0.000 | 0.000 | 0.000 |
| 0.000 | 0.000 | 0.000 | 0.000 | 0.000 | 0.000 | 0.000 | 0.000 | 0.000 | 0.000 |
| 0.000 | 0.000 | 0.000 | 0.000 | 0.000 | 0.000 | 0.000 | 0.000 | 0.000 | 0.000 |
| 0.000 | 0.000 | 0.000 | 0.000 | 0.000 | 0.000 | 0.000 | 0.000 | 0.000 | 0.000 |
| 0.000 | 0.000 | 0.000 | 0.000 | 0.000 | 0.000 | 0.000 | 0.000 | 0.000 | 0.000 |
| 0.000 | 0.000 | 0.000 | 0.000 | 0.000 | 0.000 | 0.000 | 0.000 | 0.000 | 0.000 |

Table 4.2 The singular values of Berman's "AM" matrices for the second case

| The number of measured modes (n | | | | | | | | | |
|---|---|---|---|---|---|---|---|---|---|
| 1 | 2 | 3 | 4 | 5 | 6 | 7 | 8 | 9 | 10 |
| D.0219 | 1.0390 | 0.0739 | I.1001 | D.1001 | ).1001 | ).1001 | ).1001 | D.1001 | I.1001 |
| 0.000 | ).0085 | D.0134 | I.0133 | D.0134 | ).0250 | B.0249 | I.0250 | D.0250 | I.0250 |
| 0.000 | 0.000 | 0.0029 | I.0030 | D.0036 | ).0058 | D.0074 | ).0100 | D.0198 | I.0199 |
| 0.000 | 0.000 | 0.000 | 1.0024 | D.0025 | ).0032 | D.0032 | I.0036 | D.0099 | ).0101 |
| 0.000 | 0.000 | 0.000 | 0.0000 | 0.0002 | 0.0003 | 0.0005 | 0.0006 | 0.0007 | 0.0009 |
| 0.000 | 0.000 | 0.000 | 0.0000 | 0.0000 | 0.0001 | 0.0002 | 0.0005 | 0.0007 | 0.0007 |
| 0.000 | 0.000 | 0.000 | 0.0000 | 0.0000 | 0.0000 | 0.0001 | 0.0002 | 0.0006 | 0.0006 |
| 0.000 | 0.000 | 0.000 | 0.0000 | 0.0000 | 0.0000 | 0.0000 | 0.0001 | 0.0003 | 0.0003 |
| 0.000 | 0.000 | 0.000 | 0.0000 | 0.0000 | 0.0000 | 0.0000 | 0.0000 | 0.0001 | 0.0001 |
| 0.000 | 0.000 | 0.000 | 0.0000 | 0.0000 | 0.0000 | 0.0000 | 0.0000 | 0.0000 | 0.0000 |

Table 4.3 The singular values of Berman's "AM" matrices for the second case
(noisy data)

4.5.7        ITERATIVE MODAL UPDATING TECHNIQUES USING MODAL
            DATA

So far, only non-iterative model updating methods have been presented. The main advantage of those methods is the fast computation time, and thus the implementation cost can be minimized. As a drawback, it should be noted that coordinate incompleteness causes the failure of non-iterative methods in obtaining the exact error matrices in many cases unless a reliable mode shape expansion technique is developed.

By calculating first-order sensitivities of natural frequencies (or eigenvalues) and mode shape vectors (eigenvectors) of the FE/analytical model, a relationship between modal parameters and structural elements for a particular mode can be expressed in the following form:

$$
\begin{Bmatrix} \lambda_A - \lambda_X \\ \\ \{\{\phi_A\}-\{\phi_X\}\} \end{Bmatrix} = \begin{bmatrix} [\dfrac{\partial\lambda_A}{\partial r}] \\ \\ [\dfrac{\partial\{\phi_A\}}{\partial r}] \end{bmatrix} \{r - r_A\}
\tag{4.37}
$$

where $(\lambda_A - \lambda_X)$ and $\{\phi_A - \phi_X\}$ are the differences between experimental and analytical natural frequencies and mode shape vectors respectively; $[\partial\lambda_A/\partial r],[\partial\{\phi_A\}/\partial r]$ are matrices with the partial derivatives of the analytical natural frequency and mode shape vectors with respect to the structural parameters; and $(r - r_A\}$ is a column vector with the difference between the structural parameters (mass, stiffness and damping loss factors) corresponding to the refined model and the original analytical model.

As a first step, the changes of structural parameters $\{r - r_A\}$ are determined by solving equation (4.37) when the system of equations is overdetermined. In a second step, the structural changes are then added to the original model and the generalised eigenvalue problem defined by the modified system matrices is solved. The modal parameters of the refined model are compared with the measured modal data in the third step. These three steps are repeated until a good agreement is indicated between measured and analytical modal data. The main advantage of this iterative method is that the coefficient vector and matrix can be constructed even if the mode shape vectors are incomplete in terms of the number of DoFs. The drawback of the method is the necessity to solve a generalised eigenvalue problem in each iteration.

For an algebraic eigenvalue problem (mass matrix is unity), Kublanovskaja [52] gave a convergence analysis of this method in 1970, assuming the existence of a solution. It is possible to extend his analysis to the generalised eigenvalue problem - for a system without an unit mass matrix - as long as the structural changes do not exceed a mathematical bound so that the convergence of solution can be achieved. Details of sensitivity analysis of mechanical structures will be given in Chapter 5.

### 4.5.8 MODEL UPDATING USING FREQUENCY RESPONSE FUNCTIONS

The afore-mentioned methods for updating the physical parameters of an FE/analytical model use experimentally-derived modal data. It should be noted that for a undamped mechanical structure, the information of out-of-range modes (residuals) was completely eliminated from the dynamic response at resonances. At the other frequency points, the well-known spectral decomposition of the FRF is written as :

$$H_{ij}(\omega) = \sum_{r=1}^{N} \frac{{}_r\phi_i \, {}_r\phi_j}{\omega_r^2 - \omega^2 + i\eta_r \omega_r^2} \qquad (4.38)$$

This implies that the FRF contains all information of the system matrices at any frequency point other than structural resonances. Based on this idea, Lin [53] has developed a model updating method using FRF data directly. His method uses a complete column/row of the receptance matrices at a particular frequency point and is derived as follows :

$$\{H_X(\omega)\}^T = \{H_A(\omega)\}^T - \{H_A(\omega)\}^T [\Delta Z(\omega)] \; \{H_X(\omega)\} \qquad (4.39)$$

where $\{H_X(\omega)\}$ consists of the receptances of the test structure, $\{H_A(\omega)\}$ consists of the receptances of the original analytical model and [AZ(o)] is the matrix of structural changes. Collecting equation (4.39) for several measured frequency points yields a system of equations which can be solved by a least-squares method, provided that the system of equations is overdetermined. It should be noted that the measured FRF set is generally coordinate- incomplete. In such a situation, an iterative procedure can be used whereby the unmeasured **FRFs** are predicted from **the** original or updated system matrices and are used in equation (4.39) in lieu of measurements.

## 4.6 CONCLUDING REMARKS

An attempt has been made to survey the structural identification methods which are widely used in the modal analysis community. Direct parameter extraction methods are classified with respect to the types of measurement data - frequency domain and time domain. Within these groups, a distinction is made between local and global approaches. The special features of each method are briefly described.

It may be fairly accurate to state that working methods to identify the physical mass, stiffness and damping distribution directly for mechanical structures are very scarce. As a result, the reconciliation of an FE/analytical model and modal test information is a feasible approach to derive a mathematical model which reproduces the measured data and is capable of predicting the response of a modified structure.

Although direct matrix-update methods have been developed and investigated by numerous researchers, the reason why these methods could not produce accurate mass or stiffness error matrices, even if a large number of modes have been measured, has not been well understood. Besides, the connectivity of the original analytical model is not preserved when these methods are used to determine the system error matrices. This undesirable effect can lead to physically unrealistic changes being introduced in the analytical system matrices.   In Section 4.5.1, it was noted that Baruch & Bar-Itzhack [43] borrowed the idea from the research work from navigation to develop the direct matrix-update method. However, the bases of these two disciplines are so different that the mapping technique in navigation should not be used in model updating. It is shown that the formula given in Berman's paper is mathematically incorrect unless the complete set of measured modes (as well as coordinate-complete) are given.

After identifying the inherent difficulties in obtaining mass error and stiffness error matrices by matrix manipulation, the orthogonality constraint method which is based on transforming the orthogonality relationships of the mass and stiffness matrices to sets of simultaneous equations is developed.   The mass error and stiffness error matrices are then obtained in a least-squares sense by calculating the Moore-Penrose generalised inverses when the system of equations is overdetermined. The eigendynamic constraint method is also presented. This method is based on the simple modal equations and mass normalisation relationships of measured modes.    By considering the state of the system of equations, a criterion for model updating using the minimum modal data is suggested from which the eigendynamic constraint method generally requires fewer measured modes than the method based on the orthogonality relationships of the mass and stiffness matrices of a mechanical structure. Numerical examples verify that if the criterion is satisfied, it is possible to determine the system error matrices and to produce an accurate updated analytical model.

The effect of modal and coordinate incompleteness is also investigated. Numerical examples show that there exist different identified systems when the modes available from measurement are incomplete in terms of the number of modes as well as the response coordinates. The values of mass and stiffness elements obtained depend on the method used to determine the response of the unmeasured coordinates. It can be concluded that when only a limited number of modes and response coordinates are measured, different identified systems can be obtained by using the eigendynamic constraint method with different approximations for the response at the unmeasured coordinates. All these systems reproduce quite accurately the measured modal properties and some of them preserve the physical characteristics of the structure, such as positive mass and stiffness elements, and the same connectivity. But only one of them is the true representation of the structure and will have the capability of

After identifying the inherent difficulties in obtaining mass error and stiffness error matrices by matrix manipulation, the orthogonality constraint method which is based on transforming the orthogonality relationships of the mass and stiffness matrices to sets of simultaneous equations is developed. The mass error and stiffness error matrices are then obtained in a least-squares sense by calculating the Moore-Penrose generalised inverses when the system of equations is overdetermined. The eigendynamic constraint method is also presented. This method is based on the simple modal equations and mass normalisation relationships of measured modes. By considering the state of the system of equations, a criterion for model updating using the minimum modal data is suggested from which the eigendynamic constraint method generally requires fewer measured modes than the method based on the orthogonality relationships of the mass and stiffness matrices of a mechanical structure. Numerical examples verify that if the criterion is satisfied, it is possible to determine the system error matrices and to produce an accurate updated analytical model.

The effect of modal and coordinate incompleteness is also investigated. Numerical examples show that there exist different identified systems when the modes available from measurement are incomplete in terms of the number of modes as well as the response coordinates. The values of mass and stiffness elements obtained depend on the method used to determine the response of the unmeasured coordinates. It can be concluded that when only a limited number of modes and response coordinates are measured, different identified systems can be obtained by using the eigendynamic constraint method with different approximations for the response at the unmeasured coordinates. All these systems reproduce quite accurately the measured modal properties and some of them preserve the physical characteristics of the structure, such as positive mass and stiffness elements, and the same connectivity. But only one of them is the true representation of the structure and will have the capability of

reproducing the measured modal properties exactly and of predicting the effects of changes in physical parameters.

A separate subsection is devoted to the characteristic of direct matrix-update method. It is proved that in general Berman's "AM" matrix is a projection of the actual mass error matrix in an $NxN$ subspace when sufficient modes are available. Also, the number of mass mismodelling sites can be determined when Berman's "AM" matrix is factorized using the SVD. This technique is not affected by the number of stiffness errors for any system. By following Berman's method, a pseudo "AK" matrix can be constructed based on measured modal data. Again, the number of stiffness mismodelling sites are determined when the pseudo "AK" matrix is factorized using the SVD.

The least two subsections in model updating present the iterative methods based on inverse sensitivity analysis and the latest model updating techniques using FRFs. Both of them relax the strict restriction that the measured coordinates should be complete in order to work effectively. However, the main drawback of iterative methods is the necessity of solving an generalised eigenvalue problem in each iteration.

# 5 SENSITIVITY ANALYSIS OF MECHANICAL STRUCTURES

## 5.1 INTRODUCTION

A good finite element (FE) or analytical model of a mechanical structure is important for structural integrity analysis. In practice, a high degree of confidence can be placed on such a FE/analytical model when the dynamic response of that model closely resembles experimental data. However, updating the FE model or identifying the analytical model directly is usually not the main objective of structural vibration analysis because there are many situations when the dynamic response of the mechanical structure does not satisfy the requirement set by the structural analyst (designer). In such situations, the dynamic response of the mechanical structure has to be altered either (i) by controlling the forcing inputs to the structure, or (ii) by changing the dynamic characteristics of the structure. The forcing inputs often result from interaction with the structure's environment and so cannot easily be controlled at will. When this is the case, it is important to be able to alter the structural response by redesigning the dynamic characteristics of the structure. To this end, the use of structural reanalysis techniques to obtain the optimum condition of an FE model of a mechanical structure has grown considerably in recent years.

A number of techniques exist that can be applied to the dynamic reanalysis of mechanical structures. One of the most popular of these is sensitivity analysis which has been developed and applied by several workers to the general eigenvalue problem

[54-70] and, more specifically, to applications of structural dynamic modification analysis in references [71-74]. In this area, both first- and higher-order eigenvalue and eigenvector sensitivities have been investigated with a view to predicting the dynamic response of a modified structure from knowledge of its spatial and modal properties in the original, or unmodified, state.  As the sensitivity analysis of a mechanical structure is based on a Taylor expansion of eigenvalues and eigenvectors of the unmodified structure, and the computation of the higher-order terms of this series is difficult and time consuming, the effectiveness of this method is limited to small modifications. However, it is not easy to determine what constitutes "small". In this chapter, a condition number is presented to indicate how sensitive the eigenvalues and eigenvectors of a mechanical structure are to small modifications. The value of this condition number can be used to determine a limit of applicability for first-order eigenvalue and eigenvector sensitivities.

## 5.2 THE ORIGINAL PURPOSE OF DEVELOPING THE **FIRST-**ORDER PERTURBATION

First-order perturbation estimates (eigenvalue and eigenvector sensitivities) have long been used by numerical analysts and scientists to investigate the stability of the eigenvalue problem, $[A]\{\phi\}=\lambda\{\phi\}$. These estimates have the advantage that they provide a quick, nonrigorous look at how eigenvalues and eigenvectors change when the elements of matrix $[A]$ vary within the limits of permissible error. Faddeev and Faddeeva [54] stated that the results obtained from perturbation theory are based on differentials but not finite increments. Perturbation theory has also been used for improving the accuracy of the complete eigenvalue problem. In most matrix computational textbooks, first-order perturbation theory is used to obtain the error bounds in computing eigenvalues and eigenvectors on a digital computer.

By translating the above-mentioned feature to suit structural analysts, a first-order sensitivity analysis is used to determine the "order of importance" ranking of a structure's degrees of freedom for structural modification, for each mode of vibration. To the greatest extent in an engineering application, it has been stated in a paper written by Fox and Kapoor [55] that the concept of introducing first-order eigenvalue and eigenvector derivatives is used to *approximate the* analysis of modified designs.

## 5.3 HISTORICAL DEVELOPMENT OF FIRST- (AND HIGHER-) ORDER SENSITIVITY

The basic sensitivity analysis is to compute partial derivatives of eigenvalues and eigenvectors with respect to the elements of two *NxN* system matrices [A] and [B] in a generalised eigenvalue problem. For reference purposes, the most general case considered is the following eigenvalue problem:

$$[A]\{\phi_r\} = \lambda_r [B]\{\phi\}_r \tag{5.1}$$

$$\{_l\phi\}_r^T[A] = \lambda_r \{_l\phi\}_r^T[B] \tag{5.2}$$

$$\{_l\phi\}_r^T[B]\{\phi\}_r = 1 \tag{5.3}$$

where $\lambda_r$ is an eigenvalue (generally complex); and $\{_l\phi\}_r$ and $\{\phi\}_r$ are the corresponding normalised left-hand and right-hand eigenvectors of the matrix pencil (A,B).

In 1846, Jacobi [56] published a result on first-order eigenvalue sensitivities for an eigenvalue problem [A] $\{\phi\} = \lambda\{\phi\}$ for the special case [B] = [I]:

$$\frac{\partial \lambda_r}{\partial \alpha} = \{_l\phi\}_r^T [\frac{\partial A}{\partial \alpha}] \{\phi\}_r \tag{5.4}$$

Van de Vooren [57] used sensitivity analysis (perturbation) in investigating the effects of small changes in a parameter on the flutter characteristics of an aircraft. The problem in which nearly equal natural frequencies arise is approached via that of exactly equal natural frequencies. In 1948, Jahn [58] derived first-order eigenvalue and eigenvector sensitivities in order to improve an approximate set of eigenvalues and eigenvectors of a symmetric matrix. In Jahn's paper, he extended his method to a Lagrange frequency equation of the form:

$$[ -\lambda[M] + [K] ]\{x\} = \{0\} \tag{5.5}$$

The case of coincident eigenvalues of the unmodified system and the extension of the calculations to the second-order eigenvalue sensitivities can be found in Courant and Hilbert [59] where perturbation theory has been applied to the problem of self-adjoint linear differential equations.

Lancaster [60] developed a rigorous treatment of eigenvalue sensitivities and, in particular, showed that for multiple eigenvalues the sensitivities are themselves solutions of an eigenvalue problem. Wilkinson [61] presented clear derivations for the first-order sensitivity equation of an eigenvalue in terms of the left-hand and right-hand eigenvectors. The equation presented in references [60] and [61] is

$$\frac{\partial \lambda_r}{\partial \alpha} = \frac{\{_l\psi\}_r^T [\frac{\partial A}{\partial \alpha}] \{\psi\}_r}{\{_l\psi\}_r^T \{\psi\}_r} \tag{5.6}$$

where $\{_l\psi\}_r$ and $\{\psi\}_r$ are the left-hand and right-hand eigenvectors of the matrix $\{A]$ with arbitrary scaling.

In the 1960s, some methods which are notable for their nonreliance on eigenvectors in the **eigenvalue** sensitivity formula were developed for sensitivity analysis of electronic networks. Rosenbrock **[62]**, Morgan **[63]** and Reddy **[64]** developed a formula for eigenvalue sensitivities in terms of the matrix [A] and its eigenvalues :

$$\frac{\partial \lambda_r}{\partial \alpha} = \frac{\text{trace} \{ \text{adj}([A] - \lambda_r[I])[\frac{\partial A}{\partial \alpha}] \}}{\text{trace} \{ \text{adj}([A] - \lambda_r[I]) \}} \tag{5.7}$$

Frazer et al. **[75]** showed that if $\lambda_r$ is a simple eigenvalue of the matrix A, then **adj([A]-$\lambda_r$[I])** can be expressed in terms of the corresponding left-hand and right-hand eigenvectors of $\lambda_r$ :

$$\text{adj}([A] - \lambda_r[I]) = \tau_r \{\psi\}_r \{_l\psi\}_r^T \tag{5.8}$$

where $\tau_r$ is a constant. Therefore,

$$\text{trace} \{ \text{adj}([A] - \lambda_r[I]) \} = \text{trace} (\tau_r \{\psi\}_r \{_l\psi\}_r^T)$$
$$= \tau_r \{_l\psi\}_r^T \{\psi\}_r \tag{5.9}$$

**Bodewig [76]** showed that if [Q] is square and rank [Q] = 1, so that [Q] is a simple product of a column $\{\psi\}_r$ and a row $\{_l\psi\}_r^T$ (i.e. [Q] = $\tau_r\{\psi\}_r\{_l\psi\}_r^T$), and if [$\partial$A/$\partial\alpha$] is arbitrary, but square, then

$$\text{trace} ([Q][\frac{\partial A}{\partial \alpha}]) = \text{trace} ([\frac{\partial A}{\partial \alpha}][Q]) = \tau_r\{_l\psi\}_r^T [\frac{\partial A}{\partial \alpha}]\{\psi\}_r \tag{5.10}$$

By substituting equations (5.9) and (5.10) in equation (5.7), equation (5.6) is obtained. Thus, in the computation of adj($[A] - \lambda_r[I]$), both left-hand and right-hand eigenvectors are implicitly computed, in view of equation (5.8).

Frame [77] established that the trace of the adj($[A] - \lambda_r[I]$) is equal to the derivative of the characteristic polynomial, det($[A] - \lambda_r[I]$).

$$\text{trace } \{\text{adj}([A] - \lambda_r[I])\} = \prod_{r \; r \neq s}^{N} (\lambda_s - \lambda_r) \tag{5.11}$$

Now, consider the trace of the product of the following two matrices.

$$
\begin{bmatrix}
\Delta_{11}(\lambda_r) \, \Delta_{21}(\lambda_r) \, \ldots \, \Delta_{N1}(\lambda_r) \\
\Delta_{12}(\lambda_r) \, \Delta_{22}(\lambda_r) \, \ldots \, \Delta_{N2}(\lambda_r) \\
. \qquad\qquad\qquad . \\
. \qquad\qquad\qquad . \\
\Delta_{1N}(\lambda_r) \; \Delta_{2N}(\lambda_r) \; \ldots \; \Delta_{NN}(\lambda_r)
\end{bmatrix}
\begin{bmatrix}
\dfrac{\partial a_{11}}{\partial \alpha} & \dfrac{\partial a_{12}}{\partial \alpha} & \ldots & \dfrac{\partial a_{1N}}{\partial \alpha} \\
\dfrac{\partial a_{21}}{\partial \alpha} & \dfrac{\partial a_{22}}{\partial \alpha} & \ldots & \dfrac{\partial a_{2N}}{\partial \alpha} \\
. & & & . \\
. & & & . \\
\dfrac{\partial a_{N1}}{\partial \alpha} & \dfrac{\partial a_{N2}}{\partial \alpha} & \ldots & \dfrac{\partial a_{NN}}{\partial \alpha}
\end{bmatrix}
$$

$$\tag{5.12}$$

where $\Delta_{ij}$ is the (i,j)th cofactor of ($[A] - \&[I]$).

In structural analysis $[A]$ is related to the stiffness matrix (usually written as $[K]$) and $[I]$ is the unit mass matrix. If a point Single Degree of Freedom (SDoF) stiffness modification is made at location j, the numerator of equation (5.7) can be written as :

$$\text{trace} \left\{ \begin{bmatrix} \Delta_{11}(\lambda_r) \, \Delta_{21}(\lambda_r) \dots \Delta_{N1}(\lambda_r) \\ \Delta_{12}(\lambda_r) \, \Delta_{22}(\lambda_r) \dots \Delta_{N2}(\lambda_r) \\ \cdot \qquad\qquad \cdot \\ \cdot \qquad\qquad \cdot \\ \Delta_{1N}(\lambda_r) \, \Delta_{2N}(\lambda_r) \dots A_{N\ N\&} \end{bmatrix} \begin{bmatrix} 0 & 0 & \dots & 0 \\ 0 & 0 & \dots & 0 \\ \cdot & & 1_{(j,j)} & \cdot \\ \cdot & & & \cdot \\ 0 & 0 & \dots & 0 \end{bmatrix} \right\}$$

$$= \text{trace} \left\{ \begin{bmatrix} 0.. & 0.. & \Delta_{j1}(\lambda_r) & ..0 & ..0 \\ \cdot & & & & \cdot \\ \cdot & & \Delta_{jj}(\lambda_r) & & \cdot \\ \cdot & & & & \cdot \\ 0.. & 0.. & \Delta_{jN}(\lambda_r) & ..0 & ..0 \end{bmatrix} \right\}$$

$$= \ \Delta_{jj}(\lambda_r)$$

$$= \ \text{the (j,j) cofactor of } ([A] - \lambda_r[I]) \qquad\qquad\qquad (5.13)$$

The equation of motion for a linear system is:

$$([A] - \lambda[I])\{x\} = \{f\} \qquad\qquad\qquad (5.14)$$

It has been shown in several references [e.g.78,79] that any frequency response function (FRF) of a grounded undamped structure can be described completely in terms of its poles or eigenvalues (squares of natural frequencies), its zeros (squares of anti-resonance frequencies), and a constant ($C_{jj}$).

$$H_{jj}(\lambda) \ = \frac{C_{jj} \displaystyle\prod_{k=1}^{N-1} \left(1 - \frac{\lambda}{jj\beta_k}\right)}{\displaystyle\prod_{s=1}^{N} \left(1 - \frac{\lambda}{\lambda_s}\right)} \qquad\qquad\qquad \textbf{(5.15)}$$

where   $H_{jj}(\lambda)$ = receptance of point measurement at location j

$\qquad\quad C_{jj}$    = static flexibility

$$\lambda_s \quad = sth \;\; \text{pole}$$

$$^{jj}\beta_k \quad = kth \;\; \text{zero for } H_{jj}(\lambda)$$

The FRF $H_{jj}(\lambda)$ can also be obtained from equation (5.14).

$$H_{jj}(\lambda) \;=\; \frac{x_j}{f_j}(\lambda) \;=\; \frac{\text{the (j,j) cofactor of } ([A] - \lambda_s[I])}{\det\,([A] - \lambda_s[I])} \tag{5.16}$$

**since**

$$\det\,([A] - \lambda\,[I]) \;=\; \prod_{s=1}^{N} (\lambda - \lambda_s) \;=\; \prod_{s=1}^{N} (1 - \frac{\lambda}{\lambda_s}) \prod_{r=1}^{N} \lambda_s \tag{5.17}$$

Using equations (5.15), (5.16) and (5.17), the (j,j)th cofactor of $([A] - \lambda\,[I])$ can be expressed as :

$$\text{the (j,j) cofactor of } ([A] - \&[I]) = \; C_{jj} \prod_{k=1}^{N-1} (1 - \frac{\lambda}{^{jj}\beta_k}) \prod_{s=1}^{N} \lambda_s$$

$$= \; \frac{C_{jj} \displaystyle\prod_{s=1}^{N} \lambda_s \prod_{k=1}^{N-1} (^{jj}\beta_k - \lambda)}{\displaystyle\prod_{k=1}^{N-1} {}^{jj}\beta_k} \tag{5.18}$$

Substituting equations (5.11) and (5.18) in equation (5.7) gives :

$$\frac{\partial \lambda_r}{\partial \alpha} \;=\; \frac{C_{jj} \displaystyle\prod_{s=1}^{N} \lambda_s \prod_{k=1}^{N-1} (^{jj}\beta_k - \lambda_r)}{\displaystyle\prod_{k=1}^{N-1} {}^{jj}\beta_k \prod_{r\;rfs}^{n} (\lambda_s - \lambda_r)} \tag{5.19}$$

and this is the equation for a point **SDoF** stiffness modification obtained independently by Skingle and Ewins [71].

The formula shown above for calculating the sensitivity of an eigenvalue to changes in the matrix (equation (5.19)) is implicitly the same as those shown in equations (5.6) **&** (5.7). This is to be expected if one begins with equation $[A] \{\phi\} = \lambda \{\phi\}$. As the system properties do not vary under a harmonic excitation, the difference between equation (5.19) and equations (5.6) **&** (5.7) is the number of design parameters used to calculate the first-order eigenvalue sensitivity.

Fox and Kapoor [55], apparently being unaware of earlier work such as that of Jahn [58], rediscovered the eigenvalue and eigenvector sensitivities by considering the special case of symmetric stiffness [K] and mass [M] matrices. For eigenvalues their formula is :

$$\frac{\partial \lambda_r}{\partial \alpha} = \{\phi\}_r^T \left( [\frac{\partial K}{\partial \alpha}] - \lambda_r [\frac{\partial M}{\partial \alpha}] \right) \{\phi\}_r \qquad (5.20)$$

in which it is assumed that the eigenvectors are normalised such that

$$\{\phi\}_r^T [M] \{\phi\}_r = 1 \qquad (5.21)$$

The first-order eigenvector sensitivity of the *rth* mode is :

$$\frac{\partial \{\phi\}_r}{\partial \alpha} = -\frac{1}{2} \{\phi\}_r \{\phi\}_r^T [\frac{\partial M}{\partial \alpha}] \{\phi\}_r + \sum_{\substack{s=1 \\ s \neq r}}^{N} \frac{1}{(\lambda_r - \lambda_s)} \{\phi\}_s \{\phi\}_r^T \left( [\frac{\partial K}{\partial \alpha}] - \lambda_r [\frac{\partial M}{\partial \alpha}] \right) \{\phi\}_s$$

$$(5.22)$$

Rogers [65] derived sensitivity formulae for the eigenvalues and eigenvectors of a general problem and stated the need for two sets of normalisation conditions for a non-self-adjoint system. These conditions have been largely ignored in subsequent work, resulting in some confusion in the literature on eigenvector sensitivities. Lim et *al.* [72] reviewed the development of eigenvalue and eigenvector sensitivities and highlighted the need for two independent sets of normalisations to define uniquely the left-hand and right-hand eigenvector sets. The first-order eigenvalue sensitivity for a general system is:

$$\frac{\partial \lambda_r}{\partial \alpha} = \{_l\phi\}_r^T \left(\left[\frac{\partial K}{\partial \alpha}\right] - \lambda_r\left[\frac{\partial M}{\partial \alpha}\right]\right) \{\phi\}_r \tag{5.23}$$

with biorthogonality and normalisations relationships as:

$$\{_l\phi\}_s^T [M] \{\phi\}_r = \delta_{rs} \qquad\qquad r,s = 1, 2, \ldots . N \tag{5.24}$$

$$\{\phi\}_r^T [M] \{\phi\}_r = 1 \qquad\qquad r = 1, 2, \ldots . N \tag{5.25}$$

The left-hand and right-hand eigenvector sensitivities are :

$$\frac{\partial \{\phi\}_r}{\partial \alpha} = \sum_{s=1}^{N} \sigma_{rs}\{\phi\}_r \;,\quad \frac{\partial \{_l\phi\}_r}{\partial \alpha} = \sum_{s=1}^{N} \rho_{rs}\{_l\phi\}_r \tag{5.26}$$

where

$$\sigma_{rs} = \frac{\{_l\phi\}_s^T \left(\left[\frac{\partial K}{\partial \alpha}\right] - \frac{\partial \lambda_r}{\partial \alpha}[M] - \lambda_r\left[\frac{\partial M}{\partial \alpha}\right]\right) \{\phi\}_r}{(\lambda_r - \lambda_s)} \;,\quad r \neq s \tag{5.27}$$

$$\rho_{rs} = \frac{\{_l\phi\}_r^T \left(\left[\frac{\partial K}{\partial \alpha}\right] - \frac{\partial \lambda_r}{\partial \alpha}[M] - \lambda_r\left[\frac{\partial M}{\partial \alpha}\right]\right) \{\phi\}_s}{(\lambda_r - \lambda_s)} \;,\quad r \neq s \tag{5.28}$$

Vanhonacker [66] derived some formulae calculating the sensitivities of a mechanical structure subjected to parameter changes. The formulae obtained were based on an

nDoF system under a sinusoidal excitation. Comparing his derivations with the equations shown above, it can be observed that the sensitivity is a special case in the classical methods of sensitivity analysis.

Many papers [67-70] have presented higher-order eigenvalue and eigenvector sensitivities. Wang et al. [73] have investigated the accuracy of structural modification analyses by calculating the first- and second-order eigenvalue and eigenvector sensitivities and showed the divergence phenomenon for large structural modification. The second-order eigenvalue sensitivity of a structure with symmetric system matrices is obtained by differentiating equation (5.20) :

$$
\frac{\partial^2 \lambda_r}{\partial \alpha^2} = \{\phi\}_r^T([\frac{\partial^2 K}{\partial \alpha^2}] - \lambda_r[\frac{\partial^2 M}{\partial \alpha^2}])\{\phi\}_r - 2\{\phi\}_r^T(\frac{\partial \lambda_r}{\partial \alpha}[\frac{\partial M}{\partial \alpha}])\{\phi\}_r
$$
$$
+ 2\{\phi\}^T([\frac{\partial K}{\partial \alpha}] - \frac{\partial \lambda_r}{\partial \alpha}[M] - \lambda_r[\frac{\partial M}{\partial \alpha}])\frac{\partial \{\phi\}_r}{\partial \alpha} \qquad (5.29)
$$

From this equation, it can be seen that the second-order eigenvalue sensitivity is dependent on the first-order eigenvalue and the first-order eigenvector sensitivities. Using the relationships shown in equations (5.20) and (5.21), equation (5.29) can be rewritten as :

$$
\frac{\partial^2 \lambda_r}{\partial \alpha^2} = \{\phi\}_r^T([\frac{\partial^2 K}{\partial \alpha^2}] - \lambda_r[\frac{\partial^2 M}{\partial \alpha^2}])\{\phi\}_r - 2\{\phi\}_r^T([\frac{\partial K}{\partial \alpha}] - \lambda_r[\frac{\partial M}{\partial \alpha}])\{\phi\}_r\{\phi\}_r^T[\frac{\partial M}{\partial \alpha}]\{\phi\}_r
$$
$$
- 2\{\phi\}_r^T([\frac{\partial K}{\partial \alpha}] - \lambda_r[\frac{\partial M}{\partial \alpha}])\{\phi\}_r\{\phi\}_r^T[M] \sum_{s=1 \; s\neq r}^{N} \frac{1}{(\lambda_r - \lambda_s)}\{\phi\}_s\{\phi\}_r^T([\frac{\partial K}{\partial \alpha}] - \lambda_r[\frac{\partial M}{\partial \alpha}])\{\phi\}_s
$$
$$
+ 2\{\phi\}_r^T([\frac{\partial K}{\partial \alpha}] - \lambda_r[\frac{\partial M}{\partial \alpha}]) \sum_{s=1 \; s\neq r}^{N} \frac{1}{(\lambda_r - \lambda_s)}\{\phi\}_s\{\phi\}_r^T([\frac{\partial K}{\partial \alpha}] - \lambda_r[\frac{\partial M}{\partial \alpha}])\{\phi\}_s
$$

$$(5.30)$$

Noor and Whitworth [74] have calculated the first four orders of eigenvalue sensitivities in order to predict the modified eigenvalues for a large beamlike lattice

structure following a large modification. The results predicted by truncated Taylor's expansions shown below were far from satisfactory.

$$\lambda'_r = \lambda_o + \frac{\partial \lambda_r}{\partial \alpha} \cdot \Delta\alpha + \frac{1}{2!}\frac{\partial^2 \lambda_r}{\partial \alpha^2} \cdot (\Delta\alpha)^2 + \frac{1}{3!}\frac{\partial^3 \lambda_r}{\partial \alpha^3} \cdot (\Delta\alpha)^3 + \frac{1}{4!}\frac{\partial^4 \lambda_r}{\partial \alpha^4} \cdot (\Delta\alpha)^4 \qquad (5.31)$$

and

$$\{\phi'\}_r = \{\phi\}_r + \frac{\partial \{\phi\}_r}{\partial \alpha} \cdot \Delta\alpha + \frac{1}{2!}\frac{\partial^2 \{\phi\}_r}{\partial \alpha^2} \cdot (\Delta\alpha)^2 + \frac{1}{3!}\frac{\partial^3 \{\phi\}_r}{\partial \alpha^3} \cdot (\Delta\alpha)^3 + \frac{1}{4!}\frac{\partial^4 \{\phi\}_r}{\partial \alpha^4} \cdot (\Delta\alpha)^4 \qquad (5.32)$$

In fact, the limited success of sensitivity analysis in large modification prediction is inevitable because the value of higher-order sensitivity coefficients increase drastically when the size of structural modification is increased. Unfortunately, some structural analysts still believe that including some higher-order terms will produce a more accurate prediction for large modifications. Such thoughts contradict the original purpose of developing the sensitivity analysis/perturbation technique in numerical analysis as mentioned in the preceding section; namely, to investigate the stability of the eigenvalue problem .

## 5.4 CONDITION NUMBERS OF AN EIGENVALUE, EIGENVECTOR AND THE LIMITED BOUND OF FIRST ORDER SENSITIVITY ANALYSIS

Perturbation theory is based on Taylor's series expansions of the eigenvalues and eigenvectors of an unmodified system. Although these two Taylor's series converge for small structural modifications, it is not easy to specify what constitutes "small". In this section, condition numbers of an eigenvalue and eigenvectors of an eigenvalue problem are presented. A condition number to determine the limit of applicability for the first-order eigenvalue and eigenvector sensitivities is also given.

Suppose $\lambda_r$ is a simple eigenvalue of a general real matrix [A] and $\{_l\psi\}_r$ and $\{\psi\}_r$ are the corresponding left-hand and right-hand eigenvectors. Then as [AA] tends to the null matrix, [A+AA] has an eigenvalue $\lambda_r+\Delta\lambda_r$ in accordance with the stationary property of eigenvalue (Rayleigh principal) or, by using first-order eigenvalue sensitivity such that the change of the *rth* eigenvalue can be calculated by :

$$\Delta\lambda_r \cong \frac{\{_l\psi\}_r^T[\Delta A]\{\psi\}_r}{|\{_l\psi\}_r^T\{\psi\}_r|} \tag{5.33}$$

From equation (5.33), the absolute value of $\Delta\lambda_r$ is expressed as :

$$|\Delta\lambda_r| \leq \frac{\|\{_l\psi\}_r\|_2\|[\Delta A]\{\psi\}_r\|_2}{|\{_l\psi\}_r^T\{\psi\}_r|}$$

$$\leq \frac{\|[\Delta A]\|_2\|\{_l\psi\}_r\|_2\|\{\psi\}_r\|_2}{|\{_l\psi\}_r^T\{\psi\}_r|} \tag{5.34}$$

and $|\{_l\psi\}_r^T\{\psi\}_r|$ is the cosine of the angle $\theta_r$ between the left- and right-hand eigenvectors, $\{_l\psi\}_r$ and $\{\psi\}_r$. When $\cos\theta_r$ is very small, the corresponding eigenvalue is very sensitive to perturbations in the elements of [A]. Wilkinson[61] suggested that $|\{_l\psi\}_r^T\{\psi\}_r|^{-1}$ is a condition number for a nonrepeated eigenvalue. When the matrix [A] is symmetric and $\{_l\psi\}_r$ is equal to $\{\psi\}_r$. Since $\{_l\psi\}_r^T\{\psi\}_r$ is normalised to unity, the condition number for a nonrepeated eigenvalue is dependent on the spectral norm of modification matrix [AA].

For a general matrix with distinct eigenvalues, the eigenvector $\{\psi'\}_r$ of [A+AA] corresponding to $\{\psi\}_r$ is such that as $\|[\Delta A]\| \to 0$

$$\{\psi'\}_r - \{\psi\}_r \cong \sum_{\substack{s=1\\sfr}}^{N} \frac{\{\psi\}_s\{_l\psi\}_s^T[\Delta A]\{\psi\}_s}{\{_l\psi\}_s^T\{\psi\}_s(\lambda_r-\lambda_s)}$$

$$= \sum_{\substack{s=1\\sfr}}^{N} \frac{\{\psi\}_s\{_l\psi\}_s^T[\Delta A]\{\psi\}_s}{\cos\theta_s(\lambda_r-\lambda_s)} \tag{5.35}$$

Again, it can be seen that the quantity $\cos\theta_s$ is important, however, the sensitivity of the eigenvector is also dependent on the proximity of $\lambda_r$ to other eigenvalues. From equation (5.35), the smallest value of $(\lambda_r - \lambda_s)$, indicating the separation of eigenvalue $\lambda_r$ from its neighbours, is usually defined as a condition number for the corresponding eigenvector $\{\psi\}_r$.

The condition numbers for eigenvalues and eigenvectors have been presented and discussed in Wilkinson's classical monograph [61]. However, the limited bound of application for the first-order eigenvalue and eigenvector sensitivities was not fully discussed until Stewart published two papers concerning sensitivity of the generalised eigenvalue problem [80] in 1972 and error and perturbation bounds for subspaces associated with certain eigenvalue problems [81] in 1973. In Stewart's book [82], the following theorem is given:

THEOREM . Let $\lambda$ be a simple eigenvalue of $[A] \in \mathbb{C}^{N \times N}$ with right-hand eigenvector $\{\psi\}_r$ and left hand eigenvector $\{_l\psi\}_r$. Suppose $\{\psi\}_r$ has been scaled so that $\|\{\psi\}_r\|_2 = 1$ and $\{_l\psi\}_r$ has been scaled so that $\{_l\psi\}_r^H \{\psi\}_r = 1$. Let $[U] \in \mathbb{C}^{N \times (N-1)}$ be chosen so that $(\{\psi\}_r, [\Psi])$ is unitary and set

$$(\{\psi\}_r, [\Psi])^H [A](\{\psi\}_r, [\Psi]) = \begin{bmatrix} \lambda_r & \{\psi\}_r^H[A][\Psi] \\ 0 & [\Psi]^H[A][\Psi] \end{bmatrix} \qquad (5.36)$$

Let $[\Delta A] \in \mathbb{C}^{N \times N}$ be given and let

$$\delta = \|[\Delta A]\|_2, \ v = \|[\Psi]^H[A]^H\{\psi\}_r\|_2, \ \gamma = \|[\Psi]^H[\Delta A]\{\psi\}_r\|_2$$

and $\quad \mu = \|(\lambda_r[I] - [\Psi]^H[A][\Psi])^{-1}\|, \qquad (5.37)$

Then if

$$\frac{\gamma(v + \delta)}{(\mu - \delta)^2} < \frac{1}{4} \qquad (5.38)$$

there exists an eigenvalue $\lambda'_r$ of $[A + \Delta A]$ with eigenvector $\{\psi'\}_r$ which can be predicted accurately by first-order perturbation theory.

This theorem can be modified to deal with the generalised eigenvalue problem $[K+\Delta K]\{\phi'\}_r = \lambda'_r[M+\Delta M]\{\phi'\}_r$. The system matrix $[A]$ is substituted by the matrix $[M]^{-1}[K]$ if $[M]$ is invertible, the perturbation matrix $[\Delta A]$ is approximated by $[M+\Delta M]^{-1}([\Delta K] - \lambda_r[\Delta M])$ if $[M+\Delta M]$ is invertible. It should be noted that the approximate inequality (5.38) bounds the applicable range for first-order perturbation theory.

## 5.5 RELATIONSHIP BETWEEN **RAYLEIGH** QUOTIENT AND FIRST-ORDER SENSITIVITY ANALYSIS

The **Rayleigh** quotient provides an approximation of the eigenvalues based on trial vectors which are often the approximated eigenvectors of a self-adjoint system (Rayleigh [83] and Lancaster [84]) or the approximated left-hand and right-hand eigenvectors of a non-self-adjoint system (Lancaster [84]). So if the eigenvector of a modified system $\{\phi'\}_r$ is approximated by the eigenvector of the original system $\{\phi\}_r$, then for a self-adjoint system :

$$\lambda_R = \frac{\{\phi\}_r^T[K+\Delta K]\{\phi\}_r}{\{\phi\}_r^T[M+\Delta M]\{\phi\}_r} \qquad (5.39)$$

where $\lambda_R$ is called the **Rayleigh** quotient.

Normally, the unperturbed eigenvector $\{\phi\}_r$ is a reasonable estimate for the eigenvector of the modified system, and in that case, equation (5.39) gives an approximation of the modified eigenvalue.

For a stiffness modification, the **Rayleigh** quotient is expressed as :

$$\lambda_R = \lambda_r + \frac{\{\phi\}_r^T[\Delta K]\{\phi\}_r}{\{\phi\}_r^T[M]\{\phi\}_r} \tag{5.40}$$

Comparing the results obtained by **Rayleigh** quotient (equation (5.40)) with the results obtained by perturbation theory (equation (5.20)), it is found that when there is no mass perturbation ([AM]=[O]), the **Rayleigh** quotient and first-order perturbation theory yield identical results for a self-adjoint system.

For a mass modification, the **Rayleigh** quotient is expressed as :

$$\lambda_R = \frac{\{\phi\}_r^T[K]\{\phi\}_r}{\{\phi\}_r^T[M]\{\phi\}_r \left(1 + \dfrac{\{\phi\}_r^T[\Delta M]\{\phi\}_r}{\{\phi\}_r^T[M]\{\phi\}_r}\right)} \tag{5.41}$$

Expanding the above **Rayleigh** quotient to a power series, we have

$$\lambda_R = \lambda_r + \frac{-\lambda_r\{\phi\}_r^T[\Delta M]\{\phi\}_r}{\{\phi\}_r^T[M]\{\phi\}_r} + \lambda_r\frac{(\{\phi\}_r^T[\Delta M]\{\phi\}_r)^2}{(\{\phi\}_r^T[M]\{\phi\}_r)^2}$$
$$- \lambda_r\frac{(\{\phi\}_r^T[\Delta M]\{\phi\}_r)^3}{(\{\phi\}_r^T[M]\{\phi\}_r)^3} + \ldots \tag{5.42}$$

Hence, the first-order term in the **Rayleigh** quotient is the first-order eigenvalue perturbation $((\partial\lambda_r/\partial\alpha)\Delta\alpha)$. The second-order term is one of the mass perturbation terms which appear in the second-order eigenvalue sensitivity as shown in equation (5.30). Some higher-order mass perturbations terms are present because mass terms appear in the denominator of the **Rayleigh** quotient. However, most of the mass perturbation terms for the second-order eigenvalue sensitivity are not accounted for in the **Rayleigh** quotient expression. As a result one should not conclude that **Rayleigh** quotient is equivalent to a second-order eigenvalue perturbation procedure for mass perturbations. This can be seen from equation (5.30) of $\partial\lambda_r/\partial\alpha$, the other mass

perturbation terms are not accounted for in equation (5.42). Therefore, even though it keeps some higher-order mass perturbation terms, the **Rayleigh** quotient is in essence a first-order approximation.

It is fair to state that the **Rayleigh** quotient is almost equivalent to first-order perturbation theory, provided the trial vectors chosen in the **Rayleigh** quotient are the unperturbed eigenvectors.

## 5.6 **STRUCTURAL MODIFICATION ANALYSIS USING RAYLEIGH QUOTIENT ITERATION**

As mentioned before, when $\{\phi\}_r$ is an approximate eigenvector for the modified system, $\lambda_R$ (as defined in equation (5.40)) is a reasonable estimate for the corresponding eigenvalue. On the other hand, if $\lambda_R$ is an approximate eigenvalue, inverse iteration theory shows that the solution to $([K+\Delta K] - \lambda_R[M+\Delta M])\{\phi'\}_r = [M+\Delta M](\phi)_r$ will almost always provide a good approximate vector in a least-squares sense.

Combining these two ideas gives rise to **Rayleigh** quotient iteration. For a self-adjoint system $[K+\Delta K]$ is symmetric and $[M+\Delta M]$ is symmetric and positive definite, and the **Rayleigh** quotient iteration is expressed as follows [85]:

Assign $\{\psi'\}_r^0 = \{\phi\}_r$ and $\lambda_r'^0 = \lambda_r$     Ii $\{\psi'\}_r^0$ II, $= 1$

For k = 0, 1, . . .

$$\lambda'^{k+1}_r = \frac{\{\psi'\}_r^{k\,T}\,[K+\Delta K]\,\{\psi'\}_r^k}{\{\psi'\}_r^{k\,T}\,[M+\Delta M]\,\{\psi'\}_r^k}$$

Solve   $([K+\Delta K] - \lambda'^{k+1}_r[M+\Delta M])\{\phi'\}_r^{k+1} = [M+\Delta M]\,\{\psi'\}_r^k$   for $\{\phi'\}_r^{k+1}$

$$\{\psi'\}_r^{k+1} = \frac{\{\phi'\}_r^{k+1}}{\|\{\phi'\}_r^{k+1}\|_2}$$

A criterion should be set in order to terminate the iterative procedure after a finite number of steps. The appropriate criterion is to compare the difference between successive estimates of eigenvalues $\lambda'^{k+1}_r$ and $\lambda'^{k}_r$ such that when the ratio of these two estimates is smaller than a prescribed value, say $1 \mp 1\mathrm{E}\text{-}6$, $\lambda'^{k+1}_r$ is taken as the eigenvalue of the modified structure and $\{\phi'\}_r^k$ is the associated eigenvector. After the iterative procedure has been terminated, the eigenvector $\{\psi'\}_r^k$ is normalised with respect to the mass matrix of the modified structure by using the following equation :

$$\{\phi'\}_r = \frac{1}{\sqrt{(\{\psi'\}_r^{kT}[M+\Delta M])\{\psi'\}_r^k}} \{\psi'\}_r^k \qquad (5.43)$$

The mathematical basis for the **Rayleigh** quotient iteration method is that :

$$\lambda'_r = \frac{\{\phi'\}_r^T [K+\Delta K] \{\phi'\}_r}{\{\phi'\}_r^T [M+\Delta M] \{\phi'\}_r} \qquad (5.44)$$

minimises

$$f(\lambda'_r) = \|[K+\Delta K]\{\phi'\}_r - \lambda'_r[M+\Delta M]\{\phi'\}_r\|_{[M+\Delta M]} \qquad (5.45)$$

where $\| . \|_{[M+\Delta M]}$ is defined by $\|\{\phi\}\|_{[M+\Delta M]}^2 = \{\phi\}^T[M+\Delta M]^{-1}\{\phi\}$

So far, the algorithm and mathematical basis of **Rayleigh** quotient iteration have been given. However, the speed of convergence for this iterative process has not been studied. To study the speed of convergence, the estimate of *rth* eigenvector is expressed as :

$$\{\psi'\}_r^k = \{\phi'\}_r + \sum_{\substack{s=1 \ s\neq r}}^{N} \varepsilon_s \{\phi'\}_s \tag{5.46}$$

Then, from the well-known property of the **Rayleigh** quotient, the estimate of the *rth* eigenvalue is:

$$\lambda'^{k+1}_r = \frac{\lambda_r + \sum_{\substack{s=1 \ s\neq r}}^{N} \lambda_s \varepsilon_s^2}{1 + \sum_{\substack{s=1 \ s\neq r}}^{N} \varepsilon_s^2} \tag{5.47}$$

and hence

$$\{\phi'\}_r^{k+1} = \frac{\{\phi'\}_r}{(\lambda'_r - \lambda'^{k+1}_r)} + \sum_{\substack{s=1 \ s\neq r}}^{N} \frac{\varepsilon_s \{\phi'\}_s}{(\lambda'_s - \lambda'^{k+1}_r)} \tag{5.48}$$

**Apart** from a normalizing factor the estimate of *rth* eigenvector after k+l number of iterations is:

$$\{\psi'\}_r^{k+1} = \{\phi'\}_r + (\lambda'_r - \lambda'^{k+1}_r) \sum_{\substack{s=1 \ s\neq r}}^{N} \frac{\varepsilon_s \{\phi'\}_s}{(\lambda'_s - \lambda'^{k+1}_r)}$$

$$\cong \{\phi'\}_r + \frac{\sum_{\substack{s=1 \ s\neq r}}^{N} (\lambda_s - \lambda_r) \varepsilon_s^2}{1 + \sum_{\substack{s=1 \ s\neq r}}^{N} \varepsilon_s^2} \sum_{\substack{s=1 \ s\neq r}}^{N} \frac{\varepsilon_s \{\phi'\}_s}{(\lambda'_s - \lambda'^{k+1}_r)} \tag{5.48}$$

and all coefficients other than that of $\{\phi'\}_r$ are cubic in $\varepsilon_s$. Therefore, it can be concluded that the process is cubically convergent in the vicinity of each eigenvector.

There is an analogous process for unsymmetric matrices in which approximate **left**-hand and right-hand eigenvectors are found at each stage. The process is given as follows :

For k = 0, 1, . . .

$$\lambda'^{k+1}_r = \frac{\{_l\psi'\}^{k\ T}_r\ [K+\Delta K]\ \{\psi'\}^k_r}{\{_l\psi'\}^{k\ T}_r\ [M+\Delta M]\ \{\psi'\}^k_r}$$

Solve $([K+\Delta K] - \lambda'^{k+1}_r[M+\Delta M])\{\varphi'\}^{k+1}_r = [M+\Delta M]\{\psi'\}^k_r$  for $\{\varphi'\}^{k+1}_r$

Solve $([K+\Delta K] - \lambda'^{k+1}_r[M+\Delta M])^T\{_l\varphi'\}^{k+1}_r = [M+\Delta M]^T\{_l\psi'\}^k_r$ for $\{_l\varphi'\}^{k+1}_r$

$$\{\psi'\}^{k+1}_r = \frac{\{\varphi'\}^{k+1}_r}{\|\ \{\varphi'\}^{k+1}_r\ \|_2}$$

$$\{_l\psi'\}^{k+1}_r = \frac{\{_l\varphi'\}^{k+1}_r}{\|\ \{_l\varphi'\}^{k+1}_r\ \|_2}$$

This process is again ultimately cubically convergent. The left-hand and right-hand eigenvectors can be re-normalised with respect to the mass matrix of the modified structure by using equations (5.24) and (5.25).

## 5.7 NUMERICAL  EXAMPLES

In order to evaluate the effectiveness of the first-order sensitivity and the **Rayleigh** quotient iteration methods, a modification study was made on the lumped spring-mass model with **7DoF** shown in Figure 5.1. Figure 5.2 shows the point frequency response function for this model when the excitation was applied on point 4 (proportional damping loss factors of 0.001 were used to produce the **FRFs**). For several parameter changes at different locations of the model the first-order sensitivity and the **Rayleigh** quotient iteration methods have been applied to the original data to predict the consequent changes to the system's natural frequencies. The results are compared with the exact solution obtained by complete reanalysis.

In Figures 5.3 - 5.5, the shifts of eigenvalues are plotted with respect to a mass change at point 6. From these figures, it is noticed that the **Rayleigh** quotient iteration method gives accurate results for modes 1 to 6 although some numerical difficulties are 'observed for modes 7. Figure **5.5** shows that mode 7 converges to mode 6 if the mass change is greater than 60%. The first-order sensitivity method is a linear approximation based on an infinitesimal change of a parameter, and it is seen that the accuracy of prediction based on this parameter decreases with increasing magnitude of the mass change. Figure 5.6 shows the condition number (**LHS** of inequality (5.38)) against the percentage of mass change. Modes 3 and 4 are close modes and for these the first-order sensitivity is applicable only for small mass changes ($\approx 2.5\%$). Modes **5, 6** and 7 are also ill-conditioned for the mass perturbation at point 6.

The accuracy of the mode shapes predicted by the two techniques is assessed by using the Modal Assurance Criterion (MAC). Tables 5.1 and 5.2 contain the MAC values between eigenvectors from the first-order sensitivity analysis and the exact solution and between the **Rayleigh** quotient iteration and the exact solution. Examining the tables, it is seen that the **Rayleigh** quotient iteration yields consistently better correlation with the exact solution except when the mass change is greater than 60%, in this case mode 7 converges to mode 6.
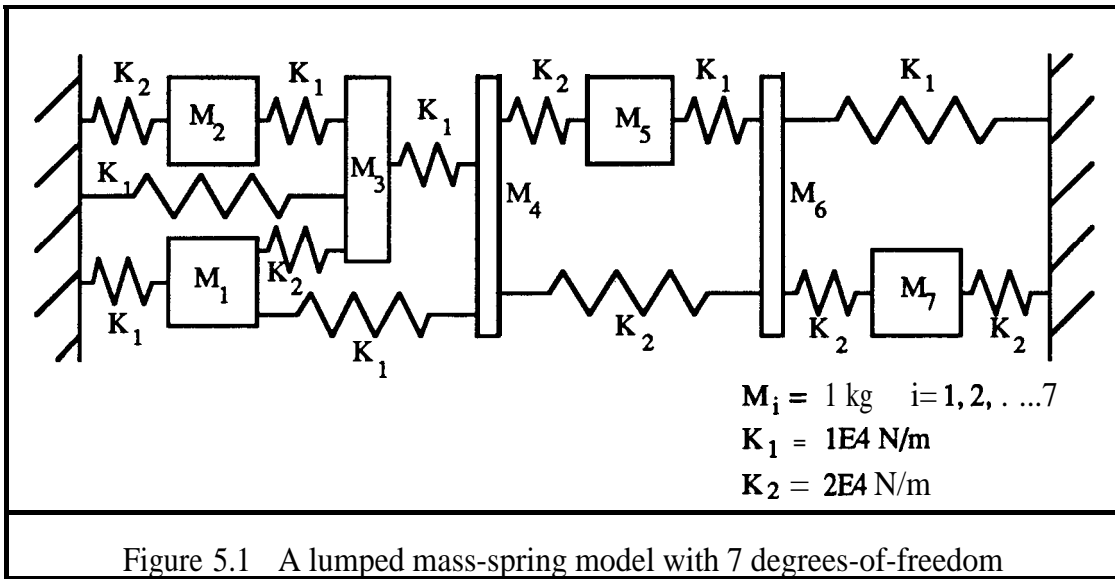
Figure 5.1   A lumped mass-spring model with 7 degrees-of-freedom
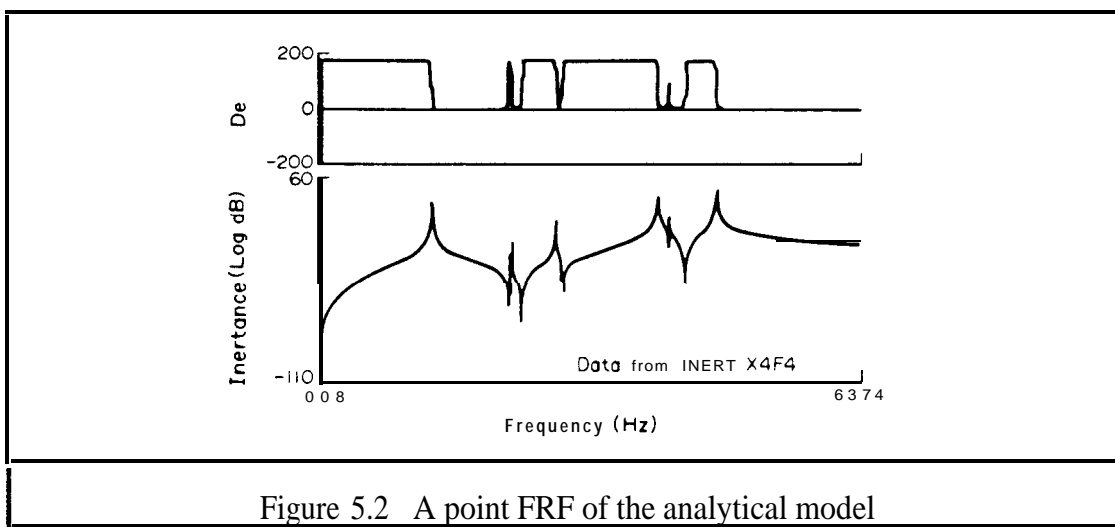


Figure 5.2   A point FRF of the analytical model
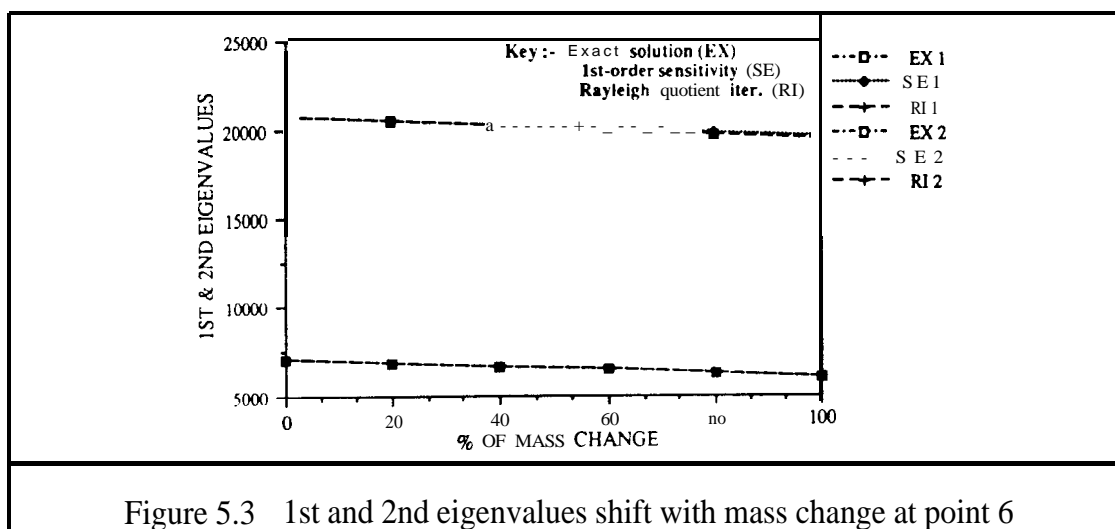


Figure 5.3   1st and 2nd eigenvalues shift with mass change at point 6

Figure 5.4   3rd and 4th eigenvalues shift with mass change at point 6



**Figure** 5.5   5th - 7th eigenvalues shift with mass change at point 6



Figure 5.6   Condition numbers vary with mass change at point 6
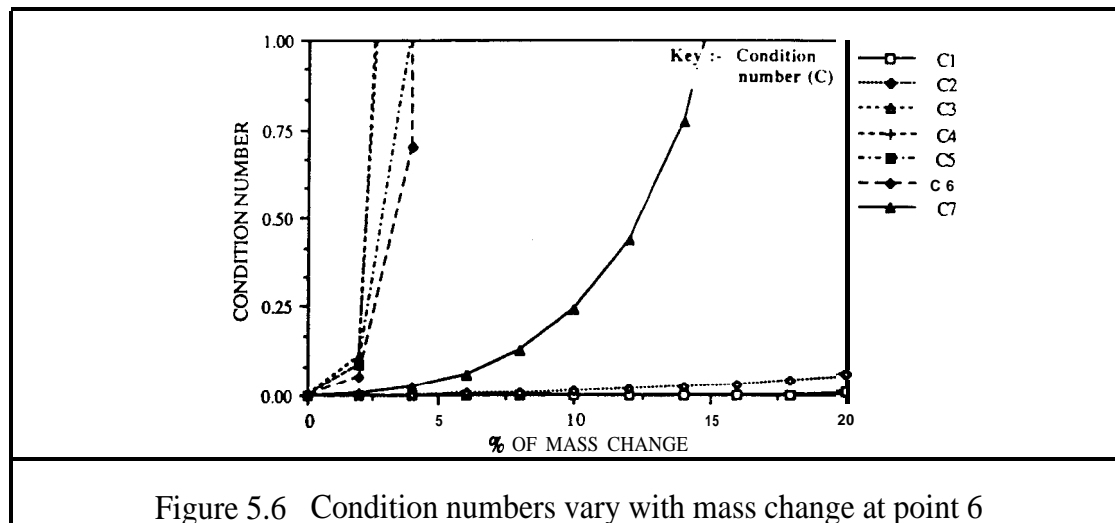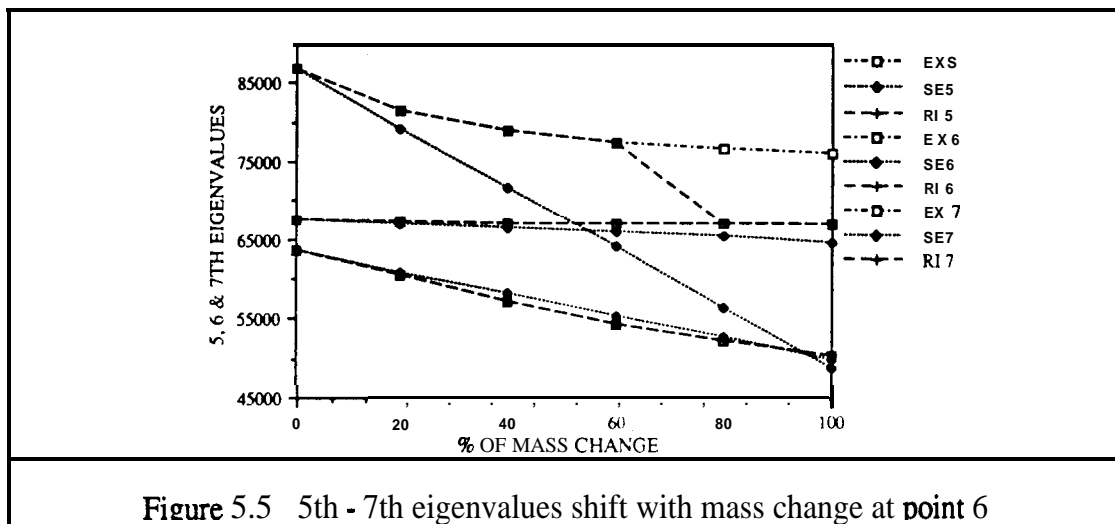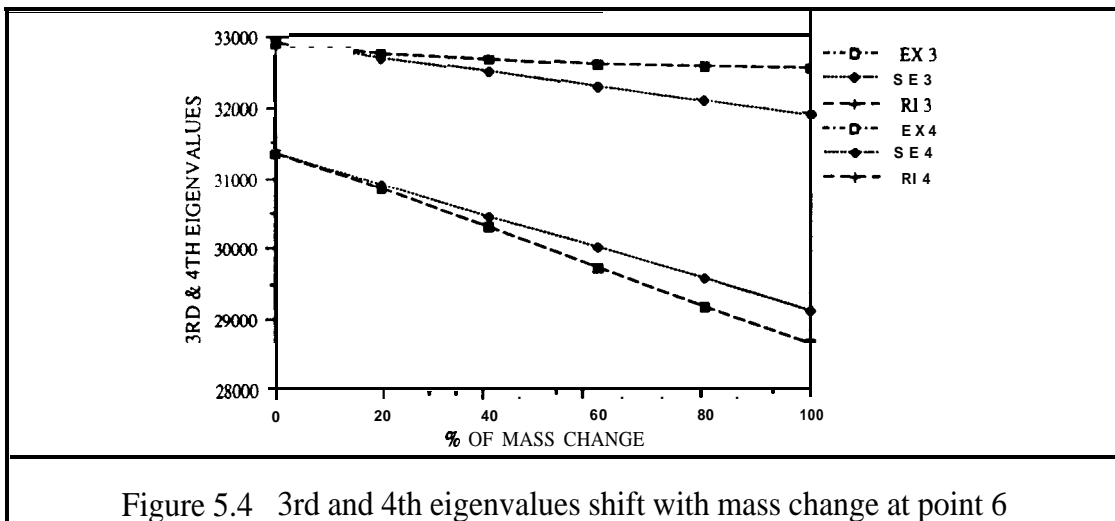
60 % Perturbation

| Exact | predicted (1st-order sensitivity) | | | | | | |
|---|---|---|---|---|---|---|---|
| | 1 | 2 | 3 | 4 | 5 | 6 | 7 |
| 1 | **1.000** | 0.003 | 0.002 | 0.002 | 0.005 | 0.002 | 0.021 |
| 2 | 0.004 | **1.000** | 0.000 | 0.003 | 0.001 | 0.001 | 0.011 |
| 3 | 0.006 | 0.003 | 0.959 | 0.035 | 0.000 | 0.004 | 0.018 |
| 4 | 0.000 | 0.000 | 0.031 | 0.964 | 0.000 | 0.000 | 0.001 |
| 5 | 0.016 | 0.007 | 0.019 | 0.003 | 0.812 | 0.094 | 0.061 |
| 6 | 0.000 | 0.000 | 0.000 | 0.000 | 0.157 | 0.834 | 0.000 |
| 7 | 0.004 | 0.002 | 0.004 | 0.000 | 0.012 | 0.082 | 0.938 |

100 % Perturbation

| Exact | Predicted (1st-order sensitivity) | | | | | | |
|---|---|---|---|---|---|---|---|
| 1 | 1.000 | 0.008 | 0.004 | 0.005 | 0.007 | 0.003 | 0.037 |
| 2 | 0.012 | 0.999 | 0.001 | 0.009 | 0.000 | 0.003 | 0.022 |
| 3 | 0.016 | 0.007 | 0.855 | 0.097 | 0.001 | 0.008 | 0.035 |
| 4 | 0.001 | 0.000 | 0.111 | 0.879 | 0.000 | 0.000 | 0.001 |
| 5 | 0.034 | 0.016 | 0.049 | 0.025 | 0.625 | 0.130 | 0.101 |
| 6 | 0.000 | 0.000 | 0.000 | 0.000 | 0.312 | 0.667 | 0.000 |
| 7 | 0.005 | 0.003 | 0.005 | 0.001 | 0.009 | 0.203 | 0.821 |

Table 5.1 MAC values for the modified eigenvectors between the 1 St-order sensitivity analysis and the exact solution for the mass modification at point 6

60 % Perturbation

| Exact | predicted (Rayleigh quotient iteration) | | | | | | |
|---|---|---|---|---|---|---|---|
| | 1 | 2 | 3 | 4 | 5 | 6 | 7 |
| 1 | 1.000 | 0.004 | 0.006 | 0.000 | 0.016 | 0.000 | 0.004 |
| 2 | 0.004 | **1.000** | 0.002 | 0.000 | 0.007 | 0.000 | 0.002 |
| 3 | 0.006 | 0.002 | 1.000 | 0.000 | 0.010 | 0.000 | 0.003 |
| 4 | 0.000 | 0.000 | 0.000 | 1.000 | 0.001 | 0.000 | 0.000 |
| 5 | 0.016 | 0.007 | 0.007 | 0.001 | **1.000** | **0.000** | 0.006 |
| 6 | 0.000 | 0.000 | 0.000 | 0.000 | 0.000 | 1.000 | 0.000 |
| 7 | 0.004 | 0.002 | 0.003 | 0.000 | 0.006 | 0.000 | 1.000 |

100 % Perturbation

| Exact | Predicted (Rayleigh quotient iteration) | | | | | | |
|---|---|---|---|---|---|---|---|
| 1 | 1.000 | 0.014 | 0.017 | 0.001 | 0.034 | 0.000 | 0.000 |
| 2 | 0.014 | **1.000** | 0.007 | 0.000 | 0.014 | 0.000 | 0.000 |
| 3 | 0.017 | 0.007 | **1.000** | **0.000** | 0.017 | 0.000 | 0.000 |
| 4 | 0.001 | 0.000 | 0.000 | 1.000 | 0.001 | 0.000 | 0.000 |
| 5 | 0.034 | 0.014 | 0.017 | 0.001 | **1.000** | **0.000** | **0.000** |
| 6 | **0.000** | **0.000** | **0.000** | **0.000** | **0.000** | 1.000 | 1.000 |
| 7 | 0.005 | 0.002 | 0.003 | 0.000 | 0.005 | 0.000 | 0.000 |

Table 5.2 MAC values for the modified eigenvectors between the Rayleigh quotient iteration and the exact solution for the mass modification at point 6

In Figures 5.7-5.9, the shifts of eigenvalues are plotted for the case of a stiffness change made between points 3 and 4. It is seen that the **Rayleigh** quotient iteration method gives accurate prediction for all modes. The condition number against the percentage of stiffness modification change is shown in Figure 5.10. From this figure, it is noticed that modes 2, 3, 5 and 6 are ill-conditioned for this stiffness modification. The limit of application for the **first-order** perturbation theory for all modes is approximately equal to 4%. The MAC values between eigenvectors **from** those two techniques and those from the exact solution are shown in Tables 5.3 and 5.4. From the results, it is observed that the **Rayleigh** quotient iteration yields better results even when the magnitude of stiffness modification is large.
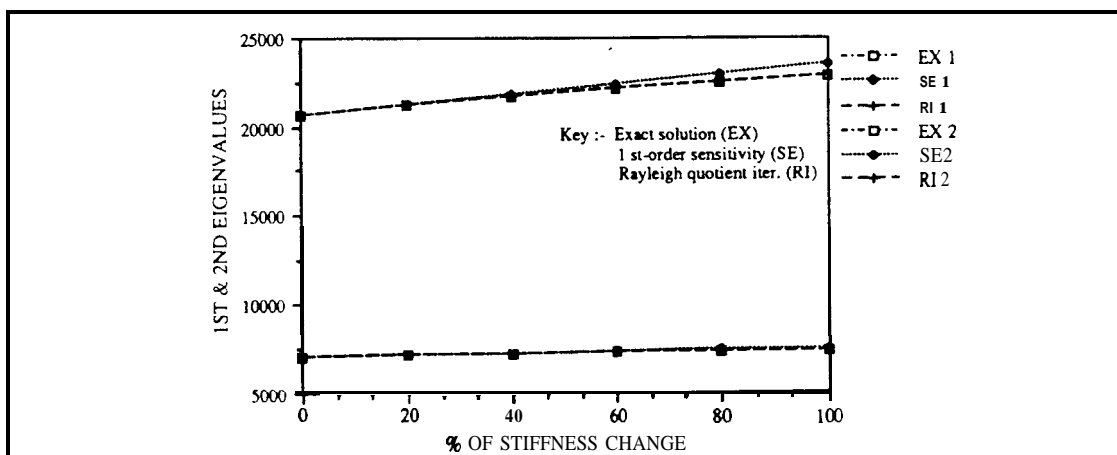


Figure 5.7   1st and 2nd eigenvalues shift with stiffness change between points 3 and 4
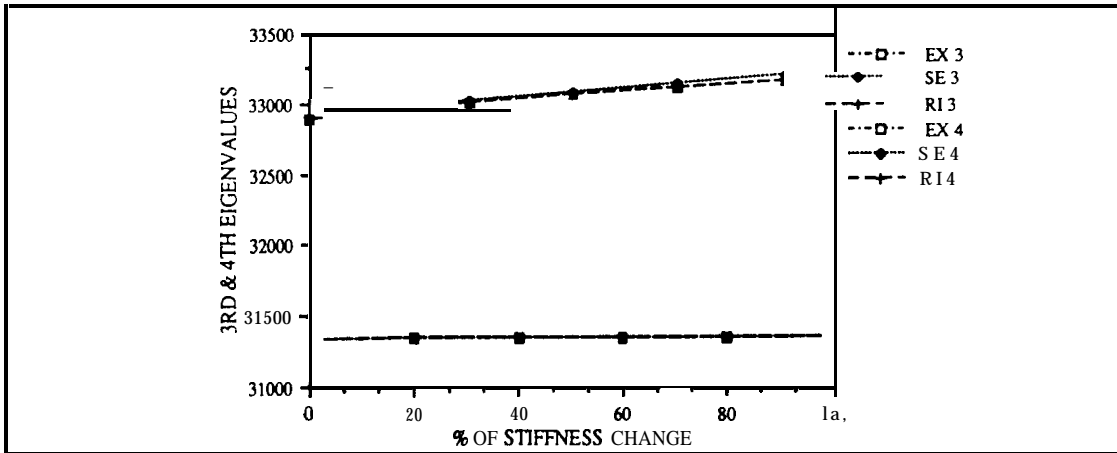
Figure 5.8   3rd and 4th eigenvalues shift with stiffness change between points 3 and 4
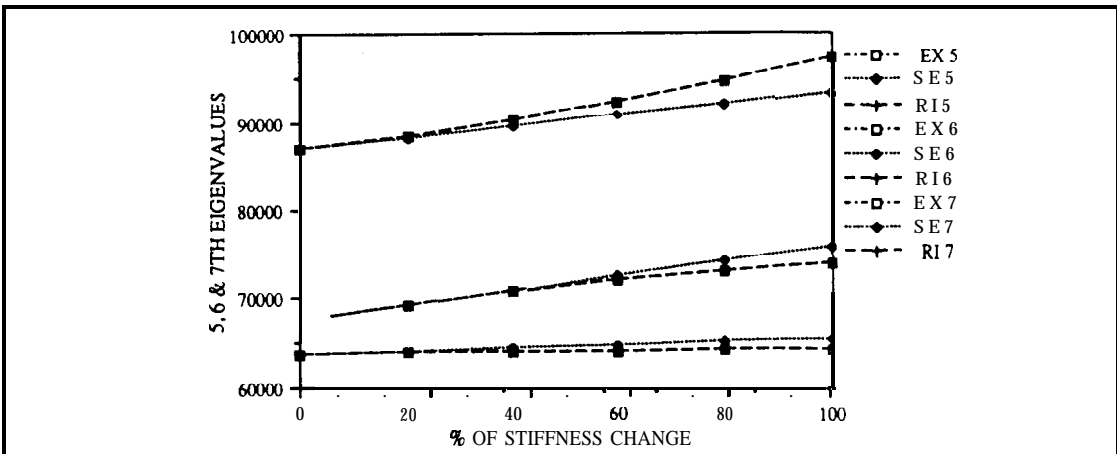


Figure 5.9   5th - 7th eigenvalues shift with stiffness change between points 3 and 4
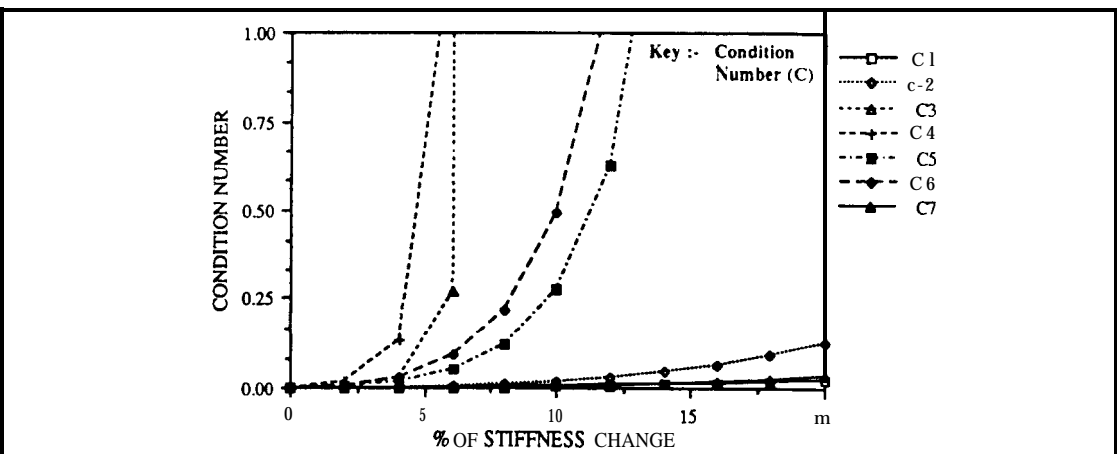


Figure 5.10   Condition numbers vary with stiffness change between points 3 and 4

100 % Perturbation

| Exact | Predicted (M-order sensitivity) | | | | | | |
|---|---|---|---|---|---|---|---|
| | 1 | 2 | 3 | 4 | 5 | 6 | 7 |
| 1 | 0.979 | 0.017 | 0.000 | 0.000 | 0.001 | 0.001 | 0.000 |
| 2 | 0.014 | 0.909 | 0.001 | 0.023 | 0.016 | 0.014 | 0.005 |
| 3 | 0.000 | 0.001 | 0.994 | 0.005 | 0.000 | 0.000 | 0.000 |
| 4 | 0.001 | 0.017 | 0.004 | 0.964 | 0.004 | 0.003 | 0.001 |
| 5 | 0.000 | 0.001 | 0.000 | 0.000 | 0.255 | 0.697 | 0.004 |
| 6 | 0.002 | 0.020 | 0.000 | 0.003 | 0.532 | 0.125 | 0.506 |
| 7 | 0.004 | 0.035 | 0.005 | 0.005 | 0.192 | 0.161 | 0.483 |

Table 5.3    MAC values for the modified eigenvectors between the 1 St-order sensitivity analysis and the exact solution for the stiffness modification between points 3 and 4

100 % Perturbation

| Exact | Predicted (Rayleigh quotient iteration) | | | | | | |
|---|---|---|---|---|---|---|---|
| | 1 | 2 | 3 | 4 | 5 | 6 | 7 |
| 1 | 1.000 | 0.000 | 0.000 | 0.000 | 0.000 | 0.000 | 0.000 |
| 2 | 0.000 | 1.000 | 0.000 | 0.000 | 0.000 | 0.000 | 0.000 |
| 3 | 0.000 | 0.000 | 1.000 | 0.000 | 0.000 | 0.000 | 0.000 |
| 4 | 0.000 | 0.000 | 0.000 | 1.000 | 0.000 | 0.000 | 0.000 |
| 5 | 0.000 | 0.000 | 0.000 | 0.000 | 1.000 | 0.000 | 0.000 |
| 6 | 0.000 | 0.000 | 0.000 | 0.000 | 0.000 | 1.000 | 0.000 |
| 7 | 0.000 | 0.000 | 0.000 | 0.000 | 0.000 | 0.000 | 1.000 |

Table 5.4    MAC values for the modified eigenvectors between the **Rayleigh** quotient iteration and the exact solution for the stiffness modification between points 3 and 4

## 5.8  ALTERNATIVE  STRUCTURAL  REANALYSIS  TECHNIQUE

In the preceding section the **Rayleigh** quotient and the inverse iteration are combined to yield the **Rayleigh** quotient iteration.  However, it should be noted that the inverse iteration is an alternative technique which is applicable in structural modification analysis when the baseline information, the modal properties of the unmodified structure, provide reasonably good approximations to the modified eigenproperties.

The inverse iteration method is expressed as follows:

Assign $\{\psi'\}_r^0 = \{\phi\}_r$          $\| \{\psi'\}_r^0 \|_2 = 1$

For k = 0, 1, . . .

Solve  $([K+\Delta K] - \lambda_r [M+\Delta M])\{\phi'\}_r^{k+1} = [M+\Delta M]\{\psi'\}_r^k$   for $\{\phi'\}_r^{k+1}$

$$\{\psi'\}_r^{k+1} = \frac{\{\phi'\}_r^{k+1}}{\| \{\phi'\}_r^{k+1} \|,}$$

The first equation is the basis of a direct iteration method for finding the eigenvectors of the modified structure. By using equation (5.46), the following explicit form for $\{\phi'\}_r$ after k number of iterations is derived:

$$\{\phi'\}_r^{k+1} = \frac{\{\psi'\}_r^k}{(\lambda_r'-\lambda_r)^k} + \sum_{\substack{s=1 \\ s\neq r}}^{N} \frac{\varepsilon_s \{\psi'\}_s^k}{(\lambda_s'-\lambda_r)^k} \tag{5.49}$$

Then, apart from a normalizing factor, the estimate of *rth* eigenvector of the modified structure is:

$$\{\psi'\}_r^{k+1} = \frac{1}{(\lambda_r'-\lambda_r)^k}\left\{\{\psi'\}_r^k + \sum_{\substack{s=1 \\ s\neq r}}^{N} \varepsilon_s \frac{(\lambda_r'-\lambda_r)^k}{(\lambda_s'-\lambda_r)^k} \{\psi'\}_s^k\right\} \tag{5.50}$$

The characteristic of this procedure is clearly illustrated by equation (5.50). It can be seen that as k gets large, $\{\psi'\}_r^{k+1}$ approaches a multiple of the mode $\{\psi'\}_r$. The convergence is geometric, i.e. like terms of the geometric progression $6, \delta^2, \delta^3, \ldots$. The speed of convergence depends essentially on how near $\lambda_r$ is taken to $\lambda_r'$.

As a practical structural reanalysis algorithm, the inverse iteration method has some attractive features and some severe limitations. Its strongest point is the simplicity of the recursion. For example, only one matrix inversion is required during the whole iterative procedure. In addition, no ill-conditioning problems will be encountered in the matrix inversion because the matrix $([K+\Delta K]-\lambda_r [M+\Delta M])$ is in general

nonsingular as it is very rare for the original and modified structure having the same eigenvalue(s). A drawback to the method is that it will converge slowly when $\lambda'_r$ is not strongly dominant. This method produces an approximation for the eigenvector, $\{\psi'\}_r$, but no information is given directly about the eigenvalue. An auxiliary computation - using the **Rayleigh** quotient in determining the corresponding eigenvalue - would be necessary.

## 5.9 POSSIBLE USE OF THESE MODIFICATION TOOLS

The FE or analytical model of a complex structure normally has a large number of degrees-of-freedom and design variables. The primary analysis yields some of the eigenvalues in a given frequency range, together with the corresponding eigenvectors.

Usually, the model needs to be progressively modified during an automated optimum design process. The first-order eigenvalue sensitivity approach ranks possible structural modification sites in their order of effectiveness at influencing each particular mode. The **Rayleigh** quotient iteration and inverse iteration methods can be used in combination in the following way : **Rayleigh** quotient iteration is used until a reasonably good value of $\lambda'_r$ is obtained, say $(\lambda'^{k+1}_r/\lambda'^k_r)$ equals to $1\pm1E-2$ and, incidentally, quite a good approximation of corresponding eigenvector. **Rayleigh** quotient iteration is then replaced by inverse iteration with the value of $\lambda'^k_r$ being fixed, starting with the final vector obtained from the **Rayleigh** quotient iteration. Finally, when the eigenvector has been determined, the refined eigenvalue is determined using **Rayleigh** quotient. The condition number monitors the behaviour of the modes in the structural modification analysis. By combining these modification tools, an iterative program can be written to calculate the optimum condition for a structure specified by the user.

If damping is included and is assumed to be viscous, its inclusion will lead to a quadratic generalised eigenvalue problem such that the matrix equation for free motion is:

$$\lambda'^2_r[M+\Delta M]\{\phi'\}_r + \lambda'_r[C+\Delta C]\{\phi'\}_r + [K+\Delta K]\{\phi'\}_r = \{0\} \qquad (5.5 \ 1)$$

where $[M]$, $[C]$ and $[K]$ are $N x N$ mass, viscous damping and stiffness matrices of the original structure; and $[AM]$, $[AC]$, $[AK]$ are the mass modification, damping modification and stiffness modification matrices respectively.

It can be shown that if the eigenvalue-eigenvector pair $(\lambda'_r, \{\phi'\}_r)$ satisfy equation (5.51), they also satisfy :

$$\left[ \begin{bmatrix} [0] & [K+\Delta K] \\ [K+\Delta K][C+\Delta C] \end{bmatrix} - \lambda'_r \begin{bmatrix} [K+\Delta K] & [0] \\ [0] & -[M+\Delta M] \end{bmatrix} \right] \begin{Bmatrix} \{\phi'\}_r \\ \lambda'_r\{\phi'\}_r \end{Bmatrix} = \begin{Bmatrix} \{0\} \\ \{0\} \end{Bmatrix} \qquad (5.52)$$

Equation (5.52) is a generalised eigenvalue problem which is described by $[[A]-\lambda'_r[B]]\{\theta\}_r=\{0\}$. The **Rayleigh** quotient iteration and inverse iteration are also applicable in solving this problem - to find an eigensolution in a $2N$ -dimensional space.

The **Rayleigh** quotient is determined by :

$$\lambda_R = \frac{\{_l\theta\}_r^T[A]\{\theta\}_r}{\{_l\theta\}_r^T[B]\{\theta\}_r} \qquad (5.53)$$

where $\{_l\theta\}_r$ is an approximate left-hand eigenvector.

Lancaster [84] has rewritten (5.53) in terms of an equation equivalent to equation (5.51) to produce a generalisation of the **Rayleigh** quotient for h-matrices of arbitrary order. For quadratic h-matrices this generalisation states that given an approximate left-hand eigenvector $\{_l\phi\}_r$, an approximate right-hand eigenvector $\{\phi\}_r$ and an approximate eigenvalue $\lambda_r$, the "best" estimate of the eigenvalue of the modified structure is given by

$$\lambda_R \;=\; \lambda_r \;-\; \frac{\{_l\phi\}_r^T[\lambda_r^2[M+\Delta M] + \lambda_r[C+\Delta C] + [K+\Delta K]]\{\phi\}_r}{\{_l\phi\}_r^T[2\lambda_r[M+\Delta M] + [C+\Delta C]]\{\phi\}_r} \qquad (5.54)$$

## 5.10    CONCLUDING  REMARKS

This chapter highlights the application of the sensitivity analysis methods to structural dynamics developed by numerical analysts as well as structural analysts and presents a historical development of first- and higher-order eigenvalue and eigenvector sensitivities. It can be concluded that first-order eigenvalue sensitivities are very useful to rank the order of importance for the sites during structural modification. First-order eigenvector sensitivities are sometimes impossible to compute because to do so requires the complete sets of left-hand and right-hand eigenvectors for a mechanical structure.  Calculation of higher-order eigenvalue and eigenvector sensitivities is difficult and expensive.  Summation of a truncated eigensystem sensitivities series does not guarantee a more accurate prediction and, even if the Taylor's series converges the speed of convergence, may be too slow to give satisfactory results in a finite summation.

Condition numbers are presented to provide information about the sensitivities of the eigenvalues and eigenvectors of the eigenvalue problem [A] $\{\phi\}_r = \lambda_r\{\phi\}_r$ to small perturbations of [A]. A condition number is presented which gives the limited bound

of the application of **first-order** sensitivity analysis. It is generalised to deal with the generalised eigenvalue problem $[K] \{\phi\}_r = \lambda_r [M] (\phi\}_r$ for small perturbations of $[K]$ and/or $[M]$.

A **Rayleigh** quotient iteration method is presented to compute the modified eigenvalues and their associated eigenvectors of a large analytical model. It has been proved that if the first prediction of an eigenvalue by using the unperturbed eigenvector is closer to the modified one than to its neighbouring eigenvalues, this iteration method converges globally and the convergence is ultimately cubic. The inverse iteration method and its convergence analysis are also presented to provide an insight into this alternative structural reanalysis technique. The advantages and drawbacks for both methods are fully discussed. It is demonstrated that it is always possible to generalise those iterative procedures in order to deal with **unsymmetric** quadratic **generalised** eigenvalue problem - the inclusion of gyroscopic force and viscous damping etc.

# 6 NON-LINEAR SENSITIVITY ANALYSIS OF MECHANICAL STRUCTURES

## 6.1 INTRODUCTION

In practice, when the modal properties of an **FE** model of a structure have been computed, it is useful to have some procedure which will enable us to determine the corresponding modal properties of the modified structure as it is progressively changed during a design optimization process. Since the determination of those modal properties will almost inevitably demand further computation, it is not unreasonable to require that the structural modification analysis (or **reanalysis** ) technique should lead directly to the modal properties of the modified structure and that it should keep the computation cost to a minimum. In Chapter 5, some structural reanalysis techniques were presented in the case that. the mass and stiffness matrices were given, together with some eigenvalues and the corresponding eigenvectors of the original structure, and the mass modification and stiffness modification matrices.

This chapter presents a new computation procedure for determining the revised modal properties (eigenvalues and mass-normalised eigenvectors) in a structural modification analysis where only the eigenvalues and the corresponding eigenvectors of the original structure, and the mass modification and stiffness modification matrices are given. This situation may arise whenever the structural modification is directly made on a practical structure whose spatial properties, the original mass and the stiffness matrices, cannot be determined precisely. The new procedure is based on expressing the

eigenvectors of the modified structure as a linear combination of the eigenvectors of the original structure and employs the stationary property of the **Rayleigh** quotient to determine the modified structure's eigenvalues. It has the same theoretical basis as first- and second-order sensitivity analysis, but here the nonlinear effects contributed by *all* high-order terms (generally assumed to be **small** relative to the effect contributed by first- and second-order terms [55,67-70,86]) are preserved in full. Hence, the usual shortcoming of sensitivity analysis - that it is limited to small modifications - is overcome.

The proposed procedure is inspired by following ***Jahn's*** method [58,87] for the improvement of approximate eigenvalues and eigenvectors of an algebraic eigenvalue problem. In Jahn's paper, he suggested that a perturbation method can be used to improve the accuracy of the eigensolutions when the complete sets of approximate eigenvalues and eigenvectors of a Lagrange frequency matrix equation for an mechanical structure are given. However, the mathematical formulation of structural modification analysis is different from refining the eigensolutions of a matrix pencil ([K], [M]) and so, the nonlinear terms not accounted for in a first-order sensitivity analysis, or in truncated Taylor's expansion approximations, have to be retained.

## *6.2* THEORETICAL BASIS OF NONLINEAR SENSITIVITY ANALYSIS

The matrix equation of free motion of an undamped mechanical structure which is characterized by an *NxN* mass matrix [M] and an *NxN* stiffness matrix [K], is

$$[M]\{\ddot{x}\} + [K]\{x\} = \{0\} \tag{6.1}$$

This equation has N eigenvalues and N mass-normalised eigenvectors, all of which are nonlinear functions of the elements of [M] and [K]. In structural dynamics, equation (6.1) is conveniently rewritten in terms of the modal properties as follows :

$$[K][\Phi] - [\lambda][M][\Phi] = \{0\} \qquad (6.2)$$

where $[\lambda]$ is an $NxN$ diagonal eigenvalue matrix and $[\Phi]$ is an $NxN$ mass-normalised eigenvector matrix.

Suppose that the mass modification and stiffness modification matrices are defined as [AM] and [AK] respectively. The *rth* eigenvalue and *rth* eigenvector for the modified structure are expressed as :

$$\lambda'_r = \lambda_r + Ah, \qquad (6.3)$$

$$\{\psi'\}_r = \{\phi\}_r + \sum_{s=1 \ s \neq r}^{n} c_{rs}\{\phi\}_s \qquad (6.4)$$

The algebraic eigenvalue properties of the modified structure are governed by :

$$[-(\lambda_r + \Delta\lambda_r)[M+\Delta M] + [K+\Delta K]]\{\{\phi\}_r + \sum_{s=1 \ s \neq r}^{n} c_{rs}\{\phi\}_s\} = \{0\} \qquad (6.5)$$

Expanding the left-hand side of equation (6.5) yields

$$[-(\lambda_r + \Delta\lambda_r)[M] - (\lambda_r + \Delta\lambda_r)[\Delta M] + [K] + [\Delta K]] \sum_{s=1 \ s \neq r}^{n} c_{rs}\{\phi\}_s +$$

$$[-\Delta\lambda_r[M] - (\lambda_r + \Delta\lambda_r)[\Delta M] + [\Delta K]]\{\{\phi\}_r\} = \{0\} \qquad (6.6)$$

In order to determine the coefficients $c_{rs}$, the mode participation factors which determine the change in the eigenvectors, equation (6.5) is post-multiplied by the transpose of $\{\phi\}_s (s \neq r)$. This gives

$$c_{rs}\left(-(\lambda_r+\Delta\lambda_r)\{\phi\}_s^T[M]\{\phi\}_s+\{\phi\}_s^T[K]\{\phi\}_s-(\lambda_r+\Delta\lambda_r)\{\phi\}_s^T[\Delta M]\{\phi\}_s+\{\phi\}_s^T[\Delta K]\{\phi\}_s\right)$$

$$-(\lambda_r+\Delta\lambda_r)\sum_{\substack{t=1 \\ t\neq r,s}}^{n}c_{rt}\{\phi\}_s^T[\Delta M]\{\phi\}_t+\sum_{\substack{t=1 \\ t\neq r,s}}^{n}c_{rt}\{\phi\}_s^T[\Delta K]\{\phi\}_t-(\lambda_r+\Delta\lambda_r)\{\phi\}_s^T[\Delta M]\{\phi\}_r+\{\phi\}_s^T[\Delta K]\{\phi\}_r=\{0\}$$

$$(6.7)$$

Hence,

$$c_{rs} = \frac{-(\lambda_r+\Delta\lambda_r)\{\phi\}_s^T[\Delta M]\{\phi\}_r+\{\phi\}_s^T[\Delta K]\{\phi\}_r-(\lambda_r+\Delta\lambda_r)\sum_{\substack{t=1 \\ t\neq r,s}}^{n}c_{rt}\{\phi\}_s^T[\Delta M]\{\phi\}_t+\sum_{\substack{t=1 \\ t\neq r,s}}^{n}c_{rt}\{\phi\}_s^T[\Delta K]\{\phi\}_t}{(\lambda_r+\Delta\lambda_r)\{\phi\}_s^T[M]\{\phi\}_s-\{\phi\}_s^T[K]\{\phi\}_s+(\lambda_r+\Delta\lambda_r)\{\phi\}_s^T[\Delta M]\{\phi\}_s-\{\phi\}_s^T[\Delta K]\{\phi\}_s}$$

$$= \frac{-(\lambda_r+\Delta\lambda_r)\{\phi\}_s^T[\Delta M]\{\phi\}_r+\{\phi\}_s^T[\Delta K]\{\phi\}_r-(\lambda_r+\Delta\lambda_r)\sum_{\substack{t=1 \\ t\neq r,s}}^{n}c_{rt}\{\phi\}_s^T[\Delta M]\{\phi\}_t+\sum_{\substack{t=1 \\ t\neq r,s}}^{n}c_{rt}\{\phi\}_s^T[\Delta K]\{\phi\}_t}{(\lambda_r+\Delta\lambda_r)-\lambda_s+(\lambda_r+\Delta\lambda_r)\{\phi\}_s^T[\Delta M]\{\phi\}_s-\{\phi\}_s^T[\Delta K]\{\phi\}_s}$$

$$(6.8)$$

where $\lambda_r$ and $\lambda_s$ are eigenvalues of the original structure.

The modal kinetic energy term $(\{\phi\}_s^T[M]\{\phi\}_s)$ is equal to unity because the eigenvectors of the original structure are mass-normalised. The terms $(\{\phi\}_s^T[\Delta M]\{\phi\}_r), (\{\phi\}_s^T[\Delta K]\{\phi\}_r)$ etc. can be calculated without knowing all elements of the eigenvectors $\{\phi\}_s$ and $\{\phi\}_r$ because only those elements of the eigenvectors used to pre-multiply or post-multiply the non-zero elements of [AM] and [AK] are required (i.e. those corresponding to modification sites).

Once the eigenvectors of the modified structure are determined using equation (6.4), they can be re-normalised in order to produce the mass-normalised eigenvectors of the modified structure by using the following equation :

$$\{\phi'\}_r \;=\; (\{\psi'\}_r^T[M+\Delta M]\{\psi'\}_r)^{-\frac{1}{2}}\;\{\psi'\}_r \tag{6.9}$$

or

$$\{\phi'\}_r = (1+ \sum_{\substack{s=1 \\ s\neq r}}^{n} c_{rs}{}^2 +\{\phi\}_r^T[\Delta M]\{\phi\}_r +2 \sum_{\substack{s=1 \\ s\neq r}}^{n} c_{rs}\{\phi\}_r^T[\Delta M]\{\phi\}_s + \sum_{\substack{t=1 \\ t\neq r}}^{n} c_{rt} \sum_{\substack{s=1 \\ s\neq r}}^{n} c_{rs}\{\phi\}_t^T[\Delta M]\{\phi\}_s)^{-\frac{1}{2}} \{\psi'\}_r$$

$$\tag{6.10}$$

The rth eigenvalue of the modified structure, $\lambda'_r$, is determined using the **Rayleigh** quotient as shown below:

$$\lambda'_r \;=\; \frac{\{\{\phi\}_r+ \displaystyle\sum_{\substack{s=1 \\ s\neq r}}^{n} c_{rs}\{\phi\}_s\}^T \,[K+\Delta K]\{\{\phi\}_r+ \displaystyle\sum_{\substack{s=1 \\ s\neq r}}^{n} c_{rs}\{\phi\}_s\}}{\{\{\phi\}_r+ \displaystyle\sum_{\substack{s=1 \\ s\neq r}}^{n} c_{rs}\{\phi\}_s\}^T \,[M+\Delta M]\{\{\phi\}_r+ \displaystyle\sum_{\substack{s=1 \\ s\neq r}}^{n} c_{rs}\{\phi\}_s\}} \tag{6.11}$$

The numerator of the right-hand side of the above equation can be expanded in the following form:

$$\{\phi\}_r^T[K]\{\phi\}_r + \sum_{\substack{s=1 \\ s\neq r}}^{n} c_{rs}{}^2\{\phi\}_s^T[K]\{\phi\}_s +\{\phi\}_r^T[\Delta K]\{\phi\}_r +2 \sum_{\substack{s=1 \\ s\neq r}}^{n} c_{rs}\{\phi\}_r^T[\Delta K]\{\phi\}_s + \sum_{\substack{t=1 \\ t\neq r}}^{n} c_{rt}( \sum_{\substack{s=1 \\ s\neq r}}^{n} c_{rs}\{\phi\}_t^T[\Delta K]\{\phi\}_s)$$

$$\tag{6.12}$$

Similarly, the denominator of the right-hand side of equation (6.11) can be expanded in a series form, as for the numerator, with the difference that the stiffness modification and stiffness matrices are replaced by the mass modification and mass matrices respectively. The eigenvectors of the original structure are mass **normalised** and so equation (6.11) can be rewritten in terms of the modal properties of the original structure, the mass modification and stiffness modification matrices as:

$$\lambda'_r = \frac{\lambda_r + \sum\limits_{s=1 \atop s\neq r}^{n} c_{rs}{}^2\lambda_s + \{\phi\}_r^T[\Delta K]\{\phi\}_r + 2\sum\limits_{s=1 \atop s\neq r}^{n} c_{rs}\{\phi\}_r^T[\Delta K]\{\phi\}_s + \sum\limits_{t=1 \atop t\neq r}^{n} c_{rt}\sum\limits_{s=1 \atop s\neq r}^{n} c_{rs}\{\phi\}_t^T[\Delta K]\{\phi\}_s}{1 + \sum\limits_{s=1 \atop s\neq r}^{n} c_{rs}{}^2 + \{\phi\}_r^T[\Delta M]\{\phi\}_r + 2\sum\limits_{s=1 \atop s\neq r}^{n} c_{rs}\{\phi\}_r^T[\Delta M]\{\phi\}_s + \sum\limits_{t=1 \atop t\neq r}^{n} c_{rt}\sum\limits_{s=1 \atop s\neq r}^{n} c_{rs}\{\phi\}_t^T[\Delta M]\{\phi\}_s}$$

$$(6.13)$$

It can be seen that the eigenvalue of each mode of the modified structure is determined by knowing the change of modal kinetic energy $(\{\phi\}_r^T[\Delta M]\{\phi\}_r)$, the change of modal potential energy $(\{\phi\}_r^T[\Delta K]\{\phi\}_r)$ and the coupling terms including the mass modification and stiffness modification matrices $(\{\phi\}_r^T[\Delta M]\{\phi\}_s), (\{\phi\}_r^T[\Delta K]\{\phi\}_s)$ etc.

## 6.3 COMPUTATION PROCEDURE

In what follows the general formulation derived in the previous section is used to develop a computation procedure (an algorithm).

Suppose that the baseline information (some of the modal properties of the original structure) are given and that the mass modification and stiffness modification matrices are specified. The first approximations for the eigenvalues of the modified structure $(\lambda'^1_r)$ can be determined by setting the initial modal participation factors ($c^0_{rs}$) and the initial eigenvalue changes $(\Delta\lambda^1_r)$ to be zero, so that

$$\lambda'^1_r = \frac{\lambda_r + \{\phi\}_r^T[\Delta K]\{\phi\}_r}{1 + \{\phi\}_r^T[\Delta M]\{\phi\}_r} \qquad (6.14)$$

Subtracting $\lambda'^1_r$ from $\lambda'^0_r$, a first approximation for the change of the *rth* eigenvalue is obtained. Hence, the first approximations for the mode participation factors are determined by :

$$c_{rs}^1 = \frac{-\lambda_r'^1\{\phi\}_s^T[\Delta M]\{\phi\}_r+\{\phi\}_s^T[\Delta K]\{\phi\}_r}{(\lambda_r'^1-\lambda_s)+\lambda_r\{\phi\}_s^T[\Delta M]\{\phi\}_s-\{\phi\}_s^T[\Delta K]\{\phi\}_s} \qquad (6.15)$$

After calculating the first approximations to the mode participation factors, the eigenvalues of the modified structure are approximated using the **Rayleigh** quotient as shown in equation (6.13). Improved estimates of the mode participation factors can then be calculated by taking into consideration the first approximations, $c_{rs}^1$, and the changes of the eigenvalues, $\Delta\lambda_r^2$. The **Rayleigh** quotients are calculated again to provide better estimates of the eigenvalues of the modified structure. Thus, equations (6.8) and (6.13) are used recursively when the number of iterations is equal to or greater than two. This process is continued until convergence of the **Rayleigh** quotients is achieved. The eigenvectors of the modified structure can then be **mass-normalised** as described in equation (6.10). It is noted that if the first prediction of a modified eigenvalue, using the eigenvectors of the original structure, is closer to a neighbouring eigenvalue than to the modified one, the *rth* mode may converge to the neighbouring mode. This can be confirmed by observing the mode participation factor relating the *rth* mode and its neighbouring mode becoming greater than unity after two or three iterations

In order to clarify the above description, the iteration loop with mass-normalization procedure for the eigenvectors of the modified structure is written below in a **program-like** format that is precise enough to convey the important algorithm concepts, but **informal** enough to permit the suppression of cumbersome details.

**FOR k=1**

$$\lambda_r'^1 := \frac{\lambda_r+\{\phi\}_r^T[\Delta K]\{\phi\}_r}{1+\{\phi\}_r^T[\Delta M]\{\phi\}_r}$$

$$c_{rs}^1 := \frac{-\lambda_r'^1\{\phi\}_s^T[\Delta M]\{\phi\}_r+\{\phi\}_s^T[\Delta K]\{\phi\}_r}{(\lambda_r'^1-\lambda_s)+\lambda_r\{\phi\}_s^T[\Delta M]\{\phi\}_s-\{\phi\}_s^T[\Delta K]\{\phi\}_s}$$

FOR k=2, . . . .

   FOR r=1, ..., n

$$\lambda_r^k := \frac{\lambda_r + \sum_{s=1\,s\neq r}^{n}(c_{rs}^k)^2\lambda_s + \{\phi\}_r^T[\Delta K]\{\phi\}_r + 2\sum_{s=1\,s\neq r}^{n}c_{rs}^k\{\phi\}_r^T[\Delta K]\{\phi\}_s + \sum_{t=1\,t\neq r}^{n}c_{rt}^k\sum_{s=1\,s\neq r}^{n}c_{rs}^k\{\phi\}_t^T[\Delta K]\{\phi\}_s}{1 + \sum_{s=1\,s\neq r}^{n}(c_{rs}^k)^2 + \{\phi\}_r^T[\Delta M]\{\phi\}_r + 2\sum_{s=1\,s\neq r}^{n}c_{rs}^k\{\phi\}_r^T[\Delta M]\{\phi\}_s + \sum_{t=1\,t\neq r}^{n}c_{rt}^k\sum_{s=1\,s\neq r}^{n}c_{rs}^k\{\phi\}_t^T[\Delta M]\{\phi\}_s}$$

$$\Delta\lambda_r^k := \lambda_r^k - \lambda_r$$

     FOR s=1, . . . . n and s≠r

$$c_{rs}^k := \frac{-(\lambda_r+\Delta\lambda_r^{k-1})\{\phi\}_s^T[\Delta M]\{\phi\}_r + \{\phi\}_s^T[\Delta K]\{\phi\}_r - (\lambda_r+\Delta\lambda_r^{k-1})\sum_{t=1\,t\neq r\,s}^{n}c_{rt}^{k-1}\{\phi\}_s^T[\Delta M]\{\phi\}_t + \sum_{t=1\,t\neq r\,s}^{n}c_{rt}^{k-1}\{\phi\}_s^T[\Delta K]\{\phi\}_t}{(\lambda_r+\Delta\lambda_r^{k-1})-\lambda_s+(\lambda_r+\Delta\lambda_r^{k-1})\{\phi\}_s^T[\Delta M]\{\phi\}_s - \{\phi\}_s^T[\Delta K]\{\phi\}_s}$$

     NEXT s

   NEXT r

IF $(\text{ABS}(\Delta\lambda_r^k - \Delta\lambda_r^{k-1}) < \text{TOLERANCE})$ THEN TERMINATE

FOR r=1, . . . . n

$$\{\psi'\}_r := \{\phi\}_r + \sum_{s=1\,s\neq r}^{n}c_{rs}\{\phi\}_s$$

$$\{\phi'\}_r := \left(1 + \sum_{s=1\,s\neq r}^{n}c_{rs}^2 + \{\phi\}_r^T[\Delta M]\{\phi\}_r + 2\sum_{s=1\,s\neq r}^{n}c_{rs}\{\phi\}_r^T[\Delta M]\{\phi\}_s + \sum_{t=1\,t\neq r}^{n}c_{rt}\sum_{s=1\,s\neq r}^{n}c_{rs}\{\phi\}_t^T[\Delta M]\{\phi\}_s\right)^{-\frac{1}{2}}\{\psi'\}_r$$

NEXT r

The symbol ":=" denotes arithmetic assignment. A statement of the form "$a := b$" should be interpreted as *"a* becomes $b$ ".

## 6.4 NUMERICAL EXAMPLES

### 6.4.1     THE FINITE ELEMENT MODEL OF A STEEL FRAME STRUCTURE

The model of a steel frame structure shown in Figure 6.1 was used to demonstrate the accuracy and the superconvergence characteristic of the proposed computation

procedure. The structure is composed of a rectangular frame and diagonal bar, all components having the same cross-sectional area, and is modelled as beam elements such that only out-of-plane flexural motion $(z, \theta_x, \theta_y)$ is considered. The geometry of the steel frame and the node numbers of the finite element model are shown in Figure 6.2.



Figure 6.1   A steel supporting frame (all dimensions are in mm)



Figure 6.2   The geometry of the steel frame
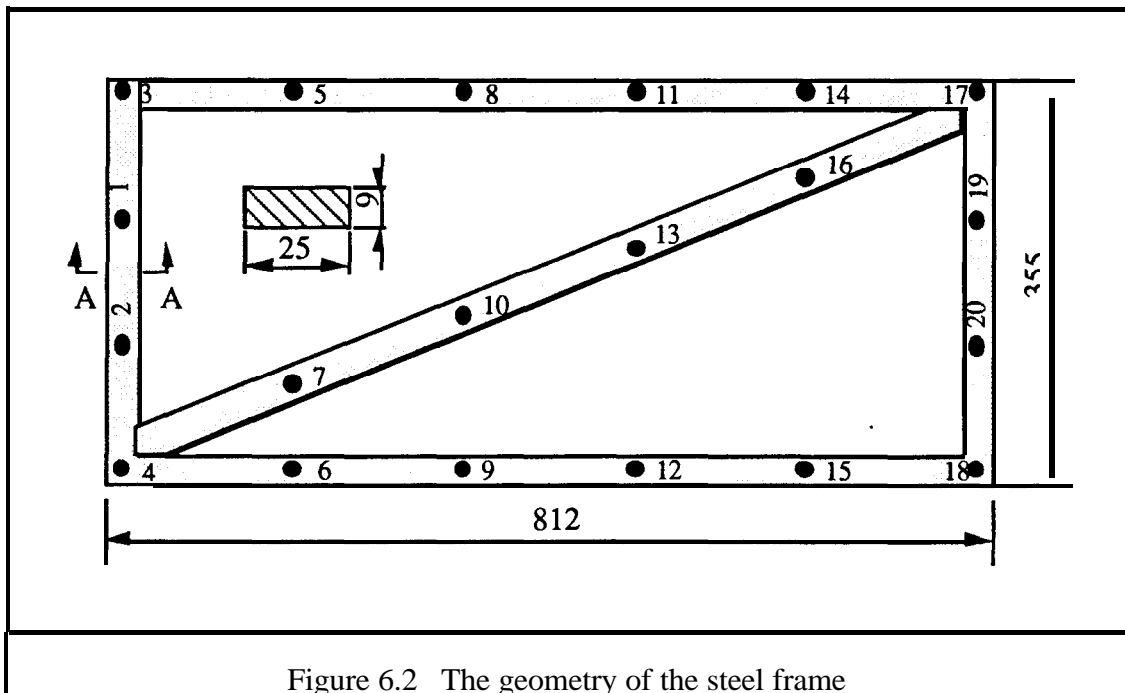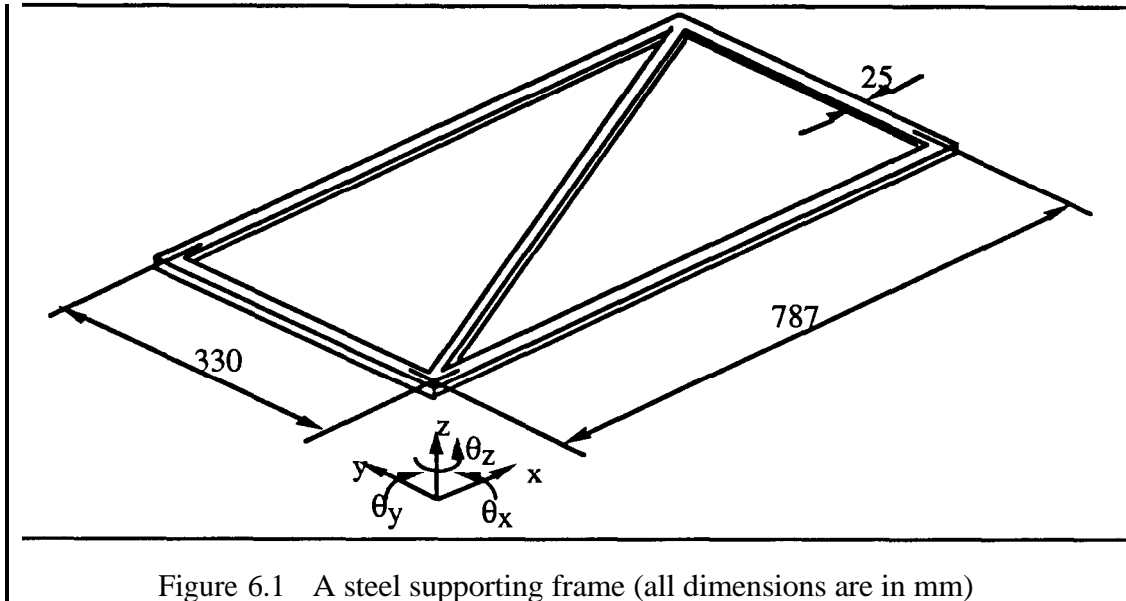
The first case considered is the effect of introducing a mass change at node 4. A mass of 0.2 kg was attached to node 4 at which point the nodal mass of the original structure is 0.2856 kg. This added mass could represent an additional unbalance weight added to the structure after the structural analysis has been performed and will be taken to have three translational degrees of freedom, although only one of these will be accounted for in this structural modification analysis (in-plane motion not being considered here). The modal properties of the modified structure were computed using the computation procedure described above. The natural frequency estimates of the first twenty modes (3 rigid body modes and 17 non-rigid body modes) through a succession of iterations are listed in Table 6.1 along with the exact solution. It can be seen that the natural frequencies computed using the proposed procedure are in very good agreement with the exact solution after a small number of iterations. The accuracy of the eigenvectors predicted by the proposed procedure was assessed by using the Modal Assurance Criterion(MAC). The results show that the first twenty diagonal MAC values which were used to compare the eigenvectors from the proposed procedure after six iterations and the exact solution converged to 1.000 in every case. The modified structure's natural frequencies and eigenvectors were also predicted by using 1st order sensitivity analysis, resulting in the last two columns shown in Table 6.1 from which it can be seen that two of the diagonal MAC values are equal to or smaller than 0.76 and some natural frequency estimates were far from satisfactory .

| | Natural Frequencies (Hz | | | | 1st Order Sen. Ana. | | |
|---|---|---|---|---|---|---|---|
| Mode | original | !nd iter. | 6th iter. /Exact | Change (abs.) $\Delta\omega(\%)$ | Nat. Freq. | iff. in freq lift(%) (i) | MAC liag.val. |
| 1 | 0.00 | 0.00 | 0.00 | 0.00 | 0.00 | 0.0 | 1.000 |
| 2 | 0.00 | 0.00 | 0.00 | 0.00 | 0.00 | 0.0 | .856 |
| 3 | 0.00 | 0.00 | 0.00 | 0.00 | 0.00 | 0.0 | .998 |
| 4 | 45.31 | 44.82 | 44.82 | 0.49  (1.1) | 44.84 | 4.1 | .983 |
| 5 | 54.99 | 52.97 | 52.97 | 2.02  (3.7) | 52.47 | 24.8 | .990 |
| 6 | 70.50 | 69.87 | 69.83 | 0.67  (1.0) | 69.59 | 35.8 | .983 |
| 7 | 91.50 | 89.77 | 89.79 | 1.71  (1.9) | 89.14 | 38.0 | .993 |
| 8 | 153.59 | 151.04 | 151.04 | 2.55  (1.7) | 150.36 | 26.7 | .993 |
| 9 | 181.41 | 179.86 | 179.85 | 1.56  (0.9) | 179.33 | 32.7 | .980 |
| 10 | 219.33 | 215.17 | 215.22 | 4.11  (1.9) | 213.58 | 39.9 | .969 |
| 11 | 263.61 | 263.11 | 263.10 | 0.51  (0.2) | 262.95 | 29.4 | .999 |
| 12 | 348.75 | 333.95 | 330.47 | 18.28  (5.2) | 334.50 | 22.0 | .428 |
| 13 | 351.82 | 341.26 | 350.42 | 1.40  (0.4) | 338.05 | 883.6 | .756 |
| 14 | 405.96 | 403.86 | 402.80 | 3.16  (0.8) | 400.90 | 60.1 | .943 |
| 15 | 444.01 | 430.27 | 434.44 | 9.57  (2.1) | 424.70 | 101.8 | .978 |
| 16 | 578.41 | 564.54 | 566.29 | 12.12  (2.1) | 556.92 | 77.3 | .921 |
| 17 | 647.56 | 646.22 | 645.11 | 2.45  (0.4) | 643.63 | 60.4 | .973 |
| 18 | 679.37 | 666.60 | 67 1.78 | 7.59  (1.1) | 663.35 | 111.1 | .970 |
| 19 | 869.59 | 865.16 | 864.50 | 5.09  (0.6) | 862.48 | 39.7 | .992 |
| 20 | 949.61 | 941.41 | 937.10 | 12.51  (1.3) | 933.48 | 28.9 | .909 |

Table 6.1   Comparison between the modal properties obtained from the proposed
technique and the exact solution

Case 1 :     Added mass at node 4

Note (i)    Diff.in (%) =  absolute value of $\left(\dfrac{\Delta\omega_{exact} - \Delta\omega_{pred.}}{\Delta\omega_{exact}}\right)$

As a second example, the width of the diagonal bar was reduced by a factor of 40%
and three 0.15 kg masses were attached to nodes 4, 10 and 17 respectively so that,
here, changes in both stiffness and mass matrices were required to correct the model.
Since the structural modification was localized and affected only a limited number of
nodal co-ordinates, the eigenvector properties at the unmodified co-ordinates were
ignored. Again, the modal properties obtained using the proposed procedure are very

accurate when compared with the exact solution of the modified structure obtained by a full reanalysis as shown in Table 6.2.

| Natural Frequencies (Hz) | | | | | |
|---|---|---|---|---|---|
| Mode | original | 2nd iter. | 6th iter. | Exact | Δω | (%) |
| 1 | 0.00 | 0.00 | 0.00 | 0.00 | 0.00 | |
| 2 | 0.00 | 0.00 | 0.00 | 0.00 | 0.00 | |
| 3 | 0.00 | 0.00 | 0.00 | 0.00 | 0.00 | |
| 4 | 45.31 | 43.78 | 43.76 | 43.76 | 1.55 | (3.4) |
| 5 | 54.99 | 48.46 | 48.80 | 48.80 | 6.19 | (12.3) |
| 6 | 70.50 | 63.22 | 63.23 | 63.23 | 7.27 | (10.3) |
| 7 | 91.50 | 88.74 | 88.73 | 88.73 | 2.77 | (3.0) |
| 8 | 153.59 | 146.62 | 146.45 | 146.45 | 7.14 | (4.6) |
| 9 | 181.41 | 172.04 | 172.96 | 172.96 | 8.45 | (4.7) |
| 10 | 219.33 | 211.68 | 211.66 | 211.66 | 7.67 | (3.5) |
| 11 | 263.61 | 257.20 | 257.22 | 257.22 | 6.39 | (2.4) |
| 12 | 348.75 | 326.50 | 326.64 | 326.64 | 22.11 | (6.3) |
| 13 | 351.82 | 335.28 | 335.68 | 335.69 | 16.13 | (4.5) |
| 14 | 405.96 | 400.24 | 399.82 | 399.74 | 6.22 | (1.5) |
| 15 | 444.01 | 418.47 | 420.07 | 420.2 1 | 23.80 | (5.4) |
| 16 | 578.41 | 509.45 | 513.57 | 513.57 | 64.84 | (11.2) |
| 17 | 647.56 | 640.14 | 640.03 | 640.03 | 7.53 | (1.2) |
| 18 | 679.37 | 653.87 | 654.42 | 654.43 | 24.94 | (3.7) |
| 19 | 869.59 | 864.73 | 864.88 | 864.88 | 4.71 | (0.5) |
| 20 | 949.61 | 934.47 | 958.82 | 928.92 | ***** | ***** |

Table 6.2   Comparison between the natural frequencies obtained from the proposed technique and the exact solution
Case 2 :  The width of the diagonal bar was reduced by a factor of 40% and three 0.15kg masses were attached to nodes 4, 10 and 17 respectively.

However, numerical results show that some high frequency modes (eg. 20th mode) did not converge because the predictions of those modes exceeded the limited bound of Rayleigh quotient which could be observed while the cross mode participation factors were greater than unity. In this case the effect of mode incompleteness was studied by limiting the first 18 modes to be used in the structural modification prediction. The numerical results are given in Table 6.3 from which it can be seen that although some

relative errors of the natural frequency predictions are large (of the order of **13%),** the

diagonal MAC values show that the modified structure's eigenvectors were well

determined by the proposed technique. Random errors of up to 1% in the eigenvalues

of the original system and up to 5% in its eigenvectors were then introduced, resulting

in the values as shown in Table 6.4.

| Natural Frequencies (Hz) | | | | | | |
|---|---|---|---|---|---|---|
| Mode | Original | 6th iter. | Exact | $\Delta\omega$ exact | $\Delta\omega$ predict. | Diff. in % | MAC diag. val. |
| 1 | 0.00 | 0.00 | 0.00 | 0.00 | 0.00 | 0.0 | 1.000 |
| 2 | 0.00 | 0.00 | 0.00 | 0.00 | 0.00 | 0.0 | 1.000 |
| 3 | 0.00 | 0.00 | 0.00 | 0.00 | 0.00 | 0.0 | 1.000 |
| 4 | 45.31 | 44.08 | 43.76 | 1.55 | 1.23 | 20.7 | .998 |
| 5 | 54.99 | 48.82 | 48.80 | 6.19 | 6.17 | 0.3 | 1.000 |
| 6 | 70.50 | 63.79 | 63.23 | 7.27 | 6.71 | 7.7 | .997 |
| 7 | 91.50 | 88.88 | 88.73 | 2.77 | 2.62 | 5.4 | 1.000 |
| 8 | 153.59 | 146.54 | 146.45 | 7.14 | 7.05 | 1.3 | 1.000 |
| 9 | 181.41 | 174.17 | 172.96 | 8.45 | 7.24 | 14.3 | .993 |
| 10 | 219.33 | 212.30 | 211.66 | 7.67 | 7.03 | 8.3 | .994 |
| 11 | 263.61 | 257.66 | 257.22 | 6.39 | 5.95 | 6.9 | .999 |
| 12 | 348.75 | 327.81 | 326.64 | 23.11 | 20.94 | 9.4 | .997 |
| 13 | 351.82 | 337.09 | 335.69 | 16.13 | 14.73 | 8.7 | .995 |
| 14 | 405.96 | 400.02 | 399.74 | 6.22 | 5.94 | 4.5 | .988 |
| 15 | 444.01 | 425.27 | 420.21 | 23.80 | 18.74 | 21.3 | .986 |
| 16 | 578.4 1 | 516.90 | 513.57 | 64.84 | 61.51 | 5.1 | .975 |
| 17 | 647.56 | 641.49 | 640.03 | 7.53 | 6.07 | 19.4 | .982 |
| 18 | 679.37 | 661.63 | 654.42 | 24.94 | 17.74 | 29.0 | .938 |

Table 6.3    Comparison between the modal properties obtained from the proposed
technique and the exact solution
Case 2 :  The width of the diagonal bar was reduced by a factor of 40% and
three 0.15kg masses were attached to nodes 4, 10 and 17 respectively.
(18 modes of the original system have been used)

relative errors of the natural frequency predictions are large (of the order of **13%**), the diagonal MAC values show that the modified structure's eigenvectors were well determined by the proposed technique. Random errors of up to 1% in the eigenvalues of the original system and up to 5% in its eigenvectors were then introduced, resulting in the values as shown in Table 6.4.

| Natural Frequencies (Hz) | | | | | | |
|---|---|---|---|---|---|---|
| Mode | Original | 6th iter. | Exact | $\Delta\omega$ exact | $\Delta\omega$ predict. | Diff. in % | MAC diag. val. |
| 1 | 0.00 | 0.00 | 0.00 | 0.00 | 0.00 | 0.0 | 1.000 |
| 2 | 0.00 | 0.00 | 0.00 | 0.00 | 0.00 | 0.0 | 1.000 |
| 3 | 0.00 | 0.00 | 0.00 | 0.00 | 0.00 | 0.0 | 1.000 |
| 4 | 45.31 | 44.08 | 43.76 | 1.55 | 1.23 | 20.7 | .998 |
| 5 | 54.99 | 48.82 | 48.80 | 6.19 | 6.17 | 0.3 | 1.000 |
| 6 | 70.50 | 63.79 | 63.23 | 7.27 | 6.71 | 7.7 | .997 |
| 7 | 91.50 | 88.88 | 88.73 | 2.77 | 2.62 | 5.4 | 1.000 |
| 8 | 153.59 | 146.54 | 146.45 | 7.14 | 7.05 | 1.3 | 1.000 |
| 9 | 181.41 | 174.17 | 172.96 | 8.45 | 7.24 | 14.3 | .993 |
| 10 | 219.33 | 212.30 | 211.66 | 7.67 | 7.03 | 8.3 | .994 |
| 11 | 263.61 | 257.66 | 257.22 | 6.39 | 5.95 | 6.9 | .999 |
| 12 | 348.75 | 327.81 | 326.64 | 23.11 | 20.94 | 9.4 | .997 |
| 13 | 351.82 | 337.09 | 335.69 | 16.13 | 14.73 | 8.7 | .995 |
| 14 | 405.96 | 400.02 | 399.74 | 6.22 | 5.94 | 4.5 | .988 |
| 15 | 444.01 | 425.27 | 420.21 | 23.80 | 18.74 | 21.3 | .986 |
| 16 | 578.4 1 | 516.90 | 513.57 | 64.84 | 61.51 | 5.1 | .975 |
| 17 | 647.56 | 641.49 | 640.03 | 7.53 | 6.07 | 19.4 | .982 |
| 18 | 679.37 | 661.63 | 654.42 | 24.94 | 17.74 | 29.0 | .938 |

Table 6.3    Comparison between the modal properties obtained from the proposed
technique and the exact solution
Case 2 :  The width of the diagonal bar was reduced by a factor of 40% and
three 0.15kg masses were attached to nodes 4, 10 and 17 respectively.
(18 modes of the original system have been used)

| Natural e q ciencies (Hi | | | | | | |
|---|---|---|---|---|---|---|
| Mode | Original | 6th iter. | Exact | A.0 exact | $\Delta\omega$ predict. | Diff. in % | MAC diag. val |
| 1 | 0.00 | 0.00 | 0.00 | 0.00 | 0.00 | 0.0 | 1.000 |
| 2 | 0.00 | 0.00 | 0.00 | 0.00 | 0.00 | 0.0 | 1.000 |
| 3 | 0.00 | 0.00 | 0.00 | 0.00 | 0.00 | 0.0 | 1.000 |
| 4 | 45.31 | 43.99 | 43.76 | 1.55 | 1.32 | 14.8 | .997 |
| 5 | 54.99 | 48.76 | 48.80 | 6.19 | 6.23 | 6.5 | .999 |
| 6 | 70.50 | 63.89 | 63.23 | 7.27 | 6.61 | 9.1 | .996 |
| 7 | 91.50 | 88.91 | 88.73 | 2.77 | 2.59 | 6.5 | .999 |
| 8 | 153.59 | 146.61 | 146.45 | 7.14 | 6.98 | 2.2 | 1.000 |
| 9 | 181.41 | 173.88 | 172.96 | 8.45 | 7.53 | 10.8 | .993 |
| 10 | 219.33 | 212.28 | 211.66 | 7.67 | 7.05 | 8.1 | .993 |
| 11 | 263.61 | 257.45 | 257.22 | 6.39 | 6.16 | 3.6 | .999 |
| 12 | 348.75 | 327.02 | 326.64 | 23.11 | 21.73 | 1.7 | .994 |
| 13 | 351.82 | 336.96 | 335.69 | 16.13 | 14.86 | 7.9 | .993 |
| 14 | 405.96 | 399.98 | 399.74 | 6.22 | 5.98 | 3.9 | .981 |
| 15 | 444.01 | 425.46 | 420.21 | 23.80 | 18.55 | 22.1 | .984 |
| 16 | 578.41 | 516.63 | 513.57 | 64.84 | 61.78 | 4.7 | .974 |
| 17 | 647.56 | 641.55 | 640.03 | 7.53 | 6.01 | 20.2 | .983 |
| 18 | 679.37 | 661.93 | 654.42 | 24.94 | 17.74 | 30.1 | .938 |

Table 6.4   Comparison between the modal properties obtained from the proposed
technique and the exact solution
Case 2 :    The width of the diagonal bar was reduced by a factor of 40%
and three 0.15kg masses were attached to nodes 4, 10 and 17 respectively.
(Eigenvalues :$\pm$ 1 %   and  Eigenvectors :$\pm 5\%$;
18 modes of the original system have been used)

## 6.4.2    AN ANALYTICAL MASS-SPRING MODEL

A mass-spring system with 10 degrees-of-freedom shown in Figure 6.3 was used to
investigate the effect of mode incompleteness and the sensitivity of the technique to
simulated measurement errors for a simple system.

Figure 6.2    A mass-spring system with 10 degrees-of-freedom

Mass modifications at points 1, 3, 6, 9 and stiffness modifications between the coordinates **2&5** and **5&7** have been made simultaneously. In this case, 50% changes in the original mass values were introduced and two springs with stiffness $K_1$ as shown in Figure 6.3 were added between the aforementioned coordinate pairs. The modal properties of the modified system were solved by the proposed technique using (i) all modes and (ii) the first five modes of the original system, respectively. The resulting eigenvalues are clearly satisfactory when compared with the exact solution of the modified system as shown in Table 6.5. A correlation between the eigenvectors obtained using the proposed technique with the first five modes available and the exact solution were again assessed using the MAC, resulting in the values as shown in Table 6.6. The diagonal elements of MAC matrix give a quantitative measure of the correlation while the off-diagonal elements are difficult to interpret because they are dependent on the form of the system mass matrix. From Table 6.6, it can be seen that all diagonal elements of the MAC matrix are greater than 0.997.

Figure 6.2 A mass-spring system with 10 degrees-of-freedom

Mass modifications at points 1, 3, 6, 9 and stiffness modifications between the coordinates **2&5** and **5&7** have been made simultaneously. In this case, 50% changes in the original mass values were introduced and two springs with stiffness $K_1$ as shown in Figure 6.3 were added between the aforementioned coordinate pairs. The modal properties of the modified system were solved by the proposed technique using (i) all modes and (ii) the first five modes of the original system, respectively. The resulting eigenvalues are clearly satisfactory when compared with the exact solution of the modified system as shown in Table 6.5. A correlation between the eigenvectors obtained using the proposed technique with the first five modes available and the exact solution were again assessed using the MAC, resulting in the values as shown in Table 6.6. The diagonal elements of MAC matrix give a quantitative measure of the correlation while the off-diagonal elements are difficult to interpret because they are dependent on the form of the system mass matrix. From Table 6.6, it can be seen that all diagonal elements of the MAC matrix are greater than 0.997.

| Natural Frequencies (Hz) | | | | | | |
|---|---|---|---|---|---|---|
| Mode | Original | Modified | Δω | (%) | Nonlin Se. (5th iter.) | | Diff. in |
| | | | | | 10 modes | 5 modes | % |
| 1 | 12.22 | 12.03 | 0.19 | (1.6) | 12.03 | 12.05 | 10.5 |
| 2 | 26.79 | 29.20 | 2.41 | (9.0) | 29.20 | 29.23 | 1.2 |
| 3 | 38.75 | 40.06 | 1.31 | (3.4) | 40.06 | 40.10 | 3.0 |
| 4 | 51.83 | 45.25 | 6.58 | (12.7) | 45.25 | 45.30 | 0.8 |
| 5 | 80.94 | 66.80 | 14.14 | (17.5) | 66.80 | 66.82 | .1 |

Table 6.5    Comparison between the eigenvalues obtained from the completed
reanalysis and the proposed technique
(noise-free data ; 10 and 5 modes of the original system have been used)

| Predicted | Exact | | | | |
|---|---|---|---|---|---|
| | 1 | 2 | 3 | 4 | 5 |
| 1 | .9999 | .0003 | .0001 | .0189 | .0012 |
| 2 | .0006 | .9990 | .0265 | .0175 | .0114 |
| 3 | .0000 | .0235 | .9984 | .1621 | .0110 |
| 4 | .0200 | .0216 | .1463 | .9978 | .0077 |
| 5 | .0009 | .0113 | .0122 | .0081 | .9985 |

Table 6.6    MAC comparison between the eigenvectors obtained from the completed
reanalysis and the proposed technique
(noise-free data ; 5 modes of the original system have been used)

Random errors of up to 1% in the eigenvalues of the original system and up to 5% in
its eigenvectors were then introduced. The modal properties of the modified system
were again obtained by the proposed technique using the first five modes of the original
system. As before, the solutions are quite accurate when compared with the exact
solution of the modified system as shown in Tables 6.7 and 6.8.

| Natural Frequencies (Hz) | | | | | |
|---|---|---|---|---|---|
| Mode | original | Modified | Δω     (%) | Nonlin. Sen 5 modes (5 ite.) | Diff. in % |
| 1 | 12.22 | 12.03 | 0.19  (1.6) | 12.03 | 0.0 |
| 2 | 26.79 | 29.20 | 2.41   (9.0) | 29.27 | 2.9 |
| 3 | 38.75 | 40.06 | 1.31  (3.4) | 40.05 | 0.8 |
| 4 | 51.83 | 45.25 | 6.58  (12.7) | 45.16 | 1.4 |
| 5 | 80.94 | 66.80 | 14.14  (17.5) | 66.83 | 0.2 |

Table 6.7   Comparison between the eigenvalues obtained from the completed
reanalysis and the proposed technique
(Eigenvalues : $\pm$ 1 %   and   Eigenvectors : $\pm$ 5 % ;
5 modes of the original system have been used)

| Predicted | Exact | | | | |
|---|---|---|---|---|---|
|  | 1 | 2 | 3 | 4 | 5 |
| 1 | .9997 | .0004 | .0002 | .0178 | .0011 |
| 2 | .0007 | .9985 | .0261 | .0169 | .0120 |
| 3 | .0000 | .0238 | .9983 | .1675 | .0106 |
| 4 | .0207 | .0221 | .1433 | .9979 | .0077 |
| 5 | .0009 | .0111 | .0121 | .0080 | .9985 |

Table 6.8   MAC comparison between the eigenvectors obtained from the completed
reanalysis and the proposed technique
(Eigenvalues : $\pm$ 1 %    and Eigenvectors : $\pm$ 5 % ;
5 modes of the original system have been used)

## 6.5  PRACTICAL  CONSIDERATIONS

An analytical or FE model of a mechanical structure normally has a large number of
degrees-of-freedom.  The primary analysis of such a model yields the same number as
the number of DoFs sets of eigenvalues and eigenvectors. However, not all modal
properties of the original structure are useful for structural modification analysis: for
example, a solid structure represented by a finite element model having perhaps
thousands of nodes, most of which are internal and therefore inaccessible for

modifications. In this case the elements of the eigenvectors of the original structure representing the structure's behaviour at the internal nodes can be deleted (or ignored) in order to minimize the computation cost and to enhance the efficiency of the proposed procedure. From equations (6.8) and **(6.13),** it can be seen that deleting the modal properties corresponding to unmodified sites will not affect the accuracy of the procedure because even if they were retained those data would be pre-multiplied or post-multiplied by zeros (elements of [AM] and [AK]).

Although all the eigenvalues and the retained elements of the eigenvectors of the original structure are sufficient to yield the exact modal properties of the modified structure, it is appropriate to investigate the accuracy of the proposed procedure when, as in practice, the eigenvalues corresponding to high frequency modes are not available. The numerical examples above show that the eigenvalues of the modified structure obtained using the proposed technique are the same as the solutions obtained using a *Newton-Ruphson* method proposed by Wang and Chu [88] and, moreover, the retained elements of the eigenvectors of the modified structure are determined.

## 6.6 OTHER REANALYSIS TECHNIQUE USING MODAL DATA

It may be advantageous to understand what has been established in Wang and Chu's paper[88]. By replacing the original mass and stiffness matrices in equation (6.1) by the modified mass and stiffness matrices, the matrix equation of free motion of the modified structure is expressed as :

$$[-\omega^2 [M+AM] + [K+\Delta K]]\{x'\} = (0) \tag{6.16}$$

or

$$[-\omega^2 [M] + [K]] (x') = [-\omega^2 [AM] + [AK]] \{x'\} \tag{6.17}$$

When the structural modification is known, equation (6.17) can be written as:

$$[-\omega^2[M] + [K]]\{x'\} = \{L(\bar{x}_r')\} \tag{6.18}$$

where $\{\bar{x}_r'\}$ contains only the DoF's affected by the modification made on the structure and each element $L_i(\bar{x}_r')$ of the vector $\{L(\bar{x}_r')\}$ is a linear function of $\{\bar{x}_r'\}$. Equation (6.18) can be rewritten as:

$$\{x_r'\} = [H(\omega)]\{L(\bar{x}_r')\} \tag{6.19}$$

where $[H(\omega)]$ is the receptance matrix of the original structure.

When the modal superposition approach is used for a harmonic response analysis, the $ij^{th}$ element of the receptance matrix is expressed as :

$$H_{ij} = \sum_{r=1}^{N} \frac{_r\phi_i\,_r\phi_j}{\omega_r^2 - \omega^2} \tag{6.20}$$

Now, a subset of equations can be extracted from equation (6.19) such that

$$\{\bar{x}_r'\} = [W(\omega)]\{\bar{x}_r'\} \tag{6.21}$$

where the element $w_{ij}$ of the matrix $[W(o)]$ is a function of elements of the receptance matrix of the original structure, the mass modification and stiffness modification matrices as well as the unknown value of $\omega$. From equation (6.19), the condition of

the nontrivial solution leads to the frequency equation for the modified system, which is :

$$\det \left([I] - [W(\omega)]\right) = 0 \tag{6.22}$$

The general formulation described above can be applied effectively to local modification. Assume that a **massless** spring, $\Delta k_{ij}$, is added between **DoF** i and **DoF** j. For this particular case,

$$\{L\{\bar{x}_r'\}\} \quad = [AK]\ \{\bar{x}_r'\} \quad = \begin{Bmatrix} -\Delta k_{ij}x_i + \Delta k_{ij}x_j \\ \Delta k_{ij}x_i - \Delta k_{ij}x_j \end{Bmatrix} \tag{6.23}$$

Substituting equation (6.23) into (6.19) and extracting the simultaneous equations corresponding to coordinates *i* and *j* , the following set of equations is obtained :

$$x_i = H_{ii}\left(-\Delta k_{ij}x_i + \Delta k_{ij}x_j,\right) + H_{ij}\left(\Delta k_{ij}x_i - \Delta k_{ij}x_j\right) \tag{6.24}$$

$$x_j = H_{ji}\left(-\Delta k_{ij}x_i + \Delta k_{ij}x_j,\right) + H_{jj}\left(\Delta k_{ij}x_i - \Delta k_{ij}x_j\right) \tag{6.25}$$

Comparing equations (6.24) and (6.25) with equation (6.21), one can identify :

$$[W(\omega)] = \Delta k_{ij}\begin{bmatrix} -H_{ii}+H_{ij} & H_{ii}-H_{ij} \\ -H_{ji}+H_{ji} & H_{ji} -H_{jj} \end{bmatrix} \tag{6.26}$$

Substituting equation (6.26) into equation (6.21) and simplifying the frequency equation of the modified structure gives :

$$1 + \Delta k_{ij}(H_{ii} + H_{jj} - 2H_{ij}) = 0 \tag{6.27}$$

By expressing $\mathbf{H_{ii}}$ and $\mathbf{H_{ij}}$ in terms of modal properties of the original structure, equation (6.27) can be written as a nonlinear algebraic equation as :

$$\frac{1}{\Delta k_{ij}} + \sum_{r=1}^{N} \frac{(_r\phi_i - {_r}\phi_j)^2}{\omega_r^2 - \omega^2} = 0 \qquad (6.28)$$

The natural frequencies of the modified structure are then obtained by solving this equation using either the Newton-Raphson's iteration method or the bisection method. Wang *et* al. [88] successfully applied this technique to a few special cases of local modification, such the change of a beam element and a plate element. Since no approximation has been made in deriving Wang and Chu's technique or the proposed technique developed in the preceding section, both of these reanalysis techniques give identical results and the same as the exact solution obtained from complete reanalysis.

## 6.7 STRUCTURAL REANALYSIS TECHNIQUE USING FRF DATA

It has long been known that for an internally coupled system, the FRF properties of the original structure and of the modified structure can be related by [89]:

$$[H'(\omega)]^{-1} = [H(o)]^{-'} + [AH(o)]^{-'} \qquad (6.29)$$

where $[H'(\omega)]^{-1}$ and $[H(\omega)]^{-1}$ are the receptance matrices of the modified structure and of the original structure respectively.

The dimension of the matrices in this equation is determined by the number of coordinates used in the connection process. By considering that a massless-spring is

added between two coordinates $i$ and j , and expressing the dynamic stiffness matrix of the original structure as

$$[H(\omega)]^{-1} = \frac{1}{H_{ii}H_{jj} - H_{ij}H_{ji}} \begin{bmatrix} H_{jj} & -H_{ij} \\ -H_{ji} & H_{ii} \end{bmatrix} \tag{6.30}$$

the dynamic stiffness matrix of the modified structure is given as:

$$[H'(\omega)]^{-1} = \begin{bmatrix} \dfrac{H_{jj}}{H_{ii}H_{jj}-H_{ij}H_{ji}} +\Delta k_{ij} & \dfrac{-H_{ij}}{H_{ii}H_{jj}-H_{ij}H_{ji}} -\Delta k_{ij} \\ \dfrac{-H_{ji}}{H_{ii}H_{jj}-H_{ij}H_{ji}} -\Delta k_{ij} & \dfrac{H_{ii}}{H_{ii}H_{jj}-H_{ij}H_{ji}} +\Delta k_{ij} \end{bmatrix} \tag{6.3 1}$$

The FRFs of the modified structure are obtained by calculating the inverse of matrix on the right hand side of equation (6.31). It should be noted that the determinant of this matrix is expressed as :

$$\det |[H'(\omega)]^{-1}| = 1 + \Delta k_{ij}(H_{ii} + H_{jj} - 2H_{ij}) \tag{6.32}$$

This equation shows that the matrix on the right hand side of equation (6.31) is invertible only if its determinant is nonsingular. A comparison of equations (6.27) and (6.32) shows that there is a close relationship between modal reanalysis technique and receptance coupling technique. In fact, they are identical in the sense that a FRF is an $N$ -degree polynomial equation and the natural frequencies are the poles of this specific equation.

6.8 CONCLUDING  REMARKS

The computation procedure for determining the modal properties of a modified structure presented above is more efficient than solving the generalised eigenvalue problem for the modified structure, since the equations employed (equations (6.8) and (6.13)) are mathematically simple. Moreover, it is more accurate than other sensitivity techniques when a large modification is considered, since the approximations for the modal properties of the modified structure are improved through an iterative process. This procedure has a useful rate of convergence owing to the quadratic convergence characteristic of the **Rayleigh** quotient which was presented in Chapter 5.

The rapid convergence of the proposed procedure was illustrated in the results of the numerical examples in the preceding section from which it can be seen that the exact modal properties of the modified structure were produced in five or six steps. The FE model of a steel frame structure showed that the exact modal properties of a modified structure could be obtained even when the **size** of structural modification was relatively large. A simple **analytical** mass-spring model illustrated that the modal properties of the modified structure obtained using the truncated modal properties of the original structure were quite accurate while the out-of-range modes - the residuals - did not have great influence on the frequency range of interest in this particular case.

However, it should be noted that when the first approximation for a modified structure's eigenvalue based on the original eigenvector is closer to a neighbouring eigenvalue than to the modified one, this iteration method may not converge as the prediction goes beyond the limited bound of **Rayleigh** quotient.

Alternative structural reanalysis techniques using either (i) modal data or, (ii) FRF data have been briefly reviewed. Although different formulae which relate the natural

frequencies of the modified structure in terms of the modal properties of the original structure and the structural modification made on the structure have been derived, it can be stated that they are simply related to each other by some kind of mathematical transformation.

# $\boxed{7}$ ERROR LOCALIZATION AND STRUCTURAL MODIFICATION PREDICTION ON A MECHANICAL STRUCTURE

## 7.1 INTRODUCTION

The numerical examples presented in Chapter 6 demonstrated the applicability of non-linear sensitivity analysis to the structural modification analysis of finite element (FE) and analytical mass-spring models. However, as a practical algorithm, it must be able to produce an accurate response prediction when the chosen modification is introduced to a real mechanical structure.

In this chapter, an experimental evaluation of the methods presented above carried out on an aluminium structure is described. Experimental data (measurements of FRF data) were analysed and collated in order to yield a consistent set of modal properties. These experimentally-derived modal properties were compared with the analytical results of an FE analysis performed on the VAX8600 machine at the Imperial College Computer Centre. When comparing the modal model obtained from experimental modal analysis with that of the FE model, it was found that the sizes of the experimental and analytical modal data were incompatible from which the problem of either (i) reducing the analytical modal data set, or (ii) expanding the measured data set, arises. In this case study, one of the physical expansion techniques based on the inversion of Kidder's reduction method [50] was selected to resolve the incompatibility problem between the measured data and the FE results. The thus-

expanded mode shape vectors were then used to locate any mismodelled region(s) in the FE model.

The experimentally-derived modal properties were then used to predict the dynamic response of the modified structure using the non-linear sensitivity analysis technique of chapter 6 when a specific structural modification was introduced analytically. The predictions were checked using the measured responses of the modified structure after the actual modification was made on the test structure.

## 7.2 COMPATIBILITY OF MEASURED AND ANALYTICAL DATA

Despite the development of finite element modelling methods, a comparison of modal data (natural frequencies and eigenvectors) reveals quite considerable discrepancies between the experimental results and the analytical ones. Since the **FRFs** were measured at a limited number of coordinates, the experimentally-derived modal data were incompatible with the analytical results obtained from the FE analysis and, as a result, the validation of an FE model of the structure requires an additional step, namely: either (i) to reduce the system matrices of the FE model to the corresponding measured **DoFs,** or (ii) to expand the measured mode shape vectors so that the dimensions of the modal models obtained from experimental modal analysis and FE modelling are compatible.

### 7.2.1      REDUCTION TECHNIQUES

The most commonly-used reduction techniques are **Guyan** reduction and similar methods **[90,91],** all of which reduce the size of mass and stiffness matrices of the FE model and, hence, the computational time for the correlation of the FE model and the

experimental modal model is reduced significantly. However, there are several disadvantages when a reduction technique is employed:

(i)     the modal properties are not exactly preserved in a reduced model and the accuracy of the modal properties for the reduced model is dependent on the expertise in choosing the Master DoFs; and,

(ii)    the connectivity of the reduced system matrices does not reflect the physical characteristics of the original FE model and, therefore, the results obtained from the error localization technique are merely vague indicators for locating the mismodelling region of the original model.

Since the connectivity of the system matrices is one of the main criteria to be satisfied in order to produce a 'good' representative model, expansion of the measured mode shape vectors is a better alternative to solve the compatibility problem.

## 7.2.2     EXPANSION TECHNIQUES

There are various methodologies for expanding the measured mode shape vectors to fill in the responses at the unmeasured DoFs.  These expansion techniques can be categorised as:

(i)     interpolation of the measured modes by applying spline functions;

(ii)    considering the experimental modal matrix as a linear combination of the corresponding analytical modal matrix;

(iii)   applying a 'physical' expansion technique which is derived from the original FE system matrices.

The first of these techniques involves fitting a spline function through the measured locations and extracting the unmeasured mode shape properties from the interpolation function [92]. It was shown in Brown's doctoral thesis [92] that this technique can be

successfully applied to some simple theoretical structures such as beams, plates and shells. However, one of the limitations in applying this technique to practical situations is that the unmeasured mode shape properties may be misinterpreted for high **frequency** modes when the number of measured **DoFs** is too small. This is analogous to the aliassing problem associated with digital spectral analysis. Besides, this technique is likely to give inaccurate results when interpolating over a region with an abrupt change in geometry or local coordinates. The second category of those expansion techniques has been fully investigated and presented by Lieven and Ewins [93] who showed that the mode shape expansion technique does not give accurate results in many examples so that it will not be discussed further in here.

In what follows, the last category - physical expansion techniques, normally derived using the connectivity of the original F.E. model of the structure - is investigated.

### 7.2.2.1    PHYSICAL EXPANSION TECHNIQUES

The most commonly used 'physical' expansion techniques are derived using an inverse process of the dynamic reduction procedure suggested by Kidder [50], which is based on the matrix equation for free motion for a structure in the form:

$$\left[ \begin{bmatrix} [_AK_{111}] & [_AK_{12}] \\ [_AK_{21}] & [_AK_{22}] \end{bmatrix} - {}_A\omega_r^2 \begin{bmatrix} [_AM_{111}] & [_AM_{12}] \\ [_AM_{21}] & [_AM_{22}] \end{bmatrix} \right] \begin{Bmatrix} {}_A\phi_1 \\ {}_A\phi_2 \end{Bmatrix}_r = \begin{Bmatrix} 0 \\ 0 \end{Bmatrix} \quad (7.1)$$

where the stiffness and mass matrices are each partitioned into four submatrices relating the measured **DoFs**, the measured/unmeasured **DoFs** and the unmeasured **DoFs** respectively; ${}_A\omega_r^2$ and $\{_A\phi_1, {}_A\phi_2\}^T_r$ are the natural frequency (square root of eigenvalue) and the mode shape vector (eigenvector) of the *rth* mode of the structure.

Equation (7.1) can be rewritten as two sets of simultaneous equations as:

$$\left[[_AK_{11}] - _A\omega_r^2[_AM_{11}]\right]\{_A\phi_1\}_r + \left[[_AK_{12}] - _A\omega_r^2[_AM_{12}]\right]\{_A\phi_2\}_r = \{0\}$$

$$(7.2)$$

and

$$\left[[_AK_{21}] - _A\omega_r^2[_AM_{21}]\right]\{_A\phi_1\}_r + \left[[_AK_{22}] - _A\omega_r^2[_AM_{22}]\right]\{_A\phi_2\}_r = \{0\}$$

$$(7.3)$$

where the vector $\{_A\phi_2\}_r$ represents the mode shape properties at the slave (unmeasured) DoFs for the *rth* mode.

## Method A

From equation (7.3), it can be shown that by calculating the inverse of the partitioned dynamic stiffness matrix corresponding to the unmeasured DoFs, the vector ($_A\phi_2\}_r$ is given by:

$$\{_A\phi_2\}_r = \left([[_AK_{22}] - _A\omega_r^2[_AM_{22}]]\right)^{-1}\left[[_AK_{21}] - _A\omega_r^2[_AM_{21}]\right]\{_A\phi_1\}_r \quad (7.4)$$

In this method the partitioned dynamic stiffness matrix corresponding to the unmeasured DoFs is a square matrix and has a dimension *(N-n)x(N-n)* where *N* is the number of DoFs for the structure and *n* is the number of measured DoFs. By calculating the inverse of this matrix and using equation (7.4), the vector $\{_A\phi_2\}_r$ is uniquely determined.

## Method B

From equation (7.3), Gysin [94] suggested that by calculating the generalised inverse of the partitioned dynamic stiffness matrix $\left([[_AK_{12}] - _A\omega_r^2[_AM_{12}]]\right)$ which has a dimension *Nx(N-n)*, the following equation is obtained:

$$\left([_AK_{12}]-_A\omega_r^2[_AM_{12}]\right)^+\left([_AK_{12}]-\omega_r^2[_AM_{12}]\right)\{_A\phi_2\}_r = \left([_AK_{12}]-_A\omega_r[_AM_{12}]\right)^+[_AK_{11}]-\omega_r^2[_AM_{11}]]\{_A\phi_1\}_r$$

$$(7.5)$$

In this method, the vector $\{_A\phi_2\}_r$ is correctly determined by calculating the solution of the right hand side of equation (7.5) **only** if the generalised inverse satisfies the following relationship:

$$\left([_AK_{12}] - _A\omega_r^2[_AM_{12}]\right)^+ \left([_AK_{12}] - _A\omega_r^2[_AM_{12}]\right) - [\,I\,] = [\,0 \quad 1 \qquad (7.6)$$

However, the number of measured **DoFs** is generally less than the number of unmeasured **DoFs,** and so this generalised inverse is just a least-squares solution that minimizes a Frobenius norm of the left hand side of equation (7.6). Hence, the solution obtained from the right hand side of equation (7.5) is merely a projection of the vector $\{_A\phi_2\}_r$ in a subspace with a dimension sxs, where s is equal to or smaller than $[\min(N\text{-}n,n\,)]$.

## Method C

From equations (7.2) and (7.3), one can define two matrices, [At] and [A₂], as:

$$[A_1] : = \left[ \begin{bmatrix} [_AK_{11}] - _A\omega_r^2[_AM_{11}] \\ [_AK_{21}] - _A\omega_r^2[_AM_{21}] \end{bmatrix} \right] \qquad (7.7)$$

and

$$[A_2] : = \left[ \begin{bmatrix} [_AK_{12}] - _A\omega_r^2[_AM_{12}] \\ [_AK_{22}] - _A\omega_r^2[_AM_{22}] \end{bmatrix} \right] \qquad (7.8)$$

and equation (7.1) can be rewritten as:

$$[A_1]\{_A\phi_1\}_r + [A_2]\{_A\phi_2\}_r = \{0\} \qquad (7.9)$$

which leads to the following equation for the unmeasured mode shape properties :

$$\{_A\phi_2\}_r = [A_2]^+ [A_1]\{_A\phi_1\}_r \qquad\qquad (7.10)$$

In contrast to Method B, the rectangular matrix $[A_2]$ used in (7.10) has a dimension Nx(N-n) so that in general its generalised inverse satisfies the relationship, $[A_2]^+[A_2]=[I]$. Hence, the vector $\{_A\phi_2\}_r$ can be uniquely determined by using equation (7.10).

Generally speaking, both Methods A and C reproduce the exact mode shape properties at the unmeasured DoFs when the FE model of the structure is correctly constructed. Method B is a mapping technique that may successfully reproduce the mode shape properties at the unmeasured DoFs when the number of unmeasured DoFs is not greater than the number of measured DoFs.

7.2.2.2    NUMERICAL SIMULATIONS

A 10 degree-of-freedom mass-spring model shown in Figure 7.1 was used to demonstrate the applicability of Methods A, B and C in the case that (i) the analytical model was correctly constructed; (ii) the analytical model was mismodelled in some measured/unmeasured DoFs.

Figure 7.1 A mass-spring system with 10 degrees-of-freedom

$M_1 = 1.0$ kg  $K_1 = 1E4$ N/m
$M_2 = 0.2$ kg  $K_2 = 2E4$ N/m
$M3 = 0.1$ kg  $K_3 = 3E4$ N/m
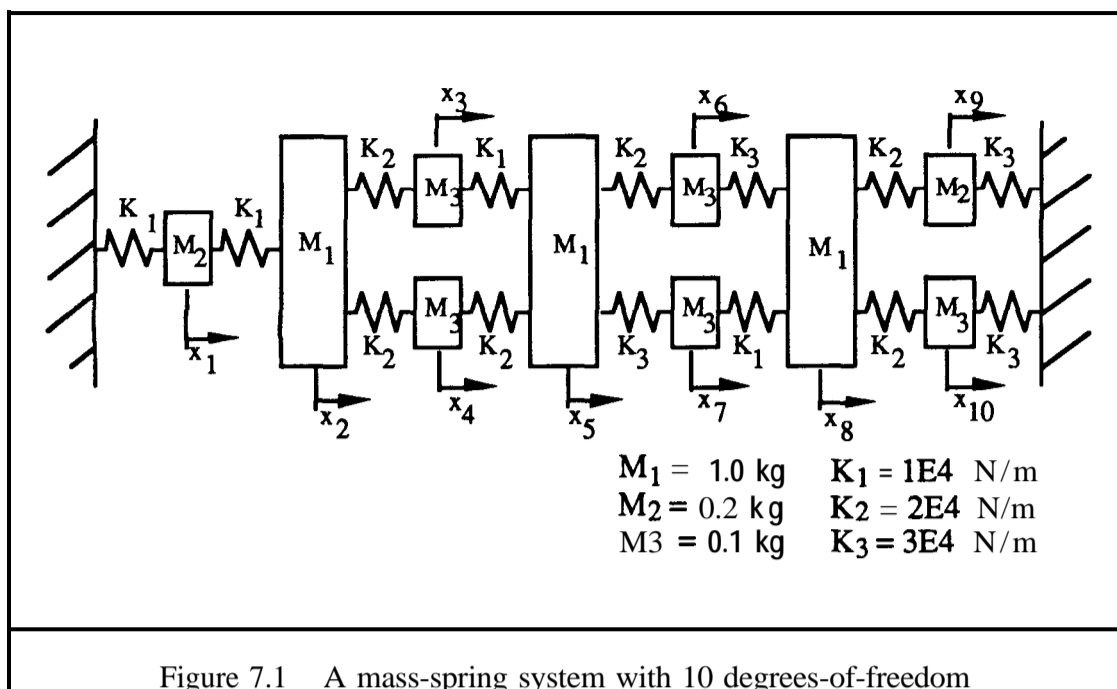
Case 1. Error-free model

The first numerical simulation assumed that only two responses were measured (at locations 1 and 6) for all modes. The mode shape properties at the unmeasured DoFs for mode 1 to 10 were calculated successively by using the formulae given in the preceding section. The accuracy of the expanded mode shape vectors obtained from Methods A, B and C was assessed by using the MAC, resulting in the values as shown in Tables 7.1 and 7.2. Both Methods A and C produced the same accurate results as shown in Table 7.1 in which the diagonal elements of the MAC matrix are unity and the off-diagonal term are 'small'. In contrast, Method B produced some unacceptable results as illustrated in Table 7.2 from which it can be observed that the diagonal MAC values are smaller than 0.2 for modes 3, 5, 6 ,7, 8 and 9.

| Predicted | Exact | | | | | | | | | |
|---|---|---|---|---|---|---|---|---|---|---|
| | 1 | 2 | 3 | 4 | 5 | 6 | 7 | 8 | 9 | 10 |
| 1 | .0000 | .0026 | .0045 | .0177 | .0016 | .0834 | .0086 | .1996 | .0064 | .1241 |
| 2 | .0026 | 1.0000 | .0000 | .0443 | .0100 | .0464 | .0681 | .0008 | .0000 | .1898 |
| 3 | .0045 | .0000 | 1.0000 | .0447 | .0422 | .0001 | .0082 | .1138 | .0352 | .0176 |
| 4 | .0177 | .0443 | .0447 | 1.0000 | .0001 | .0053 | .0032 | .0005 | .0000 | .0000 |
| 5 | .0016 | .0100 | .0422 | .0001 | 1.0000 | .0001 | .0002 | .0001 | .0004 | .0069 |
| 6 | .0834 | .0464 | .0001 | .0053 | .0001 | 1.0000 | .0005 | .0013 | .0000 | .0001 |
| 7 | .0086 | .0681 | .0082 | .0032 | .0002 | .0005 | 1.0000 | .0000 | .0000 | .0002 |
| 8 | .1996 | .0008 | .1138 | .0005 | .0001 | .0013 | .0000 | 1.0000 | .0005 | .0017 |
| 9 | .0064 | .0000 | .0352 | .0000 | .0004 | .0000 | .0000 | .0005 | 1.0000 | .0000 |
| 10 | .1241 | .1898 | .0176 | .0000 | .0069 | .0001 | .0002 | .0017 | .0000 | 1.0000 |

Table 7.1   MAC comparison between the exact mode shape vectors and the expanded mode shape vectors obtained using Method A (or C)   (2 measured DoFs)

| Predicted | Exact | | | | | | | | | |
|---|---|---|---|---|---|---|---|---|---|---|
| | 1 | 2 | 3 | 4 | 5 | 6 | 7 | 8 | 9 | 10 |
| 1 | .4688 | .0005 | .1332 | .0708 | .0058 | .0018 | .0003 | .0236 | .0254 | .0937 |
| 2 | .0029 | .7416 | .0034 | .0826 | .0067 | .0003 | .0045 | .0160 | .0344 | .1271 |
| 3 | .3976 | .0161 | .1571 | .3632 | .0031 | .0009 | .0002 | .0136 | .0153 | .0583 |
| 4 | .0337 | .0623 | .0578 | .9835 | .0000 | .0004 | .0002 | .0001 | .0000 | .0001 |
| 5 | .2089 | .3804 | .0375 | .0000 | .0130 | .0002 | .0051 | .0564 | .1081 | .4650 |
| 6 | .2063 | .0527 | .0347 | .1079 | .0008 | .0041 | .0007 | .0089 | .0054 | .0247 |
| 7 | .0161 | .4183 | .0030 | .0211 | .0085 | .0004 | .0079 | .0416 | .1134 | .5312 |
| 8 | .1614 | .1732 | .0311 | .0010 | .0107 | .0005 | .0048 | .0686 | .1490 | .7130 |
| 9 | .0752 | .1608 | .0151 | .0001 | .0089 | .0001 | .0057 | .0645 | .158 5 | .7866 |
| 10 | .0553 | .1186 | .0115 | .0001 | .0076 | .0001 | .0053 | .0616 | .1569 | .7947 |

Table 7.2   MAC comparison between the exact mode shape vectors and the expanded mode shape vectors obtained using Method B   (2 measured DoFs)

The second numerical simulation assumed that the number of measured DoFs was greater than the number of unmeasured DoFs. The unmeasured mode shape properties for all modes were again calculated by using Methods A, B and C with (i) 6 measured DoFs and (ii) 7 measured DoFs, respectively. In both cases, the MAC tables for Methods A and C are the same as the one shown in Table 7.1. This confirms that the expanded mode shape vectors obtained using Methods A and C are very accurate if the

analytical model is error-free. When there were 6 measured **DoFs** available, Table 7.3 shows the correlation between the expanded mode shape vectors obtained from Method B and the analytical solution in which the fifth and ninth diagonal MAC values are smaller than 0.6 because the partitioned dynamic stiffness matrix ($[ [_A K_{12}] - _A \omega_r^2 [_A M_{12}]]$) was rank deficient. This condition was improved by including another **DoF** (i.e. 7 measured **DoFs** were used) for which case the resulting MAC values are the same as the ones shown in Table 7.1.

| Predicted | Exact | | | | | | | | | |
|---|---|---|---|---|---|---|---|---|---|---|
| | 1 | 2 | 3 | 4 | 5 | 6 | 7 | 8 | 9 | 10 |
| 1 | **.0000** | .0026 | .0045 | .0177 | .0015 | .0834 | .0086 | .1996 | .0063 | .1242 |
| 2 | .0026 | 1.0000 | .0000 | .0443 | .0088 | .0464 | .0681 | .0008 | .0001 | .1918 |
| 3 | .0045 | .0000 | 1.0000 | .0447 | .0343 | .0001 | .0083 | .1138 | .0420 | .0196 |
| 4 | .0177 | .0443 | .0447 | 1.0000 | .0001 | .0053 | .0032 | .0005 | .0000 | .0000 |
| 5 | .0035 | .0199 | .0779 | .0002 | **.4393** | .0006 | .0028 | .0006 | .4848 | .0319 |
| 6 | .0834 | .0464 | .0001 | .0053 | .0003 | **.9999** | .0005 | .0013 | .0000 | .0001 |
| 7 | .0086 | .0681 | .0083 | .0032 | .0012 | .0005 | **.9993** | .0000 | .0003 | .0001 |
| 8 | .1996 | .0008 | .1137 | .0005 | .0003 | .0013 | .0000 | 1.0000 | .0003 | .0018 |
| 9 | .0106 | .0001 | .0714 | .0001 | .3619 | .0000 | .0005 | .0005 | **.5884** | .0488 |
| 10 | .1339 | ..2066 | .0211 | .0000 | .0151 | .0001 | .0001 | .0019 | .0309 | **.9278** |

Table 7.3  MAC comparison between the exact mode shape vectors and the expanded mode shape vectors obtained using Method B  (6 measured **DoFs**)

Case 2.  <u>Mismodelling at locations 2,7 and 8</u>

Analytical mismodelling was simulated by changing the system matrices of the original analytical model. In this example, a 50% increase on the original mass values at locations **2, 7** and 8 was introduced and an additional spring with stiffness $K_1$ (10,000 N/m) was added between coordinates 7 and 8. In order to assess the validity of each of these expansion methods in detail, three different sets of measured **DoFs** were selected. The missing quantities of the elements corresponding to the unmeasured **DoFs** were determined using the formulae given in the preceding section. The

expanded mode shape vectors were then tested on their capability to locate the mismodelled region. The localization method used here is the "Error Matrix Method" developed by He and Ewins [95]:

$$[EM] = \left[[K_A] - {}_X\omega_r^2[M_A]\right]\{{}_X\phi\}_r\{{}_X\phi\}_r^T \qquad (7.11)$$

### Case 2a : measured DoFs (2, 4, 6, 7, 8)

The error matrices of the first two modes obtained using equation (7.11) and the three expansion methods are plotted in Figures 7.2-7.4. Figure 7.2 shows that the mismodelled region of the analytical model was located precisely by using expansion Method A, for this particular case. Figure 7.3 shows that Method B could not produce any sensible results. Figure 7.4 shows that although Method C was unable to locate the mismodelled region of the analytical model exactly, the peaks in the figure do contain valuable information for the error localization.



Mode 1                    Mode 2

Figure 7.2   Error matrices  (using Method A)

Figure 7.3   Error matrices (using Method B)



Figure 7.4 Error matrices (using Method C)
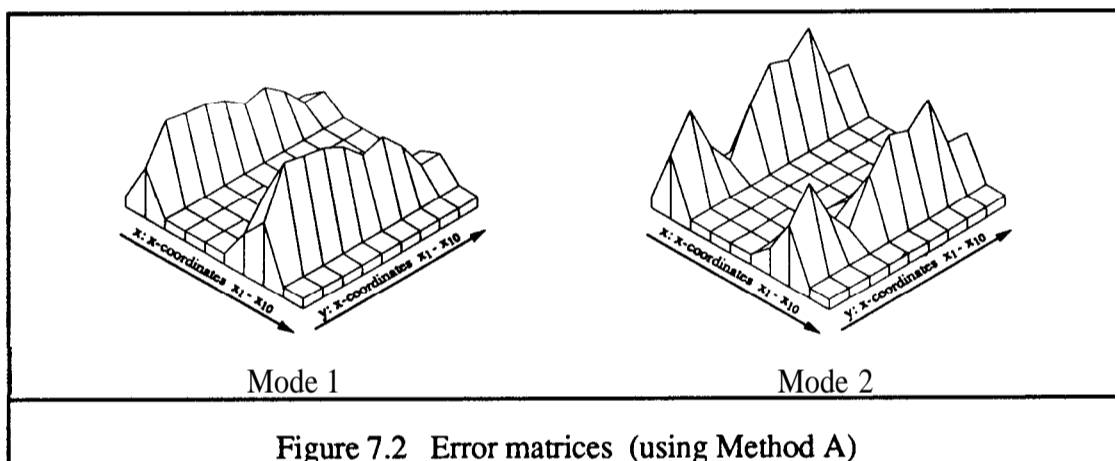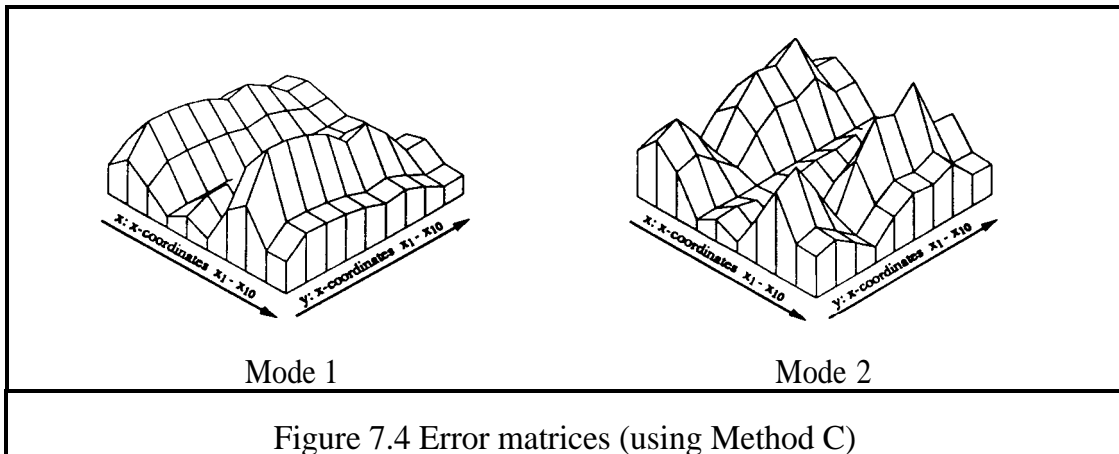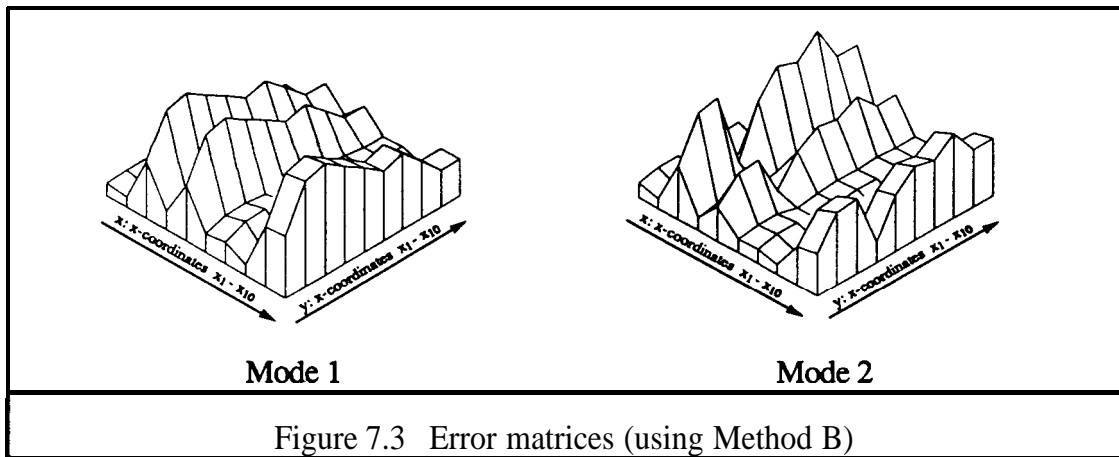
### Case 2b : measured DoFs (2, 4, 6, 8, 10)

In this case the mode shape properties at one of the mismodelled regions, location 7, was not available during the mode shape vector expansion processes. Figure 7.5 shows the error localization predictions using expanded modes 1 and 2 obtained from Method A. Since the odd-numbered DoFs in the expanded modes were produced by using the original system submatrices, $[_AK_{21}], [_AM_{21}], [_AK_{22}]$ and $[_AM_{22}]$, the modelling errors would not be expected to show up on these DoFs. This can be proved by defining the vector $\{_X\phi_2^*\}_r$ as the mode shape properties at the unmeasured DoFs. In Method A this vector is uniquely determined by :

$$\{_X\phi_2^*\}_r = \left([_AK_{22}] - _X\omega_r^2[_AM_{22}]\right)^{-1} \left[[_AK_{21}] - _X\omega_r^2[_AM_{21}]\right]\{_X\phi_1\}_r$$

$$(7.12)$$

and, substituting the expanded mode shape vectors into equation (7.1 1), one can derive :

$$[EM] = \left[\left[\begin{array}{cc}[_AK_{11}] & [_AK_{12}] \\ [_AK_{21}] & [_AK_{22}]\end{array}\right] - x\,\omega_r^2\left[\begin{array}{cc}[_AM_{11}] & [_AM_{12}] \\ [_AM_{21}] & [_AM_{22}]\end{array}\right]\right]\left\{\begin{array}{c}x\phi_1 \\ x\phi_2^*\end{array}\right\}\left\{x\phi_1\ x\phi_2^*\right\}^T = \left[\begin{array}{cc}[EM_{11}] & [EM_{12}] \\ [0] & [0]\end{array}\right]$$

(7.13)

Equation (7.13) shows that the row elements of the error matrix corresponding to the unmeasured **DoFs** must be zero. From Figure 7.5, it can be seen that Method A produced good results for modes 1 and 2. The error localization predictions using expanded modes 1 and 2 obtained from Method B are shown in Figure 7.6 from which no sensible conclusion can be drawn. Method C requires the entire system matrices, and so, there is no inherent characteristic that some rows of the error matrix are constrained to be zero because the expanded mode shape vectors are determined through a minimisation (least-squares) process. Although Method C is unable to locate the mismodelled region exactly when some modelling errors exist in the analytical model, Figure 7.7 shows that it does have the ability to locate possible mismodelled region in this specific case using modes 1 and 2.



Mode 1                                                          Mode 2

Figure 7.5 Error matrices (using Method A)

Mode 1                              Mode 2

Figure 7.6   Error matrices  (using Method B)



Mode 1                              Mode 2

Figure 7.7   Error matrices (using Method C)
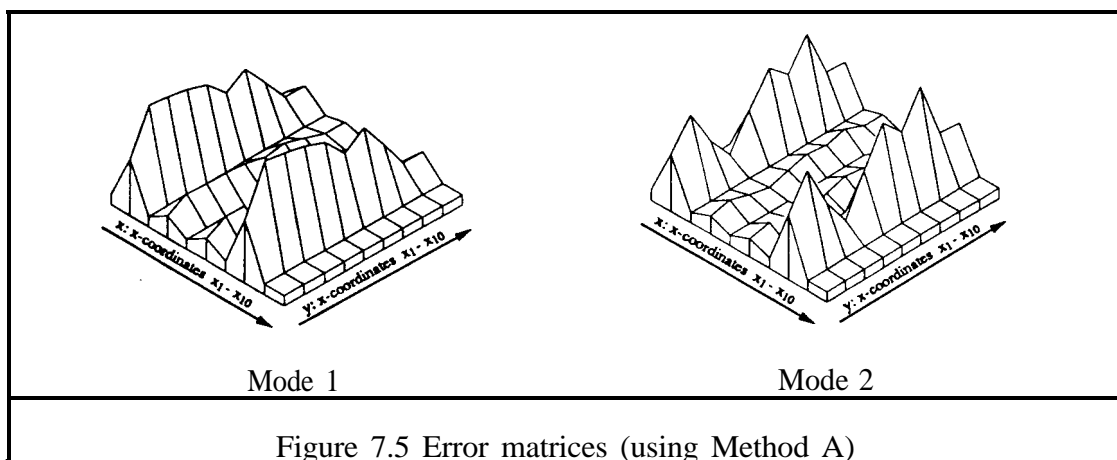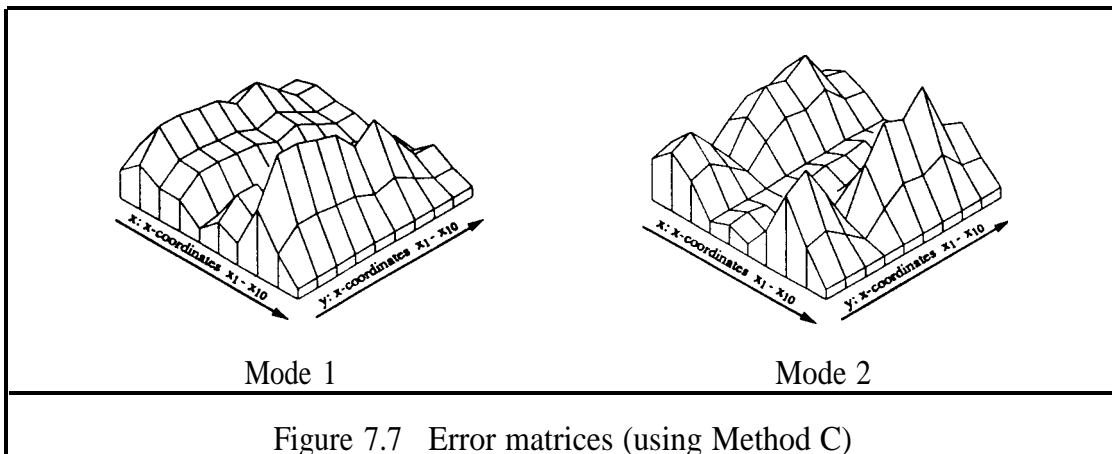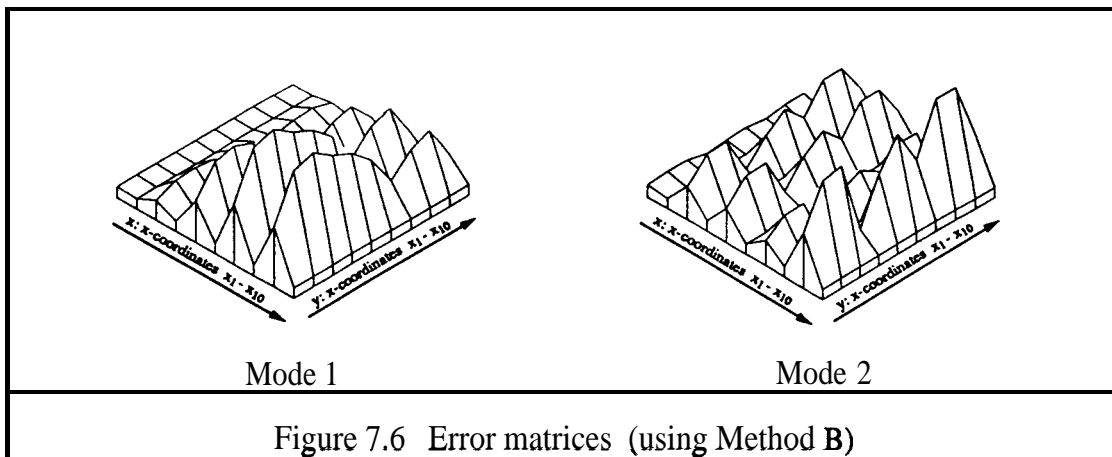
Case 2c: measured DoFs (1, 3, 5, 7, 9)

The mode shape properties corresponding to the DoFs with even numbers were selected in this case. Again, the first two modes were expanded by the three methods using the analytical system submatrices. The thus-expanded mode shape vectors were then used to locate the mismodelled region in the analytical model.

Figure 7.8 shows the error localization predictions using the expanded mode shape vectors obtained from Method A. Since the even-numbered DoFs in the expanded mode shape vectors were expanded by the original system submatrices, therefore, the modelling errors would not be revealed on these DoFs. From Figure 7.8, it can be seen that Method A produced some poor results in choosing this set of measured DoFs. The error localization predictions using the expanded mode shape vectors

obtained from Method B are plotted in Figure 7.9. Again, Method B could not produce any sensible results for this case. The results using Method C are plotted in Figure 7.10 from which it can be seen that this method has an ability to locate the mismodelled region for mode 2.



Mode 1                                   Mode 2

Figure 7.8 Error matrices (using Method A)



Mode 1                                   Mode 2

Figure 7.9  Error matrices (using Method B)

| Mode 1 | Mode 2 |

Figure 7.10 Error matrices (using Method C)
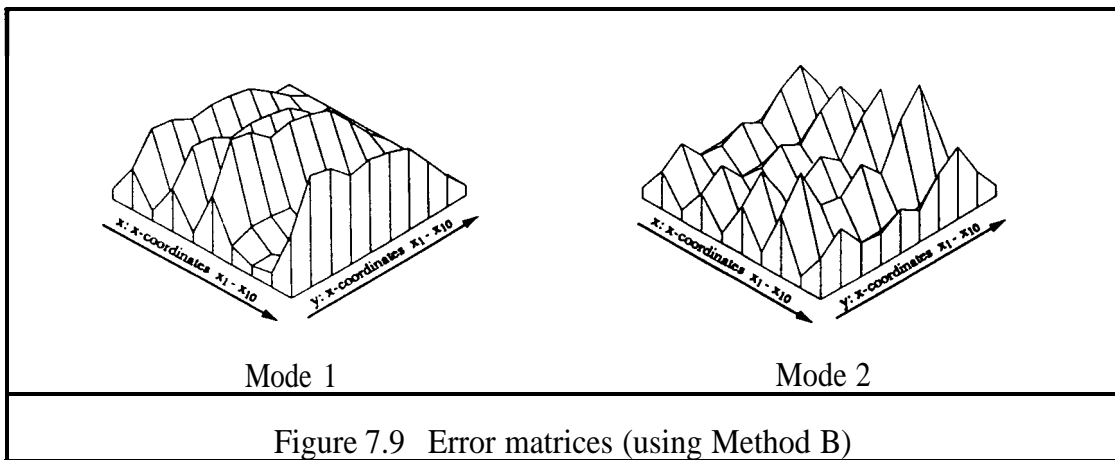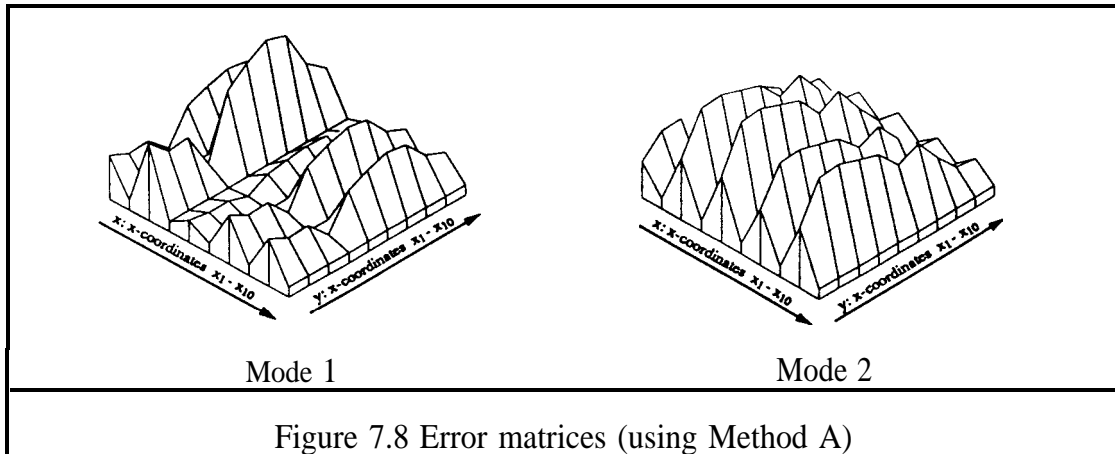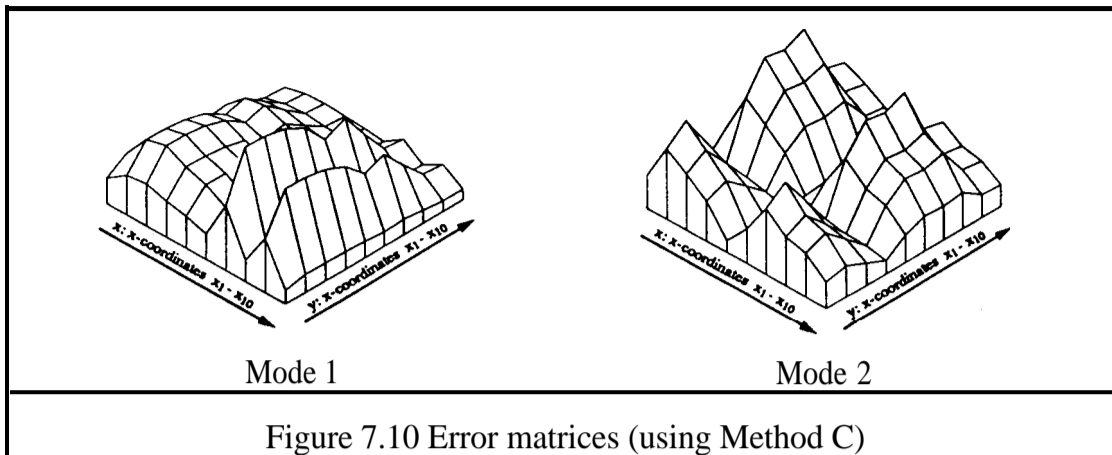
### 7.2.2.3    CHARACTERISTICS OF THE PHYSICAL EXPANSION TECHNIQUES

The following conclusions can be drawn from the numerical simulations.

a)    If no error exists in the analytical model, the missing quantities of the mode shape properties at the unmeasured DoFs can generally be reproduced by using Methods A or C. Mathematically speaking, Method B is a mapping technique that can reproduce those missing quantities if and only if the relationship shown in equation (7.6) is satisfied.   As it is usually not satisfied, this method should generally not be used.

b)    If all modelling errors lie in the measured DoFs, then only Method A works perfectly.

c)    If just some of the modelling errors lie in the measured DoFs, Methods A and C can produce some sensible results for the error localization. The capability of these methods is dependent on the choice of measured DoFs and the nature of the mode (shape) to be expanded.

If one considers the computational time and cost, Method A is superior to Method C. This is because Method A only needs to determine the inverse of an $n \times n$ matrix while

Method C needs to determine the **generalised** inverse of an $Nx(N\text{-}n)$ matrix, where in practice N and $(N\text{-}n)$ **are** much much greater than $n$ .

## 7.3 AN EXPERIMENTAL CASE STUDY

In order to study the practical problems of reliable FE modelling and to verify the applicability of non-linear sensitivity methods in real structure modification predictions, a test structure was required which would possess a number of features - it should be complicated to some degree for the experimental measurement as well as the analytical modelling but without these complications being duly extensive.

### 7.3.1      DETAILS OF THE TEST STRUCTURE

The test structure chosen is based on the casing of an instrument which is used to contain and to protect electronic equipment.  It is made of aluminium alloy and composed of three plates having different thickness and two solid bars with square section.  One end of the top plate and one end of the bottom plate are connected to both edges of the side plate by socket headed screws. Two square bars are used to connect the other edge of the top plate to the face of the bottom plate through four socket headed screws. A photograph of this structure is given in Figure 7.11.

Figure 7.11   A photograph of the aluminium test structure

## 7.3.2      DETAILS OF MEASUREMENT EQUIPMENT

The structure was excited at one point by an instrumented hammer (B&K Type 8208). It was found that for this lightly-damped structure impact testing provided a smooth, almost flat, excitation force spectrum over the frequency range of interest (O-800 Hz). A Line-Drive amplifier (Type 2644) was mounted directly in the hollow at the base of the hammer handle and this allowed the instrumented hammer to be directly connected to a dual channel signal analyser (B&K Type 2034), thus removing the need for a separate signal conditioning unit.

The translational response of the structure was measured using an accelerometer (B&K Type 4393). This accelerometer is very small and light, and is based on a simple configuration that three piezoelectric slices are clamped between a seismic mass and a triangular centre post by a preloading ring.  It has a mass of just 2.4 **g** (the mass of the

Figure 7.11   A photograph of the aluminium test structure

### 7.3.2    DETAILS OF MEASUREMENT EQUIPMENT

The structure was excited at one point by an instrumented hammer (B&K Type 8208). It was found that for this lightly-damped structure impact testing provided a smooth, almost flat, excitation force spectrum over the frequency range of interest (0-800 Hz). A Line-Drive amplifier (Type 2644) was mounted directly in the hollow at the base of the hammer handle and this allowed the instrumented hammer to be directly connected to a dual channel signal analyser  (B&K Type 2034), thus removing the need for a separate signal conditioning unit.

The translational response of the structure was measured using an accelerometer (B&K Type 4393).  This accelerometer is very small and light, and is based on a simple configuration that three piezoelectric slices are clamped between a seismic mass and a triangular centre post by a preloading ring.  It has a mass of just 2.4 g (the mass of the

test structure is 9.6 kg), and hence the loading effect of it on the structure is negligible. The accelerometer was connected to a charge amplifier (B&K Type 2653) which amplified the response signal to a suitable level for input to the dual channel signal analyser.

The B&K 2034 Dual Channel Signal Analyser is a 2-channel **FFT** analyser having all of the standard functions. It has 801 lines of resolution in dual channel operation, and so more modes of vibration can be identified and **characterised** in a single measurement than with a conventional **250-** or **400-line** analyser. However, its internal digital processor limits the dynamic range of the equipment to 80 **dB.** It was found that most of the structural resonances were captured well because the auto-range facility enabled the processor to be used to its full capability. However, in some cases when the **anti-**resonances were 3 or 4 orders of magnitude (60 or 80 **dB)** smaller than the resonance peaks, the equipment failed to give reliable information at these frequencies or frequency ranges. This could be confirmed by looking at the coherence functions corresponding to those frequency ranges. Fortunately, the anti-resonances were not required in performing the nonlinear sensitivity analysis of this structure.

A schematic diagram of the measurement chain is shown in Figure 7.12.
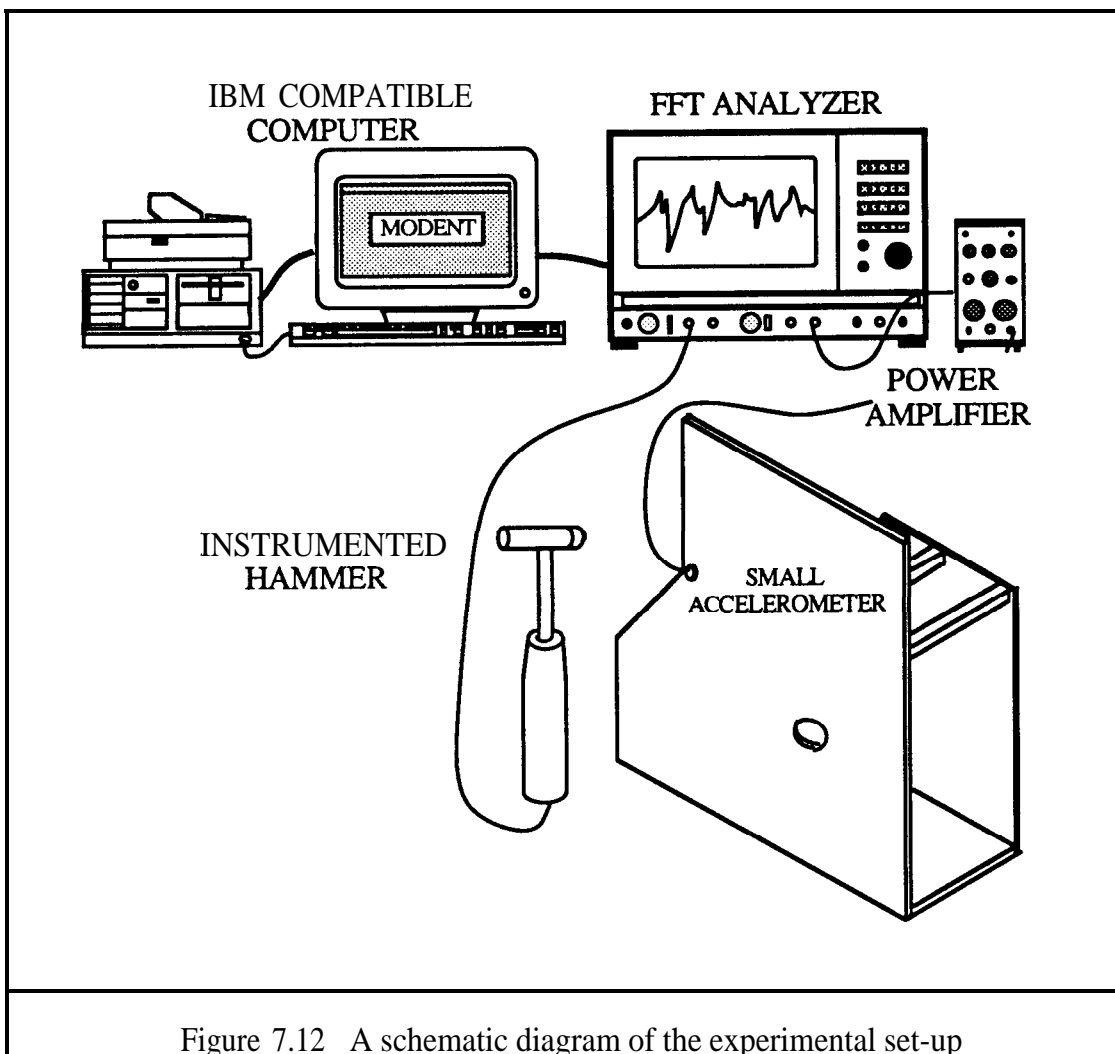
Figure 7.12   A schematic diagram of the experimental set-up

### 7.3.3    CALIBRATION OF MEASUREMENT EQUIPMENT

Before any measurement was made on the test structure, the overall calibration of the measurement chain was calibrated using a ratio-calibration technique **[8].** The accelerometer was attached to a freely suspended mass which was excited by the instrumented hammer in just the same way as measurements would be made on the structure itself. The charge amplifier gain was adjusted until the measured inertance had values equal to (l/calibration mass) across the frequency range of interest. This calibration technique has the distinct advantage that it is very easy to perform and the complete measurement chain is checked and calibrated.

### 7.3.4      MEASUREMENT OF TRANSLATIONAL DEGREES-OF-FREEDOM

The test structure was suspended by elastic bands at each of the four comers in order to achieve a **"free-free"** boundary condition so that the six rigid body modes were well below the lowest **flexural** mode of the structure. A total of 71 points were marked on the structure as measured **DoFs,** including 37 points on the top plate, 20 points on the bottom plate, 10 points on the side plate and 2 points each on the connecting bars. The positions of these measured points are shown in Figure 7.13.
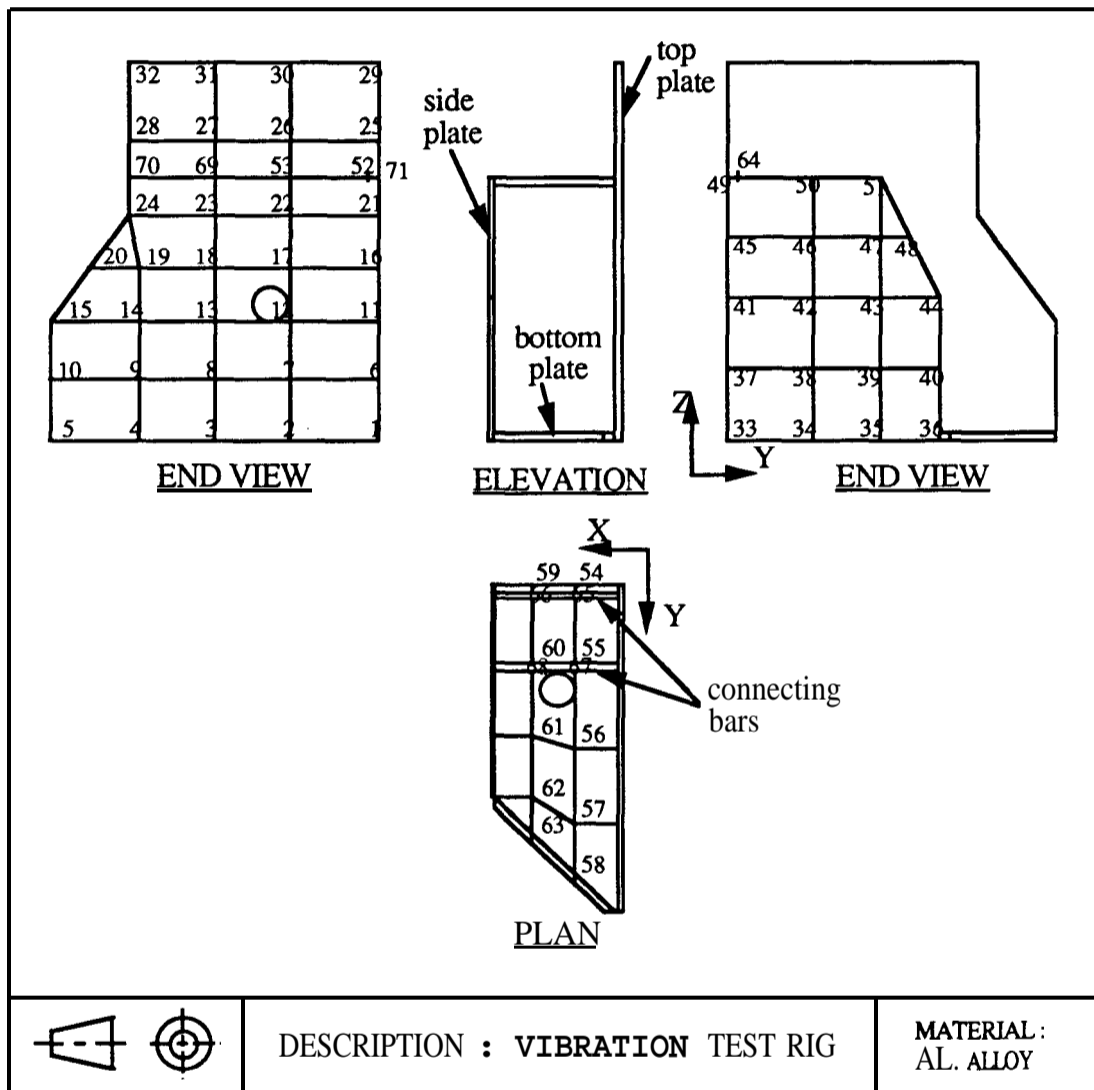


Figure 7.13   The geometry of aluminium casing

A baseband frequency range of 800 Hz was used for all FRF measurements which were made by exciting the structure at point 24 in the X-direction with the instrumented hammer. The accelerometer was moved from one location to the next location in order to collect a point FRF and 70 transfer **FRFs.** In each measurement, a good quality FRF was achieved with only ten averages. Figure 7.14 shows one of the typical **FRFs** measured and from it, 15 **flexural** modes arc clearly seen in the frequency range of interest (O-800 Hz). The identification of the modal properties for individual FRF was conducted using "MODENT" [96] in an IBM compatible 386 machine. 71 sets of analysed modal properties were then collated by using "MODESH" [97], resulting in mean values of the natural frequencies and damping loss factors as tabulated in Table 7.4. It should be noted that the tolerance was set to 3.6 per cent when collating the modal properties because for different **FRFs** there existed slight discrepancies between the identified natural frequencies and the corresponding damping loss factors.



Figure 7.14   Measured Frequency Response Function $(\ddot{x}_3/f_{24})$
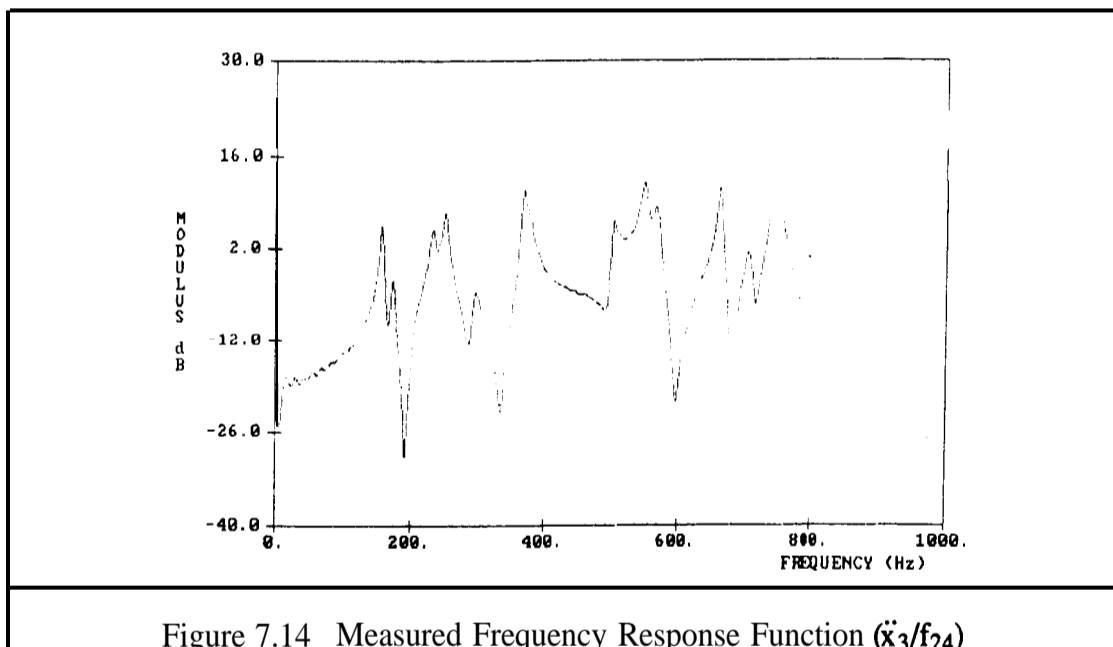
| Mode | Natural Frequency (Hz) | Damping Loss Factor (%) |
|------|------------------------|-------------------------|
| 1    | 155.91                 | .0307                   |
| 2    | 172.08                 | .0373                   |
| 3    | 203.91                 | .0686                   |
| 4    | 233.07                 | .0432                   |
| 5    | 249.66                 | .0324                   |
| 6    | 294.05                 | .0408                   |
| 7    | 370.64                 | .0239                   |
| 8    | 500.15                 | .0167                   |
| 9    | 546.54                 | .0179                   |
| 10   | 565.39                 | .0218                   |
| 11   | 661.88                 | .0112                   |
| 12   | 706.39                 | .0168                   |
| 13   | 746.18                 | .0160                   |
| 14   | 791.09                 | .0201                   |

Table 7.4   Modal properties of the test structure
(tolerance of natural frequencies = 3.6%)

## 7.4 FINITE ELEMENT ANALYSIS

The FE analysis of this structure was performed using the PAFEC code (whose name stands for Program for Automatic Finite Element Calculations), this being a comprehensive FE analysis package specially designed for static, thermal and dynamic analyses. An interactive pre-processing program called PIGS (PAFEC Interactive Graphics Suite) was used to create the mesh of the FE model. This program also provides the post-processing facilities in order to display the mode shapes, both static and animated, in a three-dimensional form.

PAFEC provides a wide range of element types for static and dynamic analyses. However, only three different types of element were used in this investigation :

(i)    Four-noded flat facet shell element.

This is a flat thin isotropic shell element which can carry bending and membrane loads and which can be used to solve any thin shell problems in which either or **both** of in-plane and out-of-plane effects are important. It has five degrees of freedom $(u_x, u_y, u_z, \phi_x, \phi_y)$ per node at the element level in a local coordinate system but after transformation to global coordinate an extra freedom $\phi_z$ may be introduced.

(ii) Three-noded flat facet shell element.

This is also a flat thin isotropic shell element and has the same properties as a four-noded flat facet shell element . However, it is generally inferior in terms of the cost of achieving the same degree of accuracy when compared with the **four-noded** flat facet shell element.

(iii) Simple beam element.

This is a straight uniform beam element with two nodes which caters for bending in two principal directions, axial forces and twisting about its shear centre. It has six degrees of freedom $(u_x, u_y, u_z, \phi_x, \phi_y, \phi_z)$ at each of the two nodes.

## 7.4.1 FINITE ELEMENT MODEL

The finite element model created was based on the afore-mentioned shell and beam elements as shown in Figure 7.15. The shell elements used were three- and **four-noded** isotopic thin facet elements, as they were recommended for thin plate structures where the aspect ratio $h/l$ ($h$=thickness, $l$=typical length of a plate) is smaller than 0.15. The simple beam element was used to model the square-section bars between the top and the bottom plates, as it was recommended to model the stiffener of a box or plate shell structure. From Figure 7.15, it can be seen that 85 nodes, which included 7 1 measurement points and some unmeasured points in the vicinity of two holes in the top and the side plates, were used to generate the FE model.

The analysis of this model was performed assuming totally unrestrained boundary conditions in order to match the "free-free" boundary condition imposed at the experimental stage, and hence no constraints had to be specified in the FE data file. Since the sole purpose of the FE analysis was to determine the natural frequencies and eigenvectors of the FE model, no dynamic loads would be considered. In the FE analysis, all **DoFs** at each node were defined as the Master **DoF** so that the "complete" system mass and stiffness matrices with 442 **DoFs** were generated.
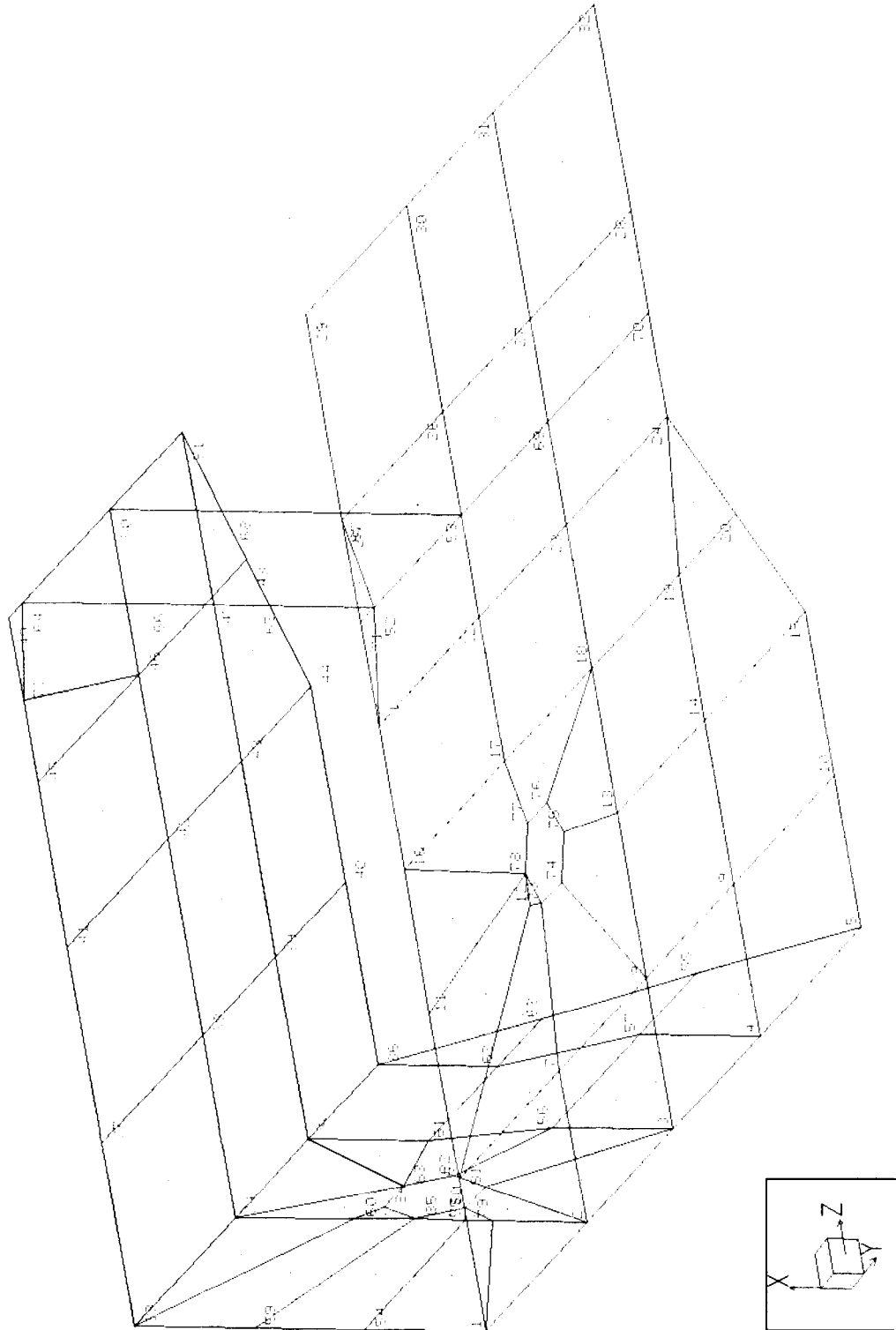
Figure 7.15   The FE model of the test structure

## 7.4.2    FINITE ELEMENT RESULTS

The first six rigid body modes were less than 0.01 Hz. The natural frequencies of the seventh to the twentieth modes are given in Table 7.5, together with the corresponding experimental results. Figures 7.16 and 7.17 depict two of the analytical mode shapes (eigenvectors).

| | Natural Frequency (Hz) | | Error | | MAC |
|---|---|---|---|---|---|
| Mode (FE) | FE | Exper. | $\Delta\omega$ | (%) | Diag. Val. |
| 7 | 145.69 | —— | —— | —— | —— |
| 8 | 165.21 | 155.91 | 9.30 | (6.0) | .9749 |
| 9 | 195.09 | 172.08 | 23.01 | (13.4) | .8043 |
| 10 | 209.41 | 203.91 | 5.50 | (2.8) | .9594 |
| | —— | 233.07 | —— | —— | —— |
| 11 | 250.07 | 249.66 | 0.41 | (0.2) | .9315 |
| 12 | 296.17 | 294.05 | 2.12 | (0.7) | .9950 |
| 13 | 384.58 | 370.64 | 13.94 | (3.8) | .9724 |
| 14 | 509.11 | 500.15 | 8.96 | (1.8) | .9544 |
| 15 | 557.94 | 546.54 | 11.40 | (2.1) | .8231 |
| 16 | 568.74 | 565.39 | 3.35 | (0.6) | .7647 |
| 17 | 656.89 | 661.88 | 4.99 | (0.8) | .7678 |
| 18 | 687.56 | 706.39 | 18.82 | (2.7) | .8092 |
| 19 | 761.65 | 746.18 | 15.47 | (2.1) | .6277 |
| 20 | 805.47 | 791.09 | 14.38 | (1.8) | .6005 |

Table 7.5    Comparison of natural frequencies obtained from FE analysis and
            experimental modal analysis

Figure 7.16    Deformed shape for mode 11 (250.07 Hz)



Figure 7.17    Deformed shape for mode 19 (761.65 Hz)
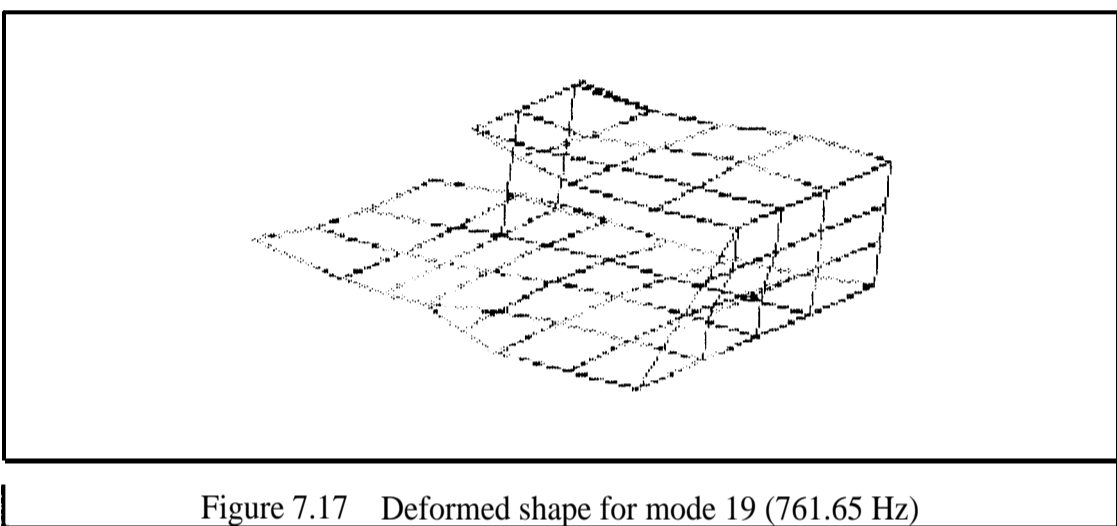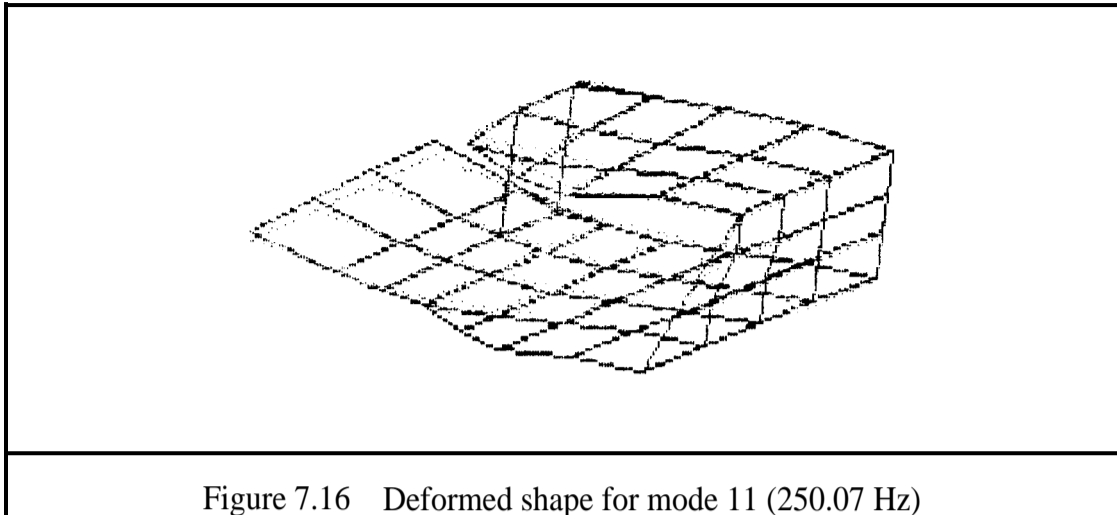
## 7.5 CORRELATION  BETWEEN  EXPERIMENTAL  AND  FE  RESULTS

As shown in Table 7.6, the natural frequencies obtained using the FE analysis are in reasonably good agreement with the experimental results except for mode 7 and for an unpredicted measured mode at 233.07 Hz. A correlation between the experimentally-derived mode shapes and the mode shape vectors obtained from the FE analysis was carried out, resulting in the MAC values given in Table 7.5 from which it can be seen that good correlations were obtained for modes 8-14.

Since **5DoFs** at each node of the shell elements and **6DoFs** at each node of the beam elements were considered in the FE analysis while, only the translational **DoFs** in the X-direction were included in the FRF measurements, the measured mode shape properties were expanded using Kidder's method (Method A). The thus-expanded mode shape vectors were used to locate the mismodelled region in the FE model. Instead of calculating the error matrix by equation **(7.11)**, an error vector for each mode was chosen and determined by :

$$\{EV\}_r \; = \; \left[ [K_A] - {}_X\omega_r^2 [M_A] \right] \{{}_X\phi\}_r \qquad\qquad (7.14)$$

Equation (7.14) is analogous to equation (7.12) so that the row elements of the error vector corresponding to the unmeasured **DoFs** must be zero. Therefore, only the elements of the error vector in the X-direction would be non-zero and useful for locating the modelling errors. The error vectors obtained using 13 measured modes are shown in Figure 7.18 from which it can be seen that modelling errors lie predominantly between nodes 1 to 5, nodes 34 to 37, and nodes 54 to 68. These nodes are the Master **DoFs** on the side plate, the square bars and at the jointed comers and modelling errors might well arise here due to limitations of the thin shell elements for in-plane motion (no in-plane shear). In addition, the joint properties were not known and the assumed fixed-fixed interface conditions at the comers might be inappropriate.
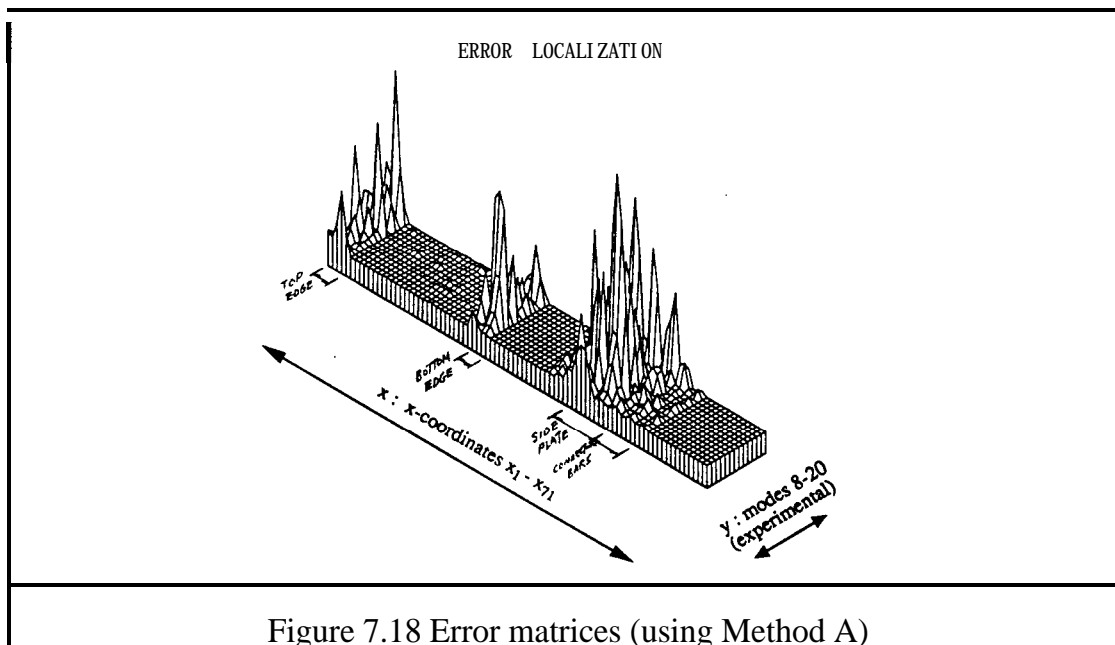
Figure 7.18 Error matrices (using Method A)

## 7.6 **STRUCTURAL MODIFICATION PREDICTION USING EXPERIMENTAL DATA**

In order to demonstrate the applicability of a structural reanalysis technique, it is desirable to obtain relatively large natural frequency shifts when a small structural modification is introduced to the test structure. This can be achieved by calculating the first-order eigenvalue sensitivity described in chapter 5 and determining the "order of importance" ranking of the structure's degrees-of-freedom for structural modification for each mode of vibration.

Since the first-order sensitivity analysis only provides a guideline to effective structural modifications, more accurate estimates of the actual shifts in natural frequencies from prescribed modifications are sought using the non-linear sensitivity analysis when the information at coordinates corresponding to structural modification sites is available. Theoretically, the FRF data in three translational and three rotational directions at each modification site ought to be measured. However, limitations imposed by currently-

used measurement techniques and equipment make the inclusion of all six coordinates at each point a very difficult task in practical situations. As a result, a lumped mass modification which is only active in the measured coordinates was made in order to minimize the discrepancies between the theoretical predictions and the **experimentally-**derived modal responses.

### 7.6.1      FIRST-ORDER EIGENVALUE SENSITIVITIES

The natural frequency sensitivities for each coordinate are shown in Table 7.6 where only the mass sensitivities in the X direction are given. Since the main purpose of calculating the first-order eigenvalue sensitivities is to provide the ranking of the degrees-of-freedom in their order of importance for modification, the values of frequency shifts would not be used to predict the modal responses of the modified structure (the limitations of the first-order sensitivity analysis have been fully discussed in chapter 5).

From the sensitivity results shown in Table 7.6, it is clear that points 11 and 32 are very sensitive to a single **DoF** mass modification in the X direction in general and will in particular produce comparatively large shifts in the resonance frequency for mode 19.

| Mode | Nat. Freq. | SDoF MASS SENSTIVITY (- Hz/kg) | | | | | | | | | |
|------|------------|------|------|------|------|------|------|------|------|------|------|
| | | 11X | 15X | 16X | 32X | 37X | 40X | 41X | 44X | 48X | 51X |
| 12 | 294.0 | 1.6 | 2.0 | 0.5 | 0.0 | 13.8 | 2.3 | 53.8 | 10.2 | 8.3 | 7.9 |
| 13 | 370.6 | 19.3 | 52.3 | 26.9 | 58.5 | 0.0 | 0.1 | 5.3 | 2.3 | 4.2 | 1.7 |
| 14 | 500.1 | 25.1 | 32.5 | 33.3 | 42.1 | 1.0 | 11.4 | 0.5 | 16.4 | 2.5 | 22.9 |
| 15 | 546.5 | 104.1 | 152.9 | 38.7 | 34.6 | 3.3 | 140.9 | 17.7 | 40.4 | 166.8 | 248.9 |
| 16 | 565.4 | 4.6 | 0.9 | 0.5 | 0.7 | 0.1 | 10.3 | 1.0 | 39.6 | 23.4 | 43.8 |
| 17 | 661.9 | 13.1 | 123.3 | 0.4 | 48.3 | 4.6 | 13.8 | 66.5 | 6.3 | 108.0 | 36.7 |
| 18 | 706.4 | 15.0 | 0.5 | 3.7 | 0.0 | 80.7 | 69.3 | 172.8 | 197.9 | 30.0 | 26.4 |
| 19 | 746.2 | 499.6 | 38.1 | 222.6 | 555.6 | 122.7 | 2.7 | 77.1 | 4.3 | 41.0 | 283.1 |
| 20 | 791.1 | 13.7 | 0.0 | 0.2 | 53.4 | 95.4 | 7.1 | 12.3 | 16.4 | 4.4 | 47.1 |

Table 7.6   Natural frequency sensitivities for the test structure

### 7.6.2     PREDICTION OF EFFECTS OF ACTUAL MODIFICATION

Once a first-order sensitivity analysis has been completed satisfactorily, the next step in the solution of a structural optimization problem is the design and selection of structural modification sites that can alter the dynamic characteristics in order to accomplish the desirable feature specified by the analyst. As the main aim of this experimental case study is to illustrate the applicability of the non-linear sensitivity analysis and so, the objective function in this excerise is to obtain maximum downwards frequency shifts for some modes when a single DoF mass modification is introduced. According to the variations in natural frequencies predicted using the first-order sensitivity analysis given in Table 7.6, the natural frequency sensitivity of mode 19 to mass modification at point 11X is 499.6 Hz/kg. Therefore, to achieve a reasonable shift in the natural frequency - say 20 Hz - the single DoF mass change required is 0.04 kg. Using a steel bar with circular cross-section, a concentrated mass of 0.05 kg was constructed. This mass was attached at point 11 (in the X-direction) by means of a silver-steel pushrod 18 mm long by 1 mm in diameter and a circular disk 2 mm thick by 10 mm in diameter, resulting in a mass modification with the total

mass of 0.0565 kg.  The geometry of the extended mass is shown in Figure 7.19. The use of a **pushrod** ensured that the concentrated mass had negligible effect in any coordinate other than 11X and would act as a single **DoF** modification. The natural frequencies of the modified structure were predicted using the non-linear sensitivity analysis. They are given in Table 7.7 from which it can be seen that the actual mass modification of 0.056 kg should produce a shift of - 16.4 Hz for mode 19.
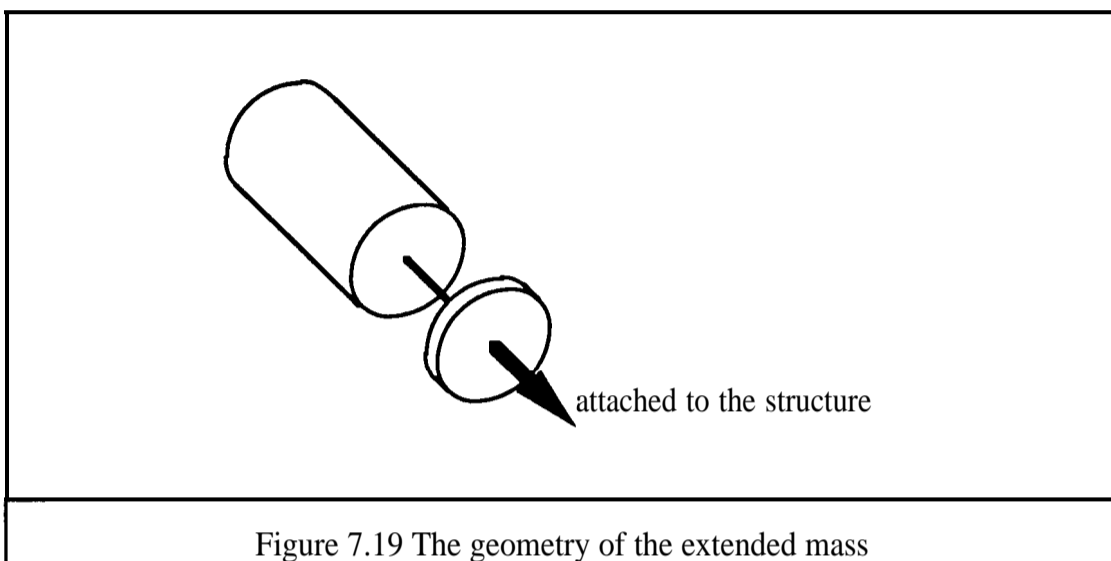


Figure 7.19 The geometry of the extended mass

The modified structure was excited in the X-direction at point 24 and a translational response measurement was made in the X direction at point 5. The transfer FRF curves of the modified and unmodified structures are shown in Figure 7.19 from which it can be seen that there was indeed a marked shift (17.7 Hz) in the natural frequency for mode 19. However, it should be noted that there was another large shift (12.2 Hz) in the natural frequency for mode 15 which was not predicted using the non-linear sensitivity analysis.  The natural frequencies have been extracted using "MODENT" and are given in Table 7.7 along with the predicted natural frequencies of the modified structure.
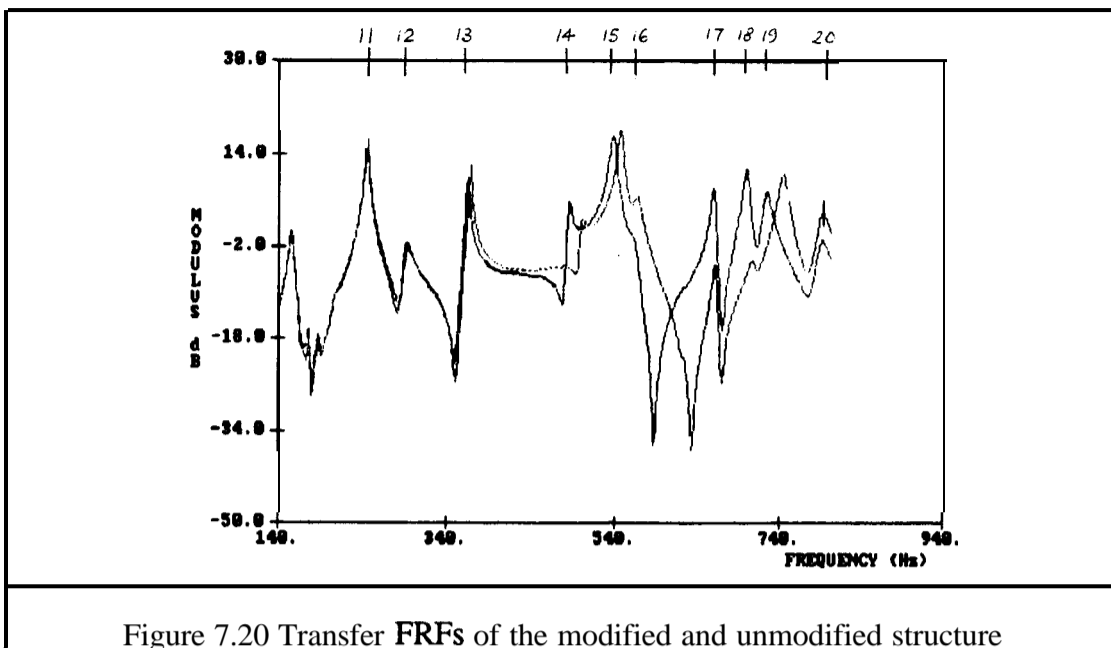
Figure 7.20 Transfer FRFs of the modified and unmodified structure

| Mode | Nat. Freq. of the original structure | Nat. Freq. of the modified structure | |
| --- | --- | --- | --- |
| | | Predicted (Non-Lin. Sen. ) | Measured |
| 8 | 155.91 | 155.90 (-0.01) | 155.90 (-0.01) |
| 9 | 172.08 | 172.07 (-0.01) | 172.07 (-0.0 1) |
| 10 | 203.91 | 203.90 (-0.01) | 203.90 (-0.01) |
| | 233.07 | 233.07 (-0.00) | 233.07 (-0.00) |
| 11 | 249.66 | 249.50 (-0.16) | 246.30 (-3.36) |
| 12 | 294.05 | 293.95 (-0.10) | 293.52 (-0.53) |
| 13 | 370.64 | 369.54 (-1.10) | 367.34 (-3.30) |
| 14 | 500.15 | 498.56 (-1.59) | 487.92 (- 12.2) |
| 15 | 546.54 | 541.17 (-5.37) | 538.92 (-7.62) |
| 16 | 565.39 | 565.17 (-0.22) | 564.90 (-0.49) |
| 17 | 661.88 | 661.05 (-0.83) | 658.90 (-2.98) |
| 18 | 706.39 | 705.13 (-1.26) | 703.23 (-3.16) |
| 19 | 746.18 | 729.77 (- 16.4) | 728.51 (-17.7) |
| 20 | 791.09 | 790.56 (-0.53) | 789.90 (-1.19) |

Table 7.7   Natural frequencies of the unmodified and modified structure

## 7.7 **CONCLUDING   REMARKS**

There were two main objectives for the case study on the aluminium test structure:

(i)     evaluation of the effectiveness of the physical expansion technique in an error localization analysis where the modelling error in a FE model should be located; and,

(ii)    justification of the applicability of non-linear sensitivity analysis in structural modification prediction using experimental data.

For the computer simulation results shown in Section 7.2, it was found that when some or all of the mismodelled sites cannot be measured directly, both Methods A and C gave quite accurate and reliable expanded mode shape vectors which can be used to indicate the modelling error in the FE/analytical model using the error matrix technique developed by He and Ewins [95].

Despite the advances in measurement technique, difficulties are encountered with attempts to measure all six DoFs - three translational and three rotational DoFs - at each measurement point. In this case study a full measurement survey of the translational DoF (in the X-direction) of the aluminium test structure was carried out. By analysing the measured FRFs using "MODENT" and "MODESH", a modal model having 16 flexural modes with 71 response coordinates was created. An FE model was set-up using the PAFEC package and a dynamic analysis was carried out by considering all 442 DoF as Master DoF. Comparing the FE results with their experimentally-derived counterparts gave satisfactory results.  The measured mode shape properties were expanded using Kidder's method (Method A) and the thus-expanded mode shape vectors were used to locate the possible mismodelled regions in the FE model. It was concluded that the main differences between the test structure and its FE model are due

to limitations of thin shell elements for representing in-plane motion and to lack of appropriate modelling for the jointed comers incoporated in the FE **model.**

In order to minimise the effects based on a model which is deficient in rotational and some translational information, a single **DoF** mass modification was achieved by attaching the added masses to the unmodified structure through a **pushrod** which has the characteristic of being stiff in one direction while at the same time being relatively flexible in the other five directions. For this modification the actual major resonance frequency shifts were predicted accurately using the non-linear sensitivity analysis technique. However, some resonance frequency shifts which could not be predicted by using the non-linear sensitivity analysis have also been measured.

The experimental case study has demonstrated that practical implementation of the error localization and non-linear sensitivity analysis methods is not simple and straightforward. The most serious problem is usually coordinate incompleteness. For the error localization, a reliable expansion technique is vital because the dimensions between experimentally-derived modal model and analytical model are almost always incompatible. For structural modification prediction, care and attention must be given to the actual modification in order to ensure that the structural modifications are only imposed in the measured coordinates.

# 8 CONCLUSIONS

## 8.1 GENERAL CONCLUSIONS

The main objective of the work was to develop new structural dynamic reanalysis tools which could be applied to both theoretical and experimental structural modification analyses. As the validity of theoretical models and the accuracy of experimental data are the key factors affecting the outcome of these structural modification analyses, the relevant topics, such as techniques for the development of model updating and sensitivity analysis of measured data, have also been included within the scope of this research.

Throughout the thesis, detailed mathematical proofs, historical backgrounds for the different methods and various numerical and/or experimental studies have been presented, because without such rigorous mathematical background and information it is difficult to ensure the applicability of the theoretical tools used in structural dynamics, such as FRF measurement, model updating and structural modification analysis. Although discussions and conclusions have also been given in each of the preceding chapters, it is appropriate now to provide a general summary of those conclusions and the important findings such that the parts of the work which constitute new developments or attempts to new developments are highlighted.

### 8.1.1    THE RELIABILITY OF FRF MEASUREMENT TECHNIQUE

At the outset of any structural identification, model updating or structural modification exercise based on the use of measured FRF or experimentally-derived modal data, it is important that the reliability and accuracy of measurement techniques are thoroughly understood so that any errors incurred in the measurement process can be minimized.

Based on a traditional open-loop measurement-system model, modal test practitioners have developed the currently-used FRF estimators $_1H(\omega), _2H(\omega), _vH(\omega)$ and $_3H(\omega)$ for a single-shaker random excitation or an impact test. In practice, neither the $_1H(\omega)$ nor the $_2H(\omega)$ FRF estimator can produce the true FRF because auto-spectra (which are greatly influenced by measurement noise) are included in their formulations. The former under-estimates the FRF while the latter over-estimates the FRF in the vicinity of structural resonances. The $_vH(\omega)$ FRF estimator is based on the calculation of the geometric mean of $_1H(\omega)$ and $_2H(\omega)$ but, unfortunately, it is also unlikely to provide a meaningful result in most cases because the noise-to-signal ratios vary with the excitation frequency and their magnitude depends on the structure's properties as well as on the excitation mechanism. By incorporating the shaker-structure interaction as a feedback path in the FRF measurement-system model, a closed-loop model for **single**-shaker modal testing has been developed from which the observed variations of measured force signal can be explained analytically. This model also reveals the relationships between the measured force and acceleration signals and the properties of the test structure and of the excitation mechanism from which it can be proved that only $_3H(\omega)$ is a "noise-free" FRF estimator.

However, FRF estimators derived from DFT analysis are also liable to a **phase**-dependent bias error which is known as "leakage" caused by windowing for a finite amount of data. Using the new closed-loop model, bias errors on the estimates of

modal parameters (natural frequencies, damping loss factors and modal constants) for the different FRF estimators have been studied analytically and numerically. It was found that the only estimate which will lie on the true modal circle is $_2H(\omega)$ under noise-free conditions. Generally speaking, it can be concluded that both $_2H(\omega)$ and $_3H(\omega)$ are likely to provide more accurate FRF estimates than other FRF estimators around structural resonances. If the frequency resolution is high and measurement noise is significant, $_3H(\omega)$ will produce the best FRF estimates across the whole frequency range of measurement. It is concluded that a full awareness of the conditions under which each measurement is made in essential if accurate data data are to be obtained.

When there is a need for application of large forces and linearization of slightly non-linear structures, multi-point excitation should be used to obtain the **FRFs** of mechanical structures. Similar to its single-shaker counterpart, the multi-shaker **sine**-dwell or random excitation test was traditionally **modelled** as a open-loop multi-input multi-output system. All existing structural identification techniques have been developed based on the open-loop MIMO model. However, those techniques have a deficiency in that they cannot be successfully applied to estimate the FRF matrix in the vicinity of structural resonances because the input cross-spectrum matrix is very **ill**-conditioned with respect to the calculation of its inverse. The closed-loop model developed above (for the SISO case) has thus been generalised for multi-shaker modal testing. By using the closed-loop model, a MIMO system with feedback path is identified from which one can explain how the shaker-structure interactions cause difficulties in controlling the orthogonality between measured force signals in a **sine**-dwell test and in maintaining the required incoherence between measured force **auto**-spectra in a random excitation test. A new FRF estimation technique has also been developed using the MIMO model. This technique has a distinct advantage that it works effectively even if the measured force signals are highly correlated.

## 8.1.2    ANALYTICAL MODEL IMPROVEMENT USING MODAL DATA

The **response** and modal models of a mechanical structure can be obtained using the traditional direct structural identification (parameter extraction) technique in the frequency-domain or the time-domain. Various parameter extraction techniques have been developed and improved by numerous researchers in the past 20 years. At the current time, the inaccuracy of experimentally-derived response and modal models comes mainly from measurement errors during the data acquisition process because, with the advent of computing facilities and by using more reliable and numerical stable mathematical techniques, the numerical errors which are introduced during the parameter extraction process can be reduced to a relatively low level. However, there are many situations where the spatial properties of the structure need to be known in order to provide a good 'representative' mathematical model for a vibrating structure and, as a result, the study of analytical model improvement using experimental data becomes increasingly important and more and more popular.

Direct matrix-update methods are amongst the most commonly-used techniques in model updating. These methods are based on the constraint minimisation method using **Lagrangian** multipliers. The physical characteristics, such as the connectivity, of the structure are generally ignored in the formulation and the updating problem is tackled from a purely mathematical viewpoint. As a consequence, the updated model can often be optimum in a mathematical sense, reproducing the modal properties of the structure which are measurable, but the model itself is generally physically unrealistic. During the literature survey of direct matrix-update method, it was found that the forerunner of this method, Baruch **&** Bar&hack, adapted the idea from research work on navigation to develop the "so-called" direct matrix-update method. Unfortunately, the physical nature of navigation and model updating problems are different so that the

mapping technique used in navigation is not appropriate to resolve the model updating problem. It has been proved in this thesis that the formulae of direct-matrix update method are mathematically incorrect unless the mode shape or/and natural frequency matrix is complete in terms of the number of modes and the number of **DoFs.**

Having identified the inherent difficulties in obtaining system error matrices by direct matrix manipulation, two other model updating methods have been formulated and shown to be effective in analytical model updating, provided a sufficient number of measured modes are available. The first of these methods, the *orthogonality constraint method,* is based on transforming the orthogonality relationships of the mass and stiffness matrices into sets of simultaneous equations. A second method, the *eigendynamic constraint method,* is based on creating a system of simultaneous equations using the simple modal equations and mass normalisation relationships of measured modes. Both methods can produce the exact system error matrices by using the generalised inverses with a SVD technique when the system of equations is overdetermined. By comparing the minimum modal data required by these two methods, it was concluded that in practice the eigendynamic constraint method is better than the orthogonality constraint method because in general it requires fewer measured modes. When the modes available from measurement are incomplete in terms of the response coordinates as well as the number of modes, there are many system error matrices which can be obtained using the OCM or ECM. The thus-updated model can reproduce quite accurately the measured modal properties: however, the reliability of this updated model depends on the expansion method used to determine the response of the unmeasured coordinates.

### 8.1.3    DEVELOPMENT OF STRUCTURAL REANALYSIS TECHNIQUES

BASED ON LINEAR AND NON-LINEAR SENSITIVITY ANALYSES

As mentioned above, the primary goal of the work was to develop new technique(s) for structural modification analysis. A major reason for starting with first- and **higher-**order sensitivity analyses was that these techniques had emerged as amongst the most popular tools in structural reanalysis. The literature survey given in chapter 5 revealed that a large number of publications were devoted to sensitivity analysis and presented in journals under different disciplines. The sensitivity eigenproblem has been viewed as a problem in numerical analysis (e.g. Jahn [58], Wilkinson [61], Stewart [81]), as a problem in perturbation theory (e.g. Jacobi [56], Courent and Hilbert [59], Lancaster [60]), as a problem in linear systems theory (**Rosenbrock** [62], Morgan [63]), and as a problem in structural reanalysis (Fox and Kapoor [55], Wang et al. [73], Skingle and Ewins [71], **Noor** and Whitworth [74] etc.). Although first-order sensitivity analysis has been presented in different forms and refined to include such considerations as coincident natural frequencies and rigid-body modes, the limits of applicability had not previously been assessed in detail and no criterion had been given to determine under what conditions the method give accurate results. For this reason, a condition number (estimator) has been presented in this work that can be used to identify the limited bound of the application of first-order sensitivity analysis.

In structural reanalysis, some analysts have over-estimated the capability of **first-** and higher-order sensitivity analyses and expected that for large structural modifications the accuracy of structure modification prediction could be improved by including some higher-order terms. However, practical experience shows that, in many cases, prediction using higher-order sensitivity analysis is even worse than the approximated one using first-order sensitivity analysis. The limited success of sensitivity analysis in large modification prediction is inevitable because the the original aim of using

sensitivities in numerical analysis was only to investigate the stability of the **generalised** eigenvalue problem, i.e. to understand how eigenvalues and eigenvectors change when the elements of system matrices vary in an infinitesimal sense.

Having identified the inherent limitations of first- and higher-order sensitivity analyses, a new structural reanalysis procedure based on the use of the **Rayleigh** quotient with the classical inverse iteration method has been formulated. It has been shown that this technique is very accurate in predicting the dynamic responses of a modified structure. Because of the cubic convergence characteristic of the **Rayleigh** quotient iteration, the exact solution of a structural modification problem can be obtained in a small number of iterations. Another structural reanalysis technique based on inverse iteration method alone is also presented and discussed. It was found that the main advantage of the inverse iteration method is the simplicity of recursion. However, a drawback of this method is that the iteration procedure converges very slowly when the modes are closely-spaced.

In practice, not all the modal properties of the original (unmodified) structure will be available and useful for structural modification analysis : for example, only the coordinates at the surface of an engine are measurable and accessible for practical modifications. In such a situation, neither the **Rayleigh** quotient iteration nor the inverse iteration method is applicable because both of them require the eigenvectors with complete coordinates. Based on the idea given by Jahn [58], a non-linear sensitivity analysis technique has been formulated and shown to be effective tools for structural reanalysis under these conditions. As this technique requires only the responses corresponding to the modification sites, it has been used to predict the responses of the modified structure not only in an FE analysis but also in an experimental case study.

## 8.2  CONTRIBUTIONS  OF  THE  PRESENT  RESEARCH

In a final review of the research presented in this thesis, the contributions made to the various areas of activity are listed as follows:

### FRF **Measurement**

the development of a new closed loop model for single- or multi-shaker modal testing based on incorporating the shaker-structure interaction(s) into the measurement-system model;

the use of a closed-loop model for single-shaker modal testing in explanation of the force drop-off phenomenon in the vicinity of structural resonances;

analysis and evaluation of the bias errors (leakage error) on modal parameters that can be incurred when finite records of time signals are to be processed using **FFT**;

the use of a closed-loop model for multi-shaker modal testing in explanation of the correlation between various signals which cause the difficulty in controlling the measured force signals in a sine-dwell test as well as a random excitation test;

the development of a new MIMO FRF estimation technique which works properly even if the measured force signals are highly correlated (in which the classical structural techniques may fail);

### **Model Updating**

critical discussion and identification of the limitations of direct matrix-update methods;

the development of a new model updating technique based on using the orthogonality relationships of the system mass and stiffness matrices;

exploitation of the capability of the orthogonality constraint and the eigendynamic constraint methods in model updating with considering the problems of modal and coordinate incompleteness, and of measurement noise;

a detailed assessment of different physical expansion techniques based on the inverse procedure of Ridder's reduction technique;

**Linear and Non-linear Sensitivity Analysis for Structural Modification**

critical discussion on the limitations of first- and/or high-order sensitivity analysis in structural modification analysis;

the development of a condition estimator which can provide the limited bound of the application of first-order sensitivity analysis;

the presentation of an alternative way of calculating the response properties of a modified structure based on the Rayleigh quotient iteration method;

the development of a new computation procedure (non-linear sensitivity analysis) which can be used to determine the exact modal properties of the modified structure in the case only the responses corresponding to the modification sites and all natural frequencies of the original structure are given.

a detailed assessment of the truncation effects of modal incompleteness on the nonlinear sensitivity analysis.

## 8.3 SIJGGESTIONS FOR FURTHER WORK

As a consequence of this work, various aspects of modal analysis have been identified for further investigation. One obvious aspect for further study is to utilize the closed-loop model for single- or multi-shaker modal testing in the development of a more realistic noise model in simulated FRF measurements. Based on the closed-loop model, a new technique used to determine the unique estimates of FRFs has been presented: however, it would be appropriate for some experimental studies to be

carried out in order to illustrate the capability of the proposed technique in real measurements. In addition, parametric structural identification technique (time-domain) needs to be updated due to recognition of the hidden feedback paths and the Non-Gaussian (or random) nature of measurement noise.

In model updating, there is an urgent need to derive a reliable mode shape expansion procedure so that those model updating techniques using modal data, such as the orthogonality constraint and eigendynamic constraint methods, can be more successfully applied to update and/or validate the analytical model using experimental results.

For structural modification analysis, further research is required to enhance the applicability of the non-linear sensitivity analysis technique for high-frequency modes because, in some cases, this newly-developed technique may not converge as the predictions go beyond the limited bounds of Rayleigh quotient, and to improve the accuracy of this technique by incorporating the effects of low- and high-frequency residuals. Finally, the development of a structural optimization procedure which is capable of solving multiple natural frequency constraint problems is essential.

# REFERENCES

1.  **Ewins, D.J.** and **Imregun, M.**
    *"State-of-the-Art Assessment of Structural Dynamic Response Analysis Methods (DYNAS)"*
    Shock and Vibration Bulletin, Vol.56, Part 1, August, 1986.

2.  **Kennedy, C.C.** and **Pancu, C.D.P.**
    "Use *of Vectors in Vibration Measurement and Analysis"*
    Journal of Aerospace Sciences, Vol.14, No.1 1, 1947, pp.603-625.

3.  **Fraeijs de Veubeke, B.M.**
    *"A Variational Approach to Pure Mode Excitation Based on Characteristics Phase Lag Theory"*
    AGARD Report 39, 1956.

4.  **Bishop, R.E.D.** and **Gladwell, G.M.L.**
    *"An Investigation into the Theory of Resonance Testing"*
    Phil. Trans. Roy. Soc., Vol.225, Ser.A.No.1055, 1963, pp.241-280.

5.  **Lewis, R.D.** and **Wrisley, D.L.**
    "A *System for the Excitation of Pure Nature Modes of Complex Structures"*
    Journal of Aeronautical Sciences, Vol. 17, No. 11, 1950, pp.705-722.

6.  **Trasill-Nash, R.W.**
    *"On the Excitation of Pure Natural Modes in Aircraft Resonance Testing"*
    Journal of Aerospace Sciences, Vol.25, Dec.1958, pp.775-778.

7.   **Asher, G.W.**
     *"A Method of Normal Mode Excitation Utilizing Admittance Measurements"*
     Proc. of IAS National Spec. Meet. on Dyns. and Aeroelasticity, Nov.1958,
     pp.69-76.

8.   **Ewins, D. J.**
     **Modal** *Testing : Theory and Practice*
     Research Studies Press, London, 1985.

9.   **Remmers, G.** and **Belsheim, R.O.**
     *"Effects of Technique on Reliability of Mechanical Impedance Measurement"*
     Shock and Vibration Bulletin, Vol.34, 1964.

10.  **Ewins, D.J.** and **Griffin, J.**
     *"A State-of-the-Art Assessment of Mobility Measurement Techniques- Results
     for the Mid-Range Structures"*
     Journal of Sound and Vibration, Vol.78, No.2, 1981, pp.197-222.

11.  **Ibrahim, S.R.** and **Mikulcik, E.C.**
     *"A Method for the Direct Identification of Vibration Parameters from Free
     Responses"*
     Shock and Vibration Bulletin, Vol.47, No.4, 1977, pp.183-198.

12.  **Tomlinson, G.R.**
     *"Force Distortion in Resonance Testing of Structures with Electro-Dynamic
     Vibration Exciters"*
     Journal of Sound and Vibration, Vol.63, No.3, 1979, pp.337-350.

13.  **Rao, D.K.**
     *"Electrodynamic Interaction between a Resonating Structure"*
     Proc. of the 5th Int. Modal Analysis Conf., 1987, pp. 1142-1 145.

14.  **Shelley, S., Zhang, Q., Luo, X.N., Allemang, R.J.** and **Brown,
     D.J.**
     *"Investigation and Modelling of Shaker Dynamic Effects"*
     Proc. of the 13th Int. Sem. on Modal Analysis, C51, 1988.

15.  **Mitchell, L.D.**
     *"Improved Methodfor the Fast Fourier Transform (FFT) Calculation of the*
     *Frequency Response Function"*
     Trans. ASME, Journal of Mech. Design, Vo.104, 1982, pp.277-279.

16.  **Elliott, K.B.** and **Mitchell, L.D.**
     *"The Improved Frequency Response Function and Its Effect on Modal Circle*
     *Fits"*
     Trans. ASME, Journal of Applied Mechanics, Vol.51, 1984, pp.657-663.

17.  **Mitchell, L.D., Cobb, R.E., Deel, J.C.** and **Luk, Y.W.**
     *"An Unbiased Frequency Response Function Estimator"*
     Journal of Modal Analysis, January 1988, pp.12-19.

18.  **Goyder, H.G.D.**
     *"Frequency Response Testing a Non-linear Structure in a Nosiy Environment*
     *with a Distorting Shakers"*
     Spring Conference, Institute of Acoustics, 1981, pp.37-40.

19.  **Wellstead, P.E.**
     *"Reference Signals for Closed-Loop Identification"*
     International Journal of Control, Vol.26, 1977, pp.945962.

20.  **Wellstead, P.E.**
     *"Non-Parametric Methods of System Identification"*
     5th IFAC Symp. on Identification and System Parameter Estimation, 1979,
     pp.115-129.

21.  **Cawley, P.**
     *"Rapid Measurement of Modal Properties Using FFT Analyzers with Random*
     *Excitation"*
     Trans. ASME, J. of Vib., Acou., Stress & Rel. in Design, Vol.108, 1986,
     pp.394-398.

22.  **Jenkins, G.** and **Watts, D.**
     *Spectral Analysis and Its Application*
     Holden-Day, San Francisco, 1968.

23. **Kabe, A.M.**
    'Multi-Shaker *Mode Testing"*
    AIAA Journal of Guidance, Vo1.7, No.6, 1984, pp.740-746.

24. **Allemang, R.J., Rost, R.W.** and **Brown, D.L.**
    *"Dual Input Estimation of Frequency Response Functions for Experimental Modal Analysis fo Aircraft Structures"*
    Proc. of the 1st Int. Modal Analysis Conf., 1982, pp.333-340.

25. **Allemang, R.J., Rost, R.W.** and **Brown, D.L.**
    *"Multiple Input Estimation of Frequency Response Functions : Excitation Considerations"*
    ASME Paper No.83-DET-73, 1983.

26. **Leuridan, J.**
    *'The Use of Principal Inputs in Multiple-Input and Multi-Output Data Analysis"*
    International Journal of Modal Analysis, July 1983, pp.1-8.

27. **Dobbs, C.J.** and **Robson, J.F.**
    *"Partial Coherence in Multivariate Random Processes"*
    Journal of Sound and Vibration, Vo1.42, 1975, pp.243-249.

28. **Bendat, J.S.**
    *"Modern Analysis Procedures for Multiple Input/Output Problems"*
    Journal of Acoustical Society of America, Vo1.68, No.2, 1980, pp.498-503.

29. **Bendat, J.S.** and **Piersol, A.G.**
    *Random Data : Analysis and Measurement Procedures*
    *New* York : John Wiley, 1984.

30. **Lembregts, F., Snoeys R.** and **Leuridan, J.**
    *"Application and Evaluation of Multiple-Input Modal-Parameter Estimation"*
    Journal of Modal Analysis, January 1987, pp. 19-31.

31. **Otte, D., Leuridan, J., Grangier, H.** and **Aquilina, R.**
    *"Coupling of Structures Using Measured FRF's by Means of SVD-Based Data Reduction Techniques"*
    Proc. of the 8th Int. Modal Analysis Conf., 1990, pp.213-220.

32.  **Brown, D.L., Allemang, R.J., Zimmermann, R.** and **Mergeay, M.**
     *"Parameter Estimation Methods for Modal Analysis"*
     SAE Paper 79022 1, 1979.

33.  **Stroud, R.C.**
     *"Excitation, Measurement and Analysis Methods for Modal Testing"*
     Joint ASME/ASCE publication, Combined Experimental/Analytical Modeling of
     Dynamic Structural Systems, June 1985.

34.  **Füllekrug, U.**
     "Survey *of Parameter Estimation Methods in Experimental Modal Analysis*
     Proc. of the 5th Int. Modal Analysis Conf., 1987, pp.460-467.

35.  **Wada, B.K.**
     *"Correlation of Modal and Test Analysis"*
     Technical Report, Jet Propulsion Laboratory, 1980.

36.  **Allemang, R.J.** and **Brown, D.L.**
     *"A Correlation Coefficient for Modal Vector Analysis"*
     Proc. of the 1st Int. Modal Analysis Conf., 1983, pp.110-116.

37.  **Lieven, N.A.J.** and **Ewins, D.J.**
     *"Spatial Correlation of Mode Shapes, the Coordinate Modal Assurance Criterion
     (COMAC)"*
     Proc. of the 6th Int. Modal Analysis Conf., 1988, pp.690-695.

38.  **Wahba, G.**
     *"A Least Squares Estimate of Satellite Attitude"*
     Problem 65-1, SIAM Review, Vol.7, July 1965, p.409.

39.  **Farrell, J.L.** and **Stuelpnagel, J.C.** (Commented by **Wessner, R.H.,
     Velmen, J.R.** and **Brock, J.E.**)
     *"Solution of the Problem - A Least Squares Estimate of Satellite Attitude"*
     Problem 65-1(Solution), SIAM Review, Vol.8, July 1966, pp.384-386.

40.  **Brock, J.E.**
     *"Optimal Matrices Describing Linear Systems"*
     AIAA Journal, Vol.6, July 1968, pp.1292-1296.

41. **Bar-Itzhack, I.Y., Mayer, J.** and **Fuhermann, P.A.**
    *"Strapdown Matrix Orthogonalization: The Dual Iterative Algorithm"*
    IEEE Trans. on Aerospace and Electronic Systems, Vol.AES-12, Jan. 1976,
    pp.32-38.

42. **Bar-Itzhack, I.Y.** and **Mayer, J.**
    *"On the Convergence of Iterative Orthogonalization Processes"*
    IEEE Trans. on Aerospace and Electronic Systems, Vol.AES-12,Mar.1976,
    pp.146-151.

43. **Baruch, M.** and **Itzhack, I.Y.B.**
    *"Optimal Weighted Orthogonalization of Measured Modes"*
    AIAA Journal, Vol.16, April 1978, pp.346-351.

44. **Berman, A.**
    *"Mass Matrix Correction Using an Incomplete Set of Measured Modes"*
    AIAA Journal, Vol.17, October 1979, pp.1 147-1148.

45. **Wei, F.S.**
    *"Stiffness Matrix Correction from Incomplete Test Data"*
    AIAA Journal, Vol.18, October 1980, pp.1274-1275.

46. **Caeser, B.**
    *"Update and Identification of Dynamic Mathematical Models"*
    Proc. of the 4th Int. Modal Analysis Conf., 1986, pp.394-401.

47. **Lin, R.M.**
    *"On Minimum Data Required to Update an Analytical Model"*
    Internal Report No.89010, Dyn. Sect., Imperial College, September 1989.

48. **Gladwell, G.M.L.** and **Gbadeyan, J.A.**
    *"On the Inverse Problem of the Vobrating String or Rod"*
    Quater. Jour. of Mech. and Appl. Math., Vol.38, 1985, pp.169-174.

49. **Gladwell, G.M.L.**
    *"The Inverse Mode Problem for Lumped-mass Systems"*
    Quater. Jour. of Mech. and Appl. Math., Vol.39, 1986, pp.297-307.

50. **Kidder, R.L.**
    *"Reduction of Structural Frequency Equations"*
    AIAA Journal, Vol. 11, June 1980, p.892.

51. **Golub, G.H., Klema, V.C.** and **Stewart, G.W.**
    *"Rank Degeneracy and Least Squares Problems"*
    Dep. Comp. Sci., Stanfor Univ. Tech. Rep.STAN-CS-76-559, August 1976.

52. **Kublanovskaja, W.N.**
    *"On an Approach to the Solution of the Inverse Eigenvalue Problem"*
    Zap. Naucn. Sem. Leningrad. Otdel. Mat. Inst., in V. A. Steklova Akad. Nauk
    SSSR, pp.138-149.

53. **Lin, R.M.**
    *"Model Updating Using Frequency Response Functions"*
    Internal Report No.9001 1, Dyn. Sect., Imperial College, 1990.

54. **Faddeev, D.K.** and **Faddeeva, V.N.**
    *Computational Methods of Linear Algebra*
    W.H. Freeman and Company, 1963.

55. **Fox, R.L.** and **Kapoor, M.P.**
    *"Rates of Changes of Eigenvalues and Eigenvectors"*
    AIAA Journal, Vol.6, 1968, pp.2426-2429.

56. **Jacobi, C.G.J.**
    *"Uber ein leichtes Verfahren die in der Theorie der Saecularstoerungen
    vorkommenden Gleichungen numerisch aufzuloesen"*
    Zeritshrift fur Reine und Angewandte Mathematik, Vol.30, 1846, pp.5 l-95; also
    NASA TT.F-13, 666, June 1971.

57. **Van De Vooren, A.I.**
    N.L.L. (Amsterdam), Rep. F 100, 1952.

58. **Jahn, H.A.**
    *"Improvement of an Approximate Set of Latent Roots and Modal Columns of a
    Matrix by Methods akin to those of Classical Perturbation Theory"*
    *Quart.* Journal of Mech. and Applied Math., Vol.1, 1948, pp.132-144.

59.  **Courent, R.** and **Hilbert, D.**
     *Methoden der Mathematischen Physik (Methods of Mathematical Physics)*
     Book 1, 1931. (Interscience, Vol.1, 1953)

60.  **Lancaster, P.**
     *"On Eigenvalues of Matrices Dependent on a Parameter"*
     Numerische Mathematick, Vo1.6, No.5, 1964, pp.377-387.

61.  **Wilkinson, J.H.**
     *The Algebraic Eigenvalue Problem*
     Oxford University Press, London, 1963, pp.62-109.

62.  **Rosenbrock, H.H.**
     *"Sensitivity of an Eigenvalue to Changes in the Matrix"*
     Electronics Letters, Vol.1, 1965, pp.278-279.

63.  **Morgan, B.S.**
     *"Computational Procedure for the Sensitivity of an Eigenvalue"*
     Electronics Letters, Vo1.2, 1966, pp.197-198.

64.  **Reddy, D.C.**
     *"Sensitivity of an Eigenvalue of a Multivariable Control System"*
     Electronics Letters, Vol.2, 1966, p.446.

65.  **Rogers, L.C.**
     *"Derivatives of Eigenvalues and Eigenvectors"*
     AIAA Journal, Vol.8, 1970, pp.943-944.

66.  **Vanhonacker, P.**
     *"Differential and Difference Sensitivities of Natural Frequencies and Mode Shapes of Mechanical Structure"*
     AIAA Journal, Vol.18, 1980, pp.151 1-1514.

67.  **Rudisill, C.S.** and **Bhatia, K.G.**
     *"Second Derivatives of the Flutter Velocity and the Optimization of Aircraft Structures"*
     AIAA Journal, Vol.10, 1972, pp.1569-1572.

68.  **Plaut, R.H.** and **Huseyin, K.**
     *"Derivatives of Eigenvalues and Eigenvectors in Non-Self-Adjoint Systems"*
     AIAA Journal, Vol.11, 1973, pp.250-251.

69.  **Rudisill, C.S.**
     *"Derivatives of Eigenvalues and Eigenvectors for a General Matrix"*
     AIAA Journal, Vol. 12, 1974, pp.721-722.

70.  **Belle, H.V.**
     *"Higher Order Sensitivities in Structural Systems"*
     AIAA Journal, Vol.20, 1982, pp.286-288.

71.  **Skingle, G.W.** and **Ewins, D.J.**
     *"Sensitivity Analysis using Resonance and Anti-resonance Frequencies - A*
     *Guide to Structural Modification"*
     Proc. of the 7th Int. Modal Analysis Conf., 1989.

72.  **Lim, K.B., Junkins, J.L.** and **Wang, B.P.**
     *"Re-examination of Eigenvector Derivatives"*
     AIAA J. Guidance, Vol.10, 1987, pp.581-587.

73.  **Wang, J., Heylen, W.** and **Sas, P.**
     *"Accuracy of Structural Modification Techniques"*
     Proc. of the 5th Int. Modal Analysis Conf., 1987, pp.65-71.

74.  **Noor, A.K.** and **Whitworth, S.**
     *"Reanalysis Procedure for Large Structural Systems"*
     Int. J. Numer. Methods Eng., Vol.26, 1988, pp.1729-1748.

75.  **Frazer, R.A., Duncan, W.J.** and **Collar A.R.**
     *Elementary Matrices*
     Cambridge University Press, London, 1935, p.61.

76.  **Bodewig, E.**
     *Matrix Calculus*
     North Holland, Amsterdam, 1959, pp.35-36.

77.  **Frame, J.S.**
     **"Matrix** *Functions* **and Applications: Part IV- Matrix Functions and Constituent**
     **Matrices"**
     IEEE Spectrum, 1964, pp.125126.

78.  **Duncan, W.J.**
     *'Mechanical Admittances and their Applications to Oscillation Problems"*
     **HMSO.,** London, 1947.

79.  **Flannelly, W.G.**
     *"Natural Anti-Resonances on Structural Dynamics"*
     **Kaman** Aerospace Corporation, September 1971.

80.  **Stewart, G.W.**
     *"On the sensitivity of the eigenvalue problem $Ax=\lambda Bx$"*
     SIAM J. Numer. Anal., Vol.9, 1972, pp.669-686.

81.  **Stewart, G.W.**
     *"Error and perturbation bounds for subspaces associated with certain eigenvalue*
     *problems"*
     SIAM Riew., Vol.15, 1973, pp.772-764.

82.  **Stewart, G.W.**
     *Introduction to Matrix Computations*
     Academic Press, New York, 1973, pp.289-307.

83.  **Lord Rayleigh**
     *The Theory of Sound : Vol.1*
     Macmillan and Co. Ltd., London, 1926, Section 90-91.

84.  **Lancaster, P.**
     *Lambda-Matrices and Vibrating Systems*
     Pergamon Press, New York, 1966.

85.  **Golub, G.H.** and **Van Loan, C.F.**
     *Matrix Computations*
     North Oxford Academic, Oxford, 1983, pp.317-318.

86.  **Noor, A.K.** and **Whitworth,  S.L.**
     *"Model-size reduction for the buckling and vibration analyses of anisotropic panels"*
     ASCE J. of Eng. Mech., Vol.113, 1987, pp.170-185.

87.  **Collar,  A.R.**
     "Some *notes on Jahn's method for the improvement of approximate latent roots and vectors of a square matrix."*
     *Quart.* J. Mech. and Appl. Math., Vol.1, 1948, pp.145148.

88.  **Wang, B.P.** and **Chu,  F.H.**
     *"Effective dynamic reanalysis of large structures"*
     Shock and Vibration Bulletin, Vol.51, Part 3, 1987, pp.73-79.

89.  **Ewins,  D.J.**
     *"Analysis of Modified or Coupled Structures Using FRF Properties"*
     Int. Rep. No.86002, Dyn. Sec., Mech. Eng. Dept., Imperial College, 1986.

90.  **Guyan,  R.J.**
     *"Reduction of Mass and Stiffness Matrices"*
     AIAA Journal, Vol.3, February 1965, p.380.

91.  **Paz,  M.**
     *"Dynamic Condensation Method"*
     AIAA Journal, Vol.22, May 1984, pp.724-727.

92.  **Brown,  T.**
     *A Unified  Approach  to  the  Identification  of Dynamic   Behaviour Using  the  Theory  of Vector  Spaces*
     PhD Thesis, Dept. of Eng. Math., University of Bristol, 1985.

93.  **Lieven,  N.A.J.** and  **Ewins,  D.J.**
     *"Expansion of Modal Data for Correlation"*
     Proc. of the 8th Int. Modal Analysis Conf., 1990, pp.605-609.

94.  **Gysin,  P.**
     *"Comparison of Expansion Methods for FE Modelling Error Localization"*
     Proc. of the 8th Int. Modal Analysis Conf., 1990, pp.195-204

95. **He, J. and Ewins, D.J.**
*"Analytical Stiffness Matrix Correction Using Measured Vibration Modes"*
*The* Int. Jour. of Analy. and Exp. Modal Analysis, **Vol.1, No.3,** July 1986.

96. **Robb, D.A.**
User's *Guide to MODENT : Version 5.1*
Modal TestingUnit, Imperial College, 1987.

97. **Imregun, M.**
*User's Guide to MODESH*
Modal Testing Unit, Imperial College, 1987.

Al. **Moore, E.H.**
*General Analysis*
Vol.1 (Mem. Amer. Phil. Soc. Vol. 1, Philadelphia, 1935) p.8 and chap.3.

A2. **Bjerhammar, A.**
*"Rectangular Reciprocal Matrices, with Special Reference to Geodetic Calculations"*
Bull. geod. int., 1951, pp.188-220.

A3. **Penrose, R.**
*"A Generalised Inverse for Matrices"*
Proc. Cambridge Philos. Soc., Vol.51, 1955, pp.406-413.

A4. **Penrose, R.**
*"On Best Approximate Solutions of Linear Matrix Equations"*
Proc. Cambridge Philos. Soc., Vol.52, 1956, pp.17-19.

A5. **Luk, W.L.**
*"Identification of Physical Mass, Stiffness and Damping Matrices Using Pseudo-Inverse"*
Proc. of the 5 th Int. Modal Analysis Conf., 1987 , pp.679-685.

A6. **Ibrahim, S.R.** and **Füllekrug, U.**
   *"Investigation into Exact Normalization of Incomplete Complex Modes by Decomposition Transformation"*
   Proc. of the *8th* Int. Modal Analysis Conf., 1990, pp.205212.

A7. **Nashed, M.Z.**
   ***Generalised Inverses and Applications***
   Academic Press, Inc., New York, U.S.A, 1976.

# APPENDIX IA/

## THE GENERALISED INVERSE AND WEIGHTED LEAST-SQUARES

### A. 1 INTRODUCTION

The generalised inverse is proving to be a very useful tool in modem linear matrix theory, in particular as a means of determining the least-squares solution of a set of simultaneous equations which are overdetermined. However, application of the generalised inverse in structural dynamics exercises is not completely successful and it is found that this failure is mainly due to a lack of understanding of the fundamental principals of the generalised inverse. The objective of this appendix is to review the basic theory of the generalised inverse and to discuss its applicability in structural dynamics. Also, a brief description of the weighted least-squares technique is included. This weighted least-squares technique is very useful in providing the optimum solution of a physical problem when a prior knowledge of the uncertainties existed in measured data is known.

### A2. HISTORICAL DEVELOPMENT OF GENERALISED INVERSE

The concept of a generalised inverse of a matrix was first introduced by E.H. Moore, who defined a unique inverse for all matrices, rectangular as well as square. He systematically investigated the properties of this inverse and showed that it has certain properties analogous to those possessed by the inverse of a non-singular matrix. Details of his work were published in 1935 as Volume 1 of the Memoirs of the

American Philosophical Society [Al]. In 1951 Bjerhammar **[A2]** rediscovered

Moore's inverse and also noted the least-squares properties (not mentioned by Moore)

of **generalised** inverses to solutions of linear system. Penrose **[A3,A4]** sharpened and

extended Bjerhammar's work on linear systems and showed that the generalised

inverse for a given matrix [A] is the unique matrix [A]+ satisfying the four equations

shown below:

$$[A][A]^+[A] \quad = \quad [A] \tag{A.1}$$

$$[A]^+[A][A]^+ \quad = \quad [A]^+ \tag{A.2}$$

$$([A][A]^+)^* \quad = \quad [A][A]^+ \tag{A.3}$$

$$([A]^+[A])^* \quad = \quad [A]^+[A] \tag{A.4}$$

This discovery has been so important and fruitful that this unique inverse is commonly

called the Moore-Penrose generalised inverse. Penrose **[A4]** showed that the

generalised inverse possesses the following least-squares property :$[A]^+[B]$ is the

unique best approximate solution of the unknown matrix [X] in the equation

[A][X]=[B], and is of smallest Euclidean norm among all possible solutions of[X].

This situation arises often in least-squares fitting, linear programming and other

statistical applications.   Best approximation solution is important in those areas

because it is the best way to solve an overdetermined problem with a set of

*inconsistent*   equations in the sense of least squares, thus to minimize the effect of

noise in a system. To this end, the word "noise" has very wide implications: any

causal or random factors which should not or cannot be modelled, about which further

information is not available, which cannot be analysed, which may not recur

periodically, etc. Thus "noise" = "something which cannot be explained". This is a

much more comprehensive category than random effects interpreted in a **well-**

developed probabilistic sense.

Since 1955 thousands of papers on various aspects of the generalised inverse and its applications in different engineering and science disciplines have appeared. In structural dynamics, the generalised inverse of matrices has been widely used in structural identification [A5], model updating [40-43], mode shape expansion [86] and normalization of incomplete complex modes [A6]. However, it seems that not enough attention has always been given to the basic theory of the generalised inverse when those structural analysts used this mathematical device to develop their own techniques. As a result, many of today's structural identification and model updating exercises are demonstrably prejudiced.

## A.3   THE GENERALISED INVERSE OF MATRICES

For an $NxN$ nonsingular square matrix [A], the **generalised** inverse is a left inverse and also a right inverse of [A]. Thus it satisfies the following relationship :

$$[A]^+[A] \; = \; [A][A]^+ \; = \; [I] \tag{A.5}$$

For an $Nxm$ matrix [B] of maximum rank $m$ ($m{\leq}N$), the columns of [B] are linearly independent and $[B]^T[B]$ is positive definite and nonsingular. The **generalised** inverse of [B] is defined as:

$$[B]+ = \; ([B]^T[B])^{-1}[B]^T \tag{A.6}$$

this generalised inverse is a left inverse of [B]. There are other left inverses, but this is the only one having rows in the row-space of $[B]^T$.

In a similar way, the **generalised** inverse of an $mxN$ matrix [C] of rank $m$ $(N \geq m)$, is defined as:

$$[C]^+ = [C]^T ([C]^T[C])^{-1} \qquad (A.7)$$

This is the only right inverse of [C] having columns in the column-space of $[C]^T$.

In the general case of any **nonzero** $Nxm$ matrix **[D]** whose rank $r$ may be less than its smaller dimension $m$, the generalised inverse of [D] cannot be determined using equations (A.6) and (A.7). In such a situation, **[D]** can be decomposed in a form of :

$$[D] = [U][\Sigma][V]^T \qquad (A.8)$$

where [U] is an $Nxm$ orthonormal matrix and [V] is an $mxm$ orthonormal matrix; $[\Sigma]$ is an $mxm$ diagonal matrix whose diagonal elements consists of $s$ **nonzero** singular values of [D] $([\Sigma] = \text{diag}(\sigma_1,...,\sigma_s,0,..., 0))$.

Having calculated the singular value decomposition of **[D],** the generalised inverse of **[D]** is determined by :

$$[D]^+ = [V][\Sigma]^+[U]^T \qquad (A.9)$$

where $[\Sigma] = \text{diag}(\sigma_1^{-1},...,\sigma_s^{-1},0,..., 0)$.

## A.4 GENERAL DISCUSSIONS

The **generalised** inverse literature is vast, as evidenced by over 1,700 references in the Proceedings of an Advanced Seminar on **Generalised** Inverses and Applications edited by M.Z. **Nashed [A7]** in 1976. However, the application of this mathematical tool to practical problems, especially to structural dynamics, has failed to give sensible results in many cases. The limited success of the generalised inverse in structure dynamics is inevitable because when the available information for structural identification, model updating, mode shape expansion and normalization of complex modes is limited and incomplete, many people misinterpret the nature of those problems, resulting in incorrect formulae from mis-using an elegant mathematical technique.

Suppose that the modal data are only incomplete in terms of the number of measured modes and are "noise-free" - not contaminated by random noise. Structural identification problems are ill-posed and underdetermined without additional information and, as a result, there will exist many possible sets of system matrices that can regenerate the (limited) measured modal data. In such a situation, using any mathematical technique will not improve the nature of problem but will only confuse the followers. As it can be realised that the rectangular modal matrix does not contain set of "inconsistent" equations or noisy data but is "insufficient" to recover the original system matrices. In model updating, the DMU method is a mapping technique (Chapter 4.3.3) so that it can be used to determine the number of mismodelling sites when sufficient modes are available. The **generalised** inverse method increases the size of matrices but cannot increase their rank, and so, alternative methods (Chapter 4.4.1) must be used if one wants to locate the mismodelling sites correctly. For mode shape expansion, a **generalised** inverse method (Method C in Chapter 7.2.2) provides a least-squares solution but does not give an "exact" or the "best" solution when all modelling errors lie in the measured **DoFs**. In normalizing complex modes, the

transformation method suggested by Ibrahim is mathematically incomplete but the numerical results shown on his paper were surprisingly promising.

Undoubtedly, the generalised inverse provides a unique solution to solve an overdetermined problem with or without noise. However, understanding the nature of problem is more important than anything such as choosing the appropriate mathematical technique since it is impossible to obtain the right answer for a specific problem which has been incorrectly constructed in the very beginning.

## A5. WEIGHTED LEAST-SQUARES

As mentioned above, the "optimum" or "best" solution (x) to an **inconsistant** (overdetermined) system of equations $[A]\{x\}=\{b)$ can be obtained using the generalised inverse technique:

$$\{x\} \ = \ [A]^+\{b\} \tag{A. 10}$$

It should be noted that the formulation of equation (A.lO) has two implicit assumptions : firstly, that all information are quantified by the same dimension, and secondly, that all observations are trusted to the same degree. As an example of the first assumption, if some of the response were in units of metres (for relative displacements) and the rest in $m/s^2$ (acceleration) the formulation of equation (A. 10) would be untenable. The second assumption implies that even if some experimental data were measured with high precision, equation (A.lO) would treat these experimental data with equal weight as the other oberservations.

The above two problems can be solved by introducing the concepts of weighting/scaling to the least-squares formulation. If the $m$ observations $b_1, \ldots b_m$ are not equally reliable, then different weights $w_1, \ldots w_m$ which depend on the knowlegde of uncertainties must be associated to the $m$ equations. This can be done by post-multplying both sides of equation [A](x)=(b) by the diagonal matix [W] whose elements are $w_1, \ldots, w_m$ in sequence. In addition to their unequal reliability, the observations may not be independent in some cases. Under these situations, a coefficient $w_{ij}$ which measures the coupling of observation $i$ to observation$j$ must be introduced. Then

$$[A]\{x\} = \{b\} \quad \text{is changed to} \quad [W][A]\{x\} = [W]\{b\} \qquad (A11)$$

To solve this new problem [W][A]{x}=[W] (b), *we* have to look back at the normal equations for the original problem, and make the appropriate changes : [A] is replaced by [W][A], and {b} is replaced by [W]{ b}. By calculating the generalised inverse of [W][A], the optimum solution of the new problem can be obtained.

# APPENDIX ☐

## BACKGROUND MATRIX ALGEBRA

### B 1. (LINEAR) SPACE

A linear space $C^N$ is a collection of mathematical (or physical) objects (say, $\{x\}$, $\{y\}$ and $\{z\} \in C^N$) which is closed relative to two operations: addition, and multiplication by all real and complex numbers; these operations satisfy the following conditions:

1. $\{x\} + \{y\} = \{y\} + (x)$ (commutative law);

2. $(\{x\} + \{y\}) + \{z\} = \{x\} + (\{y\} + \{z\})$ (associative law);

3. there exists an element "$\{0\}$" such that $\{x\} + (0) = (x)$ for all $\{x\}$;

4. for all $\{x\}$ there exists a negative element "$\{-x\}$" such that $(x) + ((-x)) = (0)$;

5. $1.\{x\} = \{x\}$;

6. $(a + b)\{x\} = a\{x\} + b(x)$;

7. $a(\{x\} + \{y\}) = a\{x\} + a\{y\}$;

8. $a(b\{x\}) = ab\{x\}$

The elements of a linear space are called *vectors*.

A space is called **real** if multiplication of its vectors is defined only for real numbers and **complex** if multiplication is defined for complex numbers.

A space is **called finite-dimensional** if the following axiom is satisfied:

9. There exists a finite number Of vectors, $\{x_1\}, \ldots \{x_N\}$ such that every vector in the space may be represented in the form

$$c_1\{x_1\} + \cdots + c_N\{x_N\}$$

The dimension of a finite-dimensional space is the least number of vectors satisfying the condition of axiom 9.

## B2. SUBSPACE

A *subspace* of a vector space $C^N$ is a subset of vectors $\{x\} \in C^N$ such that any linear combination of vectors in the subset is again a vector in this subset. It is obvious that the set consisting of the null vector and also the whole space are subspaces in the sense of this definition.

## B3. LINEARLY INDEPENDENT

If all nontrivial combinations of the vectors are nonzero,

$$c_1\{x_1\} + \ldots + c_N\{x_N\} = (0) \qquad \text{unless} \qquad c_1 = \ldots = c_N = 0,$$

then the vectors $\{x_1\}, \ldots \{x_N\}$ *are linearly independent.* Otherwise they are linearly dependent, and one of them is a linear combination of the others.

## B4. SPAN

If a vector space $C^N$ consists of all linear combinations of the particular vectors $\{x_1\}$, $\cdots, \{x_N\}$, then these vectors *span* the space. In other words, every vector (y) in $C^N$ can be expressed as some combination of the (x) 's:

$$\{y\} = c_1\{x_1\} + \ldots + c_N\{x_N\} \qquad \text{for some coefficients } c_i.$$

## B5. BASIS

A *basis* of a vector space is any ordered set of vectors of the space that

(i)   is linearly independent and

(ii)   spans the vector space.

## B6.  DIMENSION

Let N be a positive integer. If a basis of a vector space $C^N$ has N vectors, then $C^N$ has **dimension** $N$.  A vector space consisting of the zero vector only is said to have dimension zero.

## B7.  ROW(COLUMN)-SPACE

The vector space consisting of the set of all linear combinations of the *rows(columns)* of matrix [A] is called the *row(column)-space* of [A].

## B8.  PROJECTION

Let $R^k$ *be* a subspace of $C^N$ *(N>k)* and $[A] \in C^{Nxm}$.  Then each column of [A] is a vector with a dimension of N and may be projected onto $R^k$.  The matrix obtained by projecting the columns of [A] onto $R^k$ is called **the projection** of [A] onto $R^k$.

## B9.  ELEMENTARY  TRANSFORMATIONS

It is often convenient to perform the following operations on matrices :

1.    multiplying the elements of some row by a number;

2.    adding to the elements of some row numbers which are proportional to the corresponding elements of some previous/subsequent row.

These transformations may also be performed on columns. Transformations of the type indicated will be called **elementary transformations** of matrices.

## B10.    SIMILARITY TRANSFORMATIONS

A similarity transformation possesses the following properties :

1.    $[C]^{-1}[A_1][C]+[C]^{-1}[A_2][C]+ . . +[C]^{-1}[A_n][C] = [C]^{-1}([A_1]+[A_2]+...+[A_n])[C];$

2.    $[C]^{-1}[A_1][C][C]^{-1}[A_2][C]...[C]^{-1}[A_n][C] = [C]^{-1}([A_1][A_2]...[A_n])[C]$

In particular                    $([C]^{-1}[A_1][C])^n = [C]^{-1}[A_1]^n[C]$

where [C] is a non-singular matrix and $[A_1],...,[A_n]$ and [C] $\in C^{NxN}$ .

The matrix $[D]$ is said to be *similar* to that matrix [A] when $[D] = [C]^{-1}[A][C]$. The most importance property common to similar matrices is the fact that they all have the same eigenvalues, for

$$|[A] - \lambda[I]| = 0$$

implies          $|[C]^{-1}([A] - \lambda[I])[C]| = 0$

and              $|[C]^{-1}[A][C] - \lambda[I]| = 0$

so that          $|[D] - \lambda[I]| = 0$

Thus the zeros of $|[A] - \lambda[I]|$ coincide with those of $|[D] - \lambda[I]|$ and the eigenvalues of [A] and [D] therefore coincide. However, the converse statement is not necessarily true, ie., matrices having the same eigenvalues are not necessarily similar (see Wilkinson [61])

## B11.    ORTHONORMAL

A basis $\{x_1\}, .... \{x_N\}$ is called *orthonormal* if

$$\{x_i\}^H\{x_j\} = \begin{cases} 0 \quad \text{whenever } i \neq j \quad \text{giving the orthogonality} \\ 1 \quad \text{whenever } i = j \quad \text{giving the normalisation} \end{cases}$$

## B12.     RANKOFAMATRIX

If $[A] \in C^{Nxm}$, **rank** $[A]$ is the largest number of columns of $[A]$ which constitute a linearly independent set.   This set of columns is not unique, but the number of elements of this set is unique.   It is a remarkable fact that **rank**$[A]^T$ = rank$[A]$. Therefore, rank may be equivalently defined in terms of linearly independent rows. Often this is phrased as "**rank**$[A]$ = row-rank of $[A]$ = column-rank of $[A]$."

## B13.     TRACE

The roots $\lambda_i$ of the chracteristic polynomial are called the eigenvalues (or characteristic numbers) of the matrix.   The sum of the $n$ eigenvalues equals the sum of the $n$ diagonal entries of $[A]$:

$$\lambda_1 + \lambda_2 + \ldots + \lambda_N \quad = \quad a_{11} + a_{22} + \ldots + a_{NN}$$

The sum is known as the ***trace (or spur)*** of $[A]$ and this is one of the invariants of characteristic polynomial (or determinant), i.e., it does not change under similarity transformation.

## B12.     VECTOR NORM

The norm of a vector $\{x\}$ is a non-negative number $\|(x)\|$ corresponding to this vector (and in topological sense gives the length of a vector relative to origin of space) which has the following properties:

1.   $\|\{x\}\| \quad > 0$ for $\{x\} \neq \{0\}$ and $\|\{0\}\| = 0$;

2.   $\|c\{x\}\| = |c| . \|(x)\|$  for any numerical multiplier c;

3.   $\|\{x\} + \{y\}\| \leq \|\{x\}\| + \|\{y\}\|$ ("triangular inequality").

A useful class of norms are **Hölder** or p-norms defined by

$$\|\{x\}\|_p = (|x_1|_p + \ldots + |x_N|_p)^{1/p}$$

of which

$$\|\{x\}\|_1 = \sum_{i=1}^{N} |x_i|$$

$$\|\{x\}\|_2 = \sqrt{\sum_{i=1}^{N} x_i^2} = \sqrt{\{x\}^T\{x\}}$$

and

$$\|\{x\}\|_\infty = \max\{|x_i|: i=1, 2, \ldots . N\}.$$

The 2-norm is also called the Euclidean norm. It is always used in determining the solution of least-squares problem. The oo-norm is sometimes called the maximum norm (max-norm) or the Chebyshev norm. Note that the concept of norm for infinite dimensional spaces is restricted to the so-called Hilbert space.

B13.      MATRIX NORM

The norm of a matrix [A] is a non-negative number $\|[A]\|$ which satisfies the following properties :

1.    $\|[A]\| > 0$, if $[A] \neq [0]$ and $\|[0]\| = 0$;

2.    $\|c[A]\| = |c|.\|[A]\|$;

3.    $\|[A+B]\| \leq \|[A]\| + \|[B]\|$;

4.    $\|[A][B]\| \leq \|[A]\|.\|[B]\|$

It should be noticed that properties (1)-(3) are identical to the properties for a vector norm described above. A matrix norm that satisfies (1)-(3) and not necessarily (4), is often called a *generalised matrix norm*.

The most frequently-used matrix norms are the F-norm (Frobenius norm, it is also called Euclidean or Shur norm), for $[A] \in R^{Nxm}$

$$\|[A]\|_F = \sqrt{\sum_{i=1}^{N} \sum_{j=1}^{m} |a_{ij}|^2}$$

Other matrix norms are :

$$\|[A]\|_1 = \max(\sum_{i=1}^{N} |a_{ij}| : j = 1, 2, \ldots . m)$$

$$\|[A]\|_2 \leq \sqrt{\text{maximum eigenvalue of } [A]^H[A]}$$

and

$$\|[A]\|_\infty = \max(\sum_{j=1}^{m} |a_{ij}| : i = 1, 2, \ldots . N)$$

The 2-norm is often called the **spectral norm** and is useful in determining the sensitivity of eigenvalues and eigenvectors. The F-norm is always used to provide the least-squares solution of an exact- or over-determined system of equations.  Note that 2- and F-norms are invarient under similarity transformations.